Structural analysis of a bidirectional nuclear transport receptor, Importin13

Dissertation

der Mathematisch-Naturwissenschaftlichen Fakultät

der Eberhard Karls Universität Tübingen

zur Erlangung des Grades eines

Doktors der Naturwissenschaften

(Dr. rer. nat.)

vorgelegt von

Marlene Holder, geb. Grünwald

aus Ulm

Tübingen

2012

Tag der mündlichen Qualifikation: 28.05.2013
Dekan: Prof. Dr. Wolfgang Rosenstiel
1. Berichterstatter: Prof. Dr. Doron Rapaport
2. Berichterstatter: Dr. Fulvia Bono

The research described in this thesis was performed in the laboratory of Dr. Fulvia Bono at the Max-Planck-Institute for Developmental Biology. The work was supervised by Prof. Dr. Doron Rapaport at the Eberhard Karls University Tübingen. An International PhD program fellowship of the Max Planck Society and funding by the DFG supported the research.

I hereby declare that I completed the doctoral work submitted here under the title **'Structural analysis of a bidirectional nuclear transport receptor, Imp13'** independently and with no other sources, materials and aids than quoted. Wherever parts of the work have been published as well as wherever parts of the work were done by colleagues, this has been indicated accordingly. All citations, whether word for word or paraphrased are given as such. I declare that I adhered to the guidelines set forth by the University of Tübingen to guarantee proper academic scholarship (Senate Resolution 25.05.2000). I declare that these statements are true and that I am concealing nothing. I understand that any false statements can be punished with a jail term of up to three years or a financial penalty.

Marlene Holder, geb. Grünwald
Tübingen, December 2012

Acknowledgment

First of all I want to thank my supervisor Dr. Fulvia Bono for the enthusiasm she brought in the project and the encouraging words and optimism she never lost over the last years. Furthermore, I want to thank her for teaching me really "good" crystallography and for the opportunities to learn many new methods. And last but not least I want to thank her for never giving up in trying to teach me how to write scientific reports and give nice presentations.

I am very grateful to Prof. Dr. Doron Rapaport for the supervision of this thesis at the Eberhard Karls University Tübingen and for giving me the opportunity to get my first teaching experience at the University.

Furthermore, I want to thank my PhD advisory committee composed of Prof. Dr. Doron Rapaport, Prof. Dr. Andrei Lupas, Dr. Remco Sprangers and Dr. Wolfram Antonin for accompanying the thesis with excellent advice from an unbiased perspective.

My thanks go to all current and former members of the Bono group for the nice atmosphere and in particular to Daniela Lazzaretti for the collaboration on the importin project and for setting up the nice cell culture and to Katharina Veith for managing the lab. I want to thank Sophia Fahrner and notably Stefanie Wachter for helping me with the expression and purification of proteins.

I want to thank the people from the 3rd floor and Prof. Dr. Elisa Izaurralde with all the people from department II for hosting the Bono group and being patient with my abnormal long shaker usage. A special thanks goes to Dr. Oliver Weichenrieder and the "small lab" for scientific discussions and pleasant and instructive Synchroton trips as well as to Steffen Schmidt for all the great and really fast support with the crystallographic software and the servers. Moreover, I especially thank Ancilla Neu for many highly enjoyable meetings and scientific and non-scientific discussions. I want to thank all my friends in Tübingen for the kind welcome, reams of nice and amiable evenings and the grandiose fun.

Besides, I want to express my gratitude to Prof. Dr. Elena Conti for hosting me to learn new methods in her laboratory and the possibility to join the fabulous Ringberg retreats. A special thank goes to Fabien Bonneau for patient teaching how to perform nice pulldown-assays and to Gretel Buchwald for discussion about sumoylation. Moreover, I want to thank Claire Basquin who tried a lot of techniques to measure the K_Ds, introduced me to biophysical methods and constantly searched for new methods. I thank the crystallization facility for setting up thousands of thousands of crystallization drops.

I thank the staff of the SLS for providing a good scientific environment and support during the data collection.

Ancilla, Ulla, Daniela and Liz I want to thank for helpful comments on this thesis.

I want to thank Thomas Holder for assisting and solving all computer related issues, teaching me patient the basics of python and for making admirable movies with PyMOL. Yet, he merits my deepest gratitude for making my life exciting and sunshiny and holding me through the most challenging circumstances.

Last but not least, my deep gratitude goes to my family, who ever loved and supported me.

Contents

List of Figures

List of Tables

1 Summary

Zusammenfassung

Der kontrollierte Austausch von tausenden Molekülen zwischen Zytoplasma und Zellkern ist für eukaryotische Zellen überlebensnotwendig. Der Großteil des aktiven Transports von und zum Zellkern wird von Ran-abhängigen Transportproteinen ausgeführt, die als Karyopherine oder Importin β-ähnliche Proteine bezeichnet werden. Karyopherine, die den Transport von Kargos in den Zellkern durchführen, heißen Importine, während Exportine Kargos aus dem Zellkern exportieren. Die Richtung des Transports wird durch einen Konzentrationsgradienten des Proteins Ran, das zur Familie der G-Proteine gehört, gesteuert. Bei Importine führt die Bindung von RanGTP zur Freilassung des Kargos, während für Exportine die Bindung von RanGTP notwendig für die Bindung des Kargos ist. Importin 13 (Imp13) gehört zu den wenigen bidirektionalen Karyopherinen, denn es kann Kargos sowohl in den Zellkern hinein als auch aus dem Zellkern heraus transportieren. Neben vielen anderen Kargos importiert Imp13 die Proteine Mago-Y14 und Ubc9 in den Zellkern. Mago-Y14 bildet zusammen mit zwei anderen Proteinen den *Exon-Junction-Complex* (EJC) und Ubc9 ist ein an der Sumoylierungs-Reaktion beteiligtes Enzym. Das einzige bisher bekannte Kargo, das von Imp13 exportiert wird, ist der eukaryotische Initiation Faktor 1A (eIF1A). eIF1A ist für die Initiation der Translation im Zytoplasma notwendig.

Als ich mit meiner Arbeit an Imp13 begann, waren Kristallstrukturen der Importine Importinβ (Impβ) und Transportin (Tnp) sowie des Exportins CAS veröffentlicht. Allerdings waren zu diesem Zeitpunkt nur die beiden Karyopherine Msn5 und Imp13 als bidirektionale Transportproteine bekannt. Kurze Zeit später wurden die Kristallstrukturen der Exportine Crm1, ExportinT (Expt) und Exportin5 (Exp5) in Komplex mit RanGTP und einem ihrer Export-Kargos veröffentlicht. Zur gleichen Zeit wurde Exportin4 (Exp4) als ein weiteres bidirektionales Transportprotein identifiziert. Die molekulare Grundlage für die Funktion von bidirektionalen Transportproteinen, wie zum Beispiel Imp13, blieb jedoch weiterhin unbekannt. Eine weitere unbeantwortete Frage war, wie Imp13 verschiedene Proteine erkennen und transportieren kann, die keine typische Lokalisierungssequenz (nukleares Lokalisierungs-Signal (*NLS*) oder nukleares Export-Signal (*NES*)) aufweisen? Es war ebenfalls nicht geklärt, wie die Bindung von RanGTP am selben Karyopherin die Bindung eines Kargos und gleichzeitig die Abgabe eines anderen Kargos bewirken kann.

In meiner Doktorarbeit klärte ich mittels Röntgenkristallographie und biochemische Methoden den molekularen Transport-Mechanismus von Imp13 auf. Im ersten Teil meiner Arbeit befasste ich mich mit dem Import von Kargos durch Imp13 und untersuchte mit biochemischen Methoden den Zellkern-Transport-Mechanismus von Mago-Y14. Ich kristallisierte den Komplex aus Imp13 und Ubc9 und löste seine Struktur bei 2.8 Å Auflösung.

Darüber hinaus charakterisierte ich mit *in vitro* Copräzipitations-, Kompetitions- und Sumoylierungs-Untersuchungen den Transport-Mechanismus von Ubc9. Die Strukturanalyse zeigte, dass Imp13 verschiedene Interaktionsoberflächen für die Bindung von Mago-Y14 und Ubc9 verwendet. Ungewöhnlicherweise wird Ubc9 von der N-terminalen Hälfte von Imp13 an einer Stelle gebunden, die auch für die Bindung von RanGTP verwendet wird, während Mago-Y14 von der C-terminalen Hälfte von Imp13 erkannt wird. In *in vitro* Kompetitions-Untersuchungen verdrängen sich beide Proteine gleichermaßen und können nicht gleichzeitig an Imp13 binden. In Übereinstimmung mit diesem Ergebnis ergaben die Messung der Dissoziations-Konstanten (K_D) von Imp13 für beide Kargos Werte im gleichen Bereich zwischen 230 und 370 nM. Ich zeigte ebenfalls, dass die Bindung von RanGTP an Imp13 die Dissoziation beider Kargos über verschiedene Mechanismen induziert. RanGTP konkurriert direkt mit Ubc9 um dieselbe Interaktionsoberfläche, während Mago-Y14 durch eine sterische Hinderung aus dem Komplex verdrängt wird.

Im zweiten Teil meiner Doktorarbeit konzentrierte ich mich auf den Export von eIF1A durch Imp13. Ich kristallisierte einen Komplex aus Imp13-RanGTP-eIF1A und löste seine Struktur bei 3.6 Å Auflösung. Die Bindestelle für eIF1A liegt auf der Innenseite von Imp13 in dessen C-terminalen Hälfte neben der Bindestelle für RanGTP. Die Dissoziations-Konstante beträgt 3 µM. Die Interaktionsfläche von Imp13 für eIF1A wird ebenfalls für die Bindung des Import-Kargos Mago-Y14 verwendet. Der Vergleich zwischen den Import- und Export-Komplexen zeigt auf, dass die Richtung des Transports durch eine sich gegenseitige ausschließende Bindung von Import-Kargos und RanGTP und eine gleichzeitige Bindung mit dem Export-Kargo bestimmt wird. Zudem löste ich die Struktur von freiem Imp13 bei 3.0 Å Auflösung. Die Struktur von freiem Imp13 zeigt eine insgesamt offene Konformation, die größtenteils inkompatibel mit der Bindung von eIF1A ist. Dies deutet darauf hin, dass Imp13 im Zytosol nach Abgabe von RanGTP eIF1A ebenfalls nicht mehr binden kann. Zusammenfassend ist Imp13 ein außergewöhnlich vielseitiges Zellkern-Transportprotein, das mit seiner inneren Oberfläche seine Kargos an ihrer Form erkennt und dadurch seine Konformation abhängig von der Bindung von einer offenen Superhelix bis zu einem geschlossenen Ring ändern kann. Der Bidirektionalität von Imp13 liegt ein einfaches Prinzip zu Grunde, bei dem die Größe und die elektrostatische Ladung des Kargos die Transportrichtung bestimmt.

Summary

Nucleocytoplasmic transport of thousands of molecules is an essential feature of eukaryotic cells. The bulk of the active transport between cytoplasm and nucleus is performed by Ran-dependent nuclear transport receptors known as karyopherins or Importin β-like proteins. Karyopherins involved in the transport of cargoes into the nucleus are called importins, while karyopherins known as exportins export cargoes out of the nucleus. The directionality of transport is driven by a gradient of the small GTPase Ran. In case of importins, RanGTP binding triggers the release of the cargo, while for exportins, the binding of RanGTP mediates the cargo binding. One of the few bidirectional karyopherins that can both import and export cargoes is Importin13 (Imp13). In addition to several other import cargoes, Imp13 imports Mago-Y14, a core component of the exon-junction-complex (EJC), and Ubc9, the only E2-conjugating enzyme of the sumoylation pathway, into the nucleus. The only export cargo identified to date for Imp13 is the eukaryotic initiation factor 1A (eIF1A), which is essential for translation initiation in the cytoplasm.

When I started working on Imp13, detailed structural knowledge on the import factors Importinβ (Impβ) and Transportin (Tnp) and on the export receptor CAS was available. Only two karyopherins Msn5 and Imp13, were known to be bidirectional transport receptors. In 2009, the structures of the exportins Crm1, ExportinT (Expt) and Exportin5 (Exp5) in complex with RanGTP and their cargoes were published. In the same year, Exportin4 (Exp4) was also identified as a bidirectional transport receptor. However, the molecular understanding of how bidirectional transport receptors such as Imp13 function was limited. How Imp13 can recognize diverse cargoes lacking a typical nuclear localization signal (NLS) or nuclear export signal (NES) was an unresolved question. Furthermore, the means with which RanGTP associates to the same receptor to mediate both cargo release and cargo binding were unclear.

During my PhD work I used biochemical assays and x-ray crystallography to elucidate the molecular mechanism underlying Imp13 mediated transport. I first focused on the import branch of the Imp13 cycle. Using biochemical assays, I investigated the nuclear transport mechanism of Mago-Y14 by Imp13. I crystallized and solved the structure of the Imp13-Ubc9 complex at 2.8 Å resolution. Furthermore, I characterized the transport mechanism by *in vitro* co-precipitation-, competition- and sumoylation assays to further complement information obtained from the structures. I found that Imp13 employs completely different interaction surfaces for binding its import cargoes Mago-Y14 and Ubc9. Ubc9 is bound by the N-terminal arch of Imp13 with the same interaction surface also used for RanGTP binding, while Mago-Y14 is bound in the middle and C-terminal part of Imp13. In *in vitro* competition assays, both cargoes can displace each other from Imp13 to a similar extent, but cannot bind at the same time. Consistently, the dissociation constants (K_D) of Imp13 for both import cargoes is in the same range, between 230 and 370

nM. Furthermore, RanGTP induces the release of both import cargoes by different mechanisms. RanGTP directly competes for the binding surface of Ubc9 on Imp13, whereas it displaces Mago-Y14 by a steric hindrance mechanism.

In the second half of my PhD, I focused on the export part of the Imp13 cycle. I crystallized and solved the Imp13-RanGTP-eIF1A complex at 3.6 Å resolution. eIF1A is bound at the inner surface of the C-terminal arch of Imp13 adjacent to RanGTP with a K_D of 3 µM. The import cargo Mago-Y14 and the export cargo eIF1A share the same interaction surface on Imp13. The comparison between Imp13 import and export complexes reveals that the direction of the transport is determined by a mutually exclusive binding between import cargo and RanGTP and a concomitant binding with the export cargo. Furthermore, I solved the structure of the cytosolic cargo-free state of Imp13 at 3.0 Å resolution. The structure of free Imp13 reveals an overall open conformation, largely incompatible with the binding of eIF1A in the cytoplasm. In conclusion, Imp13 is a remarkably versatile nuclear transport factor which recognizes the shape of its cargoes by wrapping around them with its inner surface and thereby changing its conformation ranging from an open superhelix to a closed ring. A simple principle in which the size and charge of the cargo determines the direction of transport underlies Imp13's unusual function in nucleocytoplasmic transport.

List of publications

Results described in this thesis have been published or submitted for publication in the following research articles:

Bono F, Cook A, **Grünwald M**, Ebert J, & Conti E (2010) Nuclear Import Mechanism of the EJC Component Mago-Y14 Revealed by Structural Studies of Importin 13. *Molecular Cell* 37(2): 211-22.

Grünwald M & Bono F (2011) Structure of Importin13-Ubc9 complex: nuclear import and release of a key regulator of sumoylation. *EMBO Journal*, 30(2):427-438.

Grünwald M, Lazzaretti D & Bono F (2013) Structural basis for the nuclear export activity of Importin13. *EMBO J*, 23(6):899-913

Author's contributions to publications

The work presented in this thesis was mainly performed in the laboratory of Dr. Fulvia Bono (MPI for Developmental Biology). The research on Imp13 was started by Dr. Fulvia Bono as a post-doc fellow in the laboratory of Prof. Dr. Elena Conti (MPI for Biochemistry). The following statement summarizes the contributions by the thesis' author.

4.1 Nuclear import and release of Mago-Y14 by Imp13

Bono F, Cook A, **Grünwald M**, Ebert J, & Conti E (2010) Nuclear Import Mechanism of the EJC Component Mago-Y14 Revealed by Structural Studies of Importin 13. *Molecular Cell* 37(2): 211-22.

M. Grünwald performed all biochemical assays described in the figures and in the supplements of the paper. She prepared all proteins used for the biochemical experiments with exception of untagged Mago-Y14 and RanGTP and established conditions for the *in vitro* binding assays. She helped to complete the paper for publication.

4.2 Nuclear import and release of Ubc9 by Imp13

Grünwald M & Bono F (2011) Structure of Importin13-Ubc9 complex: nuclear import and release of a key regulator of sumoylation. *EMBO Journal*, 30(2):427-438.

M. Grünwald prepared all proteins with the exception of untagged Mago-Y14 and RanGTP. She established conditions for the assembly of stable Imp13-Ubc9 complex, optimized the Imp13-Ubc9 crystals, collected the diffraction data, solved the structure by Molecular Replacement (MR) and refined the data. She designed part of the biochemical experiments and performed all experiments described in the main body and in the supplements of the paper. She contributed to the interpretation of the data and to the writing of the manuscript (including the preparation of the figures).

4.3 Nuclear export and release of eIF1A by Imp13

Grünwald M, Lazzaretti D & Bono F (2013) Structural basis for the nuclear export activity of Importin13. *EMBO J*, 23(6):899-913

M. Grünwald prepared all recombinant proteins with the exception of untagged Mago-Y14. She established conditions and constructs for the assembly of stable and homogeneous Imp13-RanGTP-eIF1A complex, optimized the Imp13-RanGTP-eIF1A crystals, collected the diffraction data, solved the structure by MR and refined the data. Furthermore, she designed the biochemical experiments and performed all *in vitro* experiments described in the main body and in the supplements of the paper. She established the K_D measurements

by differential scanning fluorimetry and performed the experiments. In addition, she solved the structure of the free state of Imp13 by MR and refined the data. She contributed to the interpretation of the data, wrote the first draft of the manuscript and helped to complete the paper for publication (including the preparation of the figures).

2 Introduction

2.1 Compartmentalization of eukaryotic cells

Eukaryotes differ substantially from organisms of the two other domains of life, in that their cells have evolved distinct, internal compartments enclosed by intracellular membranes. These specialized micro-environments enable the cell to separate various tasks in space and time. In this context, the most prominent intracellular compartment, the nucleus, is a defining feature of eukaryotic cells. The nucleus comprises the DNA and is surrounded by a double-layered membrane called the nuclear envelope (NE). This compartment protects the genomic DNA and spatially separates replication and transcription in the nucleus from protein translation in the cytoplasm. Most likely, the presence of the nucleus enabled eukaryotes to evolve to complex multicellular organisms with large genomes and to develop diverse and elaborated mechanisms to regulate their gene expression [Martin and Koonin, 2006]. Moreover, the adoption and regulation of splicing in the nucleus allowed eukaryotes the diversification of multidomain proteins [Gilbert, 1978].

Eukaryotic cell compartmentalization has generated the requirement for inter-compartmental transport of thousands of macromolecules [Mattaj and Englmeier, 1998]. Many nuclear products, such as tRNAs, miRNAs, mRNAs and pre-ribosomal subunits, must be actively transported to the cytoplasm to fulfill their function. In contrast, nuclear proteins, like transcriptions factors, histones and polymerases, must be transported into the nucleus [Gurdon, 1970]. Many proteins oscillate between nucleoplasm and cytoplasm and therefore are continuously transported in and out of the nucleus [Mattaj and Englmeier, 1998]. During the open mitosis of higher eukaryotes, the NE breaks down and consequently nucleoplasm and cytoplasm become mixed. Therefore, after each nuclear division the nuclear-cytoplasmic distribution of proteins needs to be reestablished. [Görlich and Kutay, 1999]. Hence, the nucleocytoplasmic transport must be continuous, efficient and fast. In total, an enormous amount of traffic occurs across the NE, with a conservative estimate of more than 1 million macromolecules transferred each minute in a growing mammalian cell [Görlich and Mattaj, 1996].

2.2 Overview of nucleocytoplasmic transport

The extensive nucleocytoplasmic traffic must overcome the natural barrier formed by the NE. The NE is composed of an inner and outer membrane that fuse together to form pores in which enormous protein assemblies are embedded, the nuclear pore complexes (NPCs). NPCs are the sole gate-keepers between nucleoplasm and cytoplasm, with a channel diameter of approximately 100 nm and a molecular mass of $\sim$ 66 MDa in yeast and $\sim$ 125 MDa in metazoans [Rout and Blobel, 1993, Yang et al., 1998, Reichelt et al., 1990,

Akey and Radermacher, 1993]. Compared to most other transmembrane transporters, NPCs facilitate efficient transport in both directions without the need to unfold their protein cargoes [Görlich and Kutay, 1999]. According to the demand of nuclear transport and proliferation, the number of NPCs per cell can vary greatly, from 180 in yeast to 5 x 10^7 in *Xenopus* oocytes [Rout and Blobel, 1993, Cordes et al., 1995]. NPCs are composed of approximately 30 different proteins called nucleoporins (Nups) which occur in the NPCs in multiple copies, resulting in an eight-fold symmetry assembly [Rout et al., 2000, Cronshaw et al., 2002, Hoelz et al., 2011]. The NPCs consist of several units: the selective central channel, a core scaffold supporting the channel, a transmembrane region, the nuclear basket and the cytoplasmic filaments [Alber et al., 2007, Grünwald et al., 2011, Hoelz et al., 2011]. In the central channel, proteins rich in phenylalanine and glycine, the FG-repeat Nups, form a permeability barrier and thus function as a molecular sieve. Only small molecules up to 20-40 kDa can passively diffuse through the NPCs [Paine and Feldherr, 1972, Mohr et al., 2009]. All other macromolecules, with only a few exceptions, are actively transported by soluble receptors that specifically recognize their cargoes and allow the transit of the receptor-substrate complex through the NPCs [Mattaj and Englmeier, 1998, Görlich and Kutay, 1999, Rout and Aitchison, 2001, Vasu and Forbes, 2001]. Not all nucleocytoplasmic transport occurs via NPCs. Recently, an alternative transport pathway which bypasses the NPCs by remodeling the nuclear membrane was reported for large ribonucleoprotein (RNP) particles in neuromuscular junctions [Speese et al., 2012]. A similar process has been described for certain viruses [Johnson and Baines, 2011].

Three classes of soluble receptors are known to perform active transport through the NPCs. The first class of transport receptors is involved in the export of mRNAs through the NPCs and is composed of the heterodimer Mex67/Mtr2 in yeast and p15/NXT in metazoans [Segref et al., 1997, Grüter et al., 1998]. The second class of nuclear receptors is represented by the small nuclear transport factor 2 (NTF2), which imports the small GTPase Ran into the nucleus [Ribbeck et al., 1998, Smith et al., 1998]. Although NTF2 has only one cargo, it accounts for a large proportion of traffic, as Ran is a very abundant protein. The third class of receptors which is responsible for the bulk of the nucleocytoplasmic transport is formed by a superfamily of proteins called karyopherins or importin β-like proteins.

2.3 Nucleocytoplasmic transport mediated by karyopherins

Karyopherins can be classified as importins or exportins according to their direction of transport. Importins recognize their cargoes in the cytoplasm, either directly or using adaptor proteins, and translocate through the NPC channel via weak hydrophobic interactions with the FG-repeat Nups (see Figure 1). In the nucleoplasm, importin-cargo complexes associate with the highly abundant Ran in the GTP bound form (RanGTP),

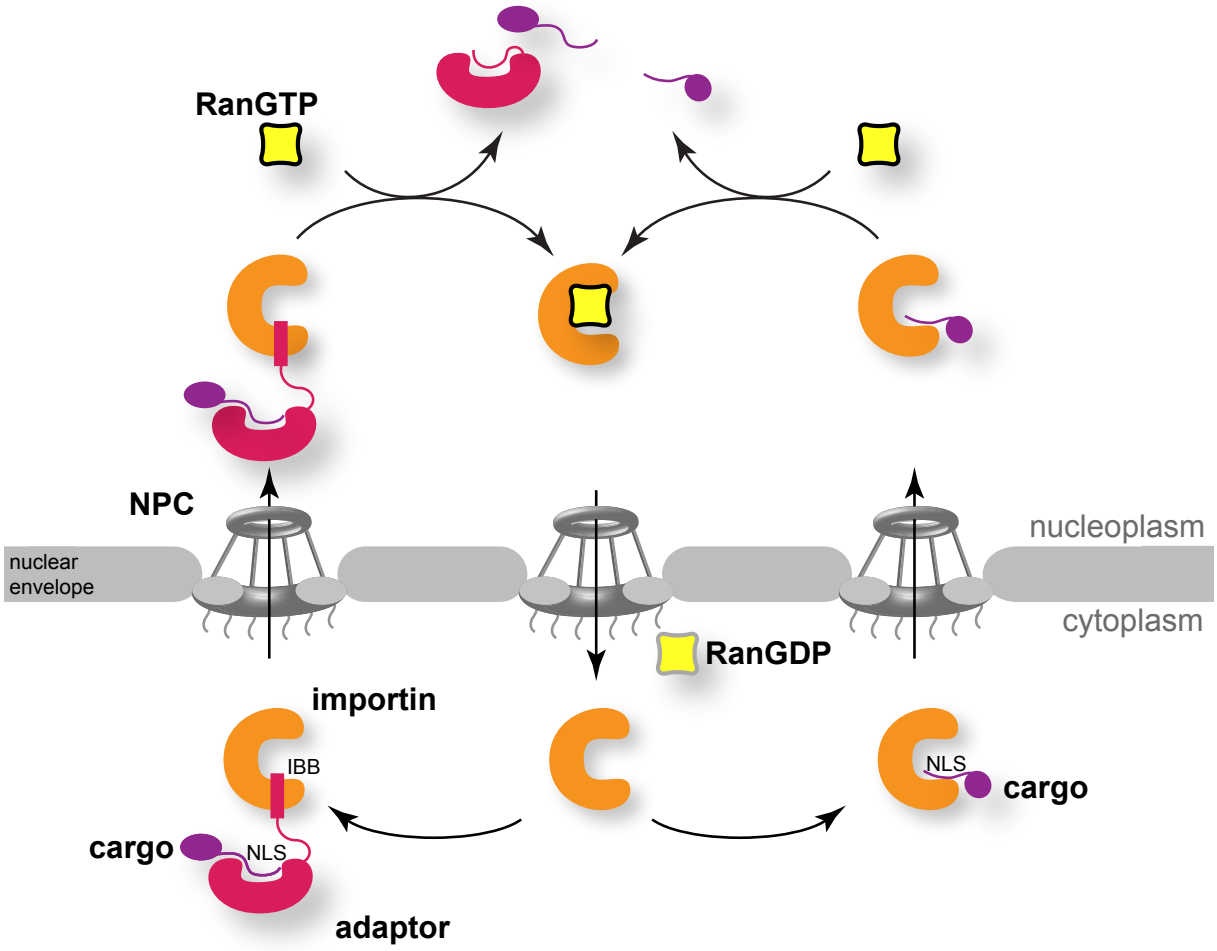

Figure 1: **Schematic illustration of importin-mediated nuclear import.** The two possible ways of cargo (purple) recognition, either by an importin (orange) or by an importin-adaptor (magenta) complex, are shown. The complexes travel through the NPCs into the nucleus, where the cargo is released via the binding of RanGTP (yellow, black outline) to the importin. The importin-RanGTP complex translocates back to the cytoplasm, where Ran is released from the complex and the GTP is hydrolysed to GDP (yellow, gray outline). The importin is then free for binding to the next cargo. This figure has been adapted from [Cook et al., 2007].

which triggers the release of the cargo. The importin-RanGTP complex then travels back to the cytoplasm where Ran is irreversibly released from the importin by the hydrolysis of GTP to GDP. In the cytoplasm, the importin is free to bind the next cargo and transport it into the nucleus. In contrast to importins, exportins bind their cargoes in the nucleus after the association with RanGTP (see Figure 2). The exportin-RanGTP-cargo complex translocates through the NPCs. In the cytoplasm, the release of Ran and the hydrolysis of GTP to GDP then causes the dissociation of the export cargo. The unbound exportin travels back into the nucleus for the next round of transport.

In humans, 19 members of the karyopherin superfamily are known, 10 of which are classified as importins (see Table 1, 2, 3) and two (RanBP6 and RanBP17) are not yet characterized [Kutay et al., 2000, O'Reilly et al., 2011]. As previously described, the ex-

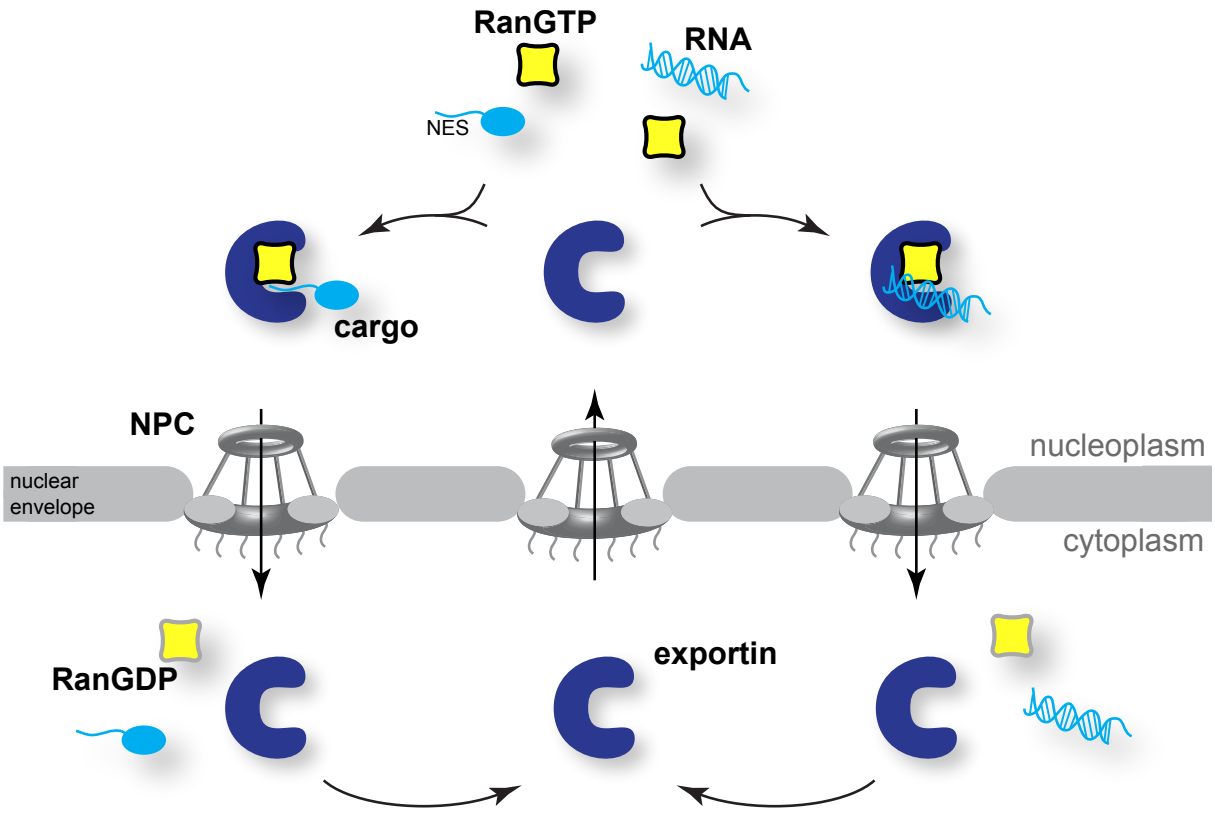

Figure 2: **Schematic illustration of exportin-mediated nuclear export.** Exportins (dark blue) bind their cargo (blue) together with RanGTP (yellow, black outline) in the nucleus and translocate through the NPCs into the cytoplasm. The dissociation of RanGTP and hydrolization of GTP to GDP (yellow, gray outline) causes the disassembling of the exportin-cargo complex. Afterwards, the free exportin travels back into the nucleus for binding to the next export cargo. This figure has been adapted from [Cook et al., 2007].

port and import of molecules is performed by distinct and specialized karopherins, with the exception of three receptors which are reported to be bidirectional transporters (see Table 2). Msn5p, a yeast specific karyopherin, Exp4 and Imp13 function in both directions, transporting and delivering different cargoes in and out of the nucleus [Yoshida and Blobel, 2001, Gontan et al., 2009, Mingot et al., 2001].

The transport function of karyopherins is well characterized, whereas the other functions of karyopherins such as their role in NE and NPC assembly, mitosis and replication have not been studied in detail [Mosammaparast and Pemberton, 2004]. Additionally, karyopherins critically influence many key cellular processes, such as gene expression, signal transduction, immune response, oncogenesis and viral propagation by the efficient and accurate transport of their cargoes [Chook and Süel, 2010].

Table 1: **Importins and their nuclear import cargoes.** Adaptor proteins and/or other receptors which redundantly transport the same cargo are listed when appropriate. The names of the importin homologs from *S. cerevisiae* are written in italics.

Importin	adaptor	other receptors	**cargoes**	**references**
Impβ (*Kap95p*)			SREBP-2	[Lee et al., 2003]
			PTHrP	[Cingolani et al., 2002, Lam et al., 2001]
		Tnp, Imp5, -7	HIV-1 Rev	[Truant and Cullen, 1999]
			HIV-1 TAT	[Truant and Cullen, 1999]
			Cyclin B	[Moore et al., 1999]
			CREB , AP-1	[Forwood et al., 2001]
	Impα	Imp5, -7, -9, Tnp	Histones	[Mühlhäusser et al., 2001, Baake et al., 2001]
	Impα	Impβ/7, -5, Tnp	ribosomal proteins	[Jäkel and Görlich, 1998]
		Exp4	SRY	[Forwood et al., 2001, Gontan et al., 2009]
	Impα		cNLS proteins	[Görlich et al., 1995, Chi et al., 1995, Radu et al., 1995]
	SPN1		U snRNPs	[Huber et al., 1998]
Tnp (Kapβ2, *Kap104*)			hnRNPs	[Lee et al., 2006]
			TAP (NXF1)	[Truant et al., 1999]
			Sox14, PQBP1, YBP1	[Lee et al., 2006]
		Imp8, -β, -5, -7	SRP19	[Dean et al., 2001]
Imp4 (*Kap123*)			Vitamin D receptor	[Miyauchi et al., 2005]
			TP2	[Pradeepa et al., 2008]
Imp5 (RanBP5, *Kap121*)			Rag-2	[Ross et al., 2003]
			Apolipoprotein A-I	[Chung et al., 2008]
			p60TRP	[Heese et al., 2004]
			Influenza A PB1, PA	[Deng et al., 2006]
Imp7 (NMD5, *Kap119*)			ERK2, MEK1, Smad3	[Chuderland et al., 2008]
		Tnp, Impβ, -5, -9	c-Jun	[Waldmann et al., 2007]
Imp8 (*Kap108*)			Ago	[Weinmann et al., 2009]
			Smad1, Smad4	[Yao et al., 2008]
Imp9 (*Kap114*)			HSP27	[Jäkel et al., 2002]
		Impβ, -13	Arx	[Lin et al., 2009]
Imp11 (*Kap120*)			UbcM2, -H6, UbeE2	[Plafker et al., 2004]
			Gag	[Gudleski et al., 2010]
TnpSR (Mtr10, *Kap111*)			ASF, SC35	[Kataoka et al., 1999]
			Tra2α, -β	[Lai et al., 2000]

Table 2: **Bidirectional karyopherins and their import and export cargoes.** Other receptors which redundantly transport the same cargo are listed. The names of the *S. cerevisae* homologs are written in italics. Import cargoes are marked with an (i), while export cargoes are labeled with (e).

bidirectional	other receptors	**cargoes**	**references**
Imp13		Ubc9, Mago/Y14, rPL5 (i)	[Mingot et al., 2001]
		NF-YB/YC (i)	[Kahle et al., 2005]
	Impα/β	NC2α/NC2β (i)	[Kahle et al., 2009]
		myopodin (i)	[Liang et al., 2008]
		Pax6, Pax3, Crx (i)	[Ploski et al., 2004]
	Imp5	CHRAC15/17, p12/CHRAC17 (i)	[Walker et al., 2009]
	Impα/β, -7	GR (i)	[Tao et al., 2006]
		eIF1A (e)	[Mingot et al., 2001]
Exp4		eIF5A (e)	[Lipowsky et al., 2000]
		Smad3 (e)	[Kurisaki et al., 2006]
	Impβ, -7, -9	Sox2, SRY (i)	[Gontan et al., 2009]
Msn5p		Pho4p (e)	[Kaffman and O'Shea, 1999]
		RPA (i)	[Yoshida and Blobel, 2001]

Table 3: **Exportins and their nuclear export cargoes.** Adaptor proteins and/or other receptors which redundantly transport the same cargo are listed when appropriate. The exportin homologs from *S. cerevisiae* are written in italics.

Exportin	adaptor	other receptors	**cargoes**	**references**
Crm1 (Exp1, Xpo1, *Kap124*)			NES proteins	[Fischer et al., 1995, Wen et al., 1995]
	HIV Rev		HIV RNA	[Fischer et al., 1995]
	Phax/Cbc		U snRNAs	[Izaurralde et al., 1995]
			SPN1	[Paraskeva et al., 1999]
CAS (Exp2, *Cse1*)			Impα	[Kutay et al., 1997, Solsbacher et al., 1998]
Expt (*Los1p*)			tRNA	[Kutay et al., 1998]
Exp5 (Xpo5)	aa-tRNA		eEF1A	[Bohnsack et al., 2002, Calado et al., 2002]
	dsRNA		dsRNA BP	[Brownawell and Macara, 2002]
			pre-miRNAs	[Yi et al., 2003]
		Crm1	60S pre-ribosomal	[Wild et al., 2010]
Exp6			Actin-profilin	[Stüven et al., 2003]
Exp7			p50RhoGAP, 14-3-3	[Mingot et al., 2004]

2.3.1 The small GTPase Ran

Many regulatory processes in cells are controlled by members of the superfamiliy of small Ras-like GTPases to which the Ras-related nuclear antigen (Ran) belongs. Human Ran consists of a G-domain, composed of a central six-stranded β-sheet surrounded by five α-helices with two characteristic loop regions (see Figure 3) [Scheffzek et al., 1995, Vetter et al., 1999a, Partridge and Schwartz, 2009] (pdb id: 3GJ0, 1RRP). C-terminal to the G-domain is an extended region (C-terminal extension) that consists of a linker and an α-helix. The two loop regions are called switch-I (or effector loop, residue 33-45) and switch-II (residue 65-78). The conformation of switch-I and switch-II vary greatly between the GTP- and GDP-bound state of Ran. This conformational change is responsible for switching Ran into the on (RanGTP) or off (RanGDP) state.

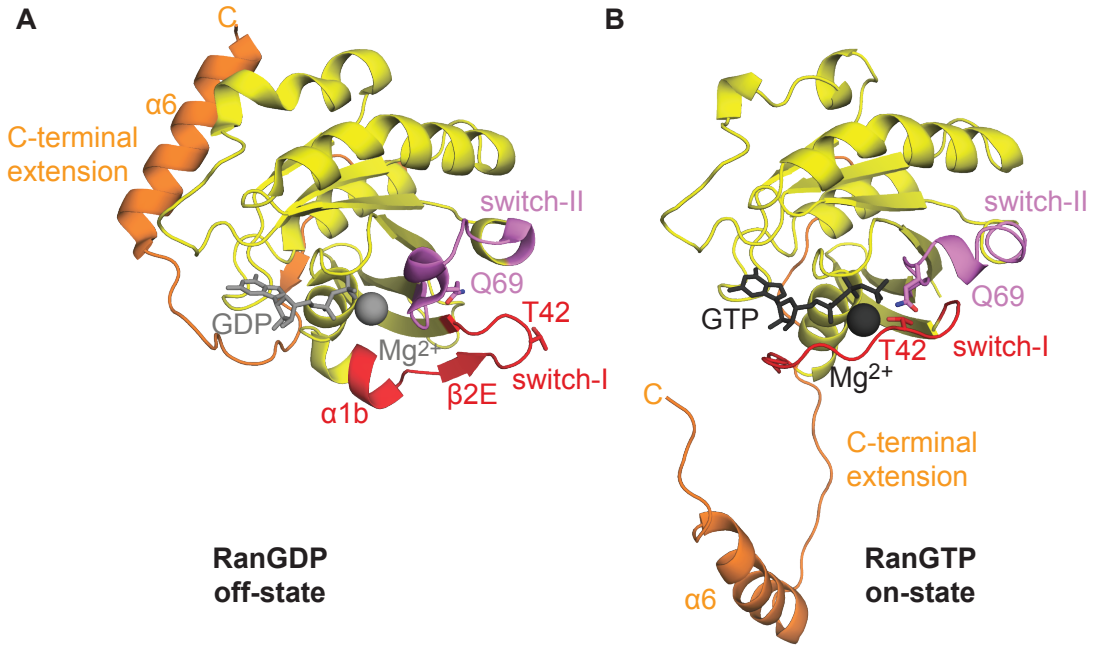

Figure 3: **Structure of Ran bound to GDP or GTP.** Cartoon view of the human Ran structure (yellow) bound to (A) GDP or (B) GTP [Partridge and Schwartz, 2009, Vetter et al., 1999a] (pdb id: 3GJ0, 1RRP). Switch-I with the helical turn α1b, short β-strand β2E and the residue Thr42 is colored in red, switch-II and the catalytic residue Gln69 are shown in pink and the C-terminal extension is marked in orange. GDP and GTP are shown as stick models in gray or in black, respectively. The Mg^{2+} ion is shown as a sphere in the same color as GDP or GTP. RanBP1, present in the structure (B), has been removed for clarity.

In the GDP-bound state, switch-I folds in a helical turn (α1b) and a β-strand (β2E) (see Figure 3A). As a consequence, the conserved nucleotide-binding residue Thr42 in switch-I and the catalytic residue Gln69 in switch-II are moved away from the nucleotide binding pocket. Furthermore, in the GDP-bound state, the C-terminal extension binds back to the G-domain, preventing karyopherin binding by blocking the interaction surface [Scheffzek et al., 1995, Stewart et al., 1998, Vetter et al., 1999a]. Conversely, in the GTP-bound

state, the secondary elements of switch-I α1b and β2E melt and this region is now in close contact with the nucleotide (see Figure 3B). In particular, Thr42 moves 14 Å closer to the nucleotide binding pocket to form a hydrogen-bond between its main chain and the γ-phosphate of the GTP. Additionally, the hydroxyl-group of Thr42 coordinates the Mg^{2+}-ion. Switch-II adopts a conformation where the catalytic residue Gln69 is in close proximity to the bound GTP. In this state, the C-terminal extension is displaced from the G-domain by switch-I and this allows the binding of the karyopherins to Ran (see Figure 3B).

The concentration of Ran in the GTP bound state is 1000 times higher in the nucleus than in the cytoplasm, generating a gradient between nucleoplasm and cytoplasm (see Figure 4). The RanGTP gradient is the sole driving force of transport directionality and

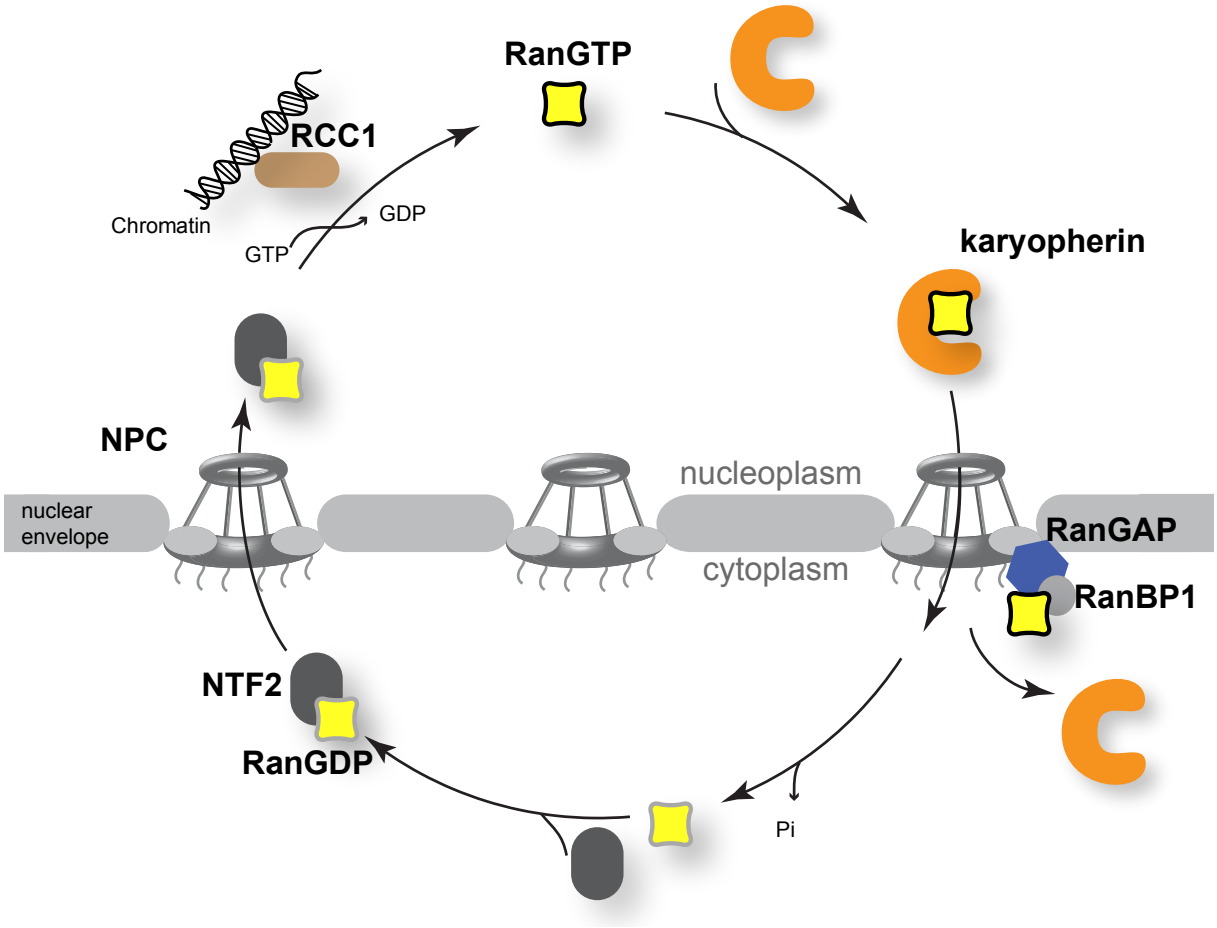

Figure 4: **Schematic illustration of the Ran cycle.** In the nucleus, RCC1 (brown) mediates the exchange of GDP to GTP and thus switches Ran into the on state (yellow, black outline). RanGTP then can bind to a karyopherin (orange) and either trigger the release of an import-cargo or promote the binding of an export-cargo. Together with the karyopherin, RanGTP translocates to the cytoplasm, where the binding of RanBP1 (gray circle) leads to the dissociation of the karyopherin-RanGTP complex. RanGAP (blue) activates the GTPase activity of Ran. Upon GTP hydrolysis, Ran undergoes a conformational change that prevents rebinding to the karyopherins. Finally, RanGDP (yellow, gray outline) is bound by NTF2 (gray) and transported back to the nucleus. This figure has been adapted from [Cook et al., 2007]

also supplies energy for the nucleocytoplasmic transport mediated by karyopherins. Consistent with this, a disruption of the gradient blocks nucleocytoplasmic transport [Moore and Blobel, 1993, Melchior et al., 1993, Corbett et al., 1995, Schlenstedt et al., 1995, Palacios et al., 1996, Richards et al., 1997, Izaurralde et al., 1997, Weis et al., 1996, Görlich et al., 1996]. High RanGTP concentration in the nucleus is maintained by the differential localization of two proteins, the guanine nucleotide exchange factor (RCC1) and the Ran GTPase-activating protein (RanGAP) (see Figure 4) [Görlich and Kutay, 1999, Görlich et al., 2003]. RCC1 is localized exclusively in the nucleus where it is stably bound to the chromatin via the histones H2A and H2B. In contrast, RanGAP is bound to the cytoplasmic site of the NPCs. Consequently, RCC1 exchanges the bound GDP from Ran into GTP and switches Ran into the on state in the nucleus [Talcott and Moore, 2000, Nemergut and Macara, 2000]. In the cytoplasm, RanGAP enhances the very low intrinsic GTPase activity (1.8×10^{-5}/s) of Ran by a factor of 10^5 and switches Ran into the off state [Klebe et al., 1995, Matunis et al., 1998]. RanGAP cannot access karyopherin-bound RanGTP, therefore the Ran-binding-protein-1 (RanBP1) or Ran-binding protein-2 (RanBP2/Nup358) are necessary to competitively induce the release of Ran [Bischoff and Görlich, 1997, Floer et al., 1997, Kutay et al., 1997, Lounsbury and Macara, 1997, Vetter et al., 1999b]. RanGTP is continuously exported from the nucleus via karyopherin association and released in the cytoplasm as RanGDP. The protein NTF2, as mentioned in section 2.2, transports RanGDP back into the nucleus [Ribbeck et al., 1998]. Therefore, the frequency of the reimport of RanGDP has to be in the same range as the transport of all other receptors together and for this reason Ran is probably the most rapidly shuttling macromolecule in the cell [Görlich and Kutay, 1999].

2.3.2 Structural aspects of karyopherins

Karyopherins are large (90-150 kDa) soluble proteins composed of 18-20 HEAT-repeats (see Figure 5 with Impβ as an example). A HEAT-repeat consists of approximately 40 amino acids forming two α-helices, A and B [Andrade and Bork, 1995, Andrade et al., 2001]. The consecutive HEAT-repeats pack against each other, usually with a 15° right-handed twist. This generates an intrinsically flexible superhelical structure in which the A helices face the outer convex surface, while the B helices form the inner concave surface. The loops between the A and B helix of the same HEAT-repeat are called intra-loops, while the loops between HEAT-repeats are called inter-loops. The sequence identity across the karyopherins is low (between 10-20 %), although the intrinsic flexibility of karyopherins appears to be conserved [Conti et al., 2006, Chook and Süel, 2010]. Structural studies on karyopherins are necessary as the accurate boundaries of HEAT-repeats are difficult to predict from the amino acid sequence and conformational changes are important for the function of karyopherins.

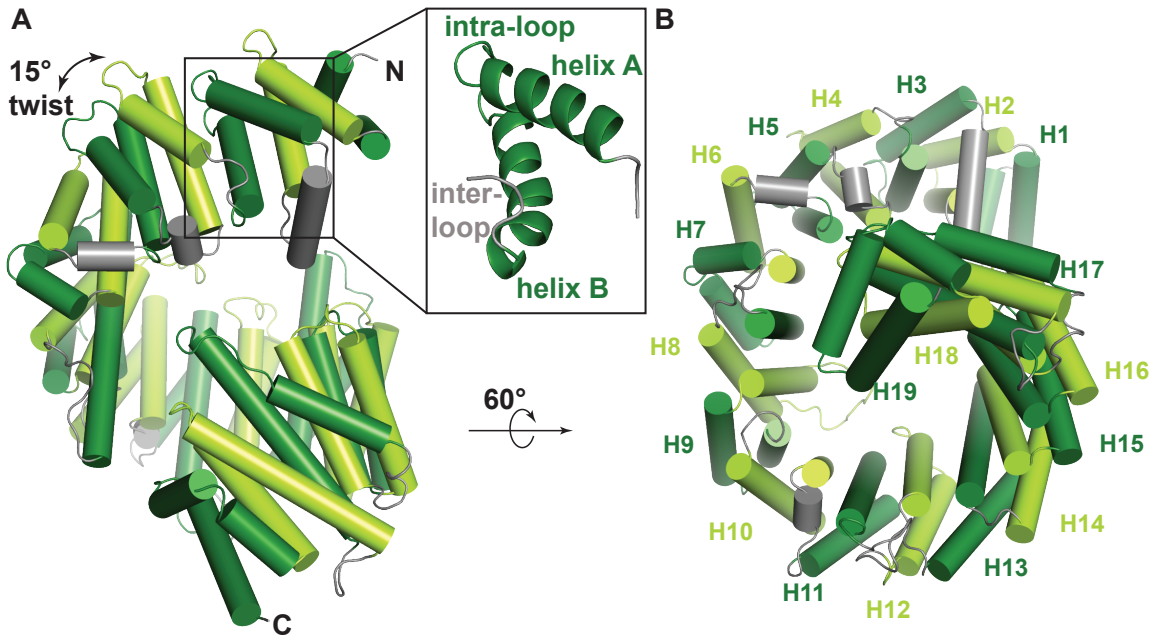

Figure 5: **Typical HEAT-repeat architecture of karyopherins** (A) Impβ structure is shown as cylndrical helices [Cingolani et al., 1999] (pdb id: 1QGK). HEAT-repeats are colored alternatively in dark and light green and the inter-loops are colored in gray. The third HEAT-repeat is zoomed-in with the helix A, B and the loops labeled. (B) View rotated 60° along the x-axis with the same colors as (A). HEAT-repeats are numbered from H1 to H19. The αIBB domain present in this crystal structure is not shown.

2.3.3 Cargo recognition by importins

Importins typically recognize their cargoes with their C-terminal half via linear nuclear localization signals (NLSs) (reviewed in [Marfori et al., 2011, Chook and Süel, 2010]). In general, NLSs are bound with high affinity in the low nanomolar range [Chook and Süel, 2010]. Impβ, the first described karyopherin, associates with its cargoes either directly or via adaptor proteins (see section 2.3 and Figure 1 and 6) [Adam and Adam, 1994, Görlich et al., 1995, Radu et al., 1995, Moroianu et al., 1995, Imamoto et al., 1995]. The Impβ adaptor Importin-α (Impα) binds classical NLSs (cNLSs) in a sequence specific manner, while

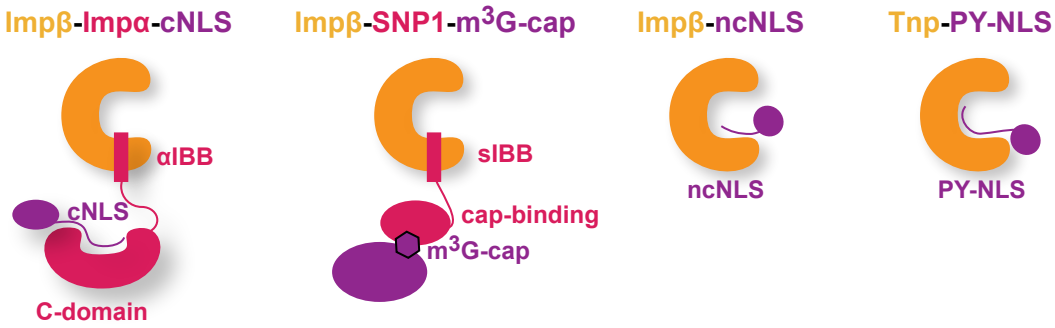

Figure 6: **Cargo recognition by importins**

another Impβ adaptor, Snurportin-1 (SPN1), recognizes a chemical structure composed of the trimethylguanosine cap (m^3G-cap). Impβ directly binds cargoes with non-classical NLSs (ncNLSs) which are generally linear sequences but may also be composed of folded domains. Tnp directly recognizes a different class of NLSs, prolin-tyrosine-NLSs (PY-NLSs). A detailed description of the different mechanisms of cargo recognition follows in the next paragraphs.

The Impβ-Impα heterodimer binds cargoes with cNLSs

The classical import mechanism is mediated by the Impβ-Impα-heterodimer. In human cells, six different Impα homologs exist, all of which bind to cNLSs (see Table 4) [Mason et al., 2009]. cNLSs are composed of one (monopartite) or two (bipartite) stretches of five to seven highly basic amino acids. P**KKKRK**V is a typical monopartite cNLS sequence of the SV40 virus protein [Fontes et al., 2000]. A typical bipartite cNLS is found in nucleoplasmin with a **KR**PAATKKAGQA**KKKK**L sequence [Stewart, 2007]. cNLSs are mainly located in solvent accessible loops to allow binding to Impα in an

Table 4: **Impα homologs and their protein cargoes for which structures are available.** The cNLS containing regions of the cargoes are indicated.

adaptor	cargo	cNLS	reference	pdb id
Impα *S.c.*	MYC	320-328	[Conti and Kuriyan, 2000]	1EE4
Impα *S.c.*	Nucleoplasmin	153-171	[Conti and Kuriyan, 2000]	1EE5
Impα *S.c.*	SV40	127-132	[Conti and Kuriyan, 2000]	1BK6
Impα2	Nucleoplasmin	155-170	[Fontes et al., 2000]	1EJY
Impα2	SV40	126-132	[Fontes et al., 2000]	1EJL
Impα2	RB1	859-878	[Fontes et al., 2003a]	1PJM
Impα2	N1N2	535-555	[Fontes et al., 2003a]	1PJN
Impα2	SV40	119-133	[Fontes et al., 2003b]	1Q1S
Impα2	SV40	119-133	[Fontes et al., 2003b]	1Q1T
Impα2	scramblase1	1-10	[Chen et al., 2005]	1Y2A
Impα2	androgen receptor	621-635	[Cutress et al., 2008]	3BTR
Impα2	CBC	1-19	[Dias et al., 2009]	3FEX
Impα2	Ku80	560-571	[Takeda et al., 2011]	3RZ9
Impα2	Ku70	558-567	[Takeda et al., 2011]	3RZX
Impα2	CLIC	198-207	[Mynott et al., 2011]	3OQS
Impα2	scramblase4	271-283	[Lott et al., 2011]	3Q5U
Impα2	MAL	118-121,151-160	[Hirano and Matsuura, 2011]	3TPM
Impα2	Fen1	352-370	[de Barros et al., 2012]	3UVU
Impα5	PB2	678-759	[Tarendeau et al., 2007]	2JDQ

extended conformation [Dingwall and Laskey, 1991, Vetter et al., 1999a, Dingwall et al., 1982]. Impα consists of two domains, an Importin-β-binding (IBB or αIBB) domain and a C-terminal domain (C-domain) (see Figure 7A). The C-domain consists of 10 armadillo (Arm) repeats which adopt a curved-shaped conformation [Conti and Kuriyan, 2000, Fontes et al., 2000, Süel et al., 2006, Marfori et al., 2011]. At the inner concave groove of this domain, highly conserved residues form two binding sites for cNLSs. The major binding site is located at the Arm repeats 2-4 (see Figure 7A) and the minor binding site is formed by the Arm repeats 6-8 (not shown). Monopartite cNLSs bind primarily to the high-affinity major binding site, while bipartite cNLSs interact with both binding sites in an arrangement antiparallel to the Impα backbone. Being short and simple motifs, cNLSs are widespread in nuclear proteins and generate a massive transport load for the Impβ-Impα heterodimer [Marfori et al., 2011].

In order to form a stable heterodimer, Impβ wraps its N-terminal arch tightly around the αIBB domain of Impα. The αIBB domain consists of a N-terminally extended region (N-extension) followed by a highly basic α-helix of approximately 40 amino acids (see Figure 7A) [Cingolani et al., 1999] (pdb id: 1QGK 1QGR). The N-extension interacts with HEAT-repeats 7-11 and with an acidic intra-repeat loop at HEAT-repeat 8, which is referred to as the 'acidic loop'. The αIBB helix interacts with HEAT-repeats 12-19. The inner surface of Impβ is negatively charged and complementary to the positively charged αIBB domain. The overall shape of Impβ, while bound to the αIBB domain is very compact with N- and C-terminal HEAT-repeats almost in contact with each other.

The Impβ-SPN1 complex binds cargoes with m^3G-cap structures

SPN1 is another adaptor protein that recognizes the m^3G-cap structure of mature uridine-rich ribonucleoproteins (U snRNAs) with its C-terminal m^3G-cap-binding domain [Huber et al., 1998, Huber et al., 2002]. SPN1 binds to Impβ with an IBB domain (sIBB). Similar to αIBB, sIBB consists of an N-extension and an α-helix [Mitrousis et al., 2008, Bhardwaj and Cingolani, 2010] (pdb id: 2P8Q, 2Q5D, 3LWW). However, the contacts between the sIBB helix and Impβ are fewer and weaker [Mitrousis et al., 2008] and surprisingly, the import of U1 snRNP and U5 snRNP is energy and Ran-independent [Huber et al., 2002]. The amino acid sequence of the sIBB N-extension is more similar to the sequence of the nuclear pore protein Nup153 than to the N-extension of αIBB. This suggests a mechanism in which Nup153 might compete with the sIBB for Impβ binding in the nucleus and thus triggers the release of sIBB in a Ran-independent manner. Several crystal structures of Impβ-sIBB domain have been solved [Wohlwend et al., 2007] (pdb id: 2QNA) [Mitrousis et al., 2008, Bhardwaj and Cingolani, 2010]. In most structures, the helical pitch of Impβ is compact and very similar to the αIBB bound state.

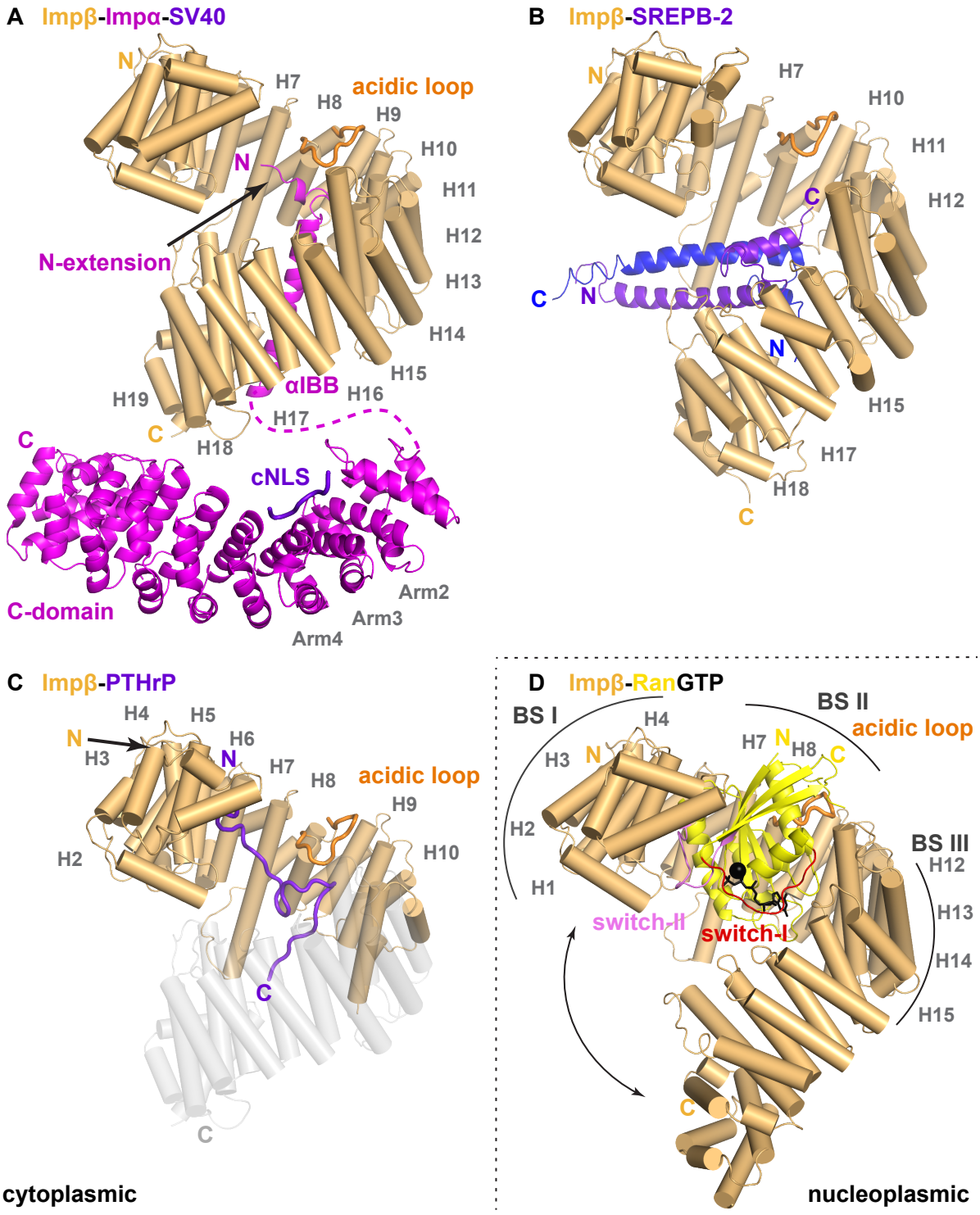

Figure 7: **Structures of Impβ-cargo and of the Impβ-RanGTP complexes.** Impβ is shown as cylindrical helices in light orange, the import cargoes in purpleblue, Impα in magenta and RanGTP in yellow. HEAT-repeats of Impβ responsible for cargo or RanGTP recognition are labeled. (A) Combined model from the Impβ-αIBB and from the Impα-SV40 structures [Cingolani et al., 1999, Fontes et al., 2000] (pdb id: 1QGK, 1EJL). The orientation of the Impα C-domain to Impβ is freely chosen. (B) Impβ-SREBP-2 complex [Lee et al., 2003] (pdb id: 1UKL). (C) Impβ-PTHrP complex [Cingolani et al., 2002] (pdb id: 1M5N). Since a truncated version of Impβ (HEAT-repeat 1-11) was used for the crystallization of this complex, the missing HEAT-repeats are indicated as transparent helices. (D) Impβ-RanGTP structure [Lee et al., 2005] (pdb id: 2BKU). The conformational change in the helical pitch of Impβ upon binding of RanGTP is indicated by an arrow.

Impβ directly binds to cargoes with ncNLSs

Impβ directly binds many cargoes directly via ncNLSs (see Table 1). ncNLS include extended sequences, helical elements and folded domains [Chook and Süel, 2010]. Unlike cNLS, ncNLS do not have shared predictable features. The crystal structures of two of these directly interacting cargoes in complex with Impβ are available. Impβ binds with the B-helices of the C-terminal arch directly to the helix-loop-helix leucine zipper domain of the sterol regulatory element binding protein 2 (SREBP-2) (see Figure 7B) [Lee et al., 2003] (pdb id: 1UKL). In this conformation, Impβ uses the long B-helices of HEAT-repeats 7 and 17 to grasp SREBP-2 like chopsticks. Impβ in complex with SREBP-2 has a more open conformation than that of Impβ in the αIBB-bound state (see Figure 7). The parathyroid hormone-related protein (PTHrP) is bound in a highly extended fashion by the N-terminal half of Impβ, spanning HEAT-repeats 2-10 (see Figure 7C) [Cingolani et al., 2002] (pdb id: 1M5N). Hydrophobic and negatively charged residues on Impβ form polar and hydrophobic contacts to PTHrP. This binding site on Impβ completely overlaps with the RanGTP binding site of Impβ.

Tnp binds cargoes with PY-NLSs

Tnp recognizes extended regions of cargoes with PY-NLSs. PY-NLS are composed of a diverse set of sequences 15 to 30 residues in length that are more complex than cNLS [Truant et al., 1998, Lee et al., 2006, Lange et al., 2008]. Many Tnp cargoes are mRNA-binding proteins with a basic or hydrophobic motif followed by the consensus sequence R/H/KX(2-5)PY (see Figure 8A) [Lee et al., 2006,Stewart, 2007]. Tnp binds the PY-NLS at two binding sites, a high affinity binding site on the B-helices of HEAT-repeats 8-13 and a low affinity binding site on the B-helices of HEAT-repeats 14-18 [Imasaki et al., 2007, Lee et al., 2006, Cansizoglu et al., 2007] (pdb id: 2Z5O, 2Z5N, 2Z5K, 2H4M, 2OT8). The overall conformation of Tnp bound to PY-NLS is rather open with a large helical pitch (see Figure 8A).

Why do some karyopherins use adaptor proteins to bind their cargoes? Adaptor proteins provide a further level of nuclear import control under different cellular conditions. For example, a change in the expression pattern of Impα isoforms triggers the neural differentiation of mouse embryonic stem cells [Yasuhara et al., 2007]. In contrast, Ran-dependent nucleocytoplasmic transport is very sensitive to a change in the expression level of the karyopherins themself [Riddick and Macara, 2007]. Thus, an increase in Impβ expression inhibits nuclear import, since the strong binding of Impβ to RanGTP depletes the RanGTP gradient [Riddick and Macara, 2007]. On the other hand, the advantage of a direct association of many cargoes to importins is that binding is faster and leads to a higher nuclear accumulation. To date, detailed molecular knowledge of the binding mode

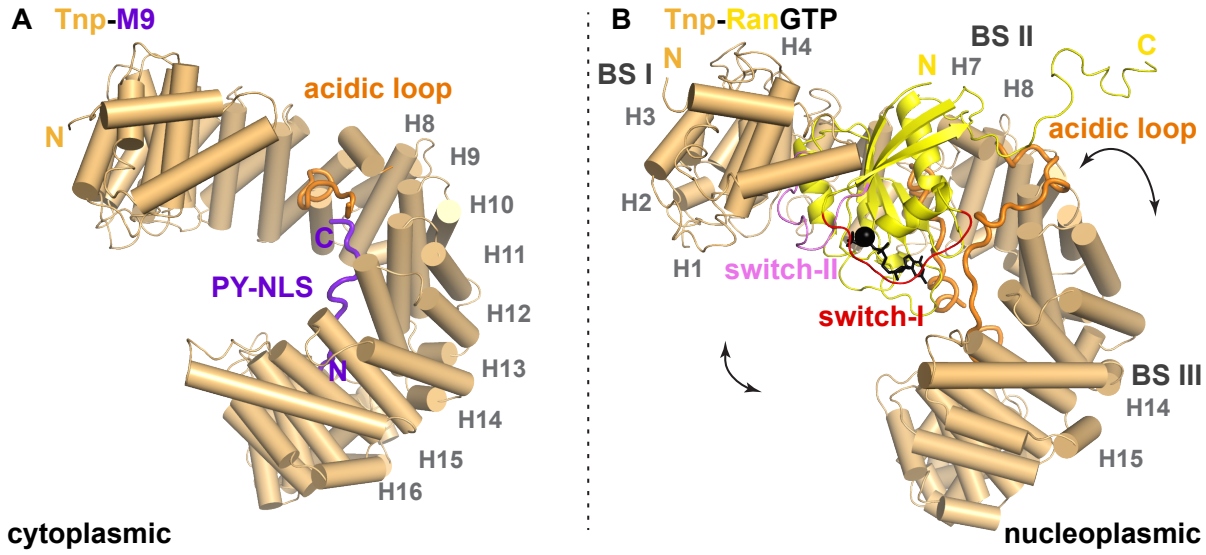

Figure 8: **Structures of the cytosolic Tnp-M9 and nuclear Tnp-RanGTP complexes** Tnp is shown as cylindrical helices in light orange. For both complexes HEAT-repeats of Tnp responsible for cargo or RanGTP recognition are labeled. In (A) the cytoplasmic state of Tnp bound to the PY-NLS of the protein M9 (purpleblue) is shown [Lee et al., 2006] (pdb id: 2H4M). (B) shows the nucleoplasmic state of Tnp bound to RanGTP (yellow) [Chook and Blobel, 1999] (pdb id: 1QBK). The conformational changes in the 'acidic loop' as well as the opening of the helical pitch of Tnp after binding of RanGTP are indicated by arrows.

of import cargoes is only available for the importins Impβ and Tnp. However, many importins bind more diverse sequences or even structural motifs, which are very difficult to predict due to their missing or more complex shared features [Chook and Süel, 2010].

2.3.4 RanGTP binding to importins and cargo release

In the nucleus RanGTP associates to importins and thereby triggers the release of the bound cargo. Typically, RanGTP is recognized by the B-helices of the N-terminal arch of karyopherins.

RanGTP binding to Impβ and cargo release

Impβ binds RanGTP at three binding sites, with a dissociation constant of approximately 250 pM (see Figure 7D) [Görlich et al., 1996, Hahn and Schlenstedt, 2011]. The first binding site (BS I) is composed of HEAT-repeats 1-4 and involves the switch-II of RanGTP [Vetter et al., 1999a, Lee et al., 2005] (pdb id: 1IBR, 2BKU). At the second binding site (BS II), HEAT-repeats 7 and 8 and the 'acidic loop' interact with RanGTP at the same position at which the C-terminal extension of Ran binds to the G-domain in the RanGDP state (see section 2.3.1 and Figure 3). The third binding site (BS III) is formed by switch-I of RanGTP and by HEAT-repeats 12-15 at the C-terminal arch of Impβ [Lee et al., 2005]. Upon binding of RanGTP, the superhelical conformation of Impβ opens to a much greater helical pitch compared to the cargo-bound cytoplasmic state (see Figure 7). Two main

mechanisms are responsible for cargo release. Mutually exclusive binding together with an allosteric mechanism result in the release of the cargo from Impβ [Lee et al., 2005, Conti et al., 2006, Stewart, 2007]. Overlapping binding interfaces prevent the simultaneous binding of cargo and RanGTP, as in the case of αIBB and PTHrP (see Figure 7). In particular, the 'acidic loop' of Impβ plays a key role in cargo binding and release, as this loop is involved in recognition of both cargo and RanGTP. The allosteric binding of RanGTP to Impβ induces a dramatic conformational change, which locks Impβ into a cargo-incompatible conformation. Since the binding affinity of Impβ for its import cargoes falls in the low nanomolar range (around 10 nM) it is likely that RanGTP promotes cargo dissociation in a stepwise manner, rather than in a single step [Stewart, 2007].

After the release of the αIBB domain from Impβ, the cargo with the cNLS has to be released from its adaptor Impα. αIBB has a cluster of basic residues that resembles a cNLS. After the dissociation from Impβ, αIBB can bind *in cis* to the NLS-binding site at the C-domain of Impα [Kobe, 1999, Catimel et al., 2001, Matsuura et al., 2003, Matsuura and Stewart, 2004] (pdb id: 1IAL, 1IQ1, 3UN0). Thus, the αIBB domain can trigger the release of the cNLS and has an autoinhibitory effect. Nup50 can also actively displace the cNLS by binding *in trans* to Impα at two distinct sites. The lower affinity binding site overlaps with the NLS-binding site [Gilchrist et al., 2002, Matsuura et al., 2003, Matsuura and Stewart, 2005] (pdb id: 2C1M, 2C1T).

RanGTP binding to Tnp and cargo release

Tnp contacts RanGTP in a manner similar to Impβ (see Figure 8B) [Chook and Blobel, 1999] (pdb id: 1QBK). Additionally, the 'acidic loop' (residue 311-373) from Tnp, which is displaced when a cargo is bound, forms extensive interactions with RanGTP as well as the C-terminal arch of Tnp. The 'acidic loop' triggers the release of the cargo by occupying the NLS-cargo binding site [Chook and Blobel, 1999, Chook et al., 2002]. Upon binding of RanGTP the conformation of Tnp changes slightly to accommodate RanGTP in the inner surface of the superhelix (see Figure 8). Unlike Impβ, Tnp couples the cargo binding and release with conformational changes in the 'acidic loop'.

Several other importins, such as Imp4, Imp7, Imp8, Imp9 and Imp11, are predicted to have loop insertions similar to Impβ or Tnp in the central HEAT-repeats, indicating that these karyopherins might employ analog mechanisms of cargo release [Lee et al., 2006]. However, detailed structural knowledge about these importins is not yet available.

2.3.5 Cargo recognition by exportins

In the case of exportins, the loading of cargo proteins as well as RNAs is coupled to RanGTP binding (reviewed in [Cook and Conti, 2010, Güttler and Görlich, 2011]). The

cooperativity of this process can be achieved via direct interactions between cargo and RanGTP or via a conformational change of the exportin induced by RanGTP.

CAS exports Impα from the nucleus

After the import of cargoes in a trimeric complex with Impβ, Impα is released in the nucleus and is actively transported back into the cytoplasm by the exportin CAS [Kutay et al., 1997]. Impα is CAS's only cargo. To avoid the rebinding of NLS-containing cargoes to Impα in the nucleus and transport back into the cytoplasm, only cargo-free Impα can be recycled by CAS. To achieve this selectivity, CAS associates with the autoinhibited state of Impα mainly with electrostatic interactions (see Figure 9B) [Matsuura and Stewart, 2004] (pdb id: 1WA5). On one side, HEAT-repeats 2-4 of CAS bind to the N-extension of the αIBB domain. On the other side, HEAT-repeats 5-7 contact the C-terminal region of the αIBB domain. CAS binds RanGTP in a manner similar to that of importins. In addition, a long intra-loop of HEAT-repeat 19 (intra-loop 19) contacts the switch-I of RanGTP. The binding affinity of CAS for RanGTP strongly increases due to the simultaneous binding of Impα [Kutay et al., 1997]. The cooperative binding of RanGTP and Impα to CAS is promoted by the intra-loop 19 of CAS, which extends back in to the inner surface of CAS to contact both proteins at the same time. In addition to the intra-loop 19, RanGTP

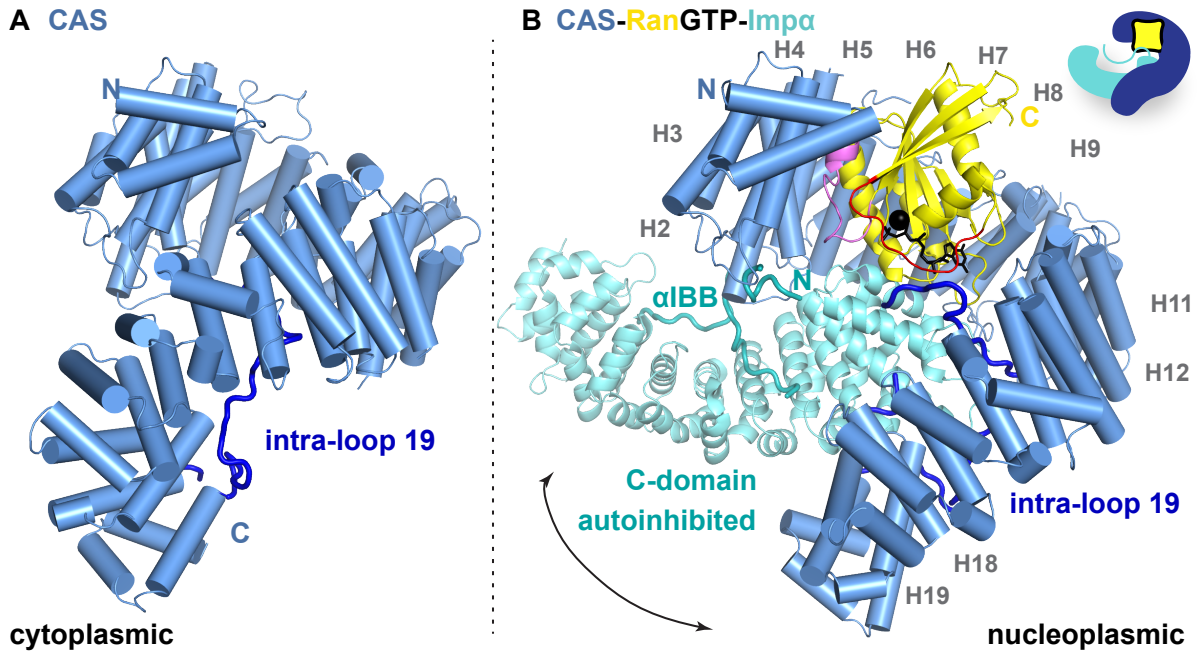

Figure 9: **Structures of free CAS and of the CAS-RanGTP-Impα complex.** CAS is shown as cylindrical helices in light blue. (A) Cytoplasmic, free state of CAS [Cook et al., 2005] (pdb id: 1Z3H). (B) CAS bound to RanGTP (yellow) and to the cargo Impα (cyan) [Matsuura and Stewart, 2004] (pdb id: 1WA5). The αIBB domain in the autoinhibited state is bound to the NLS binding site of the C-domain of Impα. HEAT-repeats of CAS responsible for cargo recognition are labeled. The conformational change that results in the opening of the helical pitch of CAS after binding of RanGTP is indicated by an arrow.

directly contacts the negatively charged C-terminal part of Impα. Instead of binding to a short extended sequence, CAS, together with RanGTP, recognizes Impα in its entirety with direct contacts to the αIBB domain and the C-domain. While the cytoplasmic, free state of CAS is tightly closed by its C-terminal arch docking to the N-terminal arch, the binding of RanGTP induces an opening of the superhelix of CAS that allows Impα association (see Figure 9) [Cook et al., 2005] (pdb id: 1Z3H).

Crm1 binds cargoes with nuclear export signals (NESs)

Crm1 recognizes over 300 different cargoes directly or via adaptor proteins, including the 40S and 60S ribosomal subunits (see Table 1) [Ho et al., 2000, Moy and Silver, 2002, Xu et al., 2012]. Usually, Crm1 recognizes short leucin-rich nuclear export signals (NESs) [Güttler et al., 2010]. NESs are composed of five hydrophobic residues with a consensus sequence of $x\Phi^0x_2\Phi^1x_3\Phi^2x_{2-3}\Phi^3x\Phi^4$ (where Φ is a hydrophobic residue) which adopt an extended or helical conformation. Crm1 binds NESs with low affinity on the outer convex surface with a hydrophobic cleft formed by the A helices of HEAT-repeat 11-12 (see Figure 10) [Monecke et al., 2009, Güttler et al., 2010]. Detailed information is available on the recognition of SPN1 by Crm1 (see Figure 10) [Monecke et al., 2009] (pdb id: 3GJX). SPN1 is recycled back to the cytoplasm by Crm1 after its release in the nucleus from Impβ and the cargo U snRNPs. Besides the typical NES located in its N-terminal region, SPN1 can interact with Crm1 with the m^3G-cap-binding domain and its C-terminal-most part through polar contacts. Since the same residues that bind the m^3G-cap structure

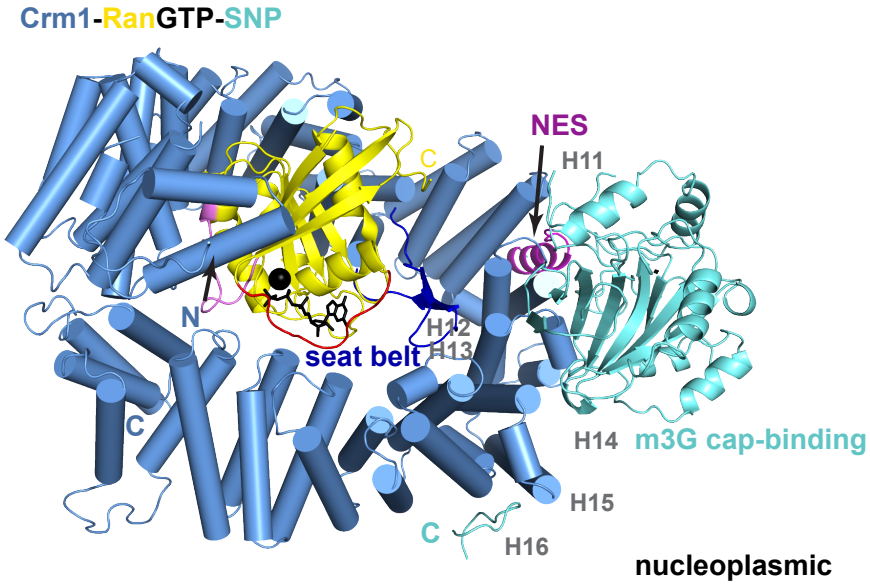

Figure 10: **Structure of the Crm1-RanGTP-SPN1 complex** [Monecke et al., 2009] (pdb id: 3GJX). Crm1 is shown as cylindrical helices in light blue. HEAT-repeats of Crm1 responsible for cargo recognition are labeled. The m^3G-cap-binding domain of SPN1 is colored in cyan, while the NES of SPN1 is shown in purple.

are involved in binding to HEAT-repeats 12-14 of Crm1, Crm1 selectively recognizes only cargo-free SPN1. The C-terminal part of SPN1 interacts with HEAT-repeats 15-16 of Crm1. RanGTP almost completely occupies the inner concave surface of Crm1 that is usually used for cargo binding. Crm1 contacts RanGTP in a similar manner to other karyopherins. However, the Ran BS III is formed by the C-terminal HEAT-repeats 17 and 19 of Crm1, instead of HEAT-repeats 12-15 as in the case of Impβ. The intra-loop of HEAT-repeat 9 forms a β-hairpin named 'seat belt'. The 'seat belt' reaches through the inner hole of Crm1 to contact HEAT-repeats 11-12 on one side and the switch-I of RanGTP on the other side. Since the cargoes bind on the outer surface of Crm1, no direct interactions between RanGTP and the cargo take place. This mode of cargo binding at the outer surface could explain how large molecules such as the ribosomal subunits can be transported by Crm1. Similar to Impβ, Tnp and CAS, a loop insertion again contacts the middle part of the karyopherin and senses if RanGTP is bound. Since HEAT-repeat 21 directly contacts HEAT-repeats 2 and 5, Crm1 adopts a completely closed, toroidal conformation. Until now, no structural information about the cytosolic, free state of Crm1 has been available and it is therefore unknown whether conformational changes occur upon binding of RanGTP by Crm1.

Expt exports tRNAs from the nucleus

RNAs are transcribed and processed in the nucleus and only correctly processed RNAs are exported to the cytoplasm. All RNAs, with exception of mRNA, are transported by karyopherins. However, since the nucleotide sequence of the different RNAs such as tRNAs or pre-miRNAs can vary strongly their recognition must therefore be sequence-independent. Expt transports processed tRNAs by clamping around the tRNA with its N- and C-terminal arch (see Figure 11B) [Cook et al., 2009] (pdb id: 3ICQ). tRNAs fold into an L-shaped structure with an acceptor arm that contains the amino-acid attachment site and an anticodon arm that base pairs with the corresponding codon in the mRNA [Cook et al., 2009]. A groove of Expt formed by the inter-loops of HEAT-repeats 4-7 buries the 3' CCA end of the tRNA acceptor arm, which is post-transcriptionally added. The post-transcriptionally cleaved 5' end is buried between HEAT-repeats 6-8 of Expt and RanGTP. The C-terminal arch of Expt (HEAT-repeats 8-18) is involved in binding the acceptor arm of the tRNA. Expt directly probes the post-transcriptionally modified regions and is therefore able to bind mature tRNAs 5-10 times more strongly than unmodified tRNAs [Lipowsky et al., 1999]. By interacting mainly with the phospho-ribose backbone, Expt recognizes the unique structure and the charge of the tRNAs in a sequence-independent manner. Expt interacts with RanGTP in a manner similar to that of other karyopherins. As in the case of CAS, RanGTP directly contacts the cargo via charged interactions and induces a conformational change of Expt. In contrast to CAS, Expt shows an open

conformation in its free state that closes upon binding of RanGTP (see Figure 11) [Cook et al., 2009] (pdb id: 3IBV).

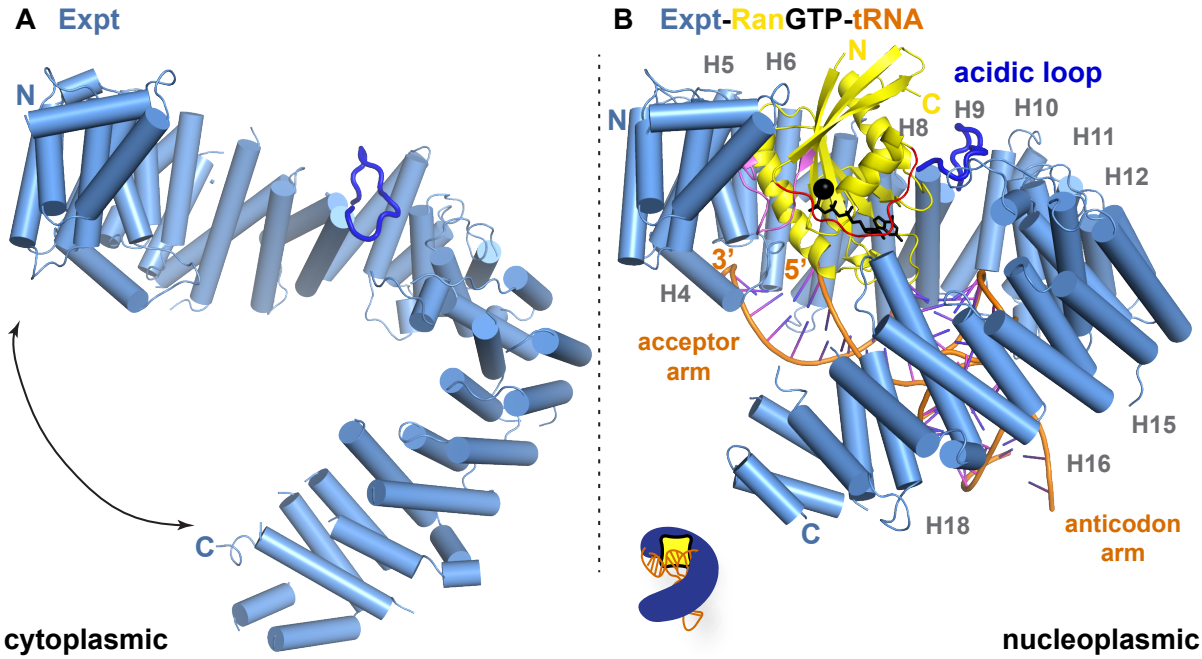

Figure 11: **Structures of free Expt and of the Expt-RanGTP-tRNA complex.** Expt is shown as cylindrical helices in light blue. (A) Cytoplasmic state of Expt [Cook et al., 2009] (pdb id: 3IBV). The conformational change that opens the helical pitch of Expt after release of RanGTP is indicated by an arrow. (B) Expt is bound to RanGTP (yellow) and to the tRNA. The tRNA is illustrated as ribbon model with the phospho-ribose backbone in orange and the bases shown as purple sticks [Cook et al., 2009] (pdb id: 3ICQ). HEAT-repeats of Expt involved in cargo recognition are labeled.

Exp5 exports miRNAs from the nucleus

Typically, pre-miRNAs consist of a stem loop of approximately 70 nucleotides with a hairpin loop and a 2 nucleotides 3' overhang. In the export complex with a pre-miRNA, Exp5 adopts a U-shaped conformation. Exp5 sandwiches the pre-miRNA stem between its two arches, while the hairpin loop faces the open end of the 'U' (see Figure 12) [Okada et al., 2009] (pdb id: 3A6P). This conformation explains why the length of the stem loop can be variable, but must be more than 14 base pairs for efficient binding to occur [Yi et al., 2003, Zeng and Cullen, 2004]. The 2 nucleotide overhang at the 3' end fits perfectly into a tunnel located at the sharp turn of the 'U' at HEAT-repeat 12-15. The main contacts between the pre-miRNA and Exp5 are between the negatively charged phospho-ribose backbone and positively charged residues of Exp5 at the central and C-terminal region that allows a sequence unspecific binding. As in the case of CAS and Expt, RanGTP directly contacts the cargo. Similar to other karyopherins, Exp5 recognizes RanGTP with the BS I and II. However, the contacts to RanGTP at BS III, formed by HEAT-repeats 17

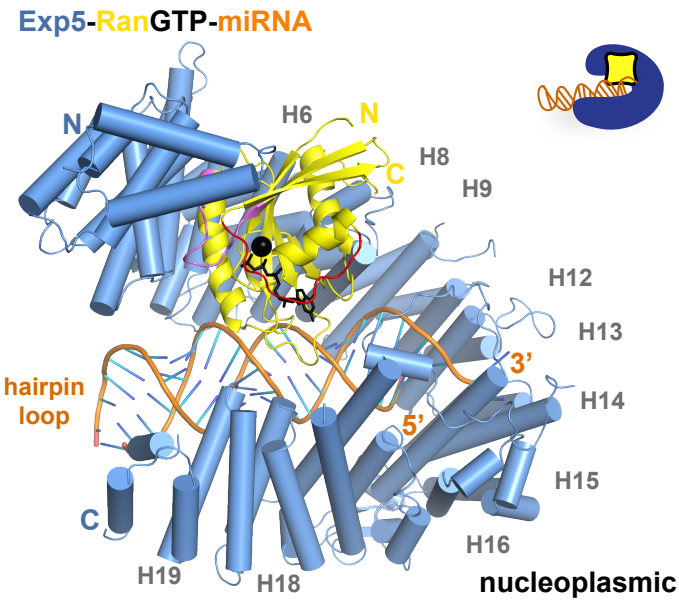

Figure 12: **Structure of the nuclear Exp5-miRNA-RanGTP complex.** [Okada et al., 2009] (pdb id: 3A6P). Exp5 is shown as cylindrical helices in light blue and RanGTP is colored in yellow. HEAT-repeats of Exp5 responsible for cargo recognition are labeled. The tRNA is shown with the phospho-ribose backbone in orange and the bases shown as purple sticks.

and 19, are fewer than compared to other karyopherins with no direct contact to switch-I of RanGTP. This suggests that Exp5 could open its C-terminal region upon binding of different cargoes, such as pre-miRNAs with bulky protrusions, or the 60S pre-ribosomal subunit (see table 3) [Okada et al., 2009, Wild et al., 2010]. Structural information on the cytosolic, free state of Exp5 is not currently available.

2.3.6 Cargo release by exportins

Export cargo release in the cytosol is coupled to RanGTP hydrolysis. As mentioned in section 2.3.1, the first step in cargo release is the extraction of RanGTP from the export complex by RanBP1 (or RanBP2), followed by the hydrolysis of the GTP bound to Ran (reviewed in [Güttler and Görlich, 2011]). The C-terminal extension of Ran, which is not involved in binding to the karyopherins, appears to extend into the solvent and could provide an initial attachment site for RanBP1 (or RanBP2) [Vetter et al., 1999b, Güttler and Görlich, 2011]. RanGTP and RanBP1 (or RanBP2) form a tight complex with the C-terminal extension of Ran that clasps RanBP1 [Vetter et al., 1999a, Koyama and Matsuura, 2010] (pdb id: 1RRP, 3M1I). In most previous studies, RanBP1 clashed with the exportin which destabilizes the exportin-RanGTP interaction dramatically. Recently, the structure of a Crm1-RanGTP-RanBP1 disassembly intermediate was solved (see Figure 13A) [Koyama and Matsuura, 2010] (pdb id: 3M1I). The structure shows that RanBP1 binding to Crm1-RanGTP induces a conformational change in the 'seat belt'. The 'seat belt' contacts the B helices of HEAT-repeats 11-12 of Crm1. The A helices of these

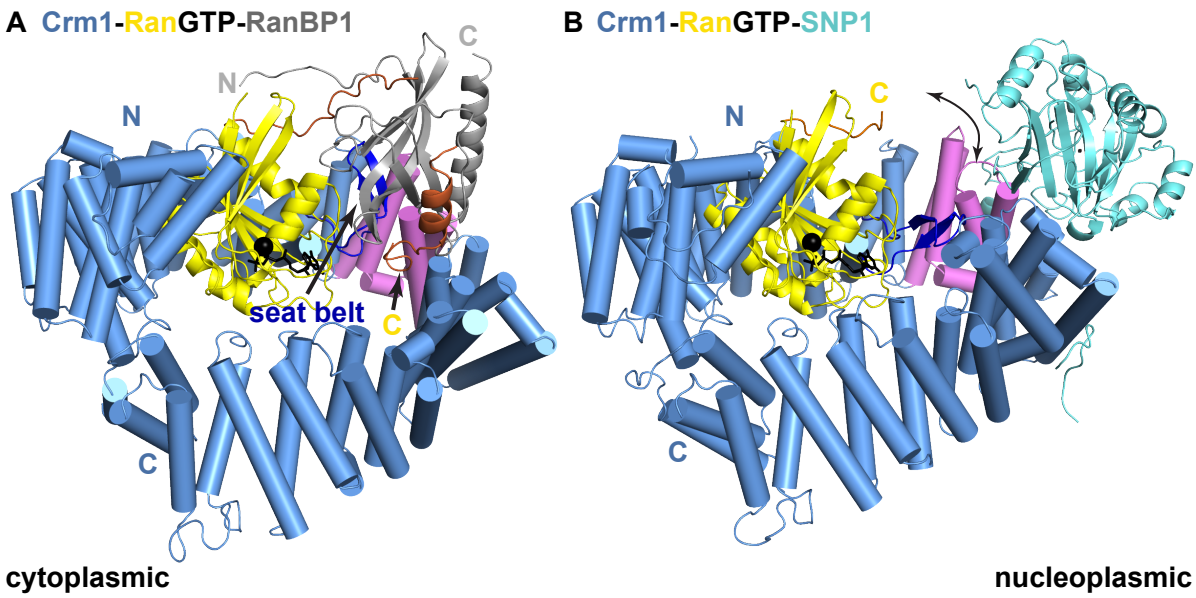

Figure 13: **Structures of the Crm1-RanGTP-RanBP1 disassembly intermediate and the nuclear Crm1-RanGTP-SPN1 complex** [Koyama and Matsuura, 2010, Monecke et al., 2009] (pdb id: 3M1I, 3GJX). Crm1 is shown as cylindrical helices in light blue with the binding cleft formed by HEAT-repeat 11-12 in purple. RanGTP is colored in yellow and the RanGTP C-terminal extension is shown in orange. In (A) the binding of RanBP1 (gray) to the Crm1-RanGTP complex is illustrated. In (B) Crm1 bound to RanGTP and the cargo SPN1 (cyan) is shown. The conformational change of the 'seat belt' and the NES binding cleft are indicated by an arrow.

HEAT-repeats form the binding cleft for NESs. Binding of the 'seat belt' at the inner surface of Crm1 causes a rearrangement that leads to a closure of the binding cleft. This allosteric mechanism strongly accelerates release of both the cargo and RanGTP from Crm1.

In addition to the RanBPs, the exportins themselves contribute to the disassembly of the export complexes. The exportins are under tension while bound to RanGTP and snap into low-energy states as soon as RanGTP is released from the complex [Matsuura and Stewart, 2004, Monecke et al., 2009]. In the case of CAS, the rebinding of the cargo in the cytoplasm is strongly inhibited by the very tight ring-like conformation which masks the cargo-binding surface [Cook et al., 2005]. Interestingly, for Expt the open cytoplasmic conformation also distorts the binding surface for the cargoes by a displacement of the HEAT-repeats that form this surface [Cook et al., 2009]. RanGTP association in the nucleus is necessary to induce a conformational change of Expt that exposes the binding surface for the cargoes.

2.3.7 Flexibility of karyopherins

As mentioned in section 2.3.2, karyopherins have an intrinsic flexibility, which is necessary for their function. Karyopherins often adopt different conformations in the cytoplas-

mic and nucleoplasmic states. The binding of RanGTP to the karyopherins triggers the most dramatic conformational changes. The superhelical structure of karyopherins can be thought of as a spring. Small changes in successive HEAT-repeats and large movements in hinge regions result in prominent changes in the overall conformation and in the helical pitch. This flexibility enables karyopherins to bind to a wide range of different cargoes by an induced-fit mechanism. Possibly, karyopherins bind to their cargoes by gradually wrapping around them [Forwood et al., 2010].

Most likely, free Impβ would adopt different open conformations in solution [Fukuhara et al., 2004] [Forwood et al., 2010]. Upon binding to a cargo such as the αIBB domain or SREBP-2, the superhelical pitch of Impβ is reduced. The extent to which the superhelical conformation of Impβ is compacted appears to depend on the size and shape of the cargo. In the nucleus, RanGTP binding to Impβ increases the helical pitch and disrupts the cargo binding surface on Impβ. Interestingly, Impβ, Tnp and CAS adopt an open conformation to accommodate RanGTP, while RanGTP closes the conformation of Expt.

2.3.8 Gating through the NPC channel

Karyopherins translocate through the NPC channel by binding to the FG-repeat Nups (see Figure 14). The mechanism triggering the gating through the channel is not yet

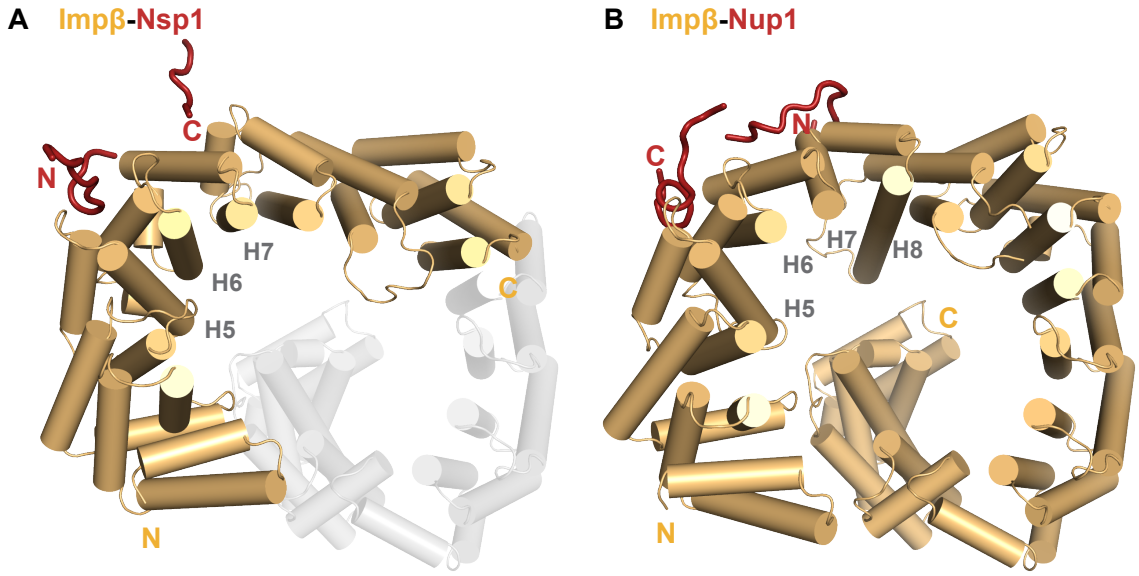

Figure 14: **Structures of the Impβ-Nsp1p and Impβ-Nup1 complexes.** Impβ is shown as cylindrical helices in light orange. HEAT-repeats of Impβ that recognize FG-repeats are labeled. In (A) the binding of the two FG-repeats of Nsp1 (red) to Impβ is illustrated [Bayliss et al., 2000] (pdb id: 1F59). Because a truncated version of Impβ (HEAT-repeat 1-11) was used for the crystallization of this complex, the missing HEAT-repeats are indicated as transparent helices. In (B) Impβ bound to the FG-repeat region of Nup1 (red) is shown [Liu and Stewart, 2005] (pdb id: 2BPT).

known. The interaction affinity between karyopherins and the FG-repeat Nups is in the µM range and is therefore rather transient [Shulga and Goldfarb, 2003]. The structures of Impβ in complex with two different FG-repeat Nups, Nsp1p and Nup1, are available. The FG-repeats are bound to the outer surface of Impβ at HEAT-repeats 5-8 (see Figure 14) [Bayliss et al., 2000, Bayliss et al., 2002, Liu and Stewart, 2005] (pdb id: 1F59, 1O6P, 1O6O, 2BPT). The conformation of Impβ bound to Nup1 is very similar to the conformation of Impβ in the Impβ-αIBB structure [Cingolani et al., 1999], suggesting that the binding of Nup1 does not change the conformation of Impβ while translocating through the NPC channel [Forwood et al., 2010]. Impβ is the only karyopherin for which detailed information of the interaction with the FG-repeat Nups is available, however all other karyopherins are thought to cross the NPC via similar interactions.

2.4 The bidirectional nuclear transport receptor Imp13

Human Imp13 was first described by the group of Dirk Görlich as a bidirectional karyopherin [Mingot et al., 2001]. Imp13 is a predominant import factor mediating the nuclear import of several cargoes including the Ubiquitin-conjugating enzyme 9 (Ubc9), the heterodimer Mago-Y14 and the ribosomal protein L5 (rPL5) (see Table 2 and Figure 15) [Mingot et al., 2001]. In addition, Imp13 recognizes heterodimers of transcription factors containing a histone fold motif (HFM) as NF-YB/NF-YC, CHRAC15/CHRAC17, p12/CHRAC17 and NC2α/NC2β and imports them into the nucleus [Kahle et al., 2005, Walker et al., 2009, Kahle et al., 2009]. The dimer formation of these proteins is necessary for the binding to Imp13, suggesting that the binding surface for Imp13 lies across the HFM of both subunits. Mutations of conserved basic residues in the HFM show a loss of binding to Imp13 and increasing accumulation of CHRAC15/CHRAC17 and p12/CHRAC17 in the cytoplasm [Walker et al., 2009]. Furthermore, Imp13 can bind single cargoes that contain a homeodomain such as Pax6, Pax3 and Crx, and facilitate the import of these proteins into the nucleus [Ploski et al., 2004]. Myopodin was also identified as an Imp13 import cargo and localizes *in vivo* to both the cytoplasm and the nucleus [Liang et al., 2008]. A knockdown of Imp13 in murine cells prevented the nuclear localization of myopodin. Some Imp13 cargoes are also imported by other karyopherins. For example, Imp13 as well as Imp7 and Impβ-Impα facilitate the import of the glucocorticoid receptor (GR) into the nucleus. However, the nuclear localization of GR was strongly affected by decreasing Imp13 expression in HeLa and epithelial cells suggesting that Imp13 might be the major transport receptor for GR [Tao et al., 2006].

Imp13 was also found to be an export factor for the eukaryotic initiaton factor 1A (eIF1A) [Mingot et al., 2001].

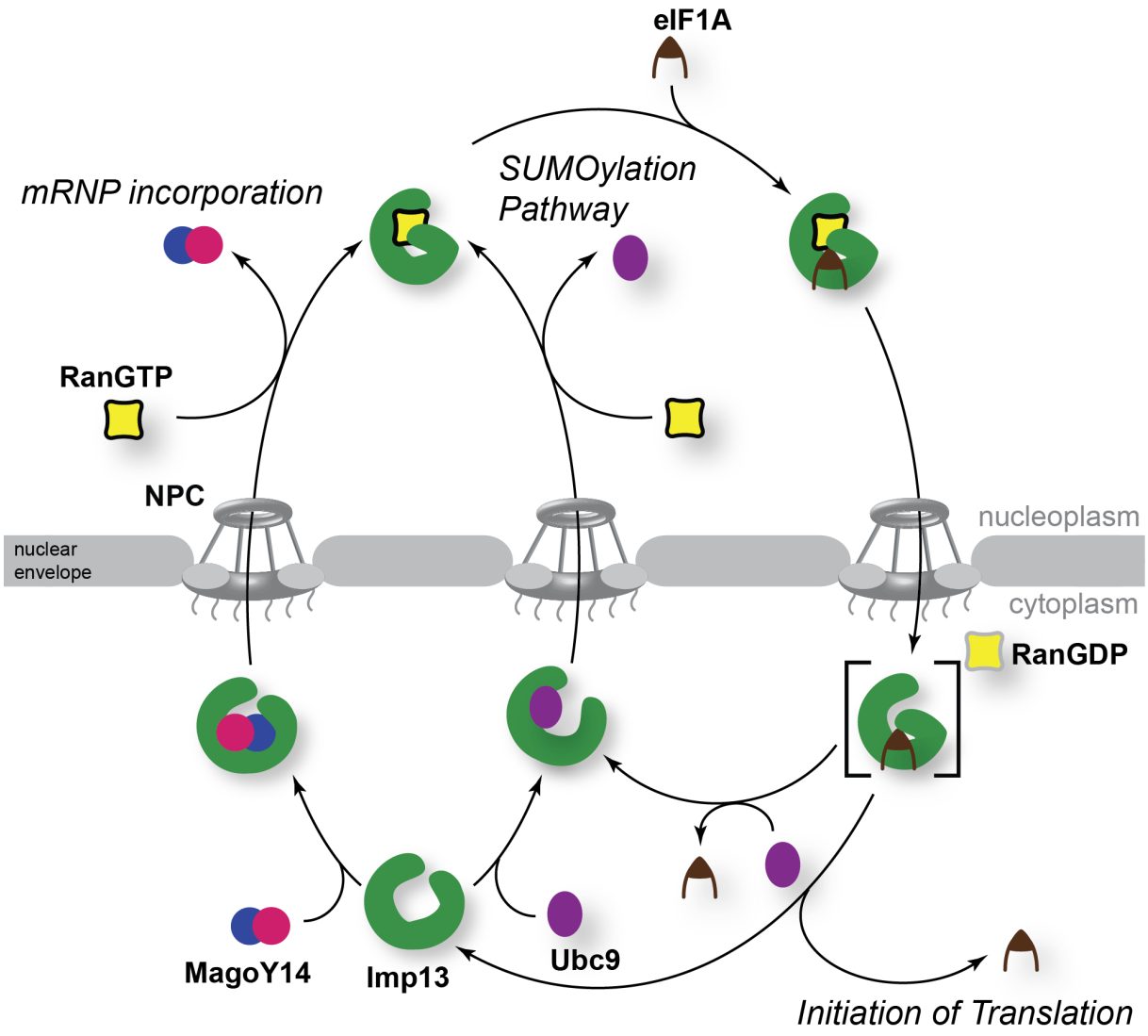

Figure 15: **Schematic illustration of the import and export pathway of Imp13.**

2.4.1 Biological function and expression of Imp13

Imp13 is highly expressed in mammalian fetal lung, brain and heart [Liang et al., 2008]. In mouse germ cells, Imp13 is expressed in a stage-specific manner with elevated expression levels in the early phase of meiosis [Yamaguchi et al., 2006]. In addition, in the fetal lung of rats, Imp13 shows a developmentally and hormonally modulated expression pattern [Zhang et al., 2000]. Mouse germ cells express two isoforms of Imp13, of which the shorter isoform, composed of the C-terminal arch, is expressed only in adult testis. Homozygous mutation of some Imp13 alleles in *Drosophila melanogaster* (*D. melanogaster*) are lethal [Giagtzoglou et al., 2009]. Imp13 affects neurotransmitter release at the larval neuromuscular junction as well as muscle growth and formation of the subsynaptic reticulum [Giagtzoglou et al., 2009].

2.4.2 Imp13 import cargo Mago-Y14

The heterodimer Mago-Y14 is a core component of the exon junction complex (EJC) together with eIF4AIII and Barentsz (Btz), [Bono and Gehring, 2011]. After splicing of the mRNA in the nucleus the EJC is assembled upstream of exon-exon junctions and thus preserves the positional information of introns after the introns have been excised [Le Hir et al., 2000]. The EJC is then exported from the nucleus together with the mRNP. In the cytoplasm, the complex is involved in a broad range of processes that range from nonsense-mediated mRNA decay (NMD) in humans to the localization of mRNAs in *Drosophila* [Hachet and Ephrussi, 2004, Palacios et al., 2004]. After release of the EJC from the mRNA by the translating ribosome and the disassembly of the EJC by the cytoplasmic protein Pym, Mago-Y14 is reimported into the nucleus by Imp13 [Gehring et al., 2009, Mingot et al., 2001].

2.4.3 Imp13 import cargo Ubc9

Ubc9 is the E2-conjugating enzyme of the sumoylation pathway [Melchior, 2000, Johnson, 2004]. Sumoylation is a post-translational modification with many features similar to the ubiquitination process. While ubiquitination commonly marks proteins for degradation, the SUMO modification alters protein-protein interactions. Proteins modified by SUMO are located predominantly in the nucleus [Rodriguez et al., 2001]. SUMO is covalently linked via an isopeptide bond to the target protein. The sumoylation reaction is catalyzed by three different enzymes (see Figure 16). 1.) The first enzyme, the E1-activating enzyme, is a heterodimer composed of the two subunits AosI and Uba2. The E1-activating enzyme forms a thioester bond between the C-terminal carboxy group of SUMO and its catalytic cysteine. 2.) SUMO is then transferred to the catalytic cysteine of the E2-conjugating enzyme Ubc9. Ubc9 is the only enzyme responsible for this step. 3.) In most cases, multiple E3 ligases are required to catalyze the last step which is the formation of the isopeptide bond between the ε-amino group of a lysine on the target protein and the C-terminal carboxy group of SUMO.

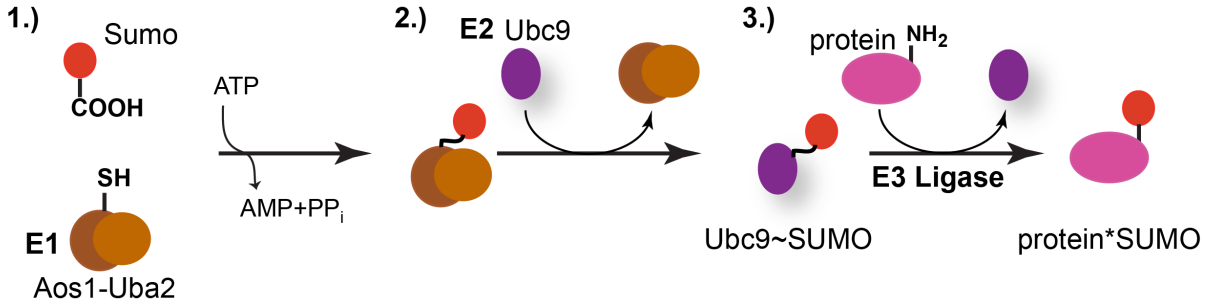

Figure 16: **Schematic illustration of the sumyolation pathway.**

2.4.4 Imp13 export cargo eIF1A

eIF1A is an essential factor for translation initiation in eukaryotes. It is necessary for the assembly of the translation pre-initiation complex (PIC), which is composed of the small ribosomal subunit and the methionyl initiator tRNA with eIF2 [Aitken and Lorsch, 2012, Jackson et al., 2010]. Together with eIF1, eIF1A promotes the scanning for the AUG start codon of the mRNA by inducing an open conformation of the 40S subunit. As soon as the start codon is reached, eIF1 dissociates and the eIF1A-40S subunit complex switches to a closed conformation, allowing binding of the 60S ribosomal subunit. Due to its small size (17 kDa), eIF1A is able to passively diffuse through the NPCs. It was hypothesized that the active export of eIF1A mediated by Imp13 depletes eIF1A from the nucleus [Mingot et al., 2001].

3 Objectives and expected output

When I started my PhD in June 2008, detailed knowledge based on structural information of the importins Impβ, Tnp and the exportin CAS was available. However, only limited information existed regarding how other karyopherins work. At the time, only two karyopherins had been identified as bidirectional transport factors, Msn5 and Imp13 [Yoshida and Blobel, 2001, Mingot et al., 2001] and no structural information for Imp13 was available. My work addressed two main questions:

3.1 How does the import mechanism of Imp13 work?

One major goal in this study was to understand the import mechanism employed by Imp13. It was unclear how Imp13 imports cargoes lacking a functional NLS. I wanted to understand the recognition of the import cargoes Mago-Y14 and Ubc9 by Imp13 and how these cargoes are released in the nucleus upon binding of RanGTP to Imp13. A combined structural and biochemical analysis on the Imp13-Mago-Y14 and Imp13-Ubc9 complexes would give detailed information on the interaction region between the karyopherin and the cargoes. Besides, the comparison of the Imp13-Mago-Y14 and Imp13-Ubc9 structure would give insights of how Imp13 distinguishes between different import cargoes. The completion of the structural data with biochemical and biophysical experiments would show whether Imp13 exhibits preferences for one or the other cargo. The comparison of the import complexes to the Imp13-RanGTP complex complemented with biochemical data would explain how both import cargoes are released in the nucleus.

3.2 How can Imp13 work as a bidirectional transport factor?

The second goal was to understand the export mechanism of Imp13 and how it can work as a bidirectional transport factor. The only export cargo identified for Imp13 is eIF1A [Mingot et al., 2001]. It was not clear how eIF1A is recognized by Imp13 and how this recognition is coupled to RanGTP binding. In addition, it was unclear how eIF1A is released in the cytoplasm after the dissociation of RanGTP from Imp13. The approach to answer this questions was to structurally and biochemically investigate the Imp13-RanGTP-eIF1A complex to obtain detailed information of the interaction region of Imp13 and eIF1A and reveal whether a cooperative binding of eIF1A and RanGTP to Imp13 is taking place. The comparison of the export complex to the free Imp13 should give profound insights into the release mechanism of the export pathway of Imp13. In addition, it was unclear why Imp13 can act as a bidirectional transport factor, while almost all other karyopherins are only unidirectional. The comparison of the import complexes of Imp13 to the export complex should be a key step to answer this question.

4 Results and discussion

One major challenge in biology is to understand which components interact at which time point in the cell and how their interaction is mediated. In particular, eukaryotic cells have to tackle the task of distinguishing between nucleoplasm and cytoplasm with very precise timing to permit necessary shifts in the localization of thousands of various molecules, while preventing the transport of the wrong molecules. RanGTP plays a key role in regulating nucleocytoplasmic transport, yet it acts on importins and exportins in opposite ways. Imp13 is a karyopherin that can function in both import and export of cargoes. The study of the transport of different import cargoes such as Mago-Y14 and Ubc9 together with the export mechanism of the only export cargo eIF1A by structural, biochemical and cell biology methods allows deep insights in the nucleocytoplasmic transport mediated by Imp13 (see Table 5). Furthermore, I aimed to understand the bidirectional regulation of Imp13 by RanGTP.

Table 5: **Imp13 complexes studied in this thesis.** Listed are the cytoplasmic Imp13 import cargo complexes and the free Imp13 state and the nuclear Imp13-RanGTP complex as well as the export complex. The resolution of the crystal structures and the pdb ids are listed.

complexes	**localization**	**resolution**	**pdb id**
Imp13-Mago-Y14	cytoplasmic	3.16 Å	2X1G
Imp13-Ubc9	cytoplasmic	2.8 Å	2XWU
free Imp13	cytoplasmic	3.0 Å	unpublished
Imp13-RanGTP	nucleoplasmic	2.8 Å	2X19
Imp13-RanGTP-eIF1A	nucleoplasmic	3.6 Å	unpublished

4.1 Nuclear import and release of Mago-Y14 by Imp13

In this study, we focused on the nuclear transport of the import cargo Mago-Y14 by Imp13. The results described in this section have been published in [Bono et al., 2010]. Detailed description of the experimental procedures and of the experimental data are available in the manuscript attached in section 5.1.

As mentioned in section 2.4.2, Mago-Y14 is a core component of the EJC. After splicing in the nucleus, the EJC assembles on the mRNA and travels with it into the cytoplasm. EJCs play a key role in mRNA metabolism and affect mRNA localization, translation and decay [Giorgi and Moore, 2007]. Since the EJC assembles only in the nucleus, an efficient nuclear import is required for its components. In this study, I investigated the Imp13 mediated nuclear import mechanism of Mago-Y14 by an extensive biochemical analysis.

The Imp13-Mago-Y14 structure

In order to understand the recognition of Mago-Y14 by Imp13 at the molecular level, Dr. Fulvia Bono solved the crystal structure of the *Drosophila* Imp13-Mago-Y14 complex at 3.16 Å resolution (pdb id: 2X1G). Imp13 features the typical HEAT-repeat architecture of karyopherins and consists of 20 consecutive HEAT-repeats (see Figure 17). The last HEAT-repeat is unusual and is composed of three parallel α-helices. A hinge region between HEAT-repeats 9 and 10 of Imp13 divides the protein into a N- and a C-terminal arch. Two further hinge regions at HEAT-repeats 4 and 14 expand the conformational flexibility of Imp13. For the binding of Mago-Y14, Imp13 employs mainly conserved and charged residues located at its C-terminal HEAT-repeats and at inter-loops. Thereby, it adopts a twisted ring-like conformation with a direct contact between residues of HEAT-repeats 1 and 20.

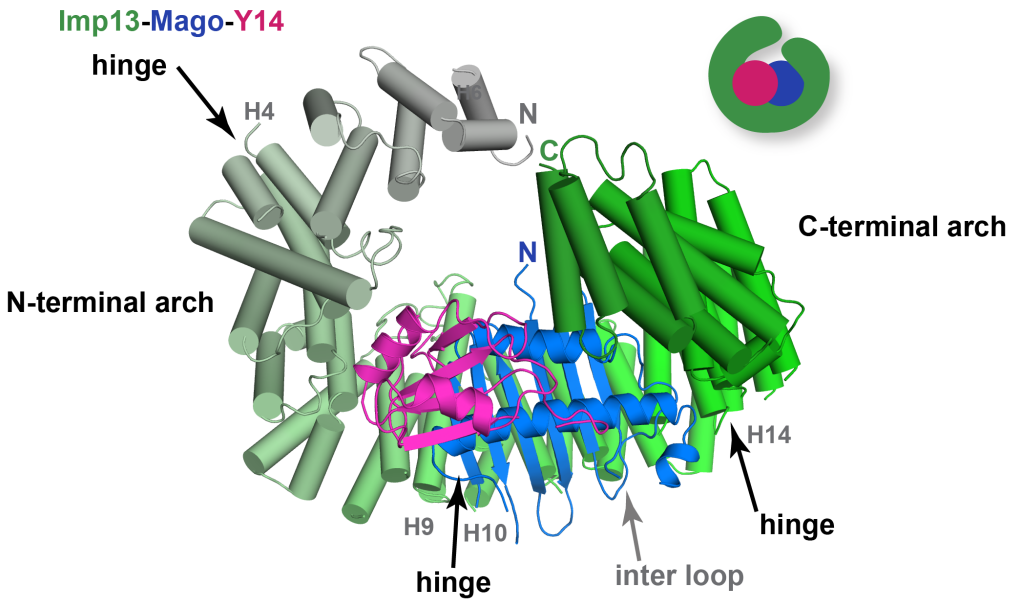

Figure 17: **Structure of the Imp13-Mago-Y14 complex.** Imp13 is shown as cylindrical helices in a color gradient from gray to green. Mago and Y14 are colored in blue and magenta, respectively. The hinge region between H9 and H10 that divides Imp13 in an N- and C-terminal arch and the two other hinges at H4 and H14 are indicated by arrows.

Based on the structure, we designed several Imp13 constructs with reverse charge mutations in residues important for binding Mago-Y14. I purified the mutant proteins recombinantly from *E. coli*. To analyze the effect of the point mutations on complex formation I performed *in vitro* coprecipitation assays. I used a GST-tagged Imp13, either wild type or mutant protein and immobilized the protein on glutathione (GSH) beads. I added the purified cargo, in this case Mago-Y14, to the beads. After extensive washing of the beads, I analyzed the bound proteins on SDS-PAGE. The mutated Imp13 constructs showed

a reduced ability in forming an Imp13-Mago-Y14 complex. In this way, I could identify several conserved amino acids on Imp13, which are important for the recognition of Mago-Y14.

Y14 is composed of a canonical RNA-recognition motif (RRM) domain with an extended N-terminal region. In complex with Mago, this N-terminal region of Y14 forms an α-helix that clamps Mago tightly between the RRM domain and the helix [Fribourg et al., 2003, Shi and Xu, 2003, Lau et al., 2003] (pdb id: 1HL6, 1OO0, 1P27). The structure of Imp13-Mago-Y14 shows that binding of the N-terminal helix of Y14 on Mago is incompatible with Imp13 association. The helix is displaced in the structure (see Figure 18). Most likely, the N-terminal region extends into the solvent. Consistently, I demonstrated by an *in vitro* coprecipitation assay that GST-tagged Imp13 is able to bind an N-terminally truncated Y14. Furthermore, both *Drosophila* and human Mago-Y14 proteins can interact with *Drosophila* Imp13 indicating that the interaction of these proteins is conserved between *Drosophila* and humans.

Figure 18: **Schematic representation of the Mago-Y14 and the Imp13-Mago-Y14 complexes.** Y14 clamps Mago between its RRM domain and the N-terminal helix. This helix is displaced in the Imp13-Mago-Y14 complex.

Imp13 and Pym compete for the binding to Mago-Y14

As mentioned in section 2.4.2, Mago-Y14 is exported from the nucleus as part of the EJC bound to mRNA. In the cytoplasm, the protein Pym is involved in EJC disassembly. After EJC disassembly, Mago-Y14 is recognized by Imp13 and reimported into the nucleus, while Pym remains in the cytoplasm. A comparison of the Pym-Mago-Y14 structure [Bono et al., 2004] (pdb id: 1RK8) with the Imp13-Mago-Y14 structure shows that Imp13 and Pym share the same binding surface on Mago-Y14 (see Figure 19). With an *in vitro*

Figure 19: **Schematic illustration of the Pym-Mago-Y14 and Imp13-Mago-Y14 complexes.** A simultaneously binding of Pym and Imp13 to Mago-Y14 is impossible, as both proteins share the same binding surface on Mago-Y14.

coprecipitation assay, I showed that a reverse charge mutation of the residue Glu73 of *Drosophila* Mago disrupts the binding of both Pym and Imp13. In addition, I performed *in vitro* competition assays demonstrating that Imp13 is able to dissociate Pym from a preformed Mago-Y14-GST-Pym complex. The competition of Pym and Imp13 for the same binding surface on Mago-Y14 explains how one protein at the time can bind to Mago-Y14.

The Imp13-RanGTP structure

To understand in detail the release mechanism of Mago-Y14 in the nucleus, Dr. Fulvia Bono solved the structure of the human Imp13-RanGTP complex at 2.8 Å resolution [Bono et al., 2010] (pdb id: 2X19). Imp13 wraps around RanGTP with its N-terminal arch (see Figure 20A). RanGTP buries a surface area of 1567.7 Å^2 on Imp13. The binding of RanGTP by Imp13 is very similar to that of other karyopherins. However, unlike most karyopherins where the RanGTP BS III is formed by the HEAT-repeats 12-15, Imp13 froms the BS III by the most C-terminal HEAT-repeats 17-19. Imp13 adopts a closed conformation when bound to RanGTP. The interaction surfaces of Mago-Y14 and RanGTP on Imp13 overlap only partially. In the Imp13-Mago-Y14 complex, the N-terminal arch of Imp13 is accessible for docking of RanGTP. However, superposition of Imp13-RanGTP and Imp13-Mago-Y14 structures suggest that a concomitant binding of RanGTP and Mago-Y14 to Imp13 is not possible (see Figure 20B). Therefore, RanGTP

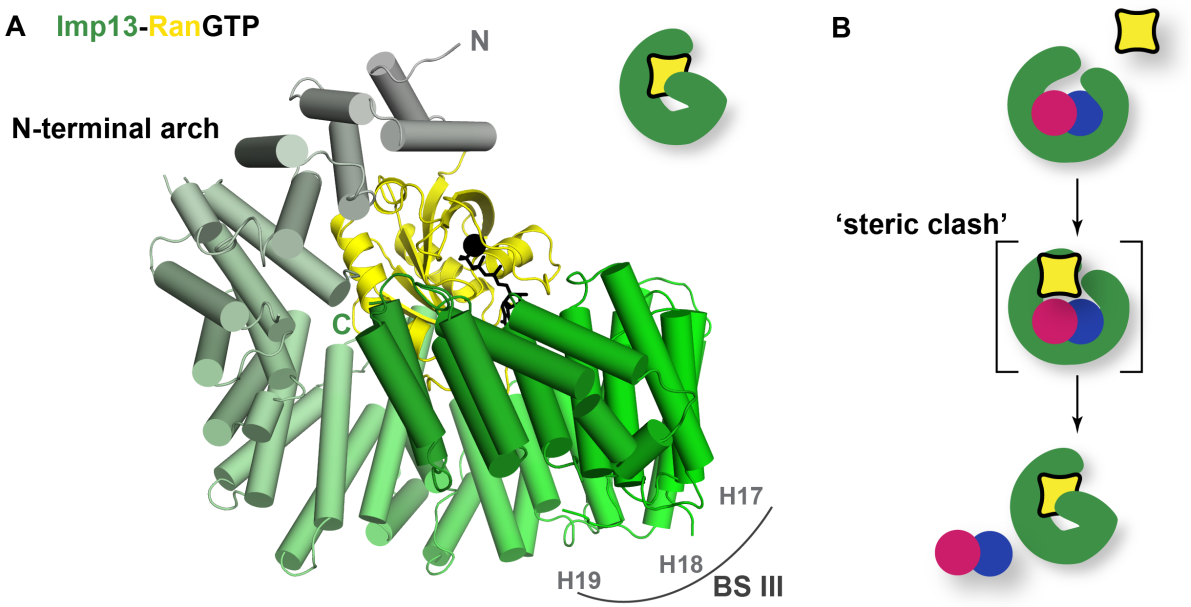

Figure 20: **Structure of the Imp13-RanGTP complex and release of Mago-Y14 from Imp13 by RanGTP.** (A) Imp13 is shown as cylindrical helices in a color gradient from gray to green. Ran is colored in yellow with GTP (black) as stick model and the Mg^{2+} ion as a black sphere. (B) Schematic illustration of the RanGTP induced release of Mago-Y14 from Imp13 by steric hindrance mechanism.

triggers the release of Mago-Y14 by a steric hindrance mechanism. In an *in vitro* competition assay, I showed that RanGTP is indeed able to trigger the release of Mago-Y14 from a preformed GST-Imp13-Mago-Y14 complex.

4.2 Nuclear import and release of Ubc9 by Imp13

The work described in this section has been published in [Grünwald and Bono, 2011]. A detailed description of the experimental data is available in the manuscript attached in section 5.2.

In this study, I investigated the import mechanism of Ubc9 by Imp13. Ubc9 is predominantly nuclear at steady state and most sumoylation targets are nuclear proteins [Rodriguez et al., 2001]. Therefore, the transport of Ubc9 into the nucleus is a very important step in the pathway.

The Imp13-Ubc9 structure

To understand the molecular mechanism of Ubc9 import by Imp13, I crystallized the human Imp13-Ubc9 complex and solved its structure by Molecular Replacement (MR) at 2.8 Å resolution. For MR, I used the structure of human Imp13 of the Imp13-RanGTP complex from our previous work (see section 4.1). In order to find a reliable MR solution of the flexible karyopherin, I had to divide Imp13 in four fragments that I used as search models. I refined the structure with the program Crystallography & NMR System (CNS) [Brünger et al., 1998] with a final R-free of 26.7 %, R-factor of 22.4 % and good stereochemistry. In the Imp13-Ubc9 structure, Imp13 adopts an open superhelical conformation with the N- and C-terminal ends twisted away from each other (see Figure 21). Unlike the majority

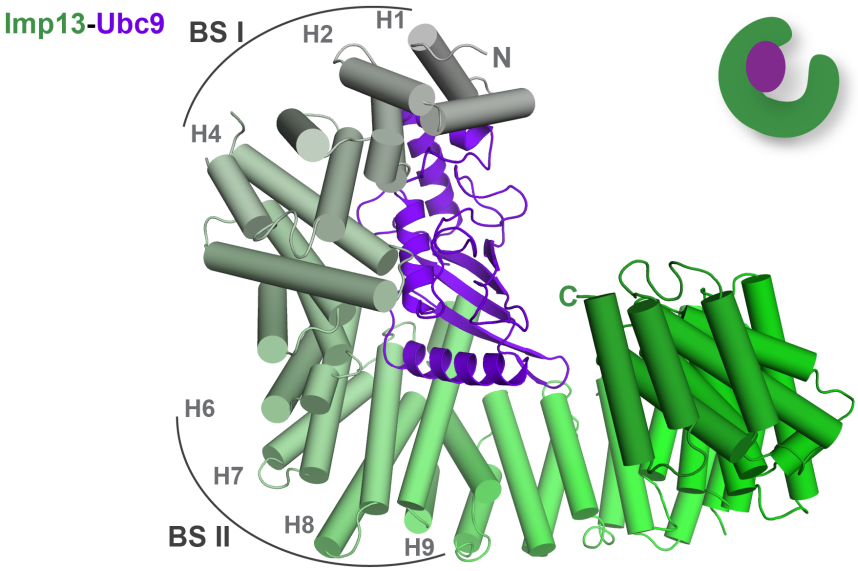

Figure 21: **Structure of the Imp13-Ubc9 complex.** Imp13 is shown as cylindrical helices in a color gradient from gray to green and Ubc9 is colored in purpleblue.

of import cargoes characterized to date that bind at the C-terminal arch of importins, Ubc9 is bound at the N-terminal arch of Imp13 with the same interaction surface used for binding RanGTP. On Imp13, Ubc9 buries a surface area of 1438.6 Å^2. Imp13 grasps Ubc9 with two opposite binding sites on its N-terminal arch. HEAT-repeats 1, 2 and 4 form the binding site I (BS I) which is engaged in mainly hydrophobic contacts. Binding site II (BS II) is composed of polar and charged residues on HEAT-repeats 6-9. In the structure, Ubc9 adopts the typical fold of E2 enzymes.

Guided by the structure, I designed an Imp13 construct with a double mutation of two tyrosine residues to arginines in BS I and another Imp13 construct with one reverse charge mutation in BS II. I purified the recombinant proteins from *E. coli*. In an *in vitro* coprecipitation assay using a GST-tagged version of Imp13, I could confirm that both sets of mutations dramatically affect the binding ability of Imp13 to Ubc9. The same mutations on Imp13 did not affect the binding of Mago-Y14. Although RanGTP and Ubc9 share the same interaction surface on Imp13, these mutations did not affect the binding of RanGTP. An explanation for this could be that, since the binding of RanGTP to Imp13 is very strong, single or double point mutations are not sufficient to reduce the binding. Furthermore, I designed an Ubc9 construct with a reverse charge mutation on Arg17 which I purified from *E. coli*. I showed that Arg17 is necessary for binding of Ubc9 to Imp13 by an *in vitro* coprecipitation assay. The previously described mutation on Imp13, which abolishes binding of Mago-Y14 (see section 4.1), does not affect the binding of Ubc9 or RanGTP.

Comparison of the import cargo recognition by Imp13

Comparison of the Imp13-Mago-Y14 and Imp13-Ubc9 complexes shows that Imp13 recognizes both cargoes with different interaction surfaces. Mago-Y14 is mainly recognized by the C-terminal HEAT-repeats and inter-loops of Imp13, while Ubc9 is bound only by the N-terminal HEAT-repeats and intra-loops. To investigate if both import cargoes can bind to Imp13 at the same time, I performed an *in vitro* competition assay. Therefore, I immobilized preformed Imp13-GST-Mago-Y14 or Imp13-GST-Ubc9 complexes to GSH beads. The addition of increasing amounts of either Ubc9 or Mago to the preformed complexes showed that both cargoes displace each other to a similar extent (see Figure 22).

Figure 22: **Schematic illustration of the competition between Mago-Y14 and Ubc9 for Imp13.** Mago-Y14 and Ubc9 can displace each other from a preformed Imp13-cargo complex.

This result showed that Ubc9 and Mago-Y14 cannot bind to Imp13 at the same time, although they use opposite interaction surfaces on Imp13.

Function of Imp13-bound Ubc9 in the sumoylation pathway

Other proteins of the sumoylation pathway are also actively imported into the nucleus. Impβ/Impα mediates the import of the E1 activating enzyme Aos1-Uba2 [Moutty et al., 2011]. The protein SUMO has a molecular weight of 11 kDa and is therefore small enough to passively diffuse through the NPCs. At present, it is not known if SUMO is actively transported into the nucleus. Ubc9 can associate to SUMO in different ways. As an intermediate of the sumoylation reaction, SUMO can be covalently linked by a thioester bond to the catalytic Cys93 of Ubc9 (Ubc9∼SUMO). Ubc9 can also bind SUMO in a non-covalent manner. Furthermore, Ubc9 can sumoylate itself at residue Lys14, via an isopeptide bond (Ubc9*SUMO). Based on the structure we hypothesized that a SUMO-modified Ubc9 could be recognized by Imp13. Therefore, I formed an Ubc9*SUMO complex by *in vitro* sumoylation. I then used an *in vitro* coprecipitation assay with GST-tagged Imp13 followed by Western blot analysis with antibodies against Ubc9 and SUMO to show that Imp13 does indeed bind an Ubc9*SUMO complex. Furthermore, I formed an Ubc9∼SUMO complex and showed that also the thioester complex Ubc9∼SUMO can bind to Imp13 by coprecipitation assay. Interestingly, Imp13 can bind both covalently linked complexes *in vitro*, suggesting a possible transport mechanism of SUMO in association to Ubc9 (see Figure 23). This will have to be confirmed by SUMO localization studies in cells.

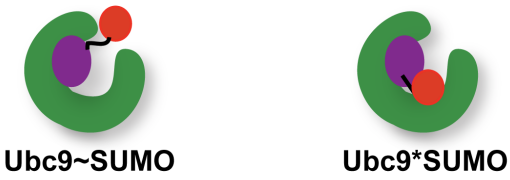

Figure 23: **Imp13 can bind SUMO-modified Ubc9.**

In the Imp13-Ubc9 complex, the active site of Ubc9 is mostly exposed to the solvent. Yet, a comparison of the Ubc9-Uba2 [Wang et al., 2007] (pdb id: 2PX9) structure with the Imp13-Ubc9 complex shows that simultaneous binding of Imp13 and Uba2 to Ubc9 is not possible due to a steric clash. RanGAP and E2-25K are sumoylation targets which are directly modified by Ubc9 without the help of an E3 ligase. Structures of both proteins in complex with Ubc9 are available [Reverter and Lima, 2005] [Walker et al., not published] (pdb id: 1Z5S, 2O25). The superposition of both structures with Ubc9 from the Imp13-Ubc9 structure shows major steric clashes, indicating that the docking of these proteins to Imp13-bound Ubc9 is not possible. Thus, Ubc9 bound to Imp13 is likely

to be catalytically inactive, at least for these two targets. To confirm this hypothesis, I performed an *in vitro* sumoylation assay using Imp13-Ubc9 complex and E2-25K and RanGAP as sumoylation targets. Ubc9 in a preformed Imp13-Ubc9 complex exhibits a dramatically reduced catalytic activity than free Ubc9 (see Figure 24).

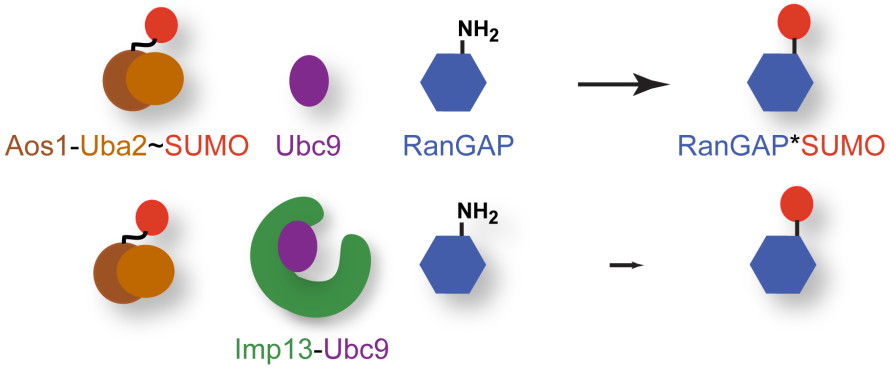

Figure 24: **Ubc9 in complex with Imp13 exhibits reduced catalytic activity.**

Ubc9 release from Imp13 by RanGTP

The comparison of the Imp13-RanGTP structure with the Imp13-Ubc9 structure suggests that Ubc9 is likely released from Imp13 by a direct competition for the same interaction surface. In an *in vitro* competition assay I showed that RanGTP is able to release Ubc9 efficiently from a preformed Imp13-Ubc9 complex (see Figure 25A).

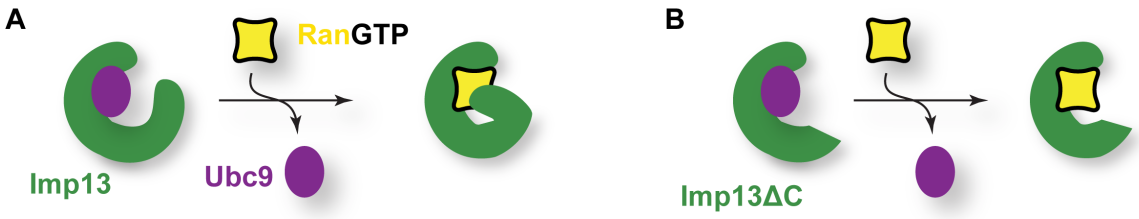

Figure 25: **Schematic illustration of Ubc9 release from Imp13 by RanGTP.** The last HEAT-repeats of the C-terminal arch of Imp13 are not necessary for the release of Ubc9 by RanGTP binding.

Ubc9 is released with similar efficiency from a complex made with a C-terminally truncated Imp13 (Imp13ΔC, residue 1-672). Therefore, the last HEAT-repeats of the C-terminal arch of Imp13 are not necessary for the release of Ubc9 by RanGTP *in vitro* (see Figure 25B). This result supports the model of a direct competition of Ubc9 and RanGTP, without the involvement of RanGTP binding to the C-terminal HEAT-repeats of Imp13. The same truncated Imp13 can bind RanGTP but not Mago-Y14 (see Figure 26). Since the RanGTP-triggered release of Mago-Y14 from preformed Imp13-Mago-Y14

complex was less efficient than the release of Ubc9, I tested whether the addition of the export cargo eIF1A had an effect on import cargo release. Surprisingly, the addition of eIF1A to RanGTP greatly enhanced the release of Mago-Y14. However, eIF1A addition did not have an effect on Ubc9 release.

Figure 26: **Schematic illustration of the cargo binding ability of Imp13ΔC.** Imp13ΔC is able to bind Ubc9 and RanGTP but not Mago-Y14.

Comparison of Imp13 to other importins

The involvement of specific loop insertions, such as the 'acidic loop' of Impβ, is widespread among karyopherins (see section 2.3.3). In the case of importins, the loop insertions are very important for RanGTP binding and cargo release. Many exportins have loop insertions that correspond structurally to importins, however, in most cases they couple the binding of RanGTP and cargo. Few karyopherins do not have a loop insertion involved in RanGTP recognition as for example Exp5 or Imp13. However, the long B helix of HEAT-repeat 9 extends into the inner concave surface of Imp13, occupying a similar position as the 'acidic loop' of Impβ. The negatively charged residues of this helix are involved in Ubc9 and RanGTP recognition, preventing a concomitant binding of the import cargo and RanGTP.

Imp13 is a highly versatile karyopherin that recognizes its import cargoes based on their shape and surface charge instead of binding short extended localization signals as Impβ and Tnp. However, Imp13 has in common with these importins that mainly basic or a combination of basic and hydrophobic residues on the cargoes are recognized. While a consensus sequence for the cNLS and PY-NLS bound by Impα and Tnp was found, only the combination of shape and charge defines Imp13 cargoes. The homeodomain of Pax6, Pax3 and Crx, which is composed of 80 amino acids, is highly conserved [Ploski et al., 2004]. It can be considered as a 'consensus domain' in which both fold and charge of the protein are conserved. Other proteins containing such a conserved homeodomain are potential Imp13 cargoes. Yet, to consider only the fold of a protein is not enough to define an Imp13 cargo. I could show that E2-25K, a E2-conjugating enzyme of the ubiquitination pathway that adopts the same fold as Ubc9 with a sequence identity of 23 % is not bound by Imp13 (see Figure 27, lane 4 & 5).

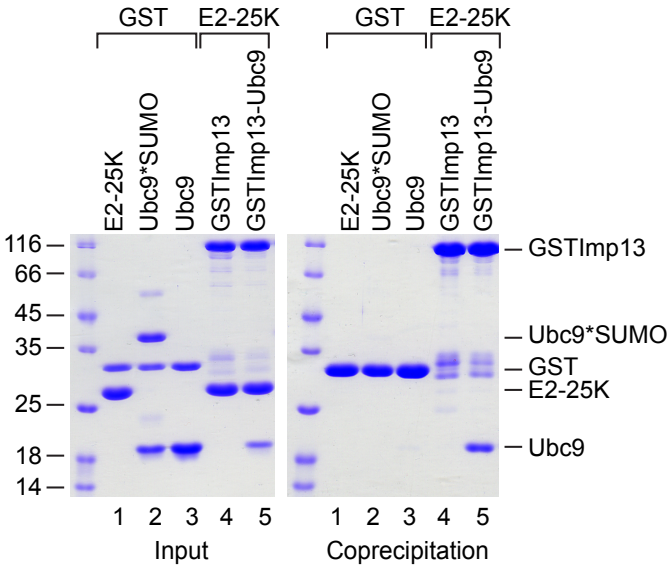

Figure 27: **Coprecipitation of GST-Imp13 with E2-25K.** Protein co-precipitation by GST-tagged Imp13 and a preformed GST-tagged Imp13-Ubc9 complex incubated together with E2-25K (lane 4 & 5). For the input control 1/6 of the samples were loaded (left panel) and the rest was co-precipitated with glutathione sepharose beads (right panel) and analyzed on Coomassie stained 15 % SDS-PAGE. The far left lane was loaded with a molecular weight marker. Lane 1-3 are GST controls.

The flexibility of karyopherins plays a key role for their function. Usually, karyopherins change their conformation upon binding RanGTP (see Figure 28). The conformational change in Impβ when bound to RanGTP is restricted to the last HEAT-repeats. In contrast, the conformational change of Tnp is small compared to Impβ and Imp13. Yet, Tnp discriminates between RanGTP- and cargo-bound states via a conformational change in the 'acidic loop'. Compared to Impβ and Tnp, Imp13 shows after binding of RanGTP a more prominent conformational change of the complete C-terminal arch. This change is induced by movements at the hinge region between HEAT-repeat 9 and 10. The two minor hinge regions at HEAT-repeat 4 and 14 further contribute to the flexibility of Imp13. From our structures we can observe that Imp13 can adopt conformations from a closed ring to an open superhelix. Such dramatic changes in the conformation have not been reported for Impβ and Tnp.

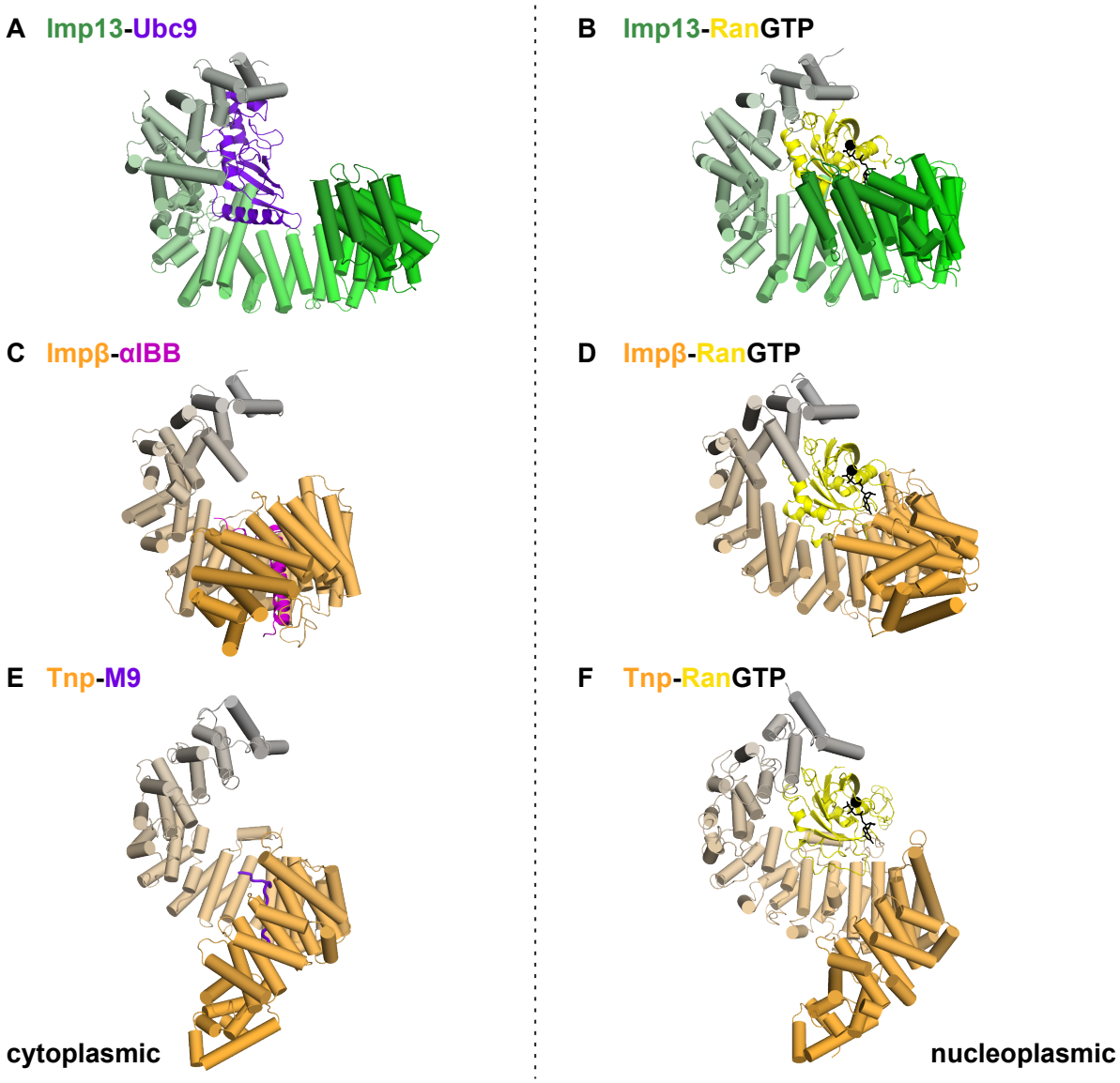

Figure 28: **Conformational changes in importins induced by RanGTP binding.**

4.3 Nuclear export and release of eIF1A by Imp13

The experimental data and detailed descriptions of the experimental procedure can be found in section 5.3. The manuscript is under review at EMBO Journal.

So far, only three karyopherins were identified to be bidirectional transport factors but little information is available on how these karyopherins function. Therefore, the study of the export pathway of Imp13 is expected to yield profound insights into how such bidirectional factors work and why only a few exist or are identified as such.

The Imp13-RanGTP-eIF1A structure

I designed different constructs of human and *Drosophila* Imp13, RanGTP and eIF1A in order to form a stoichiometric and homogenous trimeric Imp13-RanGTP-eIF1A complex.

I crystallized the human Imp13-RanGTP-eIF1A complex and solved the structure at 3.6 Å resolution by MR. As a search model I used the Imp13-RanGTP structure. I placed eIF1A manually into the density since no reliable MR solutions with the human eIF1A structure [Battiste et al., 2000] as search model could be obtained. The sequence of human eIF1A contains two methionines. I designed an human eIF1A mutant that included a third methionine at a position where a methionine is present in many eIF1A homologs. From crystals including a seleno-methionine (SeMet) substituted eIF1A with three methionines I collected a single wavelength anomalous dispersion (SAD) data set. The calculation of the anomalous Fourier map from this data resulted in three anomalous peaks corresponding to the three selenium atoms, which I used for guidance to manually place eIF1A into the density. I refined the final model with the programs BUSTER using non-crystallographic symmetry (NCS) restrains [Smart et al., 2012] and PHENIX [Adams et al., 2010] to an *R*-free of 29.9 % and *R*-factor of 26.8 % with good stereochemistry.

eIF1A is recognized by two binding sites on Imp13. The main binding site I (BS I) is composed of HEAT-repeats 7-11 whereas binding site II (BS II) consists of the last HEAT-repeat 20 (see Figure 29). eIF1A is bound mainly by electrostatic interactions. Besides the two binding sites on Imp13, RanGTP directly contacts eIF1A providing a third binding site (BS III). eIF1A adopts a typical oligonucleotide binding (OB) fold followed by an additional helix. Furthermore, eIF1A features two long unstructured N- and C-terminal tails (NTT and CTT). The overall conformation of Imp13 is very similar to the conformation of Imp13 in the Imp13-RanGTP structure, although the ring of Imp13 opens slightly to accommodate eIF1A.

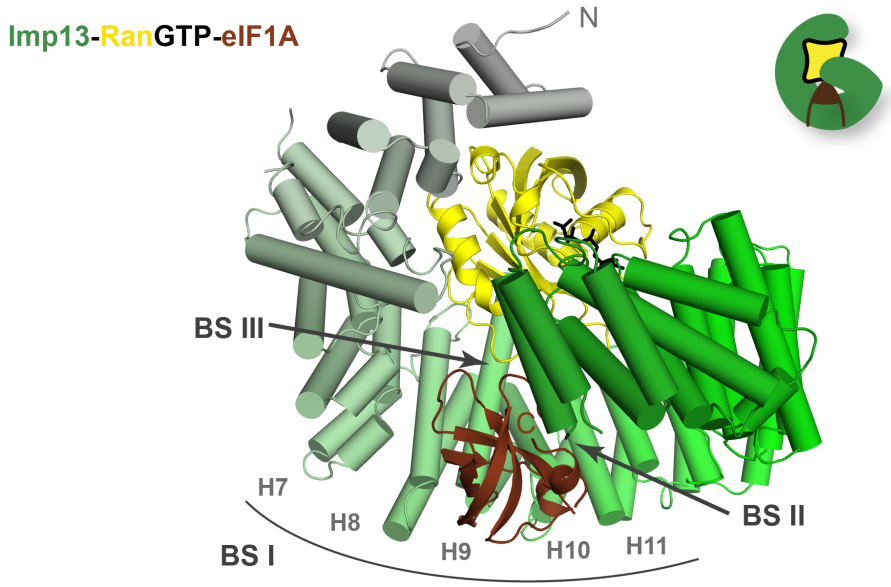

Figure 29: **Structure of the Imp13-RanGTP-eIF1A complex.** Imp13 is shown in a color gradient from gray to green with cylindrical helices, while RanGTP (yellow, black) and eIF1A (brown) are represented in cartoon view.

Based on the structure, I designed several mutants of Imp13, eIF1A and RanGTP with reverse charge mutations on residues important for binding eIF1A. I purified the recombinant proteins from *E. coli* and tested the mutated proteins for their ability to form a complex by *in vitro* coprecipitation. I could identified several residues which are necessary for the binding of eIF1A to Imp13. In addition, I showed that a double reverse charge mutation on Arg95 and Lys120 of RanGTP affects the binding of eIF1A to Imp13. I was able to dissect the molecular requirements of Imp13 for eIF1A binding, while leaving intact the import cargo binding properties of Imp13.

The bidirectionality of Imp13

Comparison of the Imp13-Mago-Y14 and the Imp13-RanGTP-eIF1A complexes shows that eIF1A and Mago-Y14 share the same interaction surface on Imp13 (see Figure 30). As previously mentioned (see section 4.1), RanGTP and Mago-Y14 cannot bind to Imp13 at the same time. However, eIF1A is much smaller than Mago-Y14 and fits adjacent to RanGTP at the same interaction surface that binds Mago-Y14. The concomitant binding of eIF1A based on its size and charge makes it possible for Imp13 to distinguish between import and export cargoes.

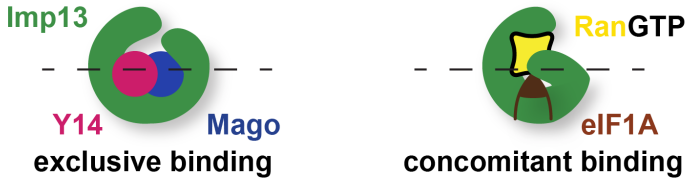

Figure 30: **Comparison of the Imp13 import and export complexes.** Schematic illustration of the Imp13-Mago-Y14 and the Imp13-RanGTP-eIF1A complexes. The import complex shows an exclusive binding of Mago-Y14, while in the case of the export complex eIF1A binds concomitantly with RanGTP to Imp13. The dashed line marks the interaction surface.

Dissociation constants of Imp13 for its cargoes

To measure the dissociation constants (K_D) of Imp13 for its cargoes I used differential scanning fluorimetry (DSF). The binding of a cargo stabilizes Imp13, resulting in a higher melting temperature (T_M) of the complex. The T_M increment depends on the concentration of the added cargo. Therefore, a plot of T_M against cargo concentrations results in an exponential curve, from which the K_D can be calculated [Niesen et al., 2007, Hintersteiner et al., 2010]. The K_D for the import cargoes Mago-Y14 and Ubc9 is in the same range (between 230 and 370 nM) (see Table 6). The release of bound cargo in the nucleus is facilitated by a higher affinity of Imp13 for RanGTP with a K_D below 100 nM. Due to the detection limit of the DSF, the precise K_D for RanGTP could not be calculated. Interestingly, an Imp13-RanGTP complex binds the export cargo eIF1A an order of magnitude less strongly than the import cargoes with a K_D of 3.0 µM.

Table 6: **K_D values of Imp13 for different cargoes and RanGTP.** Listed are K_D values of Imp13 for the import cargoes Mago-Y14 and Ubc9 as well as RanGTP. A preformed Imp13-RanGTP complex was used to determine the K_D for the export cargo eIF1A. All K_Ds were measured by DSF.

complexes	**K_D (nM)**	**localization**
Imp13-Mago-Y14	235 ± 30	cytoplasmic
Imp13-Ubc9	370 ± 20	cytoplasmic
Imp13-RanGTP	≤ 100	nucleoplasmic
Imp13-RanGTP-eIF1A	3000 ± 380	nucleoplasmic

The free Imp13 structure

I solved the crystal structure of *Drosophila* Imp13 in the unbound state at 3.0 Å resolution. As a search model for MR, I used the *Drosophila* Imp13 structure from the Imp13-Mago-Y14 complex. I refined the model with the program PHENIX [Adams et al., 2010] to a *R*-free of 31.0 %, *R*-factor of 28.7 % and good stereochemistry. A combination of weak diffraction and relatively large disorder regions at the N-terminal HEAT-repeats (approximately 100 residues) likely explains the high *R*-free value. In the ligand-free state, Imp13 adopts an open conformation similar to the Mago-Y14 bound state (see Figure 31). In the cell, free Imp13 is present in the cytosol after the release of RanGTP from Imp13. The comparison of the Imp13-RanGTP-eIF1A complex with free Imp13 explains how eIF1A is released from Imp13 after reaching the cytoplasm. The BS II for eIF1A is displaced in the free state as well as the additional contact between eIF1A and RanGTP (BS III). Furthermore, the conformational change of Imp13 after release of

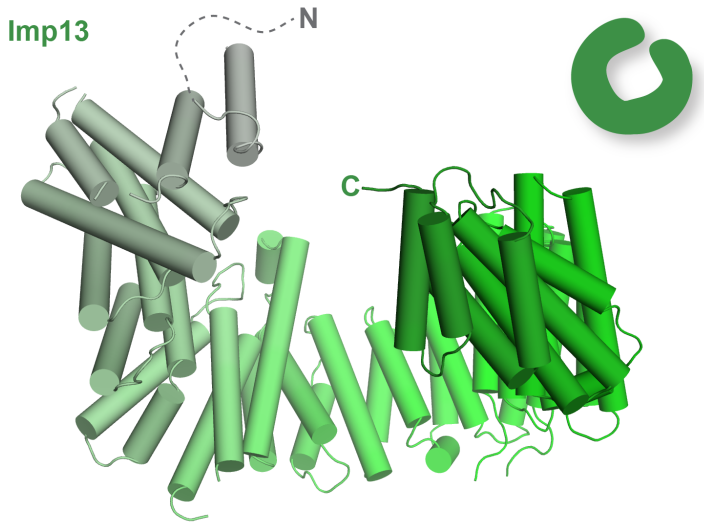

Figure 31: **Structure of free Imp13.** Imp13 is shown as cylindrical helices in a color gradient from gray to green. The first HEAT-repeats of Imp13 are disordered in the free state.

RanGTP disrupts partially BS I of eIF1A. By an *in vitro* coprecipitation assay I could show that a C-terminally truncated version of Imp13 (1-672) that lacks BS II for eIF1A can no longer bind eIF1A although eIF1A BS I and RanGTP binding are not affected. Therefore, the disruption of BS II is sufficient to impair eIF1A binding to Imp13. This result suggests that Imp13 in an open conformation is incompatible with eIF1A binding. Furthermore, Imp13 changes its conformation dramatically between nuclear and cytosolic states.

In vivo function of Imp13

To answer the question of how important Imp13 transport is in cells, Dr. Daniela Lazzaretti performed a knockdown of Imp13 in HeLa cells. She showed that Imp13 is essential for cell viability. At steady state, eIF1A is mainly localized in the cytoplasm and in the nucleoli in HeLa and H4 cells. Furthermore, Dr. Daniela Lazzaretti could show that eIF1A is recognized and exported by Imp13 *in vivo*, although it is likely that other transport pathways are also involved in eIF1A export.

Comparison of Imp13 with other exportins

As mentioned, all exportins with the exception of Crm1, bind their cargoes at the inner concave surface and RanGTP directly contacts their cargoes. This contact together with the conformational changes of exportins induced by RanGTP explain the highly cooperative binding of exportins to RanGTP and cargo. Since the structures of cargo free Exp5 and Crm1 are not available, for these exportins it is not clear whether conformational changes are involved upon cargo and RanGTP binding. CAS and Expt show major conformational changes upon binding of RanGTP and their cargo (see Figure 32). Interestingly, while the helical pitch of CAS opens to accommodate RanGTP and cargo, Expt conformation closes upon binding of RanGTP. The conformational change of Imp13 upon export cargo binding resembles the changes of the exportin Expt. As Expt, Imp13 shows an open conformation in the free state which closes after RanGTP binding.

Crm1 binds its cargoes via a NES, a short hydrophobic sequence in an exposed region of the cargo. However, other exportins recognize their cargoes based on the shape and charge. This type of recognition allows CAS to distinguish a NLS-bound from a cargo-free Impα. Furthermore, Expt and Exp5 can discriminate between premature and mature tRNAs or miRNAs. The selection of the correct forms of cargoes is essential for an efficient nucleocytoplasmic transport. In a similar manner, Imp13 recognizesits cargoes by size, shape and charge. Therefore, it avoids simultaneous binding of factors which could be bound to the cargo, like the cytoplasmic protein Pym to Mago-Y14 and it can discriminate between an import and export cargo. In summary, the conformational changes in Imp13 and the recognition of its cargoes by shape and charge bears similarity with exportins more than importins.

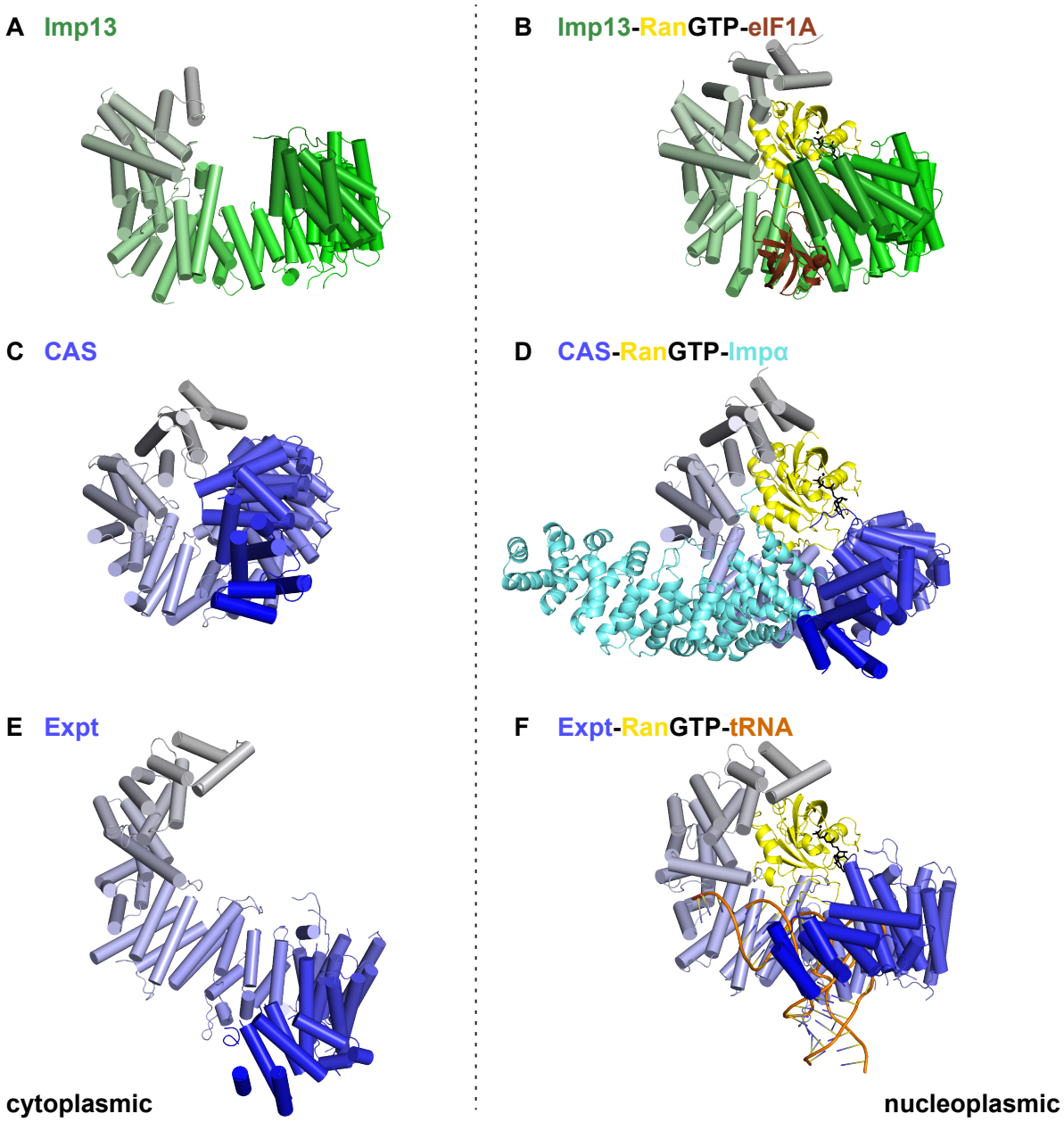

Figure 32: **Conformational changes in exportins upon RanGTP and cargo binding.**

4.4 Concluding remarks

Imp13 distinguishes between import and export cargo by antagonistic or cooperative binding of RanGTP based on shape, charge and size of the cargo. This simple principle of Imp13 bidirectionality could be a general way exploited by other karyopherins that have not been yet characterized as bidirectional receptors. Interestingly, Impβ has a low K_D of approximately 0.25 nM for RanGTP, while the exportin Crm1 binds RanGTP with a high K_D of 3 µM [Görlich et al., 1996, Bischoff and Görlich, 1997, Paraskeva et al., 1999]. The binding of RanGTP has to be strong enough to displace an import cargo from the karyopherin and to mediate at the same time cooperative binding with an export cargo [Güttler

and Görlich, 2011]. One prerequisite for bidirectional transport could be an intermediate K_D for RanGTP. Consistently, the K_Ds for RanGTP of all three bidirectional transport factors are in the low nanomolar range with 30 nM for Exp4, 52 nM for Msn5p and below 100 nM for Imp13 [Lipowsky et al., 2000, Hahn and Schlenstedt, 2011]. Interestingly, several other karyopherins that are less well characterized like Imp4, Imp7, Imp9 and TnpSR have K_D values for RanGTP similar to the bidirectional karyopherins [Hahn and Schlenstedt, 2011] and might therefore be potential bidirectional transport factors.

In this work Dr. Daniela Lazzaretti showed that eIF1A is localized in the nucleoli. The nucleolus is the site of ribosome assembly, suggesting that eIF1A at this location could be bound to the pre-ribosomal 40S subunit. FRAP experiments indicate a fast exchange between the nucleoli- and nucleoplasm-localized fraction of eIF1A (data not shown). The retention of eIF1A in the nucleus after blocking the Crm1 export pathway by leptomycin B indicates that Crm1 might play a role in the localization of eIF1A. Yet, Crm1 cannot bind directly to eIF1A [Mingot et al., 2001], which is why eIF1A has to be bound to other export cargoes of Crm1. The function of eIF1A in the nucleoli is still unclear and further investigations are necessary to show if eIF1A is in fact bound to the pre-ribosomal 40S subunit and whether it can be exported by Crm1 piggybacking on the pre-ribosomal 40S.

For many karyopherins structural data are still not available. Furthermore, consensus motifs for NLS or NES have been identified only for Impα, Tnp and Crm1. All other karyopherins use more complex localization signals, some similar to typical NLS and NES with short extended regions, others composed of folded domains as it is true for Imp13 [Chook and Süel, 2010]. The binding of cargoes at the outer convex surface of Crm1 or at the N-terminal arch of Imp13 and Impβ demonstrate that karyopherins are very versatile proteins which exploit interaction surfaces distributed over the entire molecule. Therefore, predictions of karyopherin-cargo interactions are very difficult and can only be advanced by the detailed knowledge of individual karyopherin-cargo complexes generated by further structural and biochemical analysis.

Many Nups are involved in binding to karyopherins. These interactions are necessary for efficient nucleocytoplasmic transport. For example, the FG domain of Nup214 binds to a Crm1-RanGTP-cargo complex with high affinity and is essential for Crm1-dependent nuclear export *in vivo* [Fornerod et al., 1997, Askjaer et al., 1999, Kehlenbach et al., 1999,Hutten and Kehlenbach, 2006]. Furthermore, the nuclear protein RanBP3 is required for an efficient Crm1-mediated export by stimulating the recruitment of certain cargoes to Crm1 [Lindsay et al., 2001, Englmeier et al., 2001]. The nucleoporin RanBP2, which stably binds RanGAP and is localized to the cytoplasmic filaments, functions as a cargo- and receptor-specific assembly platform [Wälde et al., 2012]. In the absence of RanBP2, about 200 proteins with cNLSs and NY-NLSs accumulate in the cytoplasm. RanBP2 also actively recruits the import receptors Impβ and Tnp to the NPCs [Hutten et al., 2008,

Hutten et al., 2009]. Interestingly, the RanBP2/RanGAP*SUMO complex can function as an E3 ligase, suggesting a link between sumoylation and RanGTP hydrolysis [Flotho and Werner, 2012]. As mentioned (see section 2.3.4), Nup50 is able to displace the cNLS from Impα. Most likely, more NPC proteins interact directly with karyopherins or their cargos and are necessary for efficient nucleocytoplasmic transport. Therefore, one future goal is to unravel the complicated network of interactions at the NPC at a molecular level by a combination of cell biology, biochemistry and structural biology in order to understand this additional layer of regulation.

As mentioned in section 2.4, Imp13 is developmentally and hormonally regulated in some systems, but details of how this regulation works are not known. This regulation could be determined by sequences within Imp13 or could be dependent on cargoes, that are developmentally regulated. The Imp13 mediated nuclear accumulation of myopodin suggest that cellular differentiation is regulated by the Imp13-dependent import of myopodin [Liang et al., 2008]. The correct and time-specific nuclear accumulation of developmentally important factors is critical for normal development. How nuclear transport factors such as Imp13 influence development are still unclear and remain to be determined mechanistically.

References

[Adam and Adam, 1994] Adam, E. J. and Adam, S. A. (1994). Identification of cytosolic factors required for nuclear location sequence-mediated binding to the nuclear envelope. *The Journal of Cell Biology*, 125(3):547–555. PMID: 8175880.

[Adams et al., 2010] Adams, P. D., Afonine, P. V., Bunkóczi, G., Chen, V. B., Davis, I. W., Echols, N., Headd, J. J., Hung, L.-W., Kapral, G. J., Grosse-Kunstleve, R. W., McCoy, A. J., Moriarty, N. W., Oeffner, R., Read, R. J., Richardson, D. C., Richardson, J. S., Terwilliger, T. C., and Zwart, P. H. (2010). PHENIX : a comprehensive python-based system for macromolecular structure solution. *Acta Crystallographica Section D Biological Crystallography*, 66(2):213–221.

[Aitken and Lorsch, 2012] Aitken, C. E. and Lorsch, J. R. (2012). A mechanistic overview of translation initiation in eukaryotes. *Nature Structural & Molecular Biology*, 19(6):568–576. PMID: 22664984.

[Akey and Radermacher, 1993] Akey, C. W. and Radermacher, M. (1993). Architecture of the xenopus nuclear pore complex revealed by three-dimensional cryo-electron microscopy. *The Journal of Cell Biology*, 122(1):1–19. PMID: 8314837.

[Alber et al., 2007] Alber, F., Dokudovskaya, S., Veenhoff, L. M., Zhang, W., Kipper, J., Devos, D., Suprapto, A., Karni-Schmidt, O., Williams, R., Chait, B. T., Sali, A., and Rout, M. P. (2007). The molecular architecture of the nuclear pore complex. *Nature*, 450(7170):695–701. PMID: 18046406.

[Andrade and Bork, 1995] Andrade, M. A. and Bork, P. (1995). HEAT repeats in the huntington's disease protein. *Nature Genetics*, 11(2):115–116. PMID: 7550332.

[Andrade et al., 2001] Andrade, M. A., Petosa, C., O'Donoghue, S. I., Müller, C. W., and Bork, P. (2001). Comparison of ARM and HEAT protein repeats. *Journal of Molecular Biology*, 309(1):1–18. PMID: 11491282.

[Askjaer et al., 1999] Askjaer, P., Bachi, A., Wilm, M., Bischoff, F. R., Weeks, D. L., Ogniewski, V., Ohno, M., Niehrs, C., Kjems, J., Mattaj, I. W., and Fornerod, M. (1999). RanGTP-regulated interactions of CRM1 with nucleoporins and a shuttling DEAD-box helicase. *Molecular and Cellular Biology*, 19(9):6276–6285. PMID: 10454574.

[Baake et al., 2001] Baake, M., Bäuerle, M., Doenecke, D., and Albig, W. (2001). Core histones and linker histones are imported into the nucleus by different pathways. *European Journal of Cell Biology*, 80(11):669–677. PMID: 11824786.

[Battiste et al., 2000] Battiste, J. L., Pestova, T. V., Hellen, C. U., and Wagner, G. (2000). The eIF1A solution structure reveals a large RNA-binding surface important for scanning function. *Molecular Cell*, 5(1):109–119. PMID: 10678173.

[Bayliss et al., 2000] Bayliss, R., Littlewood, T., and Stewart, M. (2000). Structural basis for the interaction between FxFG nucleoporin repeats and importin-beta in nuclear trafficking. *Cell*, 102(1):99–108. PMID: 10929717.

[Bayliss et al., 2002] Bayliss, R., Littlewood, T., Strawn, L. A., Wente, S. R., and Stewart, M. (2002). GLFG and FxFG nucleoporins bind to overlapping sites on importin-beta. *The Journal of Biological Chemistry*, 277(52):50597–50606. PMID: 12372823.

[Bhardwaj and Cingolani, 2010] Bhardwaj, A. and Cingolani, G. (2010). Conformational selection in the recognition of the snurportin importin beta binding domain by importin beta. *Biochemistry*, 49(24):5042–5047. PMID: 20476751.

[Bischoff and Görlich, 1997] Bischoff, F. R. and Görlich, D. (1997). RanBP1 is crucial for the release of RanGTP from importin beta-related nuclear transport factors. *FEBS Letters*, 419(2-3):249–254. PMID: 9428644.

[Bohnsack et al., 2002] Bohnsack, M. T., Regener, K., Schwappach, B., Saffrich, R., Paraskeva, E., Hartmann, E., and Görlich, D. (2002). Exp5 exports eEF1A via tRNA from nuclei and synergizes with other transport pathways to confine translation to the cytoplasm. *The EMBO Journal*, 21(22):6205–6215. PMID: 12426392.

[Bono et al., 2010] Bono, F., Cook, A. G., Grünwald, M., Ebert, J., and Conti, E. (2010). Nuclear import mechanism of the EJC component mago-y14 revealed by structural studies of importin 13. *Molecular Cell*, 37(2):211–222. PMID: 20122403.

[Bono et al., 2004] Bono, F., Ebert, J., Unterholzner, L., Güttler, T., Izaurralde, E., and Conti, E. (2004). Molecular insights into the interaction of PYM with the mago-y14 core of the exon junction complex. *EMBO Reports*, 5(3):304–310. PMID: 14968132.

[Bono and Gehring, 2011] Bono, F. and Gehring, N. H. (2011). Assembly, disassembly and recycling: the dynamics of exon junction complexes. *RNA Biology*, 8(1):24–29. PMID: 21289489.

[Brownawell and Macara, 2002] Brownawell, A. M. and Macara, I. G. (2002). Exportin-5, a novel karyopherin, mediates nuclear export of double-stranded RNA binding proteins. *The Journal of Cell Biology*, 156(1):53–64. PMID: 11777942.

[Brünger et al., 1998] Brünger, A. T., Adams, P. D., Clore, G. M., DeLano, W. L., Gros, P., Grosse-Kunstleve, R. W., Jiang, J. S., Kuszewski, J., Nilges, M., Pannu, N. S., Read, R. J., Rice, L. M., Simonson, T., and Warren, G. L. (1998). Crystallography & NMR system: A new software suite for macromolecular structure determination. *Acta Crystallographica. Section D, Biological Crystallography*, 54(Pt 5):905–921. PMID: 9757107.

[Calado et al., 2002] Calado, A., Treichel, N., Müller, E.-C., Otto, A., and Kutay, U. (2002). Exportin-5-mediated nuclear export of eukaryotic elongation factor 1A and tRNA. *The EMBO Journal*, 21(22):6216–6224. PMID: 12426393.

[Cansizoglu et al., 2007] Cansizoglu, A. E., Lee, B. J., Zhang, Z. C., Fontoura, B. M. A., and Chook, Y. M. (2007). Structure-based design of a pathway-specific nuclear import inhibitor. *Nature Structural & Molecular Biology*, 14(5):452–454. PMID: 17435768.

[Catimel et al., 2001] Catimel, B., Teh, T., Fontes, M. R., Jennings, I. G., Jans, D. A., Howlett, G. J., Nice, E. C., and Kobe, B. (2001). Biophysical characterization of interactions involving importin-alpha during nuclear import. *The Journal of Biological Chemistry*, 276(36):34189–34198. PMID: 11448961.

[Chen et al., 2005] Chen, M.-H., Ben-Efraim, I., Mitrousis, G., Walker-Kopp, N., Sims, P. J., and Cingolani, G. (2005). Phospholipid scramblase 1 contains a nonclassical nuclear localization signal with unique binding site in importin alpha. *The Journal of Biological Chemistry*, 280(11):10599–10606. PMID: 15611084.

[Chi et al., 1995] Chi, N. C., Adam, E. J., and Adam, S. A. (1995). Sequence and characterization of cytoplasmic nuclear protein import factor p97. *The Journal of Cell Biology*, 130(2):265–274. PMID: 7615630.

[Chook and Blobel, 1999] Chook, Y. M. and Blobel, G. (1999). Structure of the nuclear transport complex karyopherin-beta2-ran x GppNHp. *Nature*, 399(6733):230–237. PMID: 10353245.

[Chook et al., 2002] Chook, Y. M., Jung, A., Rosen, M. K., and Blobel, G. (2002). Uncoupling kapbeta2 substrate dissociation and ran binding. *Biochemistry*, 41(22):6955–6966. PMID: 12033928.

[Chook and Süel, 2010] Chook, Y. M. and Süel, K. E. (2010). Nuclear import by karyopherin-betas: Recognition and inhibition. *Biochimica Et Biophysica Acta*, 9. PMID: 21029754.

[Chuderland et al., 2008] Chuderland, D., Konson, A., and Seger, R. (2008). Identification and characterization of a general nuclear translocation signal in signaling proteins. *Molecular Cell*, 31(6):850–861. PMID: 18760948.

[Chung et al., 2008] Chung, K. M., Cha, S.-S., and Jang, S. K. (2008). A novel function of karyopherin beta3 associated with apolipoprotein a-i secretion. *Molecules and Cells*, 26(3):291–298. PMID: 18562802.

[Cingolani et al., 2002] Cingolani, G., Bednenko, J., Gillespie, M. T., and Gerace, L. (2002). Molecular basis for the recognition of a nonclassical nuclear localization signal by importin beta. *Molecular Cell*, 10(6):1345–1353. PMID: 12504010.

[Cingolani et al., 1999] Cingolani, G., Petosa, C., Weis, K., and Müller, C. W. (1999). Structure of importin-beta bound to the IBB domain of importin-alpha. *Nature*, 399(6733):221–229. PMID: 10353244.

[Conti and Kuriyan, 2000] Conti, E. and Kuriyan, J. (2000). Crystallographic analysis of the specific yet versatile recognition of distinct nuclear localization signals by karyopherin alpha. *Structure*, 8(3):329–338. PMID: 10745017.

[Conti et al., 2006] Conti, E., Müller, C. W., and Stewart, M. (2006). Karyopherin flexibility in nucleocytoplasmic transport. *Current Opinion in Structural Biology*, 16(2):237–244. PMID: 16567089.

[Cook et al., 2007] Cook, A., Bono, F., Jinek, M., and Conti, E. (2007). Structural biology of nucleocytoplasmic transport. *Annual Review of Biochemistry*, 76:647–671. PMID: 17506639.

[Cook et al., 2005] Cook, A., Fernandez, E., Lindner, D., Ebert, J., Schlenstedt, G., and Conti, E. (2005). The structure of the nuclear export receptor cse1 in its cytosolic state reveals a closed conformation incompatible with cargo binding. *Molecular Cell*, 18(3):355–367. PMID: 15866177.

[Cook and Conti, 2010] Cook, A. G. and Conti, E. (2010). Nuclear export complexes in the frame. *Current Opinion in Structural Biology*, 20(2):247–252. PMID: 20171875.

[Cook et al., 2009] Cook, A. G., Fukuhara, N., Jinek, M., and Conti, E. (2009). Structures of the tRNA export factor in the nuclear and cytosolic states. *Nature*, 461(7260):60–65. PMID: 19680239.

[Corbett et al., 1995] Corbett, A. H., Koepp, D. M., Schlenstedt, G., Lee, M. S., Hopper, A. K., and Silver, P. A. (1995). Rna1p, a Ran/TC4 GTPase activating protein, is required for nuclear import. *The Journal of Cell Biology*, 130(5):1017–1026. PMID: 7657689.

[Cordes et al., 1995] Cordes, V. C., Reidenbach, S., and Franke, W. W. (1995). High content of a nuclear pore complex protein in cytoplasmic annulate lamellae of xenopus oocytes. *European Journal of Cell Biology*, 68(3):240–255. PMID: 8603676.

[Cronshaw et al., 2002] Cronshaw, J. M., Krutchinsky, A. N., Zhang, W., Chait, B. T., and Matunis, M. J. (2002). Proteomic analysis of the mammalian nuclear pore complex. *The Journal of Cell Biology*, 158(5):915–927. PMID: 12196509.

[Cutress et al., 2008] Cutress, M. L., Whitaker, H. C., Mills, I. G., Stewart, M., and Neal, D. E. (2008). Structural basis for the nuclear import of the human androgen receptor. *Journal of Cell Science*, 121(Pt 7):957–968. PMID: 18319300.

[de Barros et al., 2012] de Barros, A. C., Takeda, A. A. S., Chang, C. W., Kobe, B., and Fontes, M. R. M. (2012). Structural basis of nuclear import of flap endonuclease 1 (FEN1). *Acta Crystallographica. Section D, Biological Crystallography*, 68(Pt 7):743–750. PMID: 22751659.

[Dean et al., 2001] Dean, K. A., von Ahsen, O., Görlich, D., and Fried, H. M. (2001). Signal recognition particle protein 19 is imported into the nucleus by importin 8 (RanBP8) and transportin. *Journal of Cell Science*, 114(Pt 19):3479–3485. PMID: 11682607.

[Deng et al., 2006] Deng, T., Engelhardt, O. G., Thomas, B., Akoulitchev, A. V., Brownlee, G. G., and Fodor, E. (2006). Role of ran binding protein 5 in nuclear import and assembly of the influenza virus RNA polymerase complex. *Journal of Virology*, 80(24):11911–11919. PMID: 17005651.

[Dias et al., 2009] Dias, S. M. G., Wilson, K. F., Rojas, K. S., Ambrosio, A. L. B., and Cerione, R. A. (2009). The molecular basis for the regulation of the cap-binding complex by the importins. *Nature Structural & Molecular Biology*, 16(9):930–937. PMID: 19668212.

[Dingwall and Laskey, 1991] Dingwall, C. and Laskey, R. A. (1991). Nuclear targeting sequences–a consensus? *Trends in Biochemical Sciences*, 16(12):478–481. PMID: 1664152.

[Dingwall et al., 1982] Dingwall, C., Sharnick, S. V., and Laskey, R. A. (1982). A polypeptide domain that specifies migration of nucleoplasmin into the nucleus. *Cell*, 30(2):449–458. PMID: 6814762.

[Englmeier et al., 2001] Englmeier, L., Fornerod, M., Bischoff, F. R., Petosa, C., Mattaj, I. W., and Kutay, U. (2001). RanBP3 influences interactions between CRM1 and its nuclear protein export substrates. *EMBO Reports*, 2(10):926–932. PMID: 11571268.

[Fischer et al., 1995] Fischer, U., Huber, J., Boelens, W. C., Mattaj, I. W., and Lührmann, R. (1995). The HIV-1 rev activation domain is a nuclear export signal that accesses an export pathway used by specific cellular RNAs. *Cell*, 82(3):475–483. PMID: 7543368.

[Floer et al., 1997] Floer, M., Blobel, G., and Rexach, M. (1997). Disassembly of RanGTP-karyopherin beta complex, an intermediate in nuclear protein import. *The Journal of Biological Chemistry*, 272(31):19538–19546. PMID: 9235958.

[Flotho and Werner, 2012] Flotho, A. and Werner, A. (2012). The RanBP2/RanGAP1*SUMO1/Ubc9 complex: A multisubunit e3 ligase at the intersection of sumoylation and the RanGTPase cycle. *Nucleus (Austin, Tex.)*, 3(5):429–432. PMID: 22925898.

[Fontes et al., 2000] Fontes, M. R., Teh, T., and Kobe, B. (2000). Structural basis of recognition of monopartite and bipartite nuclear localization sequences by mammalian importin-alpha. *Journal of Molecular Biology*, 297(5):1183–1194. PMID: 10764582.

[Fontes et al., 2003a] Fontes, M. R. M., Teh, T., Jans, D., Brinkworth, R. I., and Kobe, B. (2003a). Structural basis for the specificity of bipartite nuclear localization sequence binding by importin-alpha. *The Journal of Biological Chemistry*, 278(30):27981–27987. PMID: 12695505.

[Fontes et al., 2003b] Fontes, M. R. M., Teh, T., Toth, G., John, A., Pavo, I., Jans, D. A., and Kobe, B. (2003b). Role of flanking sequences and phosphorylation in the recognition of the simian-virus-40 large t-antigen nuclear localization sequences by importin-alpha. *The Biochemical Journal*, 375(Pt 2):339–349. PMID: 12852786.

[Fornerod et al., 1997] Fornerod, M., Ohno, M., Yoshida, M., and Mattaj, I. W. (1997). CRM1 is an export receptor for leucine-rich nuclear export signals. *Cell*, 90(6):1051–1060. PMID: 9323133.

[Forwood et al., 2001] Forwood, J. K., Lam, M. H., and Jans, D. A. (2001). Nuclear import of creb and AP-1 transcription factors requires importin-beta 1 and ran but is independent of importin-alpha. *Biochemistry*, 40(17):5208–5217. PMID: 11318643.

[Forwood et al., 2010] Forwood, J. K., Lange, A., Zachariae, U., Marfori, M., Preast, C., Grubmüller, H., Stewart, M., Corbett, A. H., and Kobe, B. (2010). Quantitative structural analysis of importin-beta flexibility: paradigm for solenoid protein structures. *Structure*, 18(9):1171–1183. PMID: 20826343.

[Fribourg et al., 2003] Fribourg, S., Gatfield, D., Izaurralde, E., and Conti, E. (2003). A novel mode of rbd-protein recognition in the y14-mago complex. *Nat.Struct.Biol.*, 10:433–. PubMed ID: 12730685.

[Fukuhara et al., 2004] Fukuhara, N., Fernandez, E., Ebert, J., Conti, E., and Svergun, D. (2004). Conformational variability of nucleo-cytoplasmic transport factors. *The Journal of Biological Chemistry*, 279(3):2176–2181. PMID: 14561738.

[Gehring et al., 2009] Gehring, N. H., Lamprinaki, S., Kulozik, A. E., and Hentze, M. W. (2009). Disassembly of exon junction complexes by PYM. *Cell*, 137(3):536–548. PMID: 19410547.

[Giagtzoglou et al., 2009] Giagtzoglou, N., Lin, Y. Q., Haueter, C., and Bellen, H. J. (2009). Importin 13 regulates neurotransmitter release at the drosophila neuromuscular junction. *The Journal of Neuroscience: The Official Journal of the Society for Neuroscience*, 29(17):5628–5639. PMID: 19403829.

[Gilbert, 1978] Gilbert, W. (1978). Why genes in pieces? *Nature*, 271(5645):501. PMID: 622185.

[Gilchrist et al., 2002] Gilchrist, D., Mykytka, B., and Rexach, M. (2002). Accelerating the rate of disassembly of karyopherin.cargo complexes. *The Journal of Biological Chemistry*, 277(20):18161–18172. PMID: 11867631.

[Giorgi and Moore, 2007] Giorgi, C. and Moore, M. J. (2007). The nuclear nurture and cytoplasmic nature of localized mRNPs. *Seminars in Cell & Developmental Biology*, 18(2):186–193. PMID: 17459736.

[Gontan et al., 2009] Gontan, C., Güttler, T., Engelen, E., Demmers, J., Fornerod, M., Grosveld, F. G., Tibboel, D., Görlich, D., Poot, R. A., and Rottier, R. J. (2009). Exportin 4 mediates a novel nuclear import pathway for sox family transcription factors. *The Journal of Cell Biology*, 185(1):27–34. PMID: 19349578.

[Grünwald et al., 2011] Grünwald, D., Singer, R. H., and Rout, M. (2011). Nuclear export dynamics of RNA-protein complexes. *Nature*, 475(7356):333–341. PMID: 21776079.

[Grünwald and Bono, 2011] Grünwald, M. and Bono, F. (2011). Structure of importin13-ubc9 complex: nuclear import and release of a key regulator of sumoylation. *The EMBO Journal*, 30(2):427–438. PMID: 21139563.

[Grüter et al., 1998] Grüter, P., Tabernero, C., von Kobbe, C., Schmitt, C., Saavedra, C., Bachi, A., Wilm, M., Felber, B. K., and Izaurralde, E. (1998). TAP, the human homolog of mex67p, mediates CTE-dependent RNA export from the nucleus. *Molecular Cell*, 1(5):649–659. PMID: 9660949.

[Gudleski et al., 2010] Gudleski, N., Flanagan, J. M., Ryan, E. P., Bewley, M. C., and Parent, L. J. (2010). Directionality of nucleocytoplasmic transport of the retroviral gag protein depends on sequential binding of karyopherins and viral RNA. *Proceedings of the National Academy of Sciences of the United States of America*, 107(20):9358–9363. PMID: 20435918.

[Gurdon, 1970] Gurdon, J. B. (1970). Nuclear transplantation and the control of gene activity in animal development. *Proceedings of the Royal Society of London. Series B*, 176(44):303–314. PMID: 4395100.

[Görlich et al., 1995] Görlich, D., Kostka, S., Kraft, R., Dingwall, C., Laskey, R. A., Hartmann, E., and Prehn, S. (1995). Two different subunits of importin cooperate to recognize nuclear localization signals and bind them to the nuclear envelope. *Current Biology: CB*, 5(4):383–392. PMID: 7627554.

[Görlich and Kutay, 1999] Görlich, D. and Kutay, U. (1999). Transport between the cell nucleus and the cytoplasm. *Annual Review of Cell and Developmental Biology*, 15:607–660. PMID: 10611974.

[Görlich and Mattaj, 1996] Görlich, D. and Mattaj, I. W. (1996). Nucleocytoplasmic transport. *Science*, 271(5255):1513–1518. PMID: 8599106.

[Görlich et al., 1996] Görlich, D., Panté, N., Kutay, U., Aebi, U., and Bischoff, F. R. (1996). Identification of different roles for RanGDP and RanGTP in nuclear protein import. *The EMBO Journal*, 15(20):5584–5594. PMID: 8896452.

[Görlich et al., 2003] Görlich, D., Seewald, M. J., and Ribbeck, K. (2003). Characterization of ran-driven cargo transport and the RanGTPase system by kinetic measurements and computer simulation. *The EMBO Journal*, 22(5):1088–1100. PMID: 12606574.

[Güttler and Görlich, 2011] Güttler, T. and Görlich, D. (2011). Ran-dependent nuclear export mediators: a structural perspective. *The EMBO Journal*, 30(17):3457–3474. PMID: 21878989.

[Güttler et al., 2010] Güttler, T., Madl, T., Neumann, P., Deichsel, D., Corsini, L., Monecke, T., Ficner, R., Sattler, M., and Görlich, D. (2010). NES consensus redefined by structures of PKI-type and rev-type nuclear export signals bound to CRM1. *Nature Structural & Molecular Biology*, 17(11):1367–1376. PMID: 20972448.

[Hachet and Ephrussi, 2004] Hachet, O. and Ephrussi, A. (2004). Splicing of oskar RNA in the nucleus is coupled to its cytoplasmic localization. *Nature*, 428(6986):959–963. PMID: 15118729.

[Hahn and Schlenstedt, 2011] Hahn, S. and Schlenstedt, G. (2011). Importin beta-type nuclear transport receptors have distinct binding affinities for ran-GTP. *Biochemical and Biophysical Research Communications*, 406(3). PMID: 21329658.

[Heese et al., 2004] Heese, K., Yamada, T., Akatsu, H., Yamamoto, T., Kosaka, K., Nagai, Y., and Sawada, T. (2004). Characterizing the new transcription regulator protein p60TRP. *Journal of Cellular Biochemistry*, 91(5):1030–1042. PMID: 15034937.

[Hintersteiner et al., 2010] Hintersteiner, M., Ambrus, G., Bednenko, J., Schmied, M., Knox, A. J. S., Meisner, N.-C., Gstach, H., Seifert, J.-M., Singer, E. L., Gerace, L., and Auer, M. (2010). Identification of a small molecule inhibitor of importin beta mediated nuclear import by confocal on-bead screening of tagged one-bead one-compound libraries. *ACS Chemical Biology*, 5(10):967–979. PMID: 20677820.

[Hirano and Matsuura, 2011] Hirano, H. and Matsuura, Y. (2011). Sensing actin dynamics: structural basis for g-actin-sensitive nuclear import of MAL. *Biochemical and Biophysical Research Communications*, 414(2):373–378. PMID: 21964294.

[Ho et al., 2000] Ho, J. H., Kallstrom, G., and Johnson, A. W. (2000). Nmd3p is a crm1p-dependent adapter protein for nuclear export of the large ribosomal subunit. *The Journal of Cell Biology*, 151(5):1057–1066. PMID: 11086007.

[Hoelz et al., 2011] Hoelz, A., Debler, E. W., and Blobel, G. (2011). The structure of the nuclear pore complex. *Annual Review of Biochemistry*, 80:613–643. PMID: 21495847.

[Huber et al., 1998] Huber, J., Cronshagen, U., Kadokura, M., Marshallsay, C., Wada, T., Sekine, M., and Lührmann, R. (1998). Snurportin1, an m3G-cap-specific nuclear import receptor with a novel domain structure. *The EMBO Journal*, 17(14):4114–4126. PMID: 9670026.

[Huber et al., 2002] Huber, J., Dickmanns, A., and Lührmann, R. (2002). The importin-beta binding domain of snurportin1 is responsible for the ran- and energy-independent nuclear import of spliceosomal u snRNPs in vitro. *The Journal of Cell Biology*, 156(3):467–479. PMID: 11815630.

[Hutten et al., 2008] Hutten, S., Flotho, A., Melchior, F., and Kehlenbach, R. H. (2008). The nup358-RanGAP complex is required for efficient importin alpha/beta-dependent nuclear import. *Molecular Biology of the Cell*, 19(5):2300–2310. PMID: 18305100.

[Hutten and Kehlenbach, 2006] Hutten, S. and Kehlenbach, R. H. (2006). Nup214 is required for CRM1-dependent nuclear protein export in vivo. *Molecular and Cellular Biology*, 26(18):6772–6785. PMID: 16943420.

[Hutten et al., 2009] Hutten, S., Wälde, S., Spillner, C., Hauber, J., and Kehlenbach, R. H. (2009). The nuclear pore component nup358 promotes transportin-dependent nuclear import. *Journal of Cell Science*, 122(Pt 8):1100–1110. PMID: 19299463.

[Imamoto et al., 1995] Imamoto, N., Tachibana, T., Matsubae, M., and Yoneda, Y. (1995). A karyophilic protein forms a stable complex with cytoplasmic components prior to nuclear pore binding. *The Journal of Biological Chemistry*, 270(15):8559–8565. PMID: 7721756.

[Imasaki et al., 2007] Imasaki, T., Shimizu, T., Hashimoto, H., Hidaka, Y., Kose, S., Imamoto, N., Yamada, M., and Sato, M. (2007). Structural basis for substrate recognition and dissociation by human transportin 1. *Molecular Cell*, 28(1):57–67. PMID: 17936704.

[Izaurralde et al., 1997] Izaurralde, E., Kutay, U., von Kobbe, C., Mattaj, I. W., and Görlich, D. (1997). The asymmetric distribution of the constituents of the ran system is essential for transport into and out of the nucleus. *The EMBO Journal*, 16(21):6535–6547. PMID: 9351834.

[Izaurralde et al., 1995] Izaurralde, E., Lewis, J., Gamberi, C., Jarmolowski, A., McGuigan, C., and Mattaj, I. W. (1995). A cap-binding protein complex mediating u snRNA export. *Nature*, 376(6542):709–712. PMID: 7651522.

[Jackson et al., 2010] Jackson, R. J., Hellen, C. U. T., and Pestova, T. V. (2010). The mechanism of eukaryotic translation initiation and principles of its regulation. *Nature Reviews. Molecular Cell Biology*, 11(2):113–127. PMID: 20094052.

[Johnson and Baines, 2011] Johnson, D. C. and Baines, J. D. (2011). Herpesviruses remodel host membranes for virus egress. *Nature Reviews. Microbiology*, 9(5):382–394. PMID: 21494278.

[Johnson, 2004] Johnson, E. S. (2004). Protein modification by SUMO. *Annual Review of Biochemistry*, 73:355–382. PMID: 15189146.

[Jäkel and Görlich, 1998] Jäkel, S. and Görlich, D. (1998). Importin beta, transportin, RanBP5 and RanBP7 mediate nuclear import of ribosomal proteins in mammalian cells. *The EMBO Journal*, 17(15):4491–4502. PMID: 9687515.

[Jäkel et al., 2002] Jäkel, S., Mingot, J.-M., Schwarzmaier, P., Hartmann, E., and Görlich, D. (2002). Importins fulfil a dual function as nuclear import receptors and cytoplasmic chaperones for exposed basic domains. *The EMBO Journal*, 21(3):377–386. PMID: 11823430.

[Kaffman and O'Shea, 1999] Kaffman, A. and O'Shea, E. K. (1999). Regulation of nuclear localization: a key to a door. *Annual Review of Cell and Developmental Biology*, 15:291–339. PMID: 10611964.

[Kahle et al., 2005] Kahle, J., Baake, M., Doenecke, D., and Albig, W. (2005). Subunits of the heterotrimeric transcription factor NF-Y are imported into the nucleus by distinct pathways involving importin beta and importin 13. *Molecular and Cellular Biology*, 25(13):5339–5354. PMID: 15964792.

[Kahle et al., 2009] Kahle, J., Piaia, E., Neimanis, S., Meisterernst, M., and Doenecke, D. (2009). Regulation of nuclear import and export of negative cofactor 2. *The Journal of Biological Chemistry*, 284(14):9382–9393. PMID: 19204005.

[Kataoka et al., 1999] Kataoka, N., Bachorik, J. L., and Dreyfuss, G. (1999). Transportin-SR, a nuclear import receptor for SR proteins. *The Journal of Cell Biology*, 145(6):1145–1152. PMID: 10366588.

[Kehlenbach et al., 1999] Kehlenbach, R. H., Dickmanns, A., Kehlenbach, A., Guan, T., and Gerace, L. (1999). A role for RanBP1 in the release of CRM1 from the nuclear pore complex in a terminal step of nuclear export. *The Journal of Cell Biology*, 145(4):645–657. PMID: 10330396.

[Klebe et al., 1995] Klebe, C., Bischoff, F. R., Ponstingl, H., and Wittinghofer, A. (1995). Interaction of the nuclear GTP-binding protein ran with its regulatory proteins RCC1 and RanGAP1. *Biochemistry*, 34(2):639–647. PMID: 7819259.

[Kobe, 1999] Kobe, B. (1999). Autoinhibition by an internal nuclear localization signal revealed by the crystal structure of mammalian importin alpha. *Nature Structural Biology*, 6(4):388–397. PMID: 10201409.

[Koyama and Matsuura, 2010] Koyama, M. and Matsuura, Y. (2010). An allosteric mechanism to displace nuclear export cargo from CRM1 and RanGTP by RanBP1. *The EMBO Journal*, 29(12):2002–2013. PMID: 20485264.

[Kurisaki et al., 2006] Kurisaki, A., Kurisaki, K., Kowanetz, M., Sugino, H., Yoneda, Y., Heldin, C.-H., and Moustakas, A. (2006). The mechanism of nuclear export of smad3 involves exportin 4 and ran. *Molecular and Cellular Biology*, 26(4):1318–1332. PMID: 16449645.

[Kutay et al., 1997] Kutay, U., Bischoff, F. R., Kostka, S., Kraft, R., and Görlich, D. (1997). Export of importin alpha from the nucleus is mediated by a specific nuclear transport factor. *Cell*, 90(6):1061–1071. PMID: 9323134.

[Kutay et al., 2000] Kutay, U., Hartmann, E., Treichel, N., Calado, A., Carmo-Fonseca, M., Prehn, S., Kraft, R., Gorlich, D., and Bischoff, F. R. (2000). Identification of two novel RanGTP-binding proteins belonging to the importin beta superfamily. *The Journal of Biological Chemistry*, 275(51):40163–40168. PMID: 11024021.

[Kutay et al., 1998] Kutay, U., Lipowsky, G., Izaurralde, E., Bischoff, F. R., Schwarzmaier, P., Hartmann, E., and Görlich, D. (1998). Identification of a tRNA-specific nuclear export receptor. *Molecular Cell*, 1(3):359–369. PMID: 9660920.

[Lai et al., 2000] Lai, M. C., Lin, R. I., Huang, S. Y., Tsai, C. W., and Tarn, W. Y. (2000). A human importin-beta family protein, transportin-SR2, interacts with the phosphorylated RS domain of SR proteins. *The Journal of Biological Chemistry*, 275(11):7950–7957. PMID: 10713112.

[Lam et al., 2001] Lam, M. H., Hu, W., Xiao, C. Y., Gillespie, M. T., and Jans, D. A. (2001). Molecular dissection of the importin beta1-recognized nuclear targeting signal of parathyroid hormone-related protein. *Biochemical and Biophysical Research Communications*, 282(2):629–634. PMID: 11401507.

[Lange et al., 2008] Lange, A., Mills, R. E., Devine, S. E., and Corbett, A. H. (2008). A PY-NLS nuclear targeting signal is required for nuclear localization and function of the saccharomyces cerevisiae mRNA-binding protein hrp1. *The Journal of Biological Chemistry*, 283(19):12926–12934. PMID: 18343812.

[Lau et al., 2003] Lau, C.-K., Diem, M. D., Dreyfuss, G., and Van Duyne, G. D. (2003). Structure of the y14-magoh core of the exon junction complex. *Current Biology: CB*, 13(11):933–941. PMID: 12781131.

[Le Hir et al., 2000] Le Hir, H., Izaurralde, E., Maquat, L. E., and Moore, M. J. (2000). The spliceosome deposits multiple proteins 20-24 nucleotides upstream of mRNA exon-exon junctions. *The EMBO Journal*, 19(24):6860–6869. PMID: 11118221.

[Lee et al., 2006] Lee, B. J., Cansizoglu, A. E., Süel, K. E., Louis, T. H., Zhang, Z., and Chook, Y. M. (2006). Rules for nuclear localization sequence recognition by karyopherin beta 2. *Cell*, 126(3):543–558. PMID: 16901787.

[Lee et al., 2005] Lee, S. J., Matsuura, Y., Liu, S. M., and Stewart, M. (2005). Structural basis for nuclear import complex dissociation by RanGTP. *Nature*, 435(7042):693–696. PMID: 15864302.

[Lee et al., 2003] Lee, S. J., Sekimoto, T., Yamashita, E., Nagoshi, E., Nakagawa, A., Imamoto, N., Yoshimura, M., Sakai, H., Chong, K. T., Tsukihara, T., and Yoneda, Y. (2003). The structure of importin-beta bound to SREBP-2: nuclear import of a transcription factor. *Science*, 302(5650):1571–1575. PMID: 14645851.

[Liang et al., 2008] Liang, J., Ke, G., You, W., Peng, Z., Lan, J., Kalesse, M., Tartakoff, A. M., Kaplan, F., and Tao, T. (2008). Interaction between importin 13 and myopodin suggests a nuclear import pathway for myopodin. *Molecular and Cellular Biochemistry*, 307(1-2):93–100. PMID: 17828378.

[Lin et al., 2009] Lin, W., Ye, W., Cai, L., Meng, X., Ke, G., Huang, C., Peng, Z., Yu, Y., Golden, J. A., Tartakoff, A. M., and Tao, T. (2009). The roles of multiple importins for nuclear import of murine aristaless-related homeobox protein. *The Journal of Biological Chemistry*, 284(30):20428–20439. PMID: 19494118.

[Lindsay et al., 2001] Lindsay, M. E., Holaska, J. M., Welch, K., Paschal, B. M., and Macara, I. G. (2001). Ran-binding protein 3 is a cofactor for crm1-mediated nuclear protein export. *The Journal of Cell Biology*, 153(7):1391–1402. PMID: 11425870.

[Lipowsky et al., 1999] Lipowsky, G., Bischoff, F. R., Izaurralde, E., Kutay, U., Schäfer, S., Gross, H. J., Beier, H., and Görlich, D. (1999). Coordination of tRNA nuclear export with processing of tRNA. *RNA*, 5(4):539–549. PMID: 10199570.

[Lipowsky et al., 2000] Lipowsky, G., Bischoff, F. R., Schwarzmaier, P., Kraft, R., Kostka, S., Hartmann, E., Kutay, U., and Görlich, D. (2000). Exportin 4: a mediator of a novel nuclear export pathway in higher eukaryotes. *The EMBO Journal*, 19(16):4362–4371. PMID: 10944119.

[Liu and Stewart, 2005] Liu, S. M. and Stewart, M. (2005). Structural basis for the high-affinity binding of nucleoporin nup1p to the saccharomyces cerevisiae importin-beta homologue, kap95p. *Journal of Molecular Biology*, 349(3):515–525. PMID: 15878174.

[Lott et al., 2011] Lott, K., Bhardwaj, A., Sims, P. J., and Cingolani, G. (2011). A minimal nuclear localization signal (NLS) in human phospholipid scramblase 4 that binds only the minor NLS-binding site of importin alpha1. *The Journal of Biological Chemistry*, 286(32):28160–28169. PMID: 21690087.

[Lounsbury and Macara, 1997] Lounsbury, K. M. and Macara, I. G. (1997). Ran-binding protein 1 (RanBP1) forms a ternary complex with ran and karyopherin beta and reduces ran GTPase-activating protein (RanGAP) inhibition by karyopherin beta. *The Journal of Biological Chemistry*, 272(1):551–555. PMID: 8995296.

[Marfori et al., 2011] Marfori, M., Mynott, A., Ellis, J. J., Mehdi, A. M., Saunders, N. F. W., Curmi, P. M., Forwood, J. K., Bodén, M., and Kobe, B. (2011). Molecular basis for specificity of nuclear import and prediction of nuclear localization. *Biochimica Et Biophysica Acta*, 1813(9):1562–1577. PMID: 20977914.

[Martin and Koonin, 2006] Martin, W. and Koonin, E. V. (2006). Introns and the origin of nucleus-cytosol compartmentalization. *Nature*, 440(7080):41–45. PMID: 16511485.

[Mason et al., 2009] Mason, D. A., Stage, D. E., and Goldfarb, D. S. (2009). Evolution of the metazoan-specific importin alpha gene family. *Journal of Molecular Evolution*, 68(4):351–365. PMID: 19308634.

[Matsuura et al., 2003] Matsuura, Y., Lange, A., Harreman, M. T., Corbett, A. H., and Stewart, M. (2003). Structural basis for nup2p function in cargo release and karyopherin recycling in nuclear import. *The EMBO Journal*, 22(20):5358–5369. PMID: 14532109.

[Matsuura and Stewart, 2004] Matsuura, Y. and Stewart, M. (2004). Structural basis for the assembly of a nuclear export complex. *Nature*, 432(7019):872–877.

[Matsuura and Stewart, 2005] Matsuura, Y. and Stewart, M. (2005). Nup50/Npap60 function in nuclear protein import complex disassembly and importin recycling. *The EMBO Journal*, 24(21):3681–3689. PMID: 16222336.

[Mattaj and Englmeier, 1998] Mattaj, I. W. and Englmeier, L. (1998). Nucleocytoplasmic transport: the soluble phase. *Annual Review of Biochemistry*, 67:265–306. PMID: 9759490.

[Matunis et al., 1998] Matunis, M. J., Wu, J., and Blobel, G. (1998). SUMO-1 modification and its role in targeting the ran GTPase-activating protein, RanGAP1, to the nuclear pore complex. *The Journal of Cell Biology*, 140(3):499–509. PMID: 9456312.

[Melchior, 2000] Melchior, F. (2000). SUMO–nonclassical ubiquitin. *Annual Review of Cell and Developmental Biology*, 16:591–626. PMID: 11031248.

[Melchior et al., 1993] Melchior, F., Paschal, B., Evans, J., and Gerace, L. (1993). Inhibition of nuclear protein import by nonhydrolyzable analogues of GTP and identification of the small GTPase Ran/TC4 as an essential transport factor. *The Journal of Cell Biology*, 123(6 Pt 2):1649–1659. PMID: 8276887.

[Mingot et al., 2004] Mingot, J.-M., Bohnsack, M. T., Jäkle, U., and Görlich, D. (2004). Exportin 7 defines a novel general nuclear export pathway. *The EMBO Journal*, 23(16):3227–3236. PMID: 15282546.

[Mingot et al., 2001] Mingot, J. M., Kostka, S., Kraft, R., Hartmann, E., and Görlich, D. (2001). Importin 13: a novel mediator of nuclear import and export. *The EMBO Journal*, 20(14):3685–3694. PMID: 11447110.

[Mitrousis et al., 2008] Mitrousis, G., Olia, A. S., Walker-Kopp, N., and Cingolani, G. (2008). Molecular basis for the recognition of snurportin 1 by importin beta. *The Journal of Biological Chemistry*, 283(12):7877–7884. PMID: 18187419.

[Miyauchi et al., 2005] Miyauchi, Y., Michigami, T., Sakaguchi, N., Sekimoto, T., Yoneda, Y., Pike, J. W., Yamagata, M., and Ozono, K. (2005). Importin 4 is responsible for ligand-independent nuclear translocation of vitamin d receptor. *The Journal of Biological Chemistry*, 280(49):40901–40908. PMID: 16207705.

[Mohr et al., 2009] Mohr, D., Frey, S., Fischer, T., Güttler, T., and Görlich, D. (2009). Characterisation of the passive permeability barrier of nuclear pore complexes. *The EMBO Journal*, 28(17):2541–2553. PMID: 19680228.

[Monecke et al., 2009] Monecke, T., Güttler, T., Neumann, P., Dickmanns, A., Görlich, D., and Ficner, R. (2009). Crystal structure of the nuclear export receptor CRM1 in complex with snurportin1 and RanGTP. *Science*, 324(5930):1087–1091. PMID: 19389996.

[Moore et al., 1999] Moore, J. D., Yang, J., Truant, R., and Kornbluth, S. (1999). Nuclear import of cdk/cyclin complexes: identification of distinct mechanisms for import of cdk2/cyclin e and cdc2/cyclin b1. *The Journal of Cell Biology*, 144(2):213–224. PMID: 9922449.

[Moore and Blobel, 1993] Moore, M. S. and Blobel, G. (1993). The GTP-binding protein Ran/TC4 is required for protein import into the nucleus. *Nature*, 365(6447):661–663. PMID: 8413630.

[Moroianu et al., 1995] Moroianu, J., Blobel, G., and Radu, A. (1995). Previously identified protein of uncertain function is karyopherin alpha and together with karyopherin beta docks import substrate at nuclear pore complexes. *Proceedings of the National Academy of Sciences of the United States of America*, 92(6):2008–2011. PMID: 7892216.

[Mosammaparast and Pemberton, 2004] Mosammaparast, N. and Pemberton, L. F. (2004). Karyopherins: from nuclear-transport mediators to nuclear-function regulators. *Trends in Cell Biology*, 14(10):547–556. PMID: 15450977.

[Moutty et al., 2011] Moutty, M. C., Sakin, V., and Melchior, F. (2011). Importin {alpha}/{beta} mediates nuclear import of individual SUMO e1 subunits and of the holo-enzyme. *Molecular Biology of the Cell*. PMID: 21209321.

[Moy and Silver, 2002] Moy, T. I. and Silver, P. A. (2002). Requirements for the nuclear export of the small ribosomal subunit. *Journal of Cell Science*, 115(Pt 14):2985–2995. PMID: 12082158.

[Mynott et al., 2011] Mynott, A. V., Harrop, S. J., Brown, L. J., Breit, S. N., Kobe, B., and Curmi, P. M. G. (2011). Crystal structure of importin-alpha bound to a peptide bearing the nuclear localisation signal from chloride intracellular channel protein 4. *The FEBS Journal*, 278(10):1662–1675. PMID: 21388519.

[Mühlhäusser et al., 2001] Mühlhäusser, P., Müller, E. C., Otto, A., and Kutay, U. (2001). Multiple pathways contribute to nuclear import of core histones. *EMBO Reports*, 2(8):690–696. PMID: 11493596.

[Nemergut and Macara, 2000] Nemergut, M. E. and Macara, I. G. (2000). Nuclear import of the ran exchange factor, RCC1, is mediated by at least two distinct mechanisms. *The Journal of Cell Biology*, 149(4):835–850. PMID: 10811825.

[Niesen et al., 2007] Niesen, F. H., Berglund, H., and Vedadi, M. (2007). The use of differential scanning fluorimetry to detect ligand interactions that promote protein stability. *Nature Protocols*, 2(9):2212–2221. PMID: 17853878.

[Okada et al., 2009] Okada, C., Yamashita, E., Lee, S. J., Shibata, S., Katahira, J., Nakagawa, A., Yoneda, Y., and Tsukihara, T. (2009). A high-resolution structure of the pre-microRNA nuclear export machinery. *Science*, 326(5957):1275–1279. PMID: 19965479.

[O'Reilly et al., 2011] O'Reilly, A. J., Dacks, J. B., and Field, M. C. (2011). Evolution of the karyopherin-beta family of nucleocytoplasmic transport factors; ancient origins and continued specialization. *PloS One*, 6(4):e19308. PMID: 21556326.

[Paine and Feldherr, 1972] Paine, P. L. and Feldherr, C. M. (1972). Nucleocytoplasmic exchange of macromolecules. *Experimental Cell Research*, 74(1):81–98. PMID: 4342186.

[Palacios et al., 1996] Palacios, I., Weis, K., Klebe, C., Mattaj, I. W., and Dingwall, C. (1996). RAN/TC4 mutants identify a common requirement for snRNP and protein import into the nucleus. *The Journal of Cell Biology*, 133(3):485–494. PMID: 8636225.

[Palacios et al., 2004] Palacios, I. M., Gatfield, D., St Johnston, D., and Izaurralde, E. (2004). An eIF4AIII-containing complex required for mRNA localization and nonsense-mediated mRNA decay. *Nature*, 427(6976):753–757. PMID: 14973490.

[Paraskeva et al., 1999] Paraskeva, E., Izaurralde, E., Bischoff, F. R., Huber, J., Kutay, U., Hartmann, E., Lührmann, R., and Görlich, D. (1999). CRM1-mediated recycling of snurportin 1 to the cytoplasm. *The Journal of Cell Biology*, 145(2):255–264. PMID: 10209022.

[Partridge and Schwartz, 2009] Partridge, J. R. and Schwartz, T. U. (2009). Crystallographic and biochemical analysis of the ran-binding zinc finger domain. *Journal of Molecular Biology*, 391(2):375–389. PMID: 19505478.

[Plafker et al., 2004] Plafker, S. M., Plafker, K. S., Weissman, A. M., and Macara, I. G. (2004). Ubiquitin charging of human class III ubiquitin-conjugating enzymes triggers their nuclear import. *The Journal of Cell Biology*, 167(4):649–659. PMID: 15545318.

[Ploski et al., 2004] Ploski, J. E., Shamsher, M. K., and Radu, A. (2004). Paired-type homeodomain transcription factors are imported into the nucleus by karyopherin 13. *Molecular and Cellular Biology*, 24(11):4824–4834. PMID: 15143176.

[Pradeepa et al., 2008] Pradeepa, M. M., Manjunatha, S., Sathish, V., Agrawal, S., and Rao, M. R. S. (2008). Involvement of importin-4 in the transport of transition protein 2 into the spermatid nucleus. *Molecular and Cellular Biology*, 28(13):4331–4341. PMID: 17682055.

[Radu et al., 1995] Radu, A., Blobel, G., and Moore, M. S. (1995). Identification of a protein complex that is required for nuclear protein import and mediates docking of import substrate to distinct nucleoporins. *Proceedings of the National Academy of Sciences of the United States of America*, 92(5):1769–1773. PMID: 7878057.

[Reichelt et al., 1990] Reichelt, R., Holzenburg, A., Buhle, E L, J., Jarnik, M., Engel, A., and Aebi, U. (1990). Correlation between structure and mass distribution of the nuclear pore complex and of distinct pore complex components. *The Journal of Cell Biology*, 110(4):883–894. PMID: 2324201.

[Reverter and Lima, 2005] Reverter, D. and Lima, C. D. (2005). Insights into e3 ligase activity revealed by a SUMO-RanGAP1-Ubc9-Nup358 complex. *Nature*, 435(7042):687–692. PMID: 15931224.

[Ribbeck et al., 1998] Ribbeck, K., Lipowsky, G., Kent, H. M., Stewart, M., and Görlich, D. (1998). NTF2 mediates nuclear import of ran. *The EMBO Journal*, 17(22):6587–6598. PMID: 9822603.

[Richards et al., 1997] Richards, S. A., Carey, K. L., and Macara, I. G. (1997). Requirement of guanosine triphosphate-bound ran for signal-mediated nuclear protein export. *Science*, 276(5320):1842–1844. PMID: 9188526.

[Riddick and Macara, 2007] Riddick, G. and Macara, I. G. (2007). The adapter importin-alpha provides flexible control of nuclear import at the expense of efficiency. *Molecular Systems Biology*, 3:118. PMID: 17551513.

[Rodriguez et al., 2001] Rodriguez, M. S., Dargemont, C., and Hay, R. T. (2001). SUMO-1 conjugation in vivo requires both a consensus modification motif and nuclear targeting. *The Journal of Biological Chemistry*, 276(16):12654–12659. PMID: 11124955.

[Ross et al., 2003] Ross, A. E., Vuica, M., and Desiderio, S. (2003). Overlapping signals for protein degradation and nuclear localization define a role for intrinsic RAG-2 nuclear uptake in dividing cells. *Molecular and Cellular Biology*, 23(15):5308–5319. PMID: 12861017.

[Rout and Aitchison, 2001] Rout, M. P. and Aitchison, J. D. (2001). The nuclear pore complex as a transport machine. *The Journal of Biological Chemistry*, 276(20):16593–16596. PMID: 11283009.

[Rout et al., 2000] Rout, M. P., Aitchison, J. D., Suprapto, A., Hjertaas, K., Zhao, Y., and Chait, B. T. (2000). The yeast nuclear pore complex: composition, architecture, and transport mechanism. *The Journal of Cell Biology*, 148(4):635–651. PMID: 10684247.

[Rout and Blobel, 1993] Rout, M. P. and Blobel, G. (1993). Isolation of the yeast nuclear pore complex. *The Journal of Cell Biology*, 123(4):771–783. PMID: 8227139.

[Scheffzek et al., 1995] Scheffzek, K., Klebe, C., Fritz-Wolf, K., Kabsch, W., and Wittinghofer, A. (1995). Crystal structure of the nuclear ras-related protein ran in its GDP-bound form. *Nature*, 374(6520):378–381. PMID: 7885480.

[Schlenstedt et al., 1995] Schlenstedt, G., Saavedra, C., Loeb, J. D., Cole, C. N., and Silver, P. A. (1995). The GTP-bound form of the yeast Ran/TC4 homologue blocks nuclear protein import and appearance of poly(a)+ RNA in the cytoplasm. *Proceedings of the National Academy of Sciences of the United States of America*, 92(1):225–229. PMID: 7816822.

[Segref et al., 1997] Segref, A., Sharma, K., Doye, V., Hellwig, A., Huber, J., Lührmann, R., and Hurt, E. (1997). Mex67p, a novel factor for nuclear mRNA export, binds to both poly(a)+ RNA and nuclear pores. *The EMBO Journal*, 16(11):3256–3271. PMID: 9214641.

[Shi and Xu, 2003] Shi, H. and Xu, R.-M. (2003). Crystal structure of the drosophila mago nashi-y14 complex. *Genes & Development*, 17(8):971–976. PMID: 12704080.

[Shulga and Goldfarb, 2003] Shulga, N. and Goldfarb, D. S. (2003). Binding dynamics of structural nucleoporins govern nuclear pore complex permeability and may mediate channel gating. *Molecular and Cellular Biology*, 23(2):534–542. PMID: 12509452.

[Smart et al., 2012] Smart, O. S., Womack, T. O., Flensburg, C., Keller, P., Paciorek, W., Sharff, A., Vonrhein, C., and Bricogne, G. (2012). Exploiting structure similarity in refinement: automated NCS and target-structure restraints in BUSTER. *Acta Crystallographica Section D Biological Crystallography*, 68(4):368–380.

[Smith et al., 1998] Smith, A., Brownawell, A., and Macara, I. G. (1998). Nuclear import of ran is mediated by the transport factor NTF2. *Current Biology: CB*, 8(25):1403–1406. PMID: 9889103.

[Solsbacher et al., 1998] Solsbacher, J., Maurer, P., Bischoff, F. R., and Schlenstedt, G. (1998). Cse1p is involved in export of yeast importin alpha from the nucleus. *Molecular and Cellular Biology*, 18(11):6805–6815. PMID: 9774694.

[Speese et al., 2012] Speese, S. D., Ashley, J., Jokhi, V., Nunnari, J., Barria, R., Li, Y., Ataman, B., Koon, A., Chang, Y.-T., Li, Q., Moore, M. J., and Budnik, V. (2012). Nuclear envelope budding enables large ribonucleoprotein particle export during synaptic wnt signaling. *Cell*, 149(4):832–846. PMID: 22579286.

[Stewart, 2007] Stewart, M. (2007). Molecular mechanism of the nuclear protein import cycle. *Nature Reviews. Molecular Cell Biology*, 8(3):195–208. PMID: 17287812.

[Stewart et al., 1998] Stewart, M., Kent, H. M., and McCoy, A. J. (1998). Structural basis for molecular recognition between nuclear transport factor 2 (NTF2) and the GDP-bound form of the ras-family GTPase ran. *Journal of Molecular Biology*, 277(3):635–646. PMID: 9533885.

[Stüven et al., 2003] Stüven, T., Hartmann, E., and Görlich, D. (2003). Exportin 6: a novel nuclear export receptor that is specific for profilin.actin complexes. *The EMBO Journal*, 22(21):5928–5940. PMID: 14592989.

[Süel et al., 2006] Süel, K. E., Cansizoglu, A. E., and Chook, Y. M. (2006). Atomic resolution structures in nuclear transport. *Methods*, 39(4):342–355. PMID: 16938467.

[Takeda et al., 2011] Takeda, A. A. S., de Barros, A. C., Chang, C.-W., Kobe, B., and Fontes, M. R. M. (2011). Structural basis of importin-alpha-mediated nuclear transport for ku70 and ku80. *Journal of Molecular Biology*, 412(2):226–234. PMID: 21806995.

[Talcott and Moore, 2000] Talcott, B. and Moore, M. S. (2000). The nuclear import of RCC1 requires a specific nuclear localization sequence receptor, karyopherin alpha3/Qip. *The Journal of Biological Chemistry*, 275(14):10099–10104. PMID: 10744690.

[Tao et al., 2006] Tao, T., Lan, J., Lukacs, G. L., Haché, R. J. G., and Kaplan, F. (2006). Importin 13 regulates nuclear import of the glucocorticoid receptor in airway epithelial cells. *American Journal of Respiratory Cell and Molecular Biology*, 35(6):668–680. PMID: 16809634.

[Tarendeau et al., 2007] Tarendeau, F., Boudet, J., Guilligay, D., Mas, P. J., Bougault, C. M., Boulo, S., Baudin, F., Ruigrok, R. W. H., Daigle, N., Ellenberg, J., Cusack, S., Simorre, J.-P., and Hart, D. J. (2007). Structure and nuclear import function of the c-terminal domain of influenza virus polymerase PB2 subunit. *Nature Structural & Molecular Biology*, 14(3):229–233. PMID: 17310249.

[Truant and Cullen, 1999] Truant, R. and Cullen, B. R. (1999). The arginine-rich domains present in human immunodeficiency virus type 1 tat and rev function as direct importin beta-dependent nuclear localization signals. *Molecular and Cellular Biology*, 19(2):1210–1217. PMID: 9891055.

[Truant et al., 1998] Truant, R., Fridell, R. A., Benson, R. E., Bogerd, H., and Cullen, B. R. (1998). Identification and functional characterization of a novel nuclear localization signal present in the yeast nab2 poly(a)+ RNA binding protein. *Molecular and Cellular Biology*, 18(3):1449–1458. PMID: 9488461.

[Truant et al., 1999] Truant, R., Kang, Y., and Cullen, B. R. (1999). The human tap nuclear RNA export factor contains a novel transportin-dependent nuclear localization signal that lacks nuclear export signal function. *The Journal of Biological Chemistry*, 274(45):32167–32171. PMID: 10542253.

[Vasu and Forbes, 2001] Vasu, S. K. and Forbes, D. J. (2001). Nuclear pores and nuclear assembly. *Current Opinion in Cell Biology*, 13(3):363–375. PMID: 11343909.

[Vetter et al., 1999a] Vetter, I. R., Arndt, A., Kutay, U., Görlich, D., and Wittinghofer, A. (1999a). Structural view of the ran-importin beta interaction at 2.3 a resolution. *Cell*, 97(5):635–646. PMID: 10367892.

[Vetter et al., 1999b] Vetter, I. R., Nowak, C., Nishimoto, T., Kuhlmann, J., and Wittinghofer, A. (1999b). Structure of a ran-binding domain complexed with ran bound to a GTP analogue: implications for nuclear transport. *Nature*, 398(6722):39–46. PMID: 10078529.

[Waldmann et al., 2007] Waldmann, I., Wälde, S., and Kehlenbach, R. H. (2007). Nuclear import of c-jun is mediated by multiple transport receptors. *The Journal of Biological Chemistry*, 282(38):27685–27692. PMID: 17652081.

[Walker et al., 2009] Walker, P., Doenecke, D., and Kahle, J. (2009). Importin 13 mediates nuclear import of histone fold-containing chromatin accessibility complex heterodimers. *The Journal of Biological Chemistry*, 284(17):11652–11662. PMID: 19218565.

[Wang et al., 2007] Wang, J., Hu, W., Cai, S., Lee, B., Song, J., and Chen, Y. (2007). The intrinsic affinity between e2 and the cys domain of e1 in ubiquitin-like modifications. *Molecular Cell*, 27(2):228–237. PMID: 17643372.

[Weinmann et al., 2009] Weinmann, L., Höck, J., Ivacevic, T., Ohrt, T., Mütze, J., Schwille, P., Kremmer, E., Benes, V., Urlaub, H., and Meister, G. (2009). Importin 8 is a gene silencing factor that targets argonaute proteins to distinct mRNAs. *Cell*, 136(3):496–507. PMID: 19167051.

[Weis et al., 1996] Weis, K., Dingwall, C., and Lamond, A. I. (1996). Characterization of the nuclear protein import mechanism using ran mutants with altered nucleotide binding specificities. *The EMBO Journal*, 15(24):7120–7128. PMID: 9003787.

[Wen et al., 1995] Wen, W., Meinkoth, J. L., Tsien, R. Y., and Taylor, S. S. (1995). Identification of a signal for rapid export of proteins from the nucleus. *Cell*, 82(3):463–473. PMID: 7634336.

[Wild et al., 2010] Wild, T., Horvath, P., Wyler, E., Widmann, B., Badertscher, L., Zemp, I., Kozak, K., Csucs, G., Lund, E., and Kutay, U. (2010). A protein inventory of human ribosome biogenesis reveals an essential function of exportin 5 in 60S subunit export. *PLoS Biology*, 8(10):e1000522. PMID: 21048991.

[Wohlwend et al., 2007] Wohlwend, D., Strasser, A., Dickmanns, A., and Ficner, R. (2007). Structural basis for RanGTP independent entry of spliceosomal u snRNPs into the nucleus. *Journal of Molecular Biology*, 374(4):1129–1138. PMID: 18028944.

[Wälde et al., 2012] Wälde, S., Thakar, K., Hutten, S., Spillner, C., Nath, A., Rothbauer, U., Wiemann, S., and Kehlenbach, R. H. (2012). The nucleoporin Nup358/RanBP2 promotes nuclear import in a cargo- and transport receptor-specific manner. *Traffic*, 13(2):218–233. PMID: 21995724.

[Xu et al., 2012] Xu, D., Grishin, N. V., and Chook, Y. M. (2012). NESdb: a database of NES-containing CRM1 cargoes. *Molecular Biology of the Cell*, 23(18):3673–3676. PMID: 22833564.

[Yamaguchi et al., 2006] Yamaguchi, Y. L., Tanaka, S. S., Yasuda, K., Matsui, Y., and Tam, P. P. L. (2006). Stage-specific importin13 activity influences meiosis of germ cells in the mouse. *Developmental Biology*, 297(2):350–360. PMID: 16908015.

[Yang et al., 1998] Yang, Q., Rout, M. P., and Akey, C. W. (1998). Three-dimensional architecture of the isolated yeast nuclear pore complex: functional and evolutionary implications. *Molecular Cell*, 1(2):223–234. PMID: 9659919.

[Yao et al., 2008] Yao, X., Chen, X., Cottonham, C., and Xu, L. (2008). Preferential utilization of imp7/8 in nuclear import of smads. *The Journal of Biological Chemistry*, 283(33):22867–22874. PMID: 18519565.

[Yasuhara et al., 2007] Yasuhara, N., Shibazaki, N., Tanaka, S., Nagai, M., Kamikawa, Y., Oe, S., Asally, M., Kamachi, Y., Kondoh, H., and Yoneda, Y. (2007). Triggering neural differentiation of ES cells by subtype switching of importin-alpha. *Nature Cell Biology*, 9(1):72–79. PMID: 17159997.

[Yi et al., 2003] Yi, R., Qin, Y., Macara, I. G., and Cullen, B. R. (2003). Exportin-5 mediates the nuclear export of pre-microRNAs and short hairpin RNAs. *Genes & Development*, 17(24):3011–3016. PMID: 14681208.

[Yoshida and Blobel, 2001] Yoshida, K. and Blobel, G. (2001). The karyopherin Kap142p/Msn5p mediates nuclear import and nuclear export of different cargo proteins. *The Journal of Cell Biology*, 152(4):729–740. PMID: 11266464.

[Zeng and Cullen, 2004] Zeng, Y. and Cullen, B. R. (2004). Structural requirements for pre-microRNA binding and nuclear export by exportin 5. *Nucleic Acids Research*, 32(16):4776–4785. PMID: 15356295.

[Zhang et al., 2000] Zhang, C., Sweezey, N. B., Gagnon, S., Muskat, B., Koehler, D., Post, M., and Kaplan, F. (2000). A novel karyopherin-beta homolog is developmentally and hormonally regulated in fetal lung. *American Journal of Respiratory Cell and Molecular Biology*, 22(4):451–459. PMID: 10745026.

Abbreviations

αIBB	**IBB** domain of Imp**α**
Å	Ångstroem
aa-tRNA	**a**mino-**a**cetylated-tRNA
Ago	**ar**g**o**naut
AP-1	**a**daptor related **p**rotein
Arm	**Arm**adillo
Arx	**A**ristaless-**r**elated homeobo**x** protein
ASF	**A**nti-**S**ilencing **f**unction protein
ATP	**a**denosin**t**ri**p**hosphate
BP	**B**inding **p**rotein
Btz	**B**aren**tz**
CAS	**c**ellular **a**poptosis **s**usceptibility
Cbc	**c**ap-**b**inding-**c**omplex
CHRAC	**chr**omatin **a**cessibility **c**omplex protein
CLIC	**c**h**l**oride **i**ntracellular **c**hannel protein 4
cNLS	**c**lassical **NLS**
CNS	**C**rystallography & **N**MR **S**ystem
CREB	**c**AMP-**r**esponsive **e**lement-**b**inding protein
Crm1	**c**hromosome **r**egion **m**aintenance **1**
Crx	**c**one-**r**od homeobo**x** protein
Cse1	**c**hromosome **se**gregation **1**
D. melanogaster	*Drosophila melanogaster*
DNA	**d**eoxyribo**n**uleic **a**cid
dsRNA	**d**ouble-**s**tranded RNA
E. coli	*Escherichia coli*
eIF	**e**ukaryotic translation **i**nitiation **f**actor
eEF	**e**ukaryotic translation **e**longation **f**actor
ERK	**e**xtracellular signal-**r**egulated **k**inase
EJC	**e**xon **j**unction **c**omplex
Exp	**exp**ortin
Fen1	**F**lap **en**donuclease **1**
FG-repeat	**p**henylalanine-**g**lycine-repeat
GDP	**g**uanosin**di****p**hosphate
GR	**g**lucocorticoid **r**ecetpor
GSH	glutathione
GTP	**g**uanosin**t**ri**p**hosphate
GTPase	GTP hydrolase
HEAT	**H**untingtin, **e**longation factor 3 protein phosphatase 2**A**, PI3-kinase **T**OR1

HFM	**h**istone **f**old **m**otif
HIV	**h**uman **i**mmunodeficiency **v**irus
hnRNP	**h**eterogeneous **n**uclear **r**ibo**n**ucleo**p**rotein
HSP	**h**eat **s**hock **p**rotein
IBB	**I**mportin-**b**eta-**b**inding
Imp	**Imp**ortin
Kap	**ka**ryo**p**herin
K_D	**d**issociation **c**onstant
kDa	**k**ilo**da**lton
m3G	2,2,7-tri**m**etyhl **g**uanosine (cap)
MEK	mitogen-activated-protein-kinase (**M**APK) **E**RK **k**inase
Mex67	**m**RNA **ex**port factor **67**
MDa	**m**ega**da**lton
MR	**M**olecular **R**eplacement
mRNA	**m**essenger **RNA**
Msn5	**m**ulticopy **s**uppressor of S**N**F1 mutation
Mtr2	**m**RNA **t**ransport **r**egulator **2**
N1N2	Histone-binding protein **N1**/**N2**
NC2	**n**egative **c**ofactor **2**
ncNLS	**n**on-**c**lassical **NLS**
NCS	**n**on-**c**rystallographic **s**ymmetry
NE	**n**uclear **e**nvelope
NES	**n**uclear **e**xport **s**ignal
NF-YB / YC	**n**uclear transcription **f**actor **YB** / **YC**
NLS	**n**uclear **l**ocalization **s**ignal
NMD	**n**onsense-**m**ediated mRNA **d**ecay
NPC	**n**uclear **p**ore **c**omplex
NTF2	**n**uclear **t**ransport **f**actor **2**
Nup	**nu**cleo**p**orin
NXF	**n**uclear RNA e**x**port **f**actor 1
NXT	**N**TF-2 related e**x**por**t** protein
p60TRP	**p60**-**t**ranscription-**r**egulator-**p**rotein
PA	**p**olymerase **a**cidic protein
Pax	**pa**ired bo**x** protein
PB	**p**olymerase **b**asic protein
PDB	**p**rotein **d**ata **b**ank
Phax	**ph**osphorylated **a**dapter RNA e**x**port protein
Pho	**ph**osphate system p**o**sitive regulatory protein
PIC	**p**re-**i**nitiation **c**omplex
PQBP	**p**olyglutamine (**Q**)-**b**inding **p**rotein
pre-miRNA	**pre**-**mi**cro **RNA**

PTHrP	**p**ara**t**hyroid **h**ormone-**r**elated **p**rotein
PY-NLS	**p**rolin-t**y**rosine-**NLS**
Rag-2	V(D)J **r**ecombination-**a**ctivating **p**rotein-2
Ran	**Ra**s-related **n**uclear antigen
RanBP	**Ran**-**b**inding-**p**rotein
RanGAP	**Ran** **G**TPase-**a**ctivating-**p**rotein
Ras	**Ra**t **s**arcoma
RB1	**r**etino**b**lastoma-associated protein **1**
RCC1	**r**egulator of **c**hromosome **c**ondensation **1**
Rev	**r**egulator of **e**xpression of **v**iral proteins
RhoGAP	**Rho** **G**TPase-**a**ctivating-**p**rotein
RNA	**r**ibo**n**ucleic **a**cid
RNP	**r**ibo**n**uleo**p**rotein
RPA	**r**eplication **p**rotein **A**
RRM	**RNA**-**r**ecognition **m**otif
rPL5	**r**ibosomal **p**rotein **L5**
S. cerevisiae	*Saccharomyces cerevisiae*
SAD	**s**ingle wavelength **a**nomalous **d**ispersion
SAE	**S**UMO-**a**ctivating **e**nzyme subunit 1
SeMet	**se**leno-**met**hionine
sIBB	**IBB** domain of **S**nurportin1
Smad	**m**others **a**gainst **d**ecapentaplegic homolog
snRNP	**s**mall **n**uclear **r**ibo**n**uleo**p**rotein
Sox	**S**RY-related high-mobility-group b**ox**
SPN1	**S**nur**p**orti**n-1**
SREBP-2	**s**terol **r**egulatory **e**lement **b**inding **p**rotein 2
SRP	**s**ignal **r**ecognition **p**article
SRY	**s**ex-determining **r**egion **Y** protein
TAP	**T**ip-**a**ssociated **p**rotein
TAT	**t**ransactivating **r**egulatory **p**rotein
T_M	**m**elting **t**emperature
TP2	nuclear **t**ransition **p**rotein **2**
Tnp	**T**rans**p**orti**n**
Tra2	**tra**nsformer **2** protein
tRNA	**t**ransfer **RNA**
U snRNP	**u**ridine-rich **s**mall **n**uclear **r**ibo**n**uleo**p**rotein
Uba2	**ub**iquitin-like 1-**a**ctivating enzyme 2
Ubc	**Ub**iquitin-**c**onjugating enzyme
UbeE2	**U**biquitin-**c**onjugating enzyme **E**2 E2
YBP	**Y**orkie homolog 1 **b**inding **p**rotein

5 Appendix

5.1 Nuclear import mechanism of the EJC component MagoY14 revealed by structural studies of Imp13

This work has been originally published in following article:

Nuclear import mechanism of the EJC component MagoY14 revealed by structural studies of Imp13

Fulvia Bono, Atlanta G. Cook, Marlene Grünwald, Judith Ebert and Elena Conti
Molecular Cell, 2010, 37(2) 211-222

Molecular Cell
Article

Nuclear Import Mechanism of the EJC Component Mago-Y14 Revealed by Structural Studies of Importin 13

Fulvia Bono,[1,2] Atlanta G. Cook,[1] Marlene Grünwald,[2] Judith Ebert,[1] and Elena Conti[1,*]
[1]Max-Planck-Institute of Biochemistry, Department of Structural Cell Biology, Am Klopferspitz 18, 82152 Martinsried, Germany
[2]Max-Planck-Institute for Developmental Biology, Spemannstrasse 35, 72076 Tübingen, Germany
*Correspondence: conti@biochem.mpg.de
DOI 10.1016/j.molcel.2010.01.007

SUMMARY

Mago and Y14 are core components of the exon junction complex (EJC), an assembly central to nonsense-mediated mRNA decay in humans and mRNA localization in flies. The Mago-Y14 heterodimer shuttles between the nucleus, where it is loaded onto specific mRNAs, and the cytoplasm, where it functions in translational regulation. The heterodimer is imported back into the nucleus by Importin 13 (Imp13), a member of the karyopherin-β family of transport factors. We have elucidated the structural basis of the Mago-Y14 nuclear import cycle. The 3.35 Å structure of the *Drosophila* Imp13-Mago-Y14 complex shows that Imp13 forms a ring-like molecule, reminiscent of Crm1, and encircles the Mago-Y14 cargo with a conserved interaction surface. The 2.8 Å structure of human Imp13 bound to RanGTP reveals how Mago-Y14 is released in the nucleus by a steric hindrance mechanism. Comparison of the two structures suggests how this unusual karyopherin might function in bidirectional nucleocytoplasmic transport.

INTRODUCTION

In eukaryotic cells, the distinct composition of the nucleoplasm is maintained by the selective and directional transport of macromolecules across the nuclear envelope. Nucleocytoplasmic transport occurs via nuclear pore complexes (NPCs) and is mediated, in the vast majority of cases, by the karyopherin-β family of receptors (Cook et al., 2007; Görlich and Kutay, 1999; Terry et al., 2007; Weis, 2003). Nuclear proteins are transported into the nucleus by a subset of karyopherins known as importins, while most classes of RNAs (with the notable exception of messenger RNAs, mRNAs) are transported out of the nucleus by karyopherins known as exportins. Directionality is determined by the RanGTP gradient, created by the presence of high levels of RanGTP in the nucleus and low levels in the cytosol. Importins bind their cargo in the cytosol in the absence of RanGTP and release it in the nucleus upon RanGTP binding. On the contrary, exportins form complexes in the nucleus with RanGTP and their cargo, which is then dissociated upon hydrolysis of GTP to GDP in the cytosol.

While several structural studies to date have revealed the mechanisms by which canonical transport factors mediate unidirectional nuclear import or export (Chook and Blobel, 1999; Cingolani et al., 1999; Cook et al., 2005, 2009; Dong et al., 2009; Lee et al., 2005, 2006; Matsuura and Stewart, 2004; Monecke et al., 2009), it is unclear how other transport factors can support bidirectional mechanisms. Karyopherins such as Importin 13 (Imp13) in metazoans and Msn5 in yeast, for example, have a double functionality in that they can either import or export depending on the specific cargo molecule to which they bind (Mingot et al., 2001; Yoshida and Blobel, 2001). In *Drosophila*, Imp13 is encoded by an essential gene that is required at the neuromuscular junction (Giagtzoglou et al., 2009). In humans, Imp13 has been shown to mediate the nuclear import of cargos, including Mago-Y14 and Ubc9, and to mediate the nuclear export of eIF1A (Mingot et al., 2001).

The import of Mago-Y14 into the nucleus is a prerequisite for its incorporation into messenger ribonucleoprotein particles (mRNPs) that assemble upon splicing (Giorgi and Moore, 2007). As the spliceosome processes intron-containing pre-mRNAs, it loads Mago and Y14 upstream of splice junctions. The loading depends on the presence of the helicase eIF4AIII, and the assembly is then stabilized by a fourth component, Barentsz (Btz, also known as MLN51) (Gehring et al., 2009a; Herold et al., 2009; Zhang and Krainer, 2007). Together, the four proteins form the core of the exon junction complex (EJC), an assembly that endows the mature mRNP with architectural information on the pre-mRNA intron structure long after the introns have been excised (Ballut et al., 2005; Le Hir et al., 2000). The EJC is an integral part of the spliced mRNP and is retained with it during its journey to the cytoplasm. In the cytoplasm, the EJC functions in different aspects of translational control of the mRNP with which it is associated, ranging from nonsense-mediated mRNA decay in human cells to localization of *oskar* mRNA at the posterior pole of *Drosophila* oocytes (Giorgi and Moore, 2007).

After carrying out their cytoplasmic function as part of the EJC, Mago and Y14 are imported back into the nucleus by Imp13 for another round of mRNP incorporation and regulation (Mingot et al., 2001). The dissociation of Mago-Y14 from the EJC requires the action of translating ribosomes on the mRNP as well as the

ribosomally associated protein PYM (Diem et al., 2007; Gehring et al., 2009b). PYM is a cytosolic protein that binds to Mago-Y14, forming a compact ternary complex (Forler et al., 2003; Bono et al., 2004) that is no longer able to interact with eIF4AIII and Barentsz (Chamieh et al., 2008). However, PYM is not imported into the nucleus with Mago-Y14 (Mingot et al., 2001), raising the question of how the Mago-Y14-PYM complex is dissociated prior to nuclear import.

To study the nuclear import mechanism of Mago-Y14, we determined the crystal structures of an Imp13-Mago-Y14 complex and of an Imp13-RanGTP complex, revealing snapshots of both the cytosolic and nuclear steps of the transport cycle. The structures show how the Mago-Y14 heterodimer is specifically recognized and selected away from its interaction with PYM and how the release of Mago-Y14 in the nucleus is achieved. Comparison of the two nuclear import complexes suggests how this unusual karyopherin might function in nuclear export.

RESULTS AND DISCUSSION

Determination of the Structures of Imp13-RanGTP and Imp13-Mago-Y14

To obtain crystals of Imp13 bound to the cargo Mago-Y14 or bound to the regulator RanGTP, we used homologous proteins from different species. This is an established crystallization strategy, based on the rationale that the solvent-exposed molecular surfaces that engage in crystal lattice contacts are often the least-conserved residues in the protein. The three components of the Imp13-Mago-Y14 complex from *H. sapiens* and *D. melanogaster* share 27%, 89%, and 60% sequence identity, respectively (Figures 1 and S1). Orthologs of the GTPase Ran also share about 90% sequence identity from yeast to human (Figure S1). The conservation is such that yeast GTP-bound Ran can interact with Imp13 from either human (see below) or fly (data not shown). Imp13 and Mago-Y14 from *Drosophila* and human can also interact across species in pull-down assays (see below).

Diffracting crystals of Imp13 bound to RanGTP were obtained with a complex composed of full-length *H. sapiens* Imp13 (residues 1–963) and a construct of *S. cerevisiae* Ran encompassing residues 8–179 and containing the Q71L mutation (which impairs the intrinsic GTPase activity of the protein [Bischoff et al., 1994]). The truncations at the N and C termini of Ran (residues 1–219 when full-length) were identified by limited proteolysis (data not shown) and map to the portion of the molecule that is ordered in the crystal structures of other karyopherin complexes (Cook et al., 2007). The 127 kDa binary complex between Imp13 and the nonhydrolytic deletion mutant of Ran (Ran 8–179 Q71L) bound to GTP crystallized in space group $P3_121$, with one molecule per asymmetric unit (ASU). The structure was solved by SAD (single-wavelength anomalous dispersion) phasing with crystals containing selenomethionine (SeMet)-derivatized Imp13. The final model (Figure 2A) has been refined to 2.8 Å resolution with an R_{free} of 26.8%, R_{factor} of 23.6%, and good stereochemistry (data collection and refinement statistics in Table 1). The atomic model consists of Imp13 residues 18–953 (with the exception of residues 153–158, 183–191, and 658–672, which show no ordered electron density) and Ran residues 8–179.

The structure of Imp13 bound to Mago-Y14 (Figure 2B) was obtained by combining full-length *Drosophila* (Dm) Imp13 (residues 1–971) and Mago-Y14 (residues 1–147 and 1–165). The 147 kDa ternary complex crystallized in space group *P*1, with two molecules per ASU. The structure was solved by a combination of molecular replacement and SeMet SAD phasing and has been refined at 3.35 Å resolution to an R_{free} of 28.9% and a R_{factor} of 26.7% (Table 1). The atomic model for Imp13 consists of residues 11–965, with the exception of a number of short inter- and intra-repeat loops that show no ordered electron density. The model of Mago includes residues 3–147, with the exception of residues 42–44 and 106–107 in disordered loops. The model for Y14 spans from residue 67 to 154. The electron density for functionally important regions of the molecules discussed in the text is shown in Figure S2.

Overall Structure of Imp13 in the Cargo-Bound and Ran-Bound Complexes

As with all members of the karyopherin-β family, Imp13 is an all α-helical protein consisting of 20 consecutive helical motifs (Figures 3 and S3). The first 19 are canonical HEAT repeats, each comprising two antiparallel α helices (A and B), while the C-terminal motif (here referred to as HEAT 20) consists of three α helices. The repeats pack side by side in a parallel fashion, generally with a right-handed twist that generates a superhelical molecule with the A helices forming the outer convex surface and the B helices forming the inner concave surface (Figures 3A and 3B, right panels). The loops that connect consecutive repeats (interrepeat) protrude on one side of the molecule, while the loops that connect the A and B helices of each repeat (intrarepeat) protrude on the opposite side (Figures 3A and 3B, left panels). These loops have variable lengths and in several instances contain insertions with small helical segments (Figure 3C). The regular right-handed arrangement of the repeats is interrupted by prominent left-handed turns at HEATs 4 and 10. Other deviations are at the first repeat, which packs with HEAT 2 in an almost perpendicular fashion, and at the last HEAT repeat that caps the superhelix. The packing of the helical repeats in both the Ran and Mago-Y14 complexes is such that the molecule is bent into a toroid shape, although the overall conformation of the karyopherin is different in the two structures (Figure 3).

When in complex with Mago-Y14, Dm Imp13 has a twisted ring-like conformation, with the edge of HEAT 20 approaching the side of HEAT 1 (Figure 3B). The inner surface of the ring measures about 60 Å in diameter, and the outer surface spans about 95 Å in diameter. Mago-Y14 binds at the inner surface of Imp13, shifted toward the side of the ring that features the interrepeat loops (Figures 3B, left panel, and 2B). When bound to RanGTP, human (Hs) Imp13 again has a toroidal conformation, but with a more pronounced twist of the N- and C-terminal repeats with respect to each other (Figure 3A). In the Imp13-RanGTP structure, the edge of HEAT 20 approaches the side of HEAT 4, creating a more compact toroid with an inner diameter of approximately 50–55 Å. Ran occupies half of the inner surface of the ring, shifted toward the protruding N-terminal HEAT repeats (Figures 3A, left panel, and 2A), i.e., toward the opposite side as compared to Mago-Y14. Hs and Dm Imp13

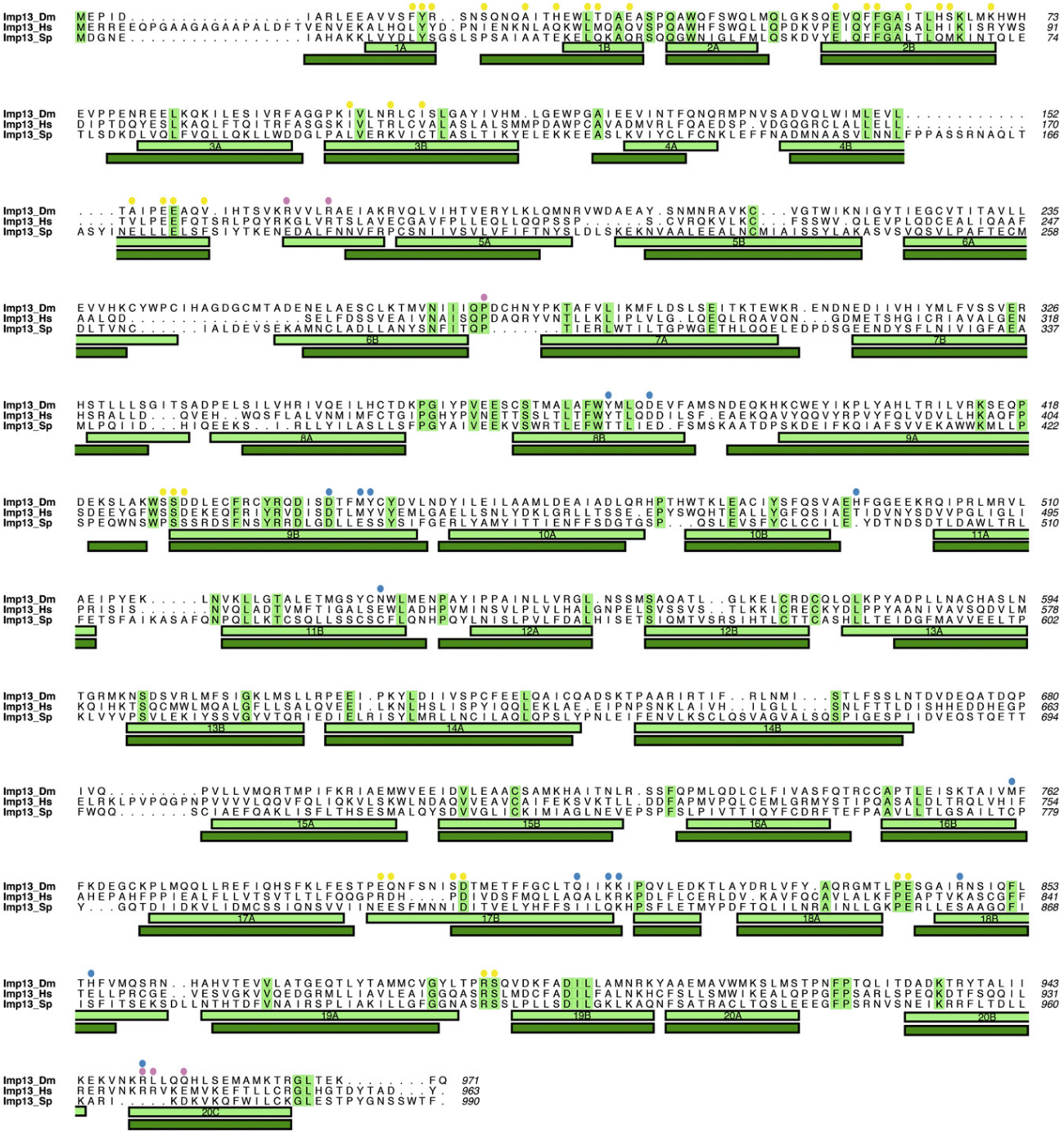

Figure 1. Structure-Based Sequence Alignment of Imp13

The alignment includes Imp13 orthologs from *D. melanogaster* (Dm), *H. sapiens* (Hs), and *S. pombe* (Sp). Highlighted in green are conserved residues. The secondary structure elements of Dm and Hs Imp13 are shown below the sequences as light and dark green rectangles, respectively. The A and B helices of the 20 HEAT repeats are labeled. Above the sequences, colored circles highlight the residues involved in the interaction with Mago (blue), Y14 (magenta), and Ran (yellow), as identified using the AquaProt server (Reichmann et al., 2007). See also Figure S1.

have similar secondary structure elements at similar positions in the sequence (Figure 1). Although the individual HEAT repeats of the two orthologs superpose with a root-mean-square deviation (rmsd) of 1.4 Å in their Cα atoms, the overall molecules superpose with a larger rmsd of 5.3 Å, reflecting the conformational differences in the two structures. The different conformations

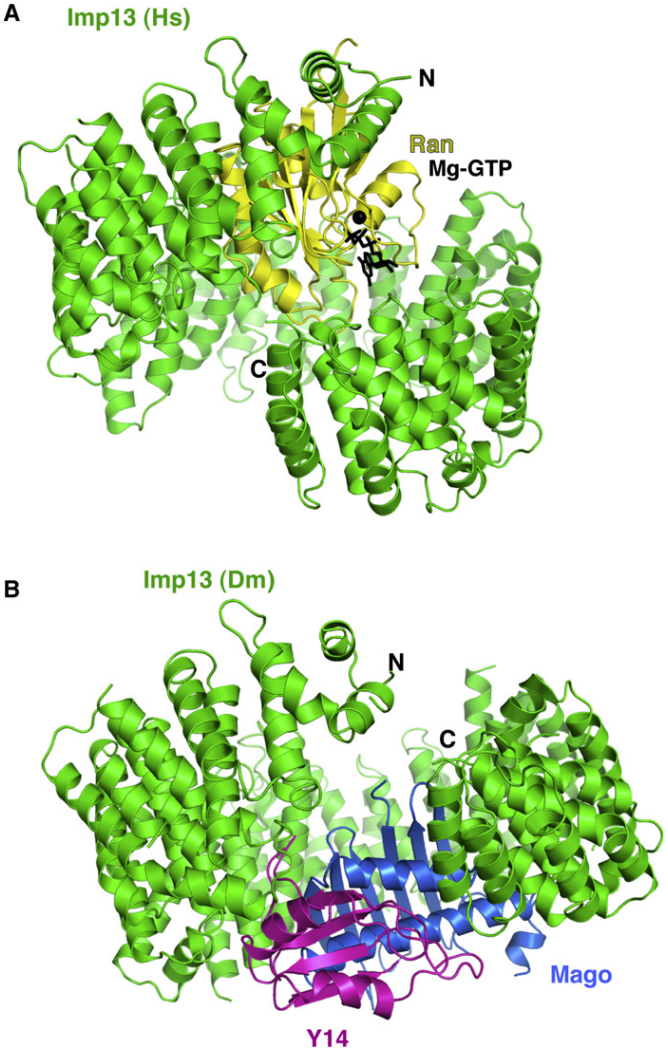

Figure 2. Structures of Imp13 Bound to the Cargo Mago-Y14 and to the Regulator Ran

(A) Structure of the Imp13-RanGTP complex. *H. sapiens* Imp13 is shown in green and Ran in yellow, with GTP and Mg^{2+} shown in ball-and-stick representation in black. The N terminus and C terminus of Imp13 are indicated. This and all other protein structure figures were generated using PyMOL (http://www.pymol.org). See also Figure S2.

(B) Structure of the Imp13-Mago-Y14 complex with *D. melanogaster* Imp13 in green, Mago in blue, and Y14 in magenta. The complex is shown in the same orientation as the RanGTP complex in (A), after optimal superposition of the karyopherin molecules.

result both from small cumulative shifts between individual HEAT repeats and from larger hinge movements.

Imp13 Binding to Mago-Y14: Snapshot of the Cytosolic Import Complex

In the complex with Imp13, Dm Mago-Y14 has a compact structure very similar to the previously reported structures of the Mago-Y14 heterodimer in isolation (rmsd of 0.98 Å over all Cα atoms) (Fribourg et al., 2003; Lau et al., 2003; Shi and Xu, 2003). Briefly, Mago is made up of a flat six-stranded antiparallel β sheet packed on one side by two long α helices (Figure 4). Y14 consists of a C-terminal region containing the fold of a canonical RRM (RNA-recognition motif) domain between residues 64 and 152, with a twisted antiparallel β sheet and two helices packing against one surface. The opposite surface of the Y14 β sheet (that is typically used by RRM domains to bind nucleic acids) interacts instead with the α helices of Mago.

In the complex with Imp13, there is no interpretable electron density for the N-terminal region of Y14. In the structure of full-length Dm Mago-Y14, the N-terminal region of Y14 was ordered between residues 10 and 39, with an α helix (residues 17–29) reaching over the β sheet surface of Mago diametrically opposite the RRM-binding surface (Fribourg et al., 2003). This conformation is not compatible with the Imp13-bound structure, as the N-terminal region of Y14 between residues 10 and 20 would clash with the B helix of HEAT 9 (Figure S4A). Thus, in the complex with Imp13, the N-terminal region of Y14 is displaced into a conformation that, from the features of the electron density, is likely to be flexible and to extend into the solvent. Consistent with this observation, in vitro pull-down experiments with recombinant proteins show that the N-terminal region of Y14 is not required for Imp13 binding (Figure S4B).

Mago fits into the arch of Imp13 formed between HEATs 8 and 20, with direct interactions at several positions (Figure 4). HEATs 8 and 9 contact one edge of the Mago β sheet (Figure 4A), at the site where the N terminus of Y14 was bound in the structure of Mago-Y14 in isolation (Fribourg et al., 2003). In particular, Asp443 of *D. melanogaster* Imp13 ($Asp443_{Dmi}$) approaches the side chain of Mago Arg34 ($Arg34_M$), while $Tyr447_{Dmi}$ and $Tyr378_{Dmi}$ contact the main chain. HEAT 15 contacts the Mago β sheet at the opposite side of the molecule, at $Leu76_M$, while HEATs 17 and 18 contact the nearby termini of the Mago α helices. In particular, $Lys815_{Dmi}$ and the adjacent $Lys814_{Dmi}$ point toward $Glu73_M$ and $Asp116_M$ (Figure 4B). Finally, HEAT 20 wraps up toward the side of the Mago α helices (Figure 4C). Here, the guanidinium groups of $Arg63_M$ and $Arg950_{Dmi}$ pack against each other. $Arg950_{Dmi}$ is in the very C-terminal helix of Imp13 and is also contacted at its main chain by Y14 Glu82 ($Glu82_Y$) and $Gln142_Y$.

Y14 is surrounded by the C-terminal HEATs 19 and 20 on one side and by HEATs 4–7 on the other. In particular, $Ile220_{Dmi}$ and $Pro275_{Dmi}$ at HEATs 5 and 6 are in van der Waals contacts with the side chains of $Leu128_Y$, $His124_Y$, and $Trp73_Y$, while $Glu132_Y$ approaches $Lys167_{Imp}$. Imp13 thus tightly and entirely encircles the Mago-Y14 heterodimer with many conserved interactions, explaining why purified Imp13 and Mago-Y14 can interact even across species (Figure S4B). Consistent with the structural analysis, mutation of $Lys815_{Dmi}$ and the adjacent $Lys814_{Dmi}$ (Figure 4B) to glutamate (thus reversing the charge) or mutation of $Tyr447_{Dmi}$ to arginine (Figure 4A) severely reduced the binding to Mago-Y14 in pull-down assays (Figure 4D, lanes 4 and 7, respectively).

Table 1. Crystallographic Statistics

Data collection			
Data set	Imp13-RanSeMet SAD	Imp13-Mago-Y14 native	Imp13-Mago-Y14 SeMet SAD
Beamline	SLS PX1	SLS PX2	SLS PX2
Space group	$P3_121$	$P1$	$P1$
Unit cell (Å)	a = b = 99.93, c = 276.52, $\alpha = \beta = 90°$, $\gamma = 120°$	a = 82.57, b = 100.79, c = 93.92, $\alpha = 89.83°$, $\beta = 110.18°$, $\gamma = 90.63°$	a = 83.28, b = 101.92,c = 94.25, $\alpha = 90.03°$, $\beta = 110.67°$, $\gamma = 89.92°$
Wavelength (Å)	0.978	0.978	0.979
Resolution range (Å)[a]	50–2.8 (3.0–2.8)	71–3.35 (3.53–3.35)	50–3.7 (3.9–3.7)
Unique reflections	76,082	39,374	29,677
Multiplicity	8.1	2.0	5.9
Completeness (%)[a]	100.0 (100.0)	96.3 (96.1)	97.1 (96.7)
Anomalous completeness (%)[a]	-	-	96.6 (96.1)
$I/\sigma(I)$[a]	15.3 (3.3)	5.7 (1.5)	9.2 (3.1)
R_{sym}(%)[a]	10.0 (66.9)	9.8 (56.0)	15.0 (55.9)
Phasing			
R_{cullis}(%)[a]	-	-	-
Phasing power	-	-	-
Refinement			
Resolution range (Å)[a]	50–2.80	50–3.35	-
R_{free} (%)[a]	26.8	28.9	-
R_{work} (%)[a]	23.6	26.7	-
Rmsd bond (Å)	0.008	0.006	-
Rmsd angle (°)	1.37	1.25	-
B factor protein (Å^2)	69.9	97.3	-
B factor ligands (Å^2)	-	-	-
Ramachandran values			
Most favored (%)	92.6	90.5	-
Additionally allowed (%)	7.4	9.5	-
Generously allowed (%)	0	0	-
Disallowed (%)	0	0	-

[a] Values in parentheses correspond to the highest-resolution shell.

Imp13 Binding to Ran: Snapshot of the Nuclear State

RanGTP has a compact core domain with a Ras-like fold that has been extensively described with previous crystal structures (Chook and Blobel, 1999; Vetter et al., 1999). The core domain features two regions that interact with the bound GTP, the switch I region (residues Thr34–Val47, yeast numbering) and switch II region (residues Thr68–Tyr82), so called because they switch conformation when the nucleotide is hydrolyzed (Milburn et al., 1990). These regions interact with two distinct surfaces of Imp13. Switch I binds the C-terminal portion of Imp13 at HEAT motifs 16–19 (Figure 5A). The interaction occurs mainly via polar and electrostatic contacts, in particular between $Lys39_{Ran}$ and $Lys40_{Ran}$ approaching $Asp785_{Hsl}$ and $Asp788_{Hsl}$. Switch II contacts the N-terminal portion of Imp13 at HEAT 1–3, with hydrophobic contacts centered at $Leu77_{Ran}$ and electrostatic contacts between $Asp79_{Ran}$ and $Arg122_{Hsl}$ (Figure 5A). The helix adjacent to switch II in the core domain contacts HEATs 3 and 4, in particular with $Arg108_{Ran}$ and $Arg112_{Ran}$ approaching $Glu175_{Hsl}$ and $Glu176_{Hsl}$. RanGTP also establishes a third interaction with the central portion of Imp13 at HEATs 8 and 9, with $Arg168_{Ran}$ and $Lys169_{Ran}$ approaching $Asp415_{Hsl}$ and $Glu416_{Hsl}$ on helix 9B (Figure 5B).

The mode of Ran binding to the N-terminal region of Imp13 is largely similar to that observed with other members of the karyopherin family, which indeed share the highest degree of conservation in the N-terminal half of the molecule (Görlich et al., 1997). The interaction in the middle region of Imp13 centered at HEAT 9 is also found in most other karyopherins, although the details differ. In importin β and transportin, this contact is mediated by a conserved acidic loop within HEAT 8 (Chook and Blobel, 1999; Lee et al., 2005). Imp13 has no such loop, but the negatively charged residues in the B helix of HEAT 9 reside in a similar structural position and serve a similar purpose. Imp13 is, in this sense, more similar to the exportins Crm1 and Cse1 (Dong et al., 2009; Matsuura and Stewart, 2004; Monecke et al., 2009). Finally, the interaction of RanGTP with the C-terminal HEATs diverges among the karyopherins studied to date. While Ran docks at HEAT 16–19 in the case of Imp13 and Crm1, it binds to HEAT 14 and 15 in the case of importin β and Cse1. These differences are reflected in the overall superhelical conformation of the karyopherins, with Imp13

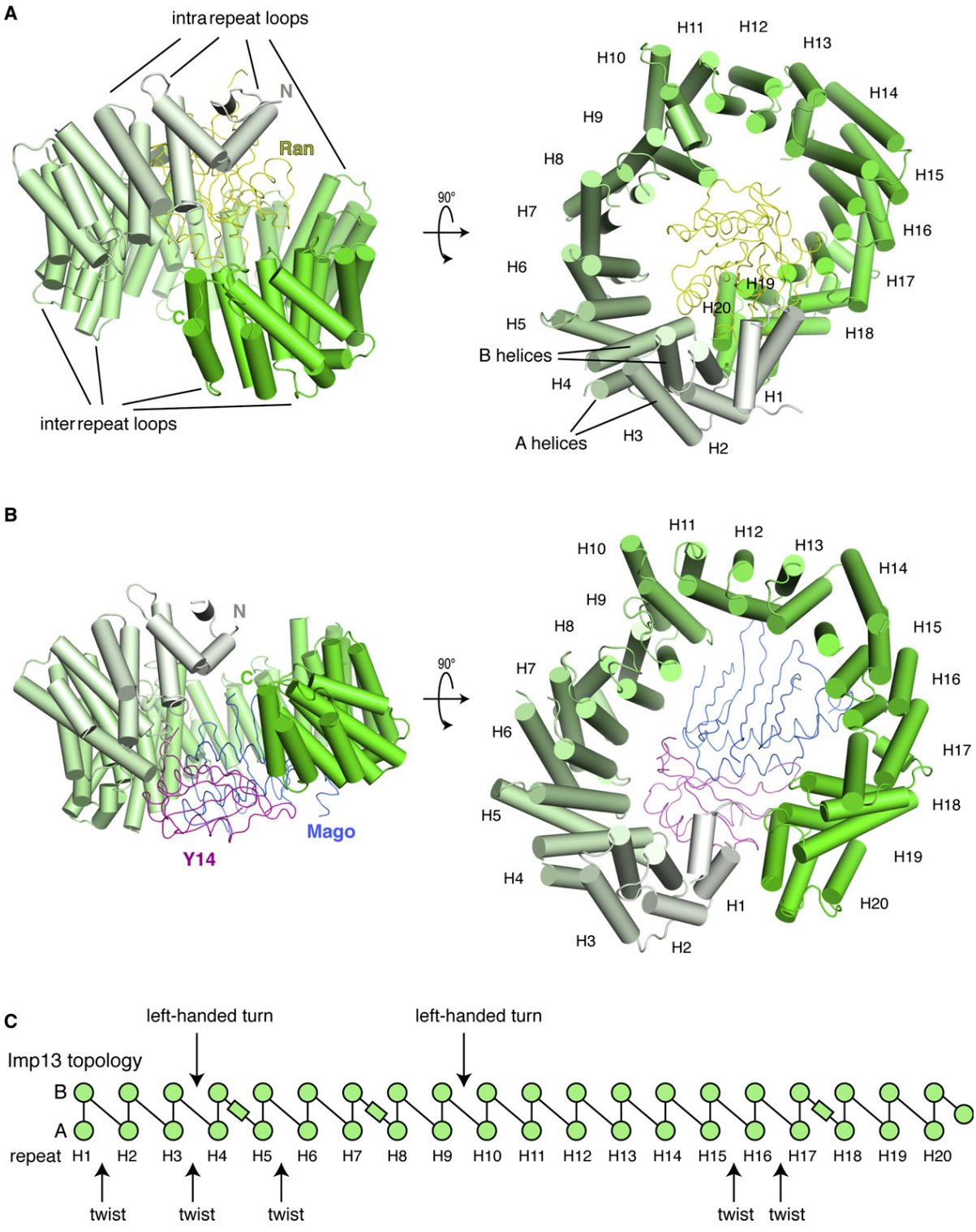

Figure 3. Conformational Variability of Imp13

(A) The Imp13-RanGTP complex is viewed in two orientations related by a 90° rotation around a horizontal axis, with the α helices of the Imp13 HEAT repeats shown as cylinders and colored with a gradient from gray (N terminus) to green (C terminus). The orientation in the left panel is the same as in Figure 2A. The HEAT repeats, as well as two of the A and B helices, are labeled on the right panel. Some of the intra- and interrepeat loops are indicated on the left panel. Ran is visible in a ribbon representation in yellow. See also Figure S3.

and Crm1 curling up in a more closed conformation than importin β and Cse1. Along the same lines, transportin makes only limited contacts with Ran at HEAT 14 and 15, and the superhelix is the most extended in comparison to the other karyopherin-β structures (Chook and Blobel, 1999) (Figure S3).

Mechanisms of Ran Dissociation and Cargo Release from Imp13

The RanGTP-bound state of Imp13 changes when the complex reaches the cytosol: as GTP is hydrolyzed to GDP, Ran dissociates from Imp13. Superposition of the RanGDP structure to the Imp13-RanGTP complex shows that the conformation of switch I and of the C-terminal tail of Ran (known as switch III) has the greatest impact on Imp13 binding. In the GDP-bound conformation, the contact between HEATs 17 and 18 to the switch I region would be lost, and this switch region would assume a conformation that would clash with HEAT 1 of Imp13 (Figure S5A). In addition, the C-terminal tail of Ran (which is known to be unstructured in the GTP-bound form and which was removed from the construct that crystallized) would assume a stable helical conformation on the surface of the Ran core domain that would clash with HEAT 9. Thus, the collapse of the Ran-bound Imp13 complex upon hydrolysis to RanGDP relies on a similar molecular mechanism observed in other karyopherins (Chook and Blobel, 1999; Cook et al., 2009; Lee et al., 2005; Monecke et al., 2009; Vetter et al., 1999).

Conversely, the cargo-bound state of Imp13 changes when the complex reaches the nucleus: upon RanGTP binding to Imp13, Mago-Y14 is dissociated. In the two importins studied to date, importin β and transportin, cargo release relies on their characteristic acidic loop at HEAT 8 (Cingolani et al., 1999; Lee et al., 2006). However, as described above, Imp13 lacks this structural feature, and therefore cargo release is likely to be mediated by a different molecular mechanism. Comparison of the structures of Imp13 bound to RanGTP and bound to Mago-Y14 shows that the GTPase and the cargo interact with different surface residues of the karyopherins and therefore do not compete for the same binding sites. The reverse-charge double mutation of $Lys814_{Dmel}$ and $Lys815_{Dmel}$, for example, impairs Mago-Y14 binding (Figure 4D, lane 4) but does not abolish Ran binding (Figure S5B). When the two structures are superposed, RanGTP and Mago-Y14 assume an almost side-by-side position when bound to Imp13, but concomitant binding would not be possible, as they would be too close: the loops on one side of the Mago β sheet would clash against the loops of the Ran β sheet (Figure 6A). As expected, increasing amounts of RanGTP progressively decrease the amount of Mago-Y14 binding to GST-Imp13 in pull-down experiments (Figure S5C).

Mutually Exclusive Binding of Mago-Y14 to Either Imp13 or PYM

Mago-Y14 is a nuclear protein at steady state, but shuttles to the cytoplasm as part of the mRNA-associated EJC (Le Hir et al., 2001). It has recently been reported, using in vitro splicing reactions and immunoprecipitations, that the protein PYM is involved in EJC dissociation (Gehring et al., 2009b), consistent with previous reports suggesting that PYM binding to Mago-Y14 would not be compatible in the context of the EJC (Bono et al., 2006). The N-terminal domain of PYM binds Mago-Y14 at a composite surface formed by a loop of the Y14 RRM (known as the β2-β3 loop) and by the α helices of Mago (Bono et al., 2004). In particular, PYM docks with electrostatic interactions at the negatively charged surface of the Mago α helices centered at $Glu73_M$. This surface is also used to bind Imp13. Superposition of the structures of Mago-Y14 bound to Imp13 and to PYM shows that Arg18 and Arg24 of PYM occupy a similar position in space as Lys815 and Lys814 of Imp13 (Figure 6B). Thus, the two interactions are mutually exclusive, as the β hairpin of PYM (residues 15–24) would clash with HEAT 16, 17, and 18 of Imp13. This prediction from the structure can be recapitulated biochemically. A reverse-charged mutation of Mago Glu73 to arginine impairs the interaction either with Imp13 or PYM (Figure 6C). Moreover, increasing amounts of Imp13 progressively reduce the amounts of PYM binding to GST-Mago-Y14 in competition experiments (Figure 6D).

Conclusions

A challenge in understanding how mRNPs function at the molecular level is to decipher how and when the composition of the protein components changes during their complex life cycle. mRNP dynamics are the result of different cellular machineries, which act with a precise sequence of events that depend on concomitant or incompatible interactions. Mago and Y14 participate in a complex set of sequential binding events: they assemble into the EJC to associate with mRNPs in the nucleus, bind to PYM during or after EJC dissociation in the cytoplasm, bind to Imp13 to return back to the nucleus, and are dissociated from it by RanGTP (Figure S6). Previous work had elucidated the first steps of the Mago-Y14 pathway at the atomic level, revealing the intricate network of interactions that form the RNA-bound EJC and its mutually exclusive interactions with PYM (Andersen et al., 2006; Bono et al., 2004, 2006). We now report the mechanisms of the nuclear import step of the cycle. Mago-Y14 is recognized by the karyopherin Imp13 via specific and evolutionarily conserved contacts. The transport factor forms a ring around the Mago-Y14 cargo, binding at a surface that is also used for PYM recognition. Concomitant binding of PYM is thus sterically incompatible, explaining how this Mago-Y14-binding partner is excluded from the nuclear import step. Similarly, Mago-Y14 is sterically inaccessible to Imp13 when in the EJC.

Binding of RanGTP in the nucleus successively displaces Mago-Y14 from the transport factor. The sites at which RanGTP binds on the karyopherin are mostly accessible in the Imp13-Mago-Y14 complex, providing a rationale for how the GTPase would be able to approach and dock to the transport factor as

(B) The Imp13-Mago-Y14 complex is shown with similar views and representations as the RanGTP complex in (A). Mago and Y14 are visible in a ribbon representation in blue and magenta.
(C) Schematic of the Dm Imp13 secondary structure, with the A and B helices of each HEAT repeat indicated. Two left-handed turns are indicated, as are disruptions between subsequent HEAT repeats that differ between the two structures (twists).

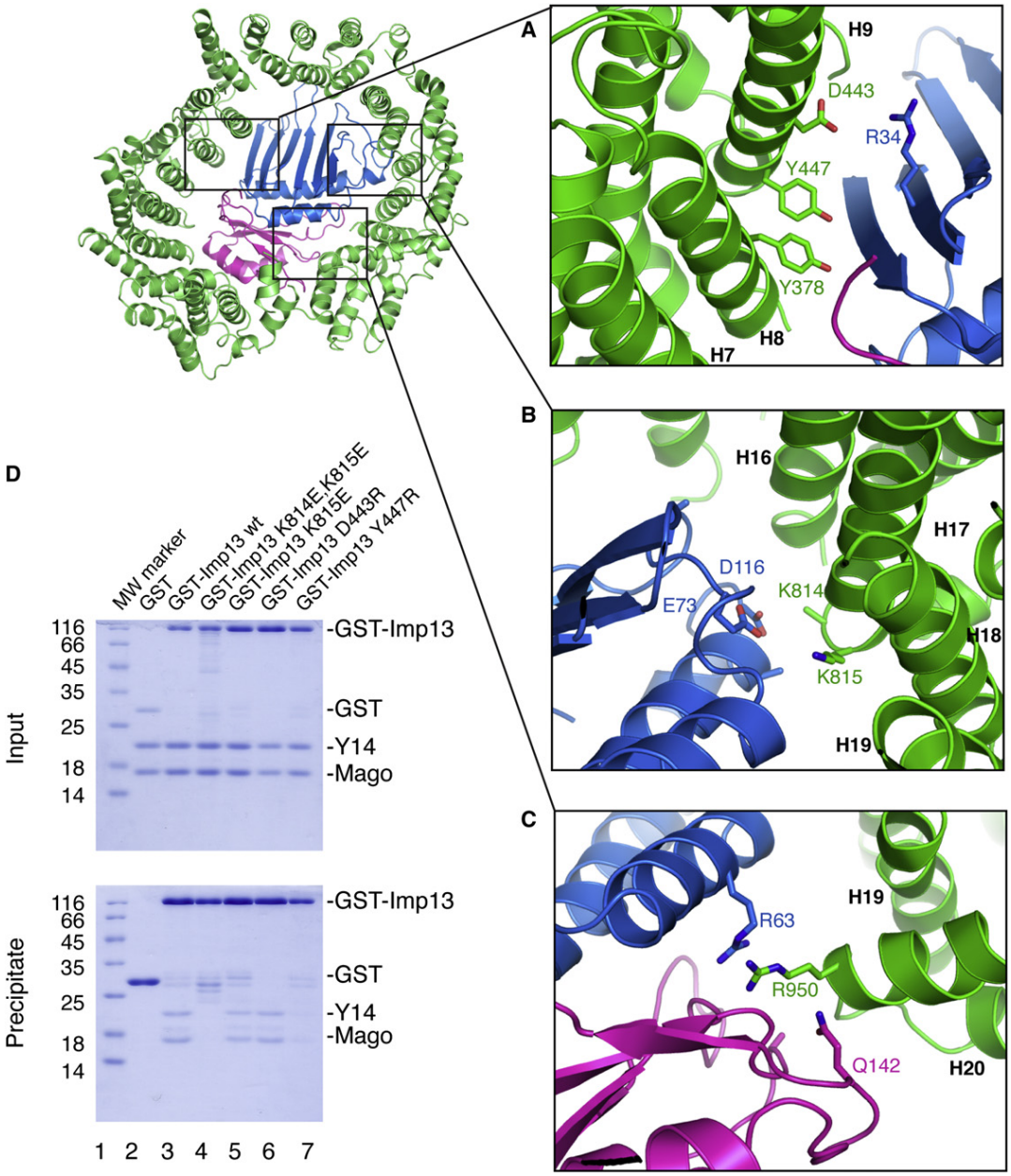

Figure 4. Conserved Interactions between Imp13 and Mago-Y14

(A–C) Close-up views of the interactions between Imp13 and Mago-Y14. The molecules are in a similar orientation as in Figure 3B, right panel. The views show the interaction between HEATs 8 and 9 of Imp13 and the Mago β sheet (A), between HEATs 17 and 18 of Imp13 and the Mago loops (B), and between HEAT 20 and the interface of the Mago-Y14 heterodimer (C). Residues of Imp13 are labeled in green, of Mago in blue, and of Y14 in magenta, and HEAT repeats are in black (bold). See also Figure S4.

(D) Protein coprecipitations by GST pull-down assays. GST-tagged *Drosophila* Imp13 wild-type or mutants were incubated with full-length Mago-Y14 in a buffer containing 50 mM NaCl. One-sixth of the sample was kept as input control (upper panel), and the rest was coprecipitated with glutathione-Sepharose beads (lower panel). Both input and pull-down samples were analyzed on Coomassie-stained 15% SDS-PAGE. Lane 1 shows binding to GST as control. The far left lane was loaded with a molecular weight marker.

it enters the nucleus in a complex. When fully bound, RanGTP binding would sterically push Mago-Y14 out of the complex: although the binding sites for cargo and Ran are positioned roughly side-by-side on the karyopherin, the molecules would come into too close a contact with each other for their binding to be simultaneous. In this scenario, it is possible to envisage how this unusual karyopherin might be able to mediate bidirectional transport, rather than being a canonical unidirectional

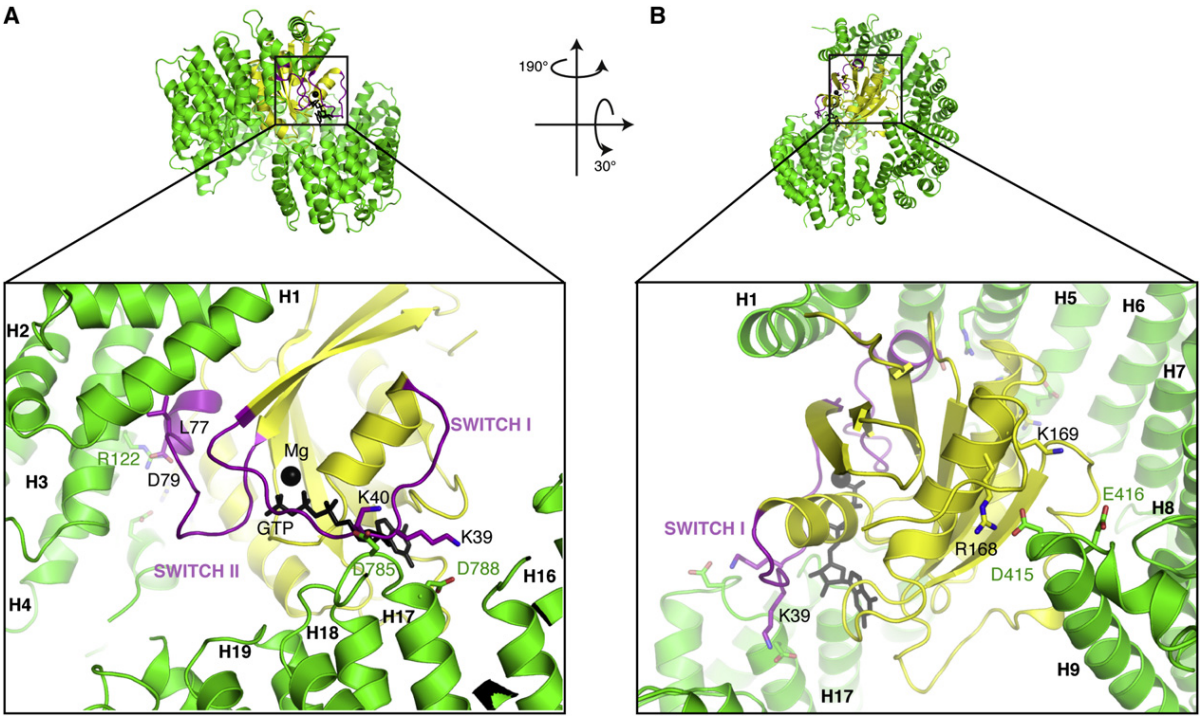

Figure 5. Conserved Interactions between Imp13 and Ran

(A) Close-up view of the interaction between the switch I region of Ran and HEATs 17 and 18 and between the switch II region of Ran and HEATs 3 and 4. The molecule is shown in the same orientation as in Figure 3A, left panel. Ran is in yellow, the switch regions in violet, and GTP and Mg in black. Residues of Imp13 are labeled in green, residues of Ran in black, and HEAT repeats are in black (bold). See also Figure S5.

(B) Close-up view of the interaction between Ran and HEATs 8 and 9 of Imp13. The molecule is shown in the same orientation as in Figure 3A, right panel.

import or export factor. An export cargo might also bind to Imp13 with a side-by-side configuration relative to Ran but occupy less space than Mago-Y14, so as not to clash with RanGTP and to require the proximity with RanGTP for increasing its binding affinity. In this situation, Imp13 would be able to mediate either the cooperative or antagonistic binding of Ran with the cargo depending on its specific structural features. This would in turn define whether a cargo is destined for import or export.

EXPERIMENTAL PROCEDURES

Protein Expression and Purification

D. melanogaster Mago and Y14 were coexpressed in *E. coli* and purified essentially as previously described (Fribourg et al., 2003). Dm *Imp13* was cloned from a full-length commercial (Drosophila Genomics Resource Center) clone and the Hs *Imp13* clone was a kind gift from Dirk Görlich (MPI; Goettingen, Germany). Dm and Hs Imp13 were expressed as N-terminal GST fusion proteins in *E. coli* BL21-GOLD pLysS cells (Stratagene; Amsterdam Zudoost, Holland) with an overnight induction at 18°C. They were affinity-purified on glutathione-Sepharose beads (GE Healthcare; Freiburg, Germany) in buffer A (20 mM Tris [pH 7.5], 100 mM NaCl, 1 mM dithiothreitol [DTT]). Binding to the resin was performed in batch, and the tag was removed by addition of Tobacco Etch Virus (TEV) protease. The cleaved proteins were further purified by anion-exchange chromatography using a HiQ column (Bio-Rad; Munich, Germany) in buffer A and eluted with a gradient of 100–750 mM NaCl. The Dm Imp13-Mago-Y14 complex was formed by adding a 1.5-fold excess of pure Mago-Y14 heterodimer to Imp13 and incubating for 2 hr at 4°C prior to loading the complex onto a Superdex 200 gel filtration column (GE Healthcare). Attempts to measure the affinity of the interaction between GST-Imp13 and Mago-Y14 either by surface plasmon resonance (SPR) or by isothermal titration calorimetry (ITC) failed, mainly because a significant percentage of Imp13 aggregates over time (as detected in static light scattering [SLS] measurements) (data not shown).

A construct of yeast RanQ71L encompassing residues 8–179 was expressed as an N-terminal His-tagged protein in *E. coli* BL21-GOLD pLysS cells with an overnight induction at 18°C. His-tagged Ran was purified by Ni^{2+}-NTA chromatography with buffer B (20 mM Tris [pH 7.5], 4 mM $MgCl_2$, 10% glycerol, and 0.5 mM DTT) supplemented with 500 mM NaCl and 5 mM imidazole. After elution (buffer B with 500 mM NaCl, 500 mM imidazole, and 1 mM β-mercaptoethanol), the protein was dialyzed in the presence of TEV protease (buffer B with 250 mM NaCl and with 1 mg TEV per 50 mg Ran). It was then loaded on a Co^{2+}-Talon (Clontech; Saint-Germain-en-Laye, France) column and collected in the flowthrough. To ensure the formation of a homogeneous nucleotide-bound state of Ran, the pure protein was incubated with 7 mM EDTA, dialyzed in buffer B supplemented with 50 mM NaCl, and then incubated with a 5-fold molar excess of GTP and 10 mM $MgCl_2$ at room temperature for 30 min. As a final purification step, RanGTP was purified by cation-exchange chromatography (ResourceS, GE Healthcare) in buffer B and eluted with a 1 M NaCl gradient. The Imp13-Ran complex was formed by adding a 1.5-fold molar excess of Ran to Imp13 for 2 hr at 4°C. The 1:1 complex was then purified on a Superdex 200 size-exclusion column.

For phasing, Hs and Dm Imp13 proteins labeled with SeMet were used to form the corresponding complexes with either unlabeled RanGTP or unlabelled Mago-Y14. The SeMet-labeled Imp13 proteins were expressed in BL21-GOLD pLysS cells grown in M9 minimal media and starved before addition of SeMet (Van Duyne et al., 1993). They were purified with the same protocol used for the unmodified proteins.

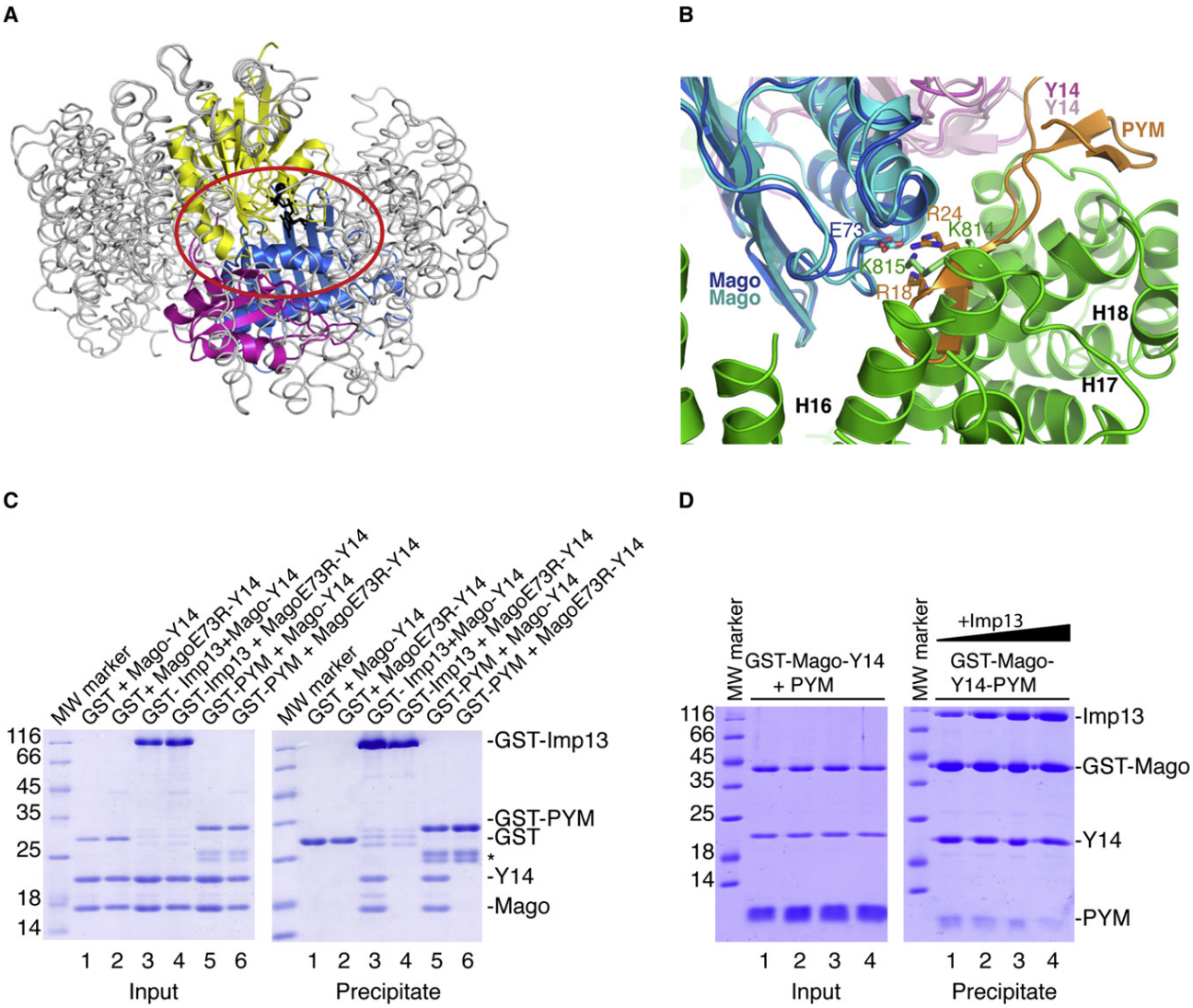

Figure 6. Mutually Exclusive Interactions on Imp13 and Mago-Y14

(A) Superposition of the structures of Imp13-Mago-Y14 and Imp13-RanGTP. The molecules are viewed in the same orientation as in Figure 2, with Imp13 shown in a ribbon representation in gray. Although Mago-Y14 and RanGTP bind to a large extent to different regions of Imp13, their concomitant binding would result in steric clashes (region highlighted with a red circle). See also Figure S6.

(B) Superposition of the structures of Imp13-Mago-Y14 and Mago-Y14-PYM. Imp13 (green) and PYM (orange) interact with the same region of Mago (blue) centered at Glu73. HEAT repeats are labeled in black (bold).

(C) Protein coprecipitations by GST pull-down assays. *Drosophila* GST-tagged Imp13 or GST-tagged PYM were incubated with full-length Mago-Y14, either wild-type or containing the Mago E73R mutation. The pull-downs were carried out with a similar protocol described in Figure 4D. The input and precipitated samples are shown in the left and right panels. The leftmost lanes were loaded with a molecular weight marker. Bands marked with an asterisk are degradation impurities of GST-PYM.

(D) Competition experiments showing the effect of Imp13 on the PYM-binding properties of Mago-Y14. GST-Mago-Y14 was incubated on beads with an excess of PYM (input, left panel). After washing, increasing amounts of Imp13 (from 2.3 μg in lane 1 to 13.8 μg in lane 4) were added in the pull-down. The competition experiments are representative of five repetitions, all showing that the amount of Imp13 precipitated is progressively increased while the amount of PYM is progressively decreased.

Crystallization, Data Collection, and Structure Determination

Crystallization experiments were carried out using the vapor diffusion method. The best crystals of the Imp13-RanGTP complex were obtained at 18°C using a reservoir solution containing 100 mM Bis-Tris (pH 6.0), 23% (w/v) PEG 3350, and 100 mM Na-thiocyanate. For data collection, the crystals were flash-cooled in liquid nitrogen after addition of 20% glycerol as cryoprotectant to the reservoir solution. The crystals diffracted to 2.8 Å resolution at the PXII beamline of the Swiss Light Source (Villigen, Switzerland). They belong to space group $P3_121$ with cell dimensions $a = b = 99.93$ Å, $c = 276.52$ Å and contain one molecule in the ASU. Diffraction data were processed with the program XDS (Kabsch, 1993). The structure was solved by SeMet SAD phasing. SHELX (Schneider and Sheldrick, 2002) was used to obtain 23 selenium sites and initial phases. Model building was carried out with Coot (Emsley and Cowtan, 2004) and alternating cycles of refinement with CNS (Brünger et al., 1998).

Initial crystals of the Imp13-Mago-Y14 complex were obtained using 100 mM MES (pH 6.5) and 26% (v/v) PEG 300 as reservoir solution and were optimized with the addition of 6% trimethylamine N-oxide dihydrate and by microseeding. The crystals were flash-cooled in liquid nitrogen after adding 40% (v/v) PEG 400. Diffraction data to 3.35 Å resolution were collected at the SLS synchrotron and were processed with the program XDS (Kabsch, 1993). The crystals belong to space group *P*1 with cell dimensions a = 82.6 Å, b = 100.8 Å, c = 93.9 Å and α = 89.8°, β = 110.2°, γ = 90.6°. The ASU of the crystals contains two independent copies of the Imp13-Mago-Y14 complex related by a noncrystallographic two-fold axis. The structure was solved with the program Phaser (McCoy et al., 2007) using a combination of molecular replacement and single-wavelength anomalous dispersion (SAD) data on a crystal grown using SeMet-substituted Imp13. Phased molecular replacement in Phaser using the structure of *Drosophila* Mago-Y14 as search model (PDB code 1HL6) allowed the location of 41 of the expected 86 selenium sites and gave initial phases. The electron density was improved with DM (CCP4, 1994), model building was performed with the program O (Jones and Kjeldgaard, 1997), and refinement with CNS (Brünger et al., 1998).

In Vitro Binding Assays

In the pull-down assays in Figures 4D and 6C, GST-tagged recombinant Imp13 or PYM proteins and purified binding partners (2 μg of each) were mixed in binding buffer (20 mM HEPES [pH 7.5], 50 mM NaCl, 1 mM DTT, 10% glycerol, 0.1% [v/v] Nonidet P40) to a final volume of 60 μl and incubated for 1 hr at 4°C. Complexes were immobilized on 15 μl glutathione agarose beads (GE Healthcare) and incubated for 1 hr at 4°C. The resin was washed three times with 500 μl binding buffer and eluted with 20 mM reduced glutathione in elution buffer (30 mM Tris-HCl [pH 8.8], 150 mM NaCl, 1 mM DTT, 14% glycerol, 0.1% [v/v] Nonidet P40). Eluates were dried down, mixed with SDS loading buffer, boiled, and loaded on 15% SDS-PAGE with a protein molecular mass marker. Proteins were visualized by Coomassie staining. In the competition experiment in Figure 6D, 4 μg GST-Mago-Y14 and PYM was incubated on beads and washed, and increasing amounts of Imp13 were added (2.3 μg, 4.6 μg, 9.2 μg, and 13.8 μg from lanes 1 to 4).

ACCESSION NUMBERS

The coordinates and structure factors have been deposited in the Macromolecular Structure Database of the European Bioinformatic Institute (EBI) with ID code 2x19 (Imp13-RanGTP complex) and 2x1g (Imp13-Mago-Y14 complex).

SUPPLEMENTAL INFORMATION

Supplemental Information includes six figures and can be found with this article online at doi:10.1016/j.molcel.2010.01.007.

ACKNOWLEDGMENTS

We would like to thank Petra Birle and Tatjana Krywcun for mutagenesis and Jerome Basquin, Karina Valer Saldana, and Sabine Pleyer at the MPI-Martinsried crystallization facility. We also thank Dirk Görlich for the Hs Imp13 clone, the staff of the PX beamlines at the Swiss Light Source (Villigen, Switzerland) for assistance during data collection, and Randy Read for suggestions with Phaser. We thank members of the lab, Esben Lorentzen and Elisa Izaurralde, for suggestions and critical reading of the manuscript. This study was supported by the Max Planck Gesellschaft, the EU grant 3D Repertoire (contract number LSHG-CT-2005-51202), the Sonderforschungsbereich SFB646, and the Gottfried Wilhelm Leibniz Program of the Deutsche Forschungsgemeinschaft (DFG).

Received: October 6, 2009
Revised: December 2, 2009
Accepted: January 6, 2010
Published: January 28, 2010

REFERENCES

Andersen, C.B., Ballut, L., Johansen, J.S., Chamieh, H., Nielsen, K.H., Oliveira, C.L., Pedersen, J.S., Séraphin, B., Le Hir, H., and Andersen, G.R. (2006). Structure of the exon junction core complex with a trapped DEAD-box ATPase bound to RNA. Science *313*, 1968–1972.

Ballut, L., Marchadier, B., Baguet, A., Tomasetto, C., Séraphin, B., and Le Hir, H. (2005). The exon junction core complex is locked onto RNA by inhibition of eIF4AIII ATPase activity. Nat. Struct. Mol. Biol. *12*, 861–869.

Bischoff, F.R., Klebe, C., Kretschmer, J., Wittinghofer, A., and Ponstingl, H. (1994). RanGAP1 induces GTPase activity of nuclear Ras-related Ran. Proc. Natl. Acad. Sci. USA *91*, 2587–2591.

Bono, F., Ebert, J., Unterholzner, L., Güttler, T., Izaurralde, E., and Conti, E. (2004). Molecular insights into the interaction of PYM with the Mago-Y14 core of the exon junction complex. EMBO Rep. *5*, 304–310.

Bono, F., Ebert, J., Lorentzen, E., and Conti, E. (2006). The crystal structure of the exon junction complex reveals how it maintains a stable grip on mRNA. Cell *126*, 713–725.

Brünger, A.T., Adams, P.D., Clore, G.M., DeLano, W.L., Gros, P., Grosse-Kunstleve, R.W., Jiang, J.S., Kuszewski, J., Nilges, M., Pannu, N.S., et al. (1998). Crystallography & NMR system: A new software suite for macromolecular structure determination. Acta Crystallogr. D Biol. Crystallogr. *54*, 905–921.

Chamieh, H., Ballut, L., Bonneau, F., and Le Hir, H. (2008). NMD factors UPF2 and UPF3 bridge UPF1 to the exon junction complex and stimulate its RNA helicase activity. Nat. Struct. Mol. Biol. *15*, 85–93.

Chook, Y.M., and Blobel, G. (1999). Structure of the nuclear transport complex karyopherin-beta2-Ran x GppNHp. Nature *399*, 230–237.

Cingolani, G., Petosa, C., Weis, K., and Müller, C.W. (1999). Structure of importin-beta bound to the IBB domain of importin-alpha. Nature *399*, 221–229.

CCP4 (Collaborative Computational Project, Number 4). (1994). The CCP4 suite: programs for protein crystallography. Acta Crystallogr. D Biol. Crystallogr. *50*, 760–763.

Cook, A., Fernandez, E., Lindner, D., Ebert, J., Schlenstedt, G., and Conti, E. (2005). The structure of the nuclear export receptor Cse1 in its cytosolic state reveals a closed conformation incompatible with cargo binding. Mol. Cell *18*, 355–367.

Cook, A., Bono, F., Jinek, M., and Conti, E. (2007). Structural biology of nucleocytoplasmic transport. Annu. Rev. Biochem. *76*, 647–671.

Cook, A.G., Fukuhara, N., Jinek, M., and Conti, E. (2009). Structures of the tRNA export factor in the nuclear and cytosolic states. Nature *461*, 60–65.

Diem, M.D., Chan, C.C., Younis, I., and Dreyfuss, G. (2007). PYM binds the cytoplasmic exon-junction complex and ribosomes to enhance translation of spliced mRNAs. Nat. Struct. Mol. Biol. *14*, 1173–1179.

Dong, X., Biswas, A., Süel, K.E., Jackson, L.K., Martinez, R., Gu, H., and Chook, Y.M. (2009). Structural basis for leucine-rich nuclear export signal recognition by CRM1. Nature *458*, 1136–1141.

Emsley, P., and Cowtan, K. (2004). Coot: model-building tools for molecular graphics. Acta Crystallogr. D Biol. Crystallogr. *60*, 2126–2132.

Forler, D., Köcher, T., Rode, M., Gentzel, M., Izaurralde, E., and Wilm, M. (2003). An efficient protein complex purification method for functional proteomics in higher eukaryotes. Nat. Biotechnol. *21*, 89–92.

Fribourg, S., Gatfield, D., Izaurralde, E., and Conti, E. (2003). A novel mode of RBD-protein recognition in the Y14-Mago complex. Nat. Struct. Biol. *10*, 433–439.

Gehring, N.H., Lamprinaki, S., Hentze, M.W., and Kulozik, A.E. (2009a). The hierarchy of exon-junction complex assembly by the spliceosome explains key features of mammalian nonsense-mediated mRNA decay. PLoS Biol. *7*, e1000120.

Gehring, N.H., Lamprinaki, S., Kulozik, A.E., and Hentze, M.W. (2009b). Disassembly of exon junction complexes by PYM. Cell *137*, 536–548.

Giagtzoglou, N., Lin, Y.Q., Haueter, C., and Bellen, H.J. (2009). Importin 13 regulates neurotransmitter release at the Drosophila neuromuscular junction. J. Neurosci. *29*, 5628–5639.

Giorgi, C., and Moore, M.J. (2007). The nuclear nurture and cytoplasmic nature of localized mRNPs. Semin. Cell Dev. Biol. *18*, 186–193.

Görlich, D., and Kutay, U. (1999). Transport between the cell nucleus and the cytoplasm. Annu. Rev. Cell Dev. Biol. *15*, 607–660.

Görlich, D., Dabrowski, M., Bischoff, F.R., Kutay, U., Bork, P., Hartmann, E., Prehn, S., and Izaurralde, E. (1997). A novel class of RanGTP binding proteins. J. Cell Biol. *138*, 65–80.

Herold, N., Will, C.L., Wolf, E., Kastner, B., Urlaub, H., and Lührmann, R. (2009). Conservation of the protein composition and electron microscopy structure of Drosophila melanogaster and human spliceosomal complexes. Mol. Cell. Biol. *29*, 281–301.

Jones, T.A., and Kjeldgaard, M. (1997). Electron-density map interpretation. Methods Enzymol. *277*, 173–208.

Kabsch, W. (1993). Automatic processing of rotation diffraction data from crystals of initially unknown symmetry and cell constants. J. Appl. Cryst. *26*, 795–800.

Lau, C.K., Diem, M.D., Dreyfuss, G., and Van Duyne, G.D. (2003). Structure of the Y14-Magoh core of the exon junction complex. Curr. Biol. *13*, 933–941.

Le Hir, H., Izaurralde, E., Maquat, L.E., and Moore, M.J. (2000). The spliceosome deposits multiple proteins 20-24 nucleotides upstream of mRNA exon-exon junctions. EMBO J. *19*, 6860–6869.

Le Hir, H., Gatfield, D., Braun, I.C., Forler, D., and Izaurralde, E. (2001). The protein Mago provides a link between splicing and mRNA localization. EMBO Rep. *2*, 1119–1124.

Lee, S.J., Matsuura, Y., Liu, S.M., and Stewart, M. (2005). Structural basis for nuclear import complex dissociation by RanGTP. Nature *435*, 693–696.

Lee, B.J., Cansizoglu, A.E., Süel, K.E., Louis, T.H., Zhang, Z., and Chook, Y.M. (2006). Rules for nuclear localization sequence recognition by karyopherin beta 2. Cell *126*, 543–558.

Matsuura, Y., and Stewart, M. (2004). Structural basis for the assembly of a nuclear export complex. Nature *432*, 872–877.

McCoy, A.J., Grosse-Kunstleve, R.W., Adams, P.D., Winn, M.D., Storoni, L.C., and Read, R.J. (2007). Phaser crystallographic software. J. Appl. Cryst. *40*, 658–674.

Milburn, M.V., Tong, L., deVos, A.M., Brünger, A., Yamaizumi, Z., Nishimura, S., and Kim, S.H. (1990). Molecular switch for signal transduction: structural differences between active and inactive forms of protooncogenic ras proteins. Science *247*, 939–945.

Mingot, J.M., Kostka, S., Kraft, R., Hartmann, E., and Görlich, D. (2001). Importin 13: a novel mediator of nuclear import and export. EMBO J. *20*, 3685–3694.

Monecke, T., Güttler, T., Neumann, P., Dickmanns, A., Görlich, D., and Ficner, R. (2009). Crystal structure of the nuclear export receptor CRM1 in complex with Snurportin1 and RanGTP. Science *324*, 1087–1091.

Reichmann, D., Cohen, M., Abramovich, R., Dym, O., Lim, D., Strynadka, N.C., and Schreiber, G. (2007). Binding hot spots in the TEM1-BLIP interface in light of its modular architecture. J. Mol. Biol. *365*, 663–679.

Schneider, T.R., and Sheldrick, G.M. (2002). Substructure solution with SHELXD. Acta Crystallogr. D Biol. Crystallogr. *58*, 1772–1779.

Shi, H., and Xu, R.M. (2003). Crystal structure of the Drosophila Mago nashi-Y14 complex. Genes Dev. *17*, 971–976.

Terry, L.J., Shows, E.B., and Wente, S.R. (2007). Crossing the nuclear envelope: hierarchical regulation of nucleocytoplasmic transport. Science *318*, 1412–1416.

Van Duyne, G.D., Standaert, R.F., Karplus, P.A., Schreiber, S.L., and Clardy, J. (1993). Atomic structures of the human immunophilin FKBP-12 complexes with FK506 and rapamycin. J. Mol. Biol. *229*, 105–124.

Vetter, I.R., Arndt, A., Kutay, U., Görlich, D., and Wittinghofer, A. (1999). Structural view of the Ran-Importin beta interaction at 2.3 A resolution. Cell *97*, 635–646.

Weis, K. (2003). Regulating access to the genome: nucleocytoplasmic transport throughout the cell cycle. Cell *112*, 441–451.

Yoshida, K., and Blobel, G. (2001). The karyopherin Kap142p/Msn5p mediates nuclear import and nuclear export of different cargo proteins. J. Cell Biol. *152*, 729–740.

Zhang, Z., and Krainer, A.R. (2007). Splicing remodels messenger ribonucleoprotein architecture via eIF4A3-dependent and -independent recruitment of exon junction complex components. Proc. Natl. Acad. Sci. USA *104*, 11574–11579.

Supplemental Information
Molecular Cell, *Volume 37*

Nuclear Import Mechanism of the EJC Components Mago-Y14 Revealed by Structural Studies of Importin 13
Fulvia Bono, Atlanta G. Cook, Marlene Grünwald, Judith Ebert, and Elena Conti

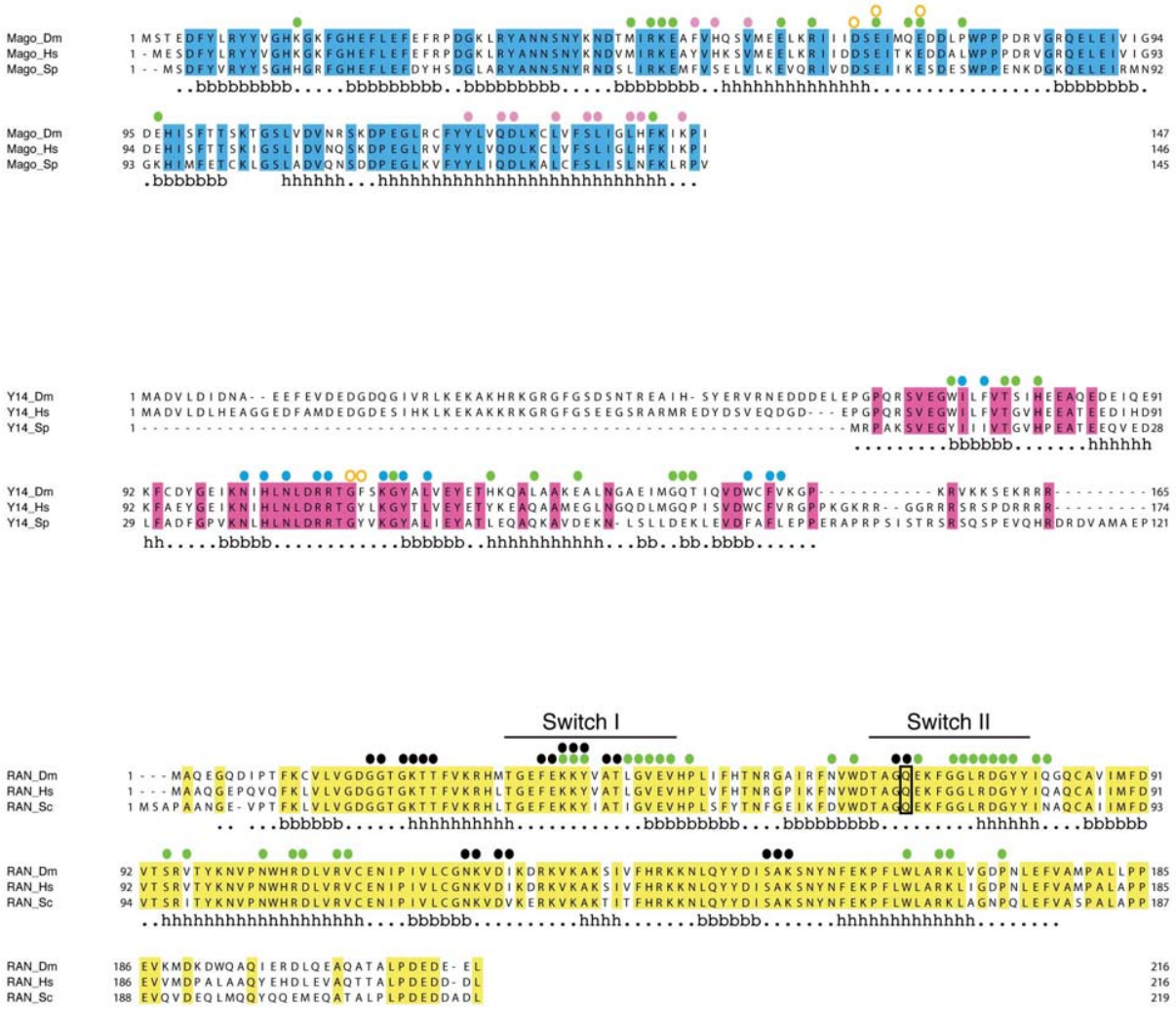

Figure S1
Structure-based sequence alignment of Mago, Y14 and Ran.
Orthologues from Dm, Hs, Sp and *S. cerevisiae* (Sc) are included. Conserved residues are highlighted in blue, magenta and yellow, respectively. Colored circles above the sequences identify the residues that interact with Imp13 (green circles), with Y14 (magenta), with Mago (blue), with PYM (orange) and with GTP (black circles). The residue mutated in Ran for structure determination (Q71L) is boxed.

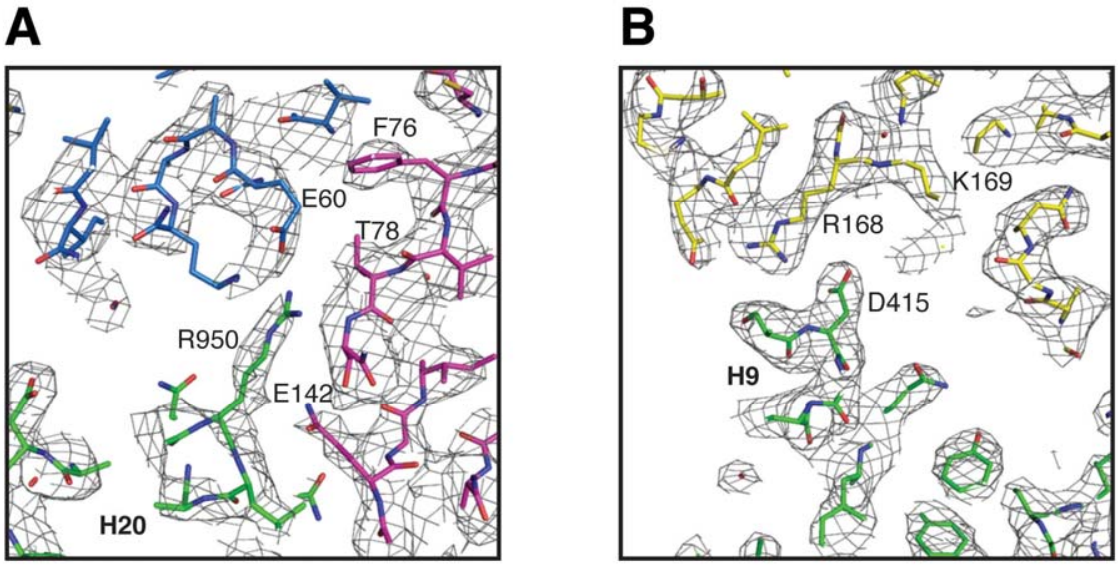

Figure S2
Electron density of regions of the Imp13-Mago-Y14 and Imp13-Ran structures.
The electron density of the refined 2Fo-Fc maps is shown as gray mesh contoured at 1σ, with the final models superposed.
A) Zoom-in view showing the interaction between the C-terminal region of Dm Imp13 (carbon atoms in green) and Mago-Y14 (carbon atoms in blue and magenta, respectively). Arg950 at HEAT 20 of Imp13 points towards Glu60 of Mago and Thr78 of Y14.
B) Zoom-in view showing the interaction between HEAT 9 of Hs Imp13 and RanGTP (similar view as in Figure 5B). Asp415 of Imp13 contacts Ran (shown with carbon atoms in yellow) at Arg168.

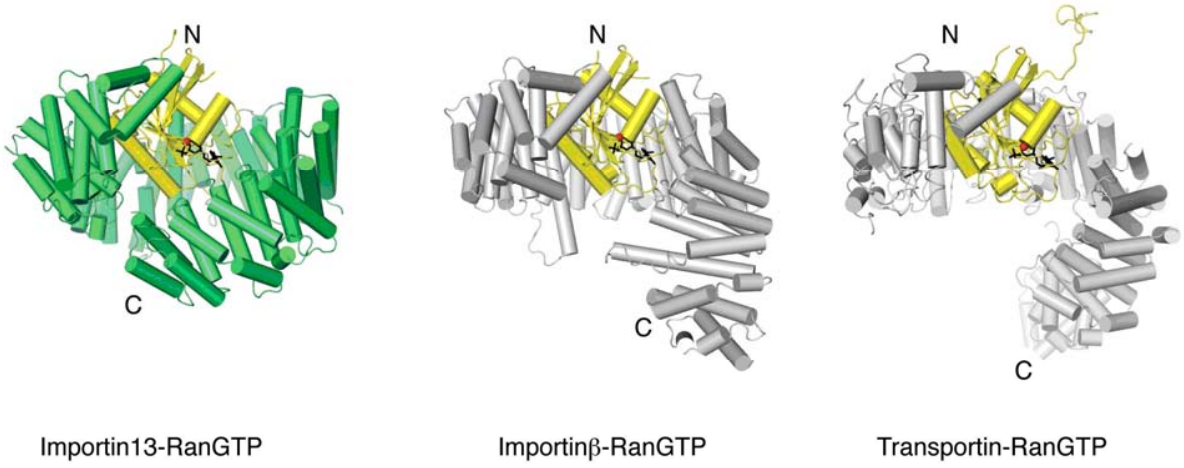

Figure S3
Imp13 is an all α-helical protein of the HEAT-repeat karyopherin family. The crystal structures of Imp13-RanGTP, Importinβ-RanGTP, Transportin-RanGTP are shown, after superposition of RanGTP in a similar orientation as in Figure 3A in the main text. RanGTP is shown in yellow, GTP in black and magnesium as a red sphere. The comparison shows the conformational variability of the three different importins bound to RanGTP.

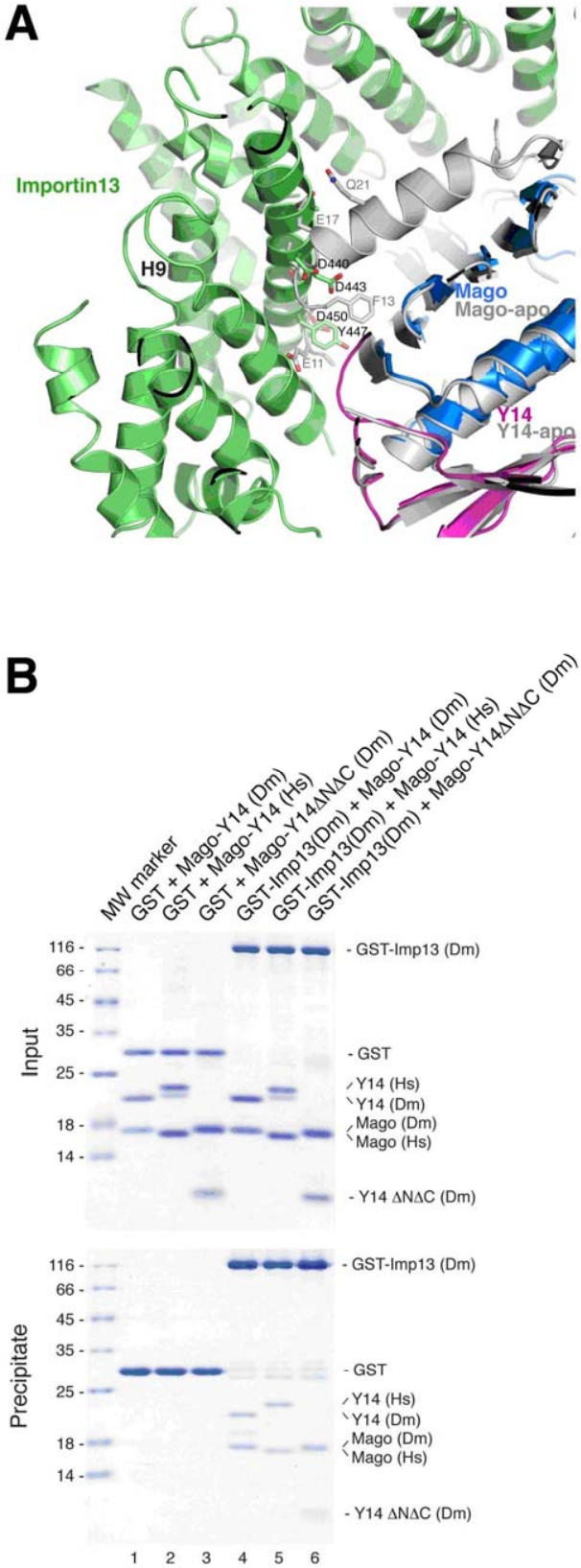

Figure S4
Requirements for the interaction between Imp13 and MagoY14.
A) Comparison of Mago-14 in the apo and Imp13-bound structures. In the apo structure, the N-terminal helix of Y14 (in gray) packs against the β-sheet of Mago. This conformation of the Y14 N-terminal helix is not compatible with Imp13 binding, since it would clash against HEAT 9. Selected residues of the Y14 N-terminus in this region are labeled in gray and of Imp13 in black. Indeed, no ordered electron density for the Y14 N-terminal helix is visible in the Imp13-bound structure, suggesting it has been displaced into solvent.
B) Protein co-precipitations were carried out by incubating GST-tagged *Drosophila* Imp13 with full-length Mago-Y14 from either *D. melanogaster* (Dm) or *H. sapiens* (Hs), or with a construct of Dm Mago-Y14 lacking the N-terminal and C-terminal regions in Y14 (Y14ΔNΔC, residues 67-154). The GST pull-down assays were performed in a buffer containing 50 mM NaCl. One sixth of the sample was kept as input control (upper panel) and the rest was precipitated with glutathione-sepharose beads (lower panel). Both input and pull-down samples were analyzed on Coomassie stained 15% SDS-PAGE. Lanes 1, 2 and 3 are the control pull-downs with GST, showing no unspecific binding of Mago-Y14 to the resin. Lanes 4, 5 and 6 show the pull-downs with GST-Imp13. The left-most lane contains the molecular weight markers. Minor bands between 25 and 35 kDa in lanes 4 to 6 are impurities from the GST-Imp13 purification.

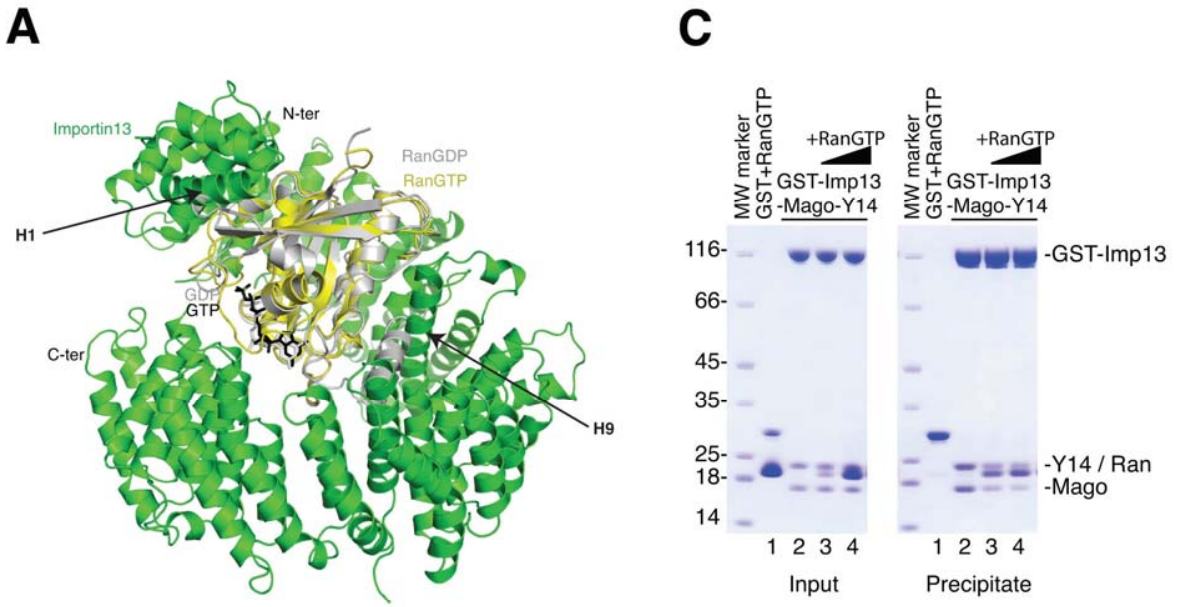

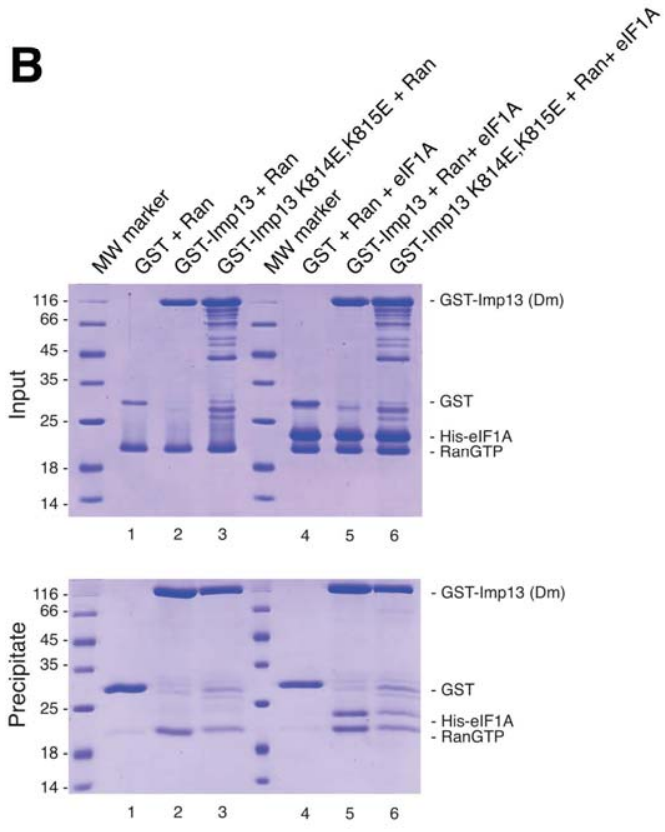

Figure S5
Requirements for the interaction between Imp13 and Ran

A) Incompatible binding of RanGDP and Importin 13. Structure of RanGDP (in gray, PDB code 1BYU) superposed to Importin13-RanGTP (in green and yellow, respectively). The superposition shows two regions (indicated with an arrow) where RanGDP would sterically clash with Importin 13.

B) Effect of Imp13 mutants on RanGTP binding. Protein co-precipitations were carried out by incubating GST-tagged *Drosophila* Imp13 (either wild-type or with the K814E-K815E mutation) with human eIF1A and/or yeast RanGTP. The GST pull-down assays were performed as described in Supplementary Figure 4. Lanes 1 and 4 show the control pull-downs with GST. While the K814E/K815E mutant disrupted the interaction with Mago-Y14 (Figure 4, lane 4), it was not sufficient to completely disrupt the formation of an Imp13-Ran and of an Imp13-Ran-eIF1A complex.

C) Competition experiment showing the effect of RanGTP on the Mago-Y14 binding properties of Imp13. The pull-down assays were carried out with GST-Imp13-Mago-Y14 and increasing amounts of RanGTP. The pull-downs were carried out with a similar protocol described in Figure 6D.

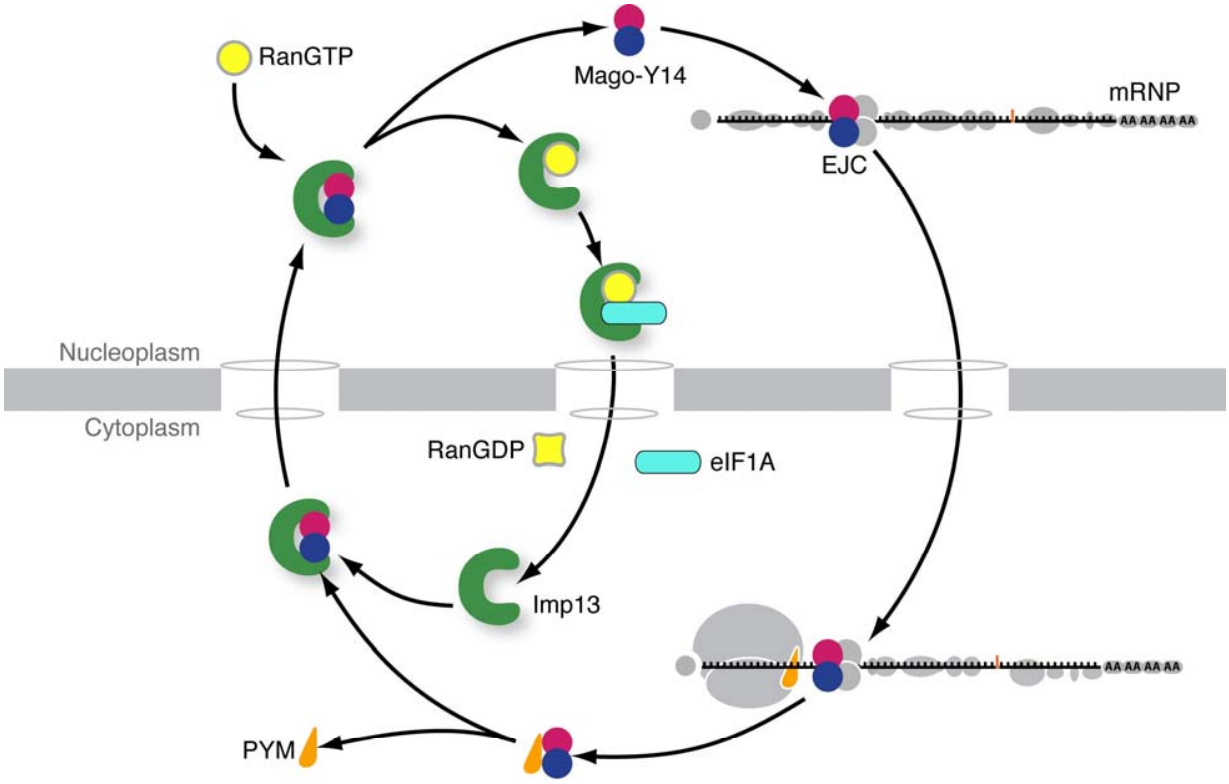

Figure S6
Interactions in the Mago-Y14 cycle
The scheme shows the sequel of either simultaneous or mutually exclusive interactions underlying Mago-Y14 function. The Mago-Y14 heterodimer (blue and magenta) is transported into the nucleus by Imp13 (in green), here released by RanGTP binding (yellow circle) and incorporated into a spliced mRNP with eIF4AIII and Btz (grey) in the form of the EJC (other mRNP proteins are shown in gray). After the mRNP is transported to the cytoplasm to function in translational regulation (ribosome in gray), the EJC is disassembled with the aid of a ribosomal-binding protein, PYM (in orange). Mago-Y14 is re-imported into the nucleus without PYM by Imp13. Imp13 also functions as a nuclear export factor for eIF1A (cyan bar). After reaching the cytoplasm, the export complex is dissociated by hydrolysis to RanGDP (yellow rectangle).

5.2 Structure of Importin13-Ubc9 complex: nuclear import and release of a key regulator of sumoylation

This work has been originally published in following article:

Structure of Importin13-Ubc9 complex: nuclear import and release of a key regulator of sumoylation

Marlene Grünwald and Fulvia Bono
EMBO Journal, 2011, 30(2):427-438

The EMBO Journal (2010), 1–12 | © 2010 European Molecular Biology Organization | All Rights Reserved 0261-4189/10
www.embojournal.org

THE
EMBO
JOURNAL

Structure of Importin13–Ubc9 complex: nuclear import and release of a key regulator of sumoylation

Marlene Grünwald and Fulvia Bono*

Max Planck Institute for Developmental Biology, Tübingen, Germany

Importin13 (Imp13) is an unusual β-karyopherin that is able to both import and export cargoes in and out of the nucleus. In the cytoplasm, Imp13 associates with different cargoes such as Mago-Y14 and Ubc9, and facilitates their import into the nucleus where RanGTP binding promotes the release of the cargo. In this study, we present the 2.8 Å resolution crystal structure of Imp13 in complex with the SUMO E2-conjugating enzyme, Ubc9. The structure shows an uncommon mode of cargo–karyopherin recognition with Ubc9 binding at the N-terminal portion of Imp13, occupying the entire RanGTP-binding site. Comparison of the Imp13–Ubc9 complex with Imp13–Mago-Y14 shows the remarkable plasticity of Imp13, whose conformation changes from a closed ring to an open superhelix when bound to the two different cargoes. The structure also shows that the binding mode is compatible with the sumoylated states of Ubc9. Indeed, we find that Imp13 is able to bind sumoylated Ubc9 *in vitro* and suppresses autosumoylation activity in the complex.

The EMBO Journal advance online publication, 7 December 2010; doi:10.1038/emboj.2010.320
Subject Categories: membranes & transport; structural biology
Keywords: Importin13; karyopherin; nuclear import; Ubc9–SUMO; X-ray crystallography

Introduction

The regulated transport of molecules through the nuclear pore complexes (NPCs) is a distinctive feature of the eukaryotic cell. The main facilitators of nucleocytoplasmic transport are cargo receptors belonging to the karyopherin-β family (Görlich and Kutay, 1999; Cook *et al*, 2007; Terry *et al*, 2007). Members of this family that transport proteins into the nucleus are called importins. In contrast, exportins facilitate the export of cargoes from the nucleus to the cytosol. Importins and exportins are regulated by RanGTP in opposite ways. In the cell, RanGTP forms a gradient with high levels of RanGTP in the nucleus and low levels in the cytoplasm. Importins associate with a cognate cargo in the cytoplasm and release it in the nucleus on RanGTP binding. Exportins, conversely, bind their cargo in the presence of RanGTP and release it in the cytoplasm when GTP is hydrolyzed to GDP (Cook and Conti, 2010). Two unusual karyopherins, Importin13 (Imp13) and yeast Msn5 (Mingot *et al*, 2001; Yoshida and Blobel, 2001) can function as both import and export receptors. In human cells, Imp13 can export the translation initiation factor eIF1A and import the exon junction complex components Mago-Y14 as well as several transcription factors that contain a histone-fold motif and the E2 SUMO-conjugating enzyme Ubc9 (Mingot *et al*, 2001; Kahle *et al*, 2005; Walker *et al*, 2009).

Recent structural studies have revealed the mechanistic basis for nuclear targeting and release of Mago-Y14 (Bono *et al*, 2010). In complex with Mago-Y14, Imp13 has a closed ring-like conformation, which can be thought of as composed of an N-terminal and a C-terminal arch facing each other. Mago-Y14 binds to the concave surface of the C-terminal arch via a set of evolutionarily conserved residues. This portion of the import factor is the common site for cargo recognition observed in all but one of the importin crystal structures known to date (Cingolani *et al*, 2002; Cook *et al*, 2007).

The complex with RanGTP (i.e., the snapshot of the nuclear state after cargo release) shows that RanGTP binds to the inner concave surface of the N-terminal arch. Although RanGTP and Mago-Y14 occupy different surfaces on the importin, their binding is nevertheless mutually exclusive because of direct steric clashes between the GTPase and the cargo. This is rather different from the mechanism of substrate release observed in importin-β and transportin, wherein an acidic loop at the interface between the N-and C-terminal arches of these karyopherins is the focal point for cargo uptake and release (Cook *et al*, 2007).

While Mago-Y14 is to date the best-studied example of Imp13-mediated transport, little is known of how Imp13 mediates the nuclear import of another evolutionarily conserved cargo, Ubc9. Ubc9 is an essential protein in mammalian cells with a predominantly nuclear localization (Firestein and Feuerstein, 1998; Rodriguez *et al*, 2001; Hayashi *et al*, 2002; Nacerddine *et al*, 2005; Geiss-Friedlander and Melchior, 2007). It is the only SUMO E2-conjugating enzyme and, as such, is a central player in specifying SUMO substrates and catalyzing all SUMO conjugations in the cell (Melchior, 2000; Johnson, 2004). Sumoylation results in the formation of an isopeptide bond between the C-terminal carboxy group of mature SUMO and the ε-amino-group of a lysine residue in the target protein. SUMO attachment occurs in an ATP-dependent reaction wherein SUMO forms a thioester bond with the E1-activating enzyme heterodimer Aos1–Uba2. SUMO is then transferred to the E2-conjugating enzyme Ubc9, again forming a thioester. The reaction is often enhanced by the intervention of E3 ligases (Melchior, 2000; Johnson, 2004). Sumoylation is crucial in a broad range of cellular processes, wherein it acts at the molecular level by altering the protein–protein interaction properties of its targets in a reversible manner (Johnson, 2004; Geiss-Friedlander

*Corresponding author. Department of Biochemistry, Max-Planck-Institute for Developmental Biology, Spemannstraße 35, Tübingen 72076, Germany. Tel.: +49 7071 6011367; Fax: +49 7071 6011353; E-mail: fulvia.bono@tuebingen.mpg.de

Received: 13 August 2010; accepted: 10 November 2010

and Melchior, 2007; Makhnevych *et al*, 2009). The structures of Ubc9 in different complexes and sumoylation states have revealed the molecular basis for E2-dependent protein conjugation (Capili and Lima, 2007b; Knipscheer *et al*, 2008; Tang *et al*, 2008; Sekiyama *et al*, 2010)). The specificity of the sumoylation reaction can be regulated at different levels. For example, it has been shown that the mammalian E2-conjugating enzyme Ubc9 is autosumoylated to regulate target discrimination (Hannich *et al*, 2005; Knipscheer *et al*, 2008; Makhnevych *et al*, 2009). To understand the mechanism by which Ubc9 is transported into the nucleus and how the import step fits into the Ubc9 sumoylation pathway, we determined the structure of the complex of Imp13 with Ubc9 and studied how the sumoylation properties of Ubc9 are affected in the import complex.

Results and discussion

Structure determination

Full-length human (Hs) Imp13 and Ubc9 were expressed independently in *Escherichia coli* and purified to homogeneity. The 126 kDa complex was reconstituted by size-exclusion chromatography using an excess of Ubc9 to saturate the complex. The binary complex crystallized in space group $P2_12_12_1$, with one molecule per asymmetric unit. The structure was solved by molecular replacement (MR) using the human Ubc9 structure (PDB ID 1U9A, (Tong *et al*, 1997)) and the human Imp13 structure (PDB ID 2X19, (Bono *et al*, 2010) as search models. A successful MR solution could only be obtained when the Imp13 search model was separated into fragments that could be fitted initially as rigid bodies (see methods). The final model (Figure 1) has been refined to 2.8 Å resolution with an *R*-free of 26.7%, *R*-factor of 22.4% and good stereochemistry (Table I). In the structure, some disordered stretches of residues at the N- and C-termini of Imp13, as well as a long inter-loop between HEAT 14 and 15 (residues 655–673) and a few residues in loops are missing in the final model; the full-length Ubc9 could be modelled. A sample view of the quality of the electron density of the Imp13–Ubc9 interacting surface is shown in Supplementary Figure S1.

Superhelical conformation of Imp13 when bound to Ubc9

Imp13 consists of 20 consecutive HEAT repeats as previously shown (Bono *et al*, 2010) (Figure 1A and B). Briefly, HEAT repeats are 40 amino-acid motifs that typically fold into two α-helices A and B (Andrade *et al*, 2001) and stack against consecutive repeats to form a superhelix. The A helices form the outer surface of the superhelix and the B helices the inner concave surface. Loops link the two helices within (intra-repeat) and between (inter-repeat) HEAT motifs. In Hs Imp13, most of these loops are short, but longer helical insertions are observed in the intra-repeat loop at HEAT 9 and in the inter-repeat loop between HEAT 17 and 18. The repeats pack against each other generally with a clockwise rotation between successive repeats. This rotation is interrupted around HEAT 4 and 10 by counter-clockwise turns that roughly correspond to hinge regions. Further deviations from canonical HEAT repeat arrangements are found at the first repeat that packs almost perpendicularly against HEAT 2 and the last repeat that consists of three parallel α-helices that cap the

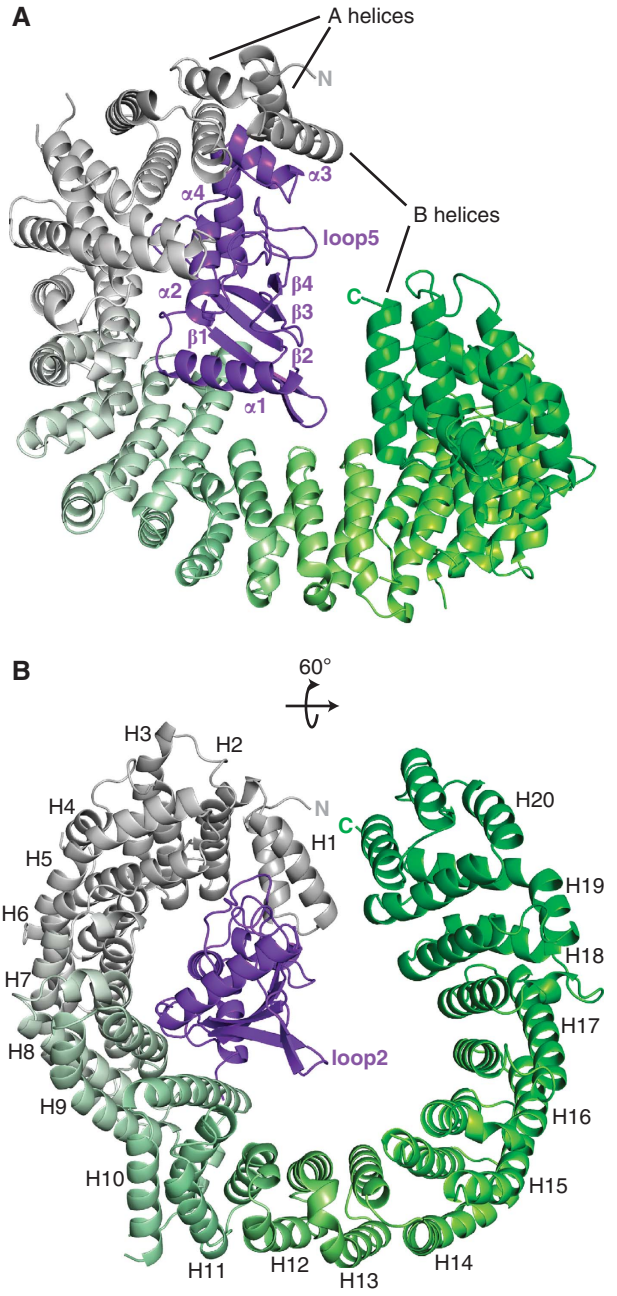

Figure 1 Structure of the Imp13–Ubc9 complex. (**A**) Cartoon view of the complex. Imp13 is shown in green with a colour gradient from grey (N-terminus) to green (C-terminus). Ubc9 is in purple. Secondary structure elements are labelled; (**B**) Cartoon view rotated 60° along the *x* axis. HEAT repeats are labelled from H1 to H20. These and all other protein structure figures were generated using PyMOL (http://www.pymol.org).

superhelix, similar to what was recently observed in the tRNA export receptor, Xpot (Cook *et al*, 2009).

In the Imp13–Ubc9 structure, the HEAT repeats are arranged to form a superhelical structure with the N- and C-terminal ends twisted away from each other. The conformation of Imp13 is, therefore, very different from the ring structure it adopts when in complex with Mago-Y14 (see below). The superhelical pitch extends for ∼57 Å with a central hole of ∼65–70 Å in diameter (longest diagonal). The C-terminal portion of the molecule is not engaged in

Table I Crystallographic statistics for data collection and refinement

Data collection	
Data set	Imp13–Ubc9
Beamline	SLS PXII
Space group	$P2_12_12_1$
Unit cell (Å)	$a=68.7$, $b=126.8$, $c=184.0$, $\alpha=\beta=\gamma=90^\circ$
Wavelength (Å)	0.9997
Resolution range (Å)[a]	50–2.8 (2.9–2.8)
Unique reflections	40287
Multiplicity	3.7
Completeness (%)[a]	99.4 (99.9)
$I/\sigma(I)$[a]	14.49 (2.37)
R_{sym}(%)[a]	6.9 (67.5)
Refinement	
Resolution range (Å)[a]	50–2.80
R-free (%)[a]	26.7
R-work (%)[a]	22.4
r.m.s.d. Bond (Å)	0.011
r.m.s.d. Angle (deg)	1.4
B factor protein (Å^2)	74.5
Ramachandran values[b]	
Favoured (%)	96.5%
Allowed (%)	99.1%

[a]Values in parentheses correspond to the highest resolution shell.
[b]Molprobity, http://molprobity.biochem.duke.edu/.

binding with the cargo. Ubc9 occupies almost exactly the N-terminal half of the inner surface of the superhelix (Figure 1B).

In the complex with Imp13, Hs Ubc9 shows the canonical E2 catalytic fold that is similar to previously reported structures of the protein in isolation and in other complexes. Ubc9 superimposes with a root mean square deviation (r.m.s.d.) between 0.435 and 1.02 Å (over all Cα atoms) on available Ubc9 structures of the mammalian proteins (Tong *et al*, 1997; Giraud *et al*, 1998; Bernier-Villamor *et al*, 2002; Reverter and Lima, 2005; Yunus and Lima, 2006; Knipscheer *et al*, 2007, 2008; Wang *et al*, 2007; Capili and Lima, 2007a). Ubc9 has an asymmetric structure that contains a four-stranded anti-parallel β-sheet (β1–4) on one side delimited by four α-helices (α1–4) on the other side (Figure 1A). A finer comparison of Ubc9 when in complex with Imp13 and in other structures, detects minor conformational variability in only two loops of Ubc9. The loop between helices α2 and α3 (loop6) is slightly displaced (r.m.s.d. 1.958 Å over 9 Cα atoms) in the Imp13–Ubc9 structure and is engaged in the binding to Imp13. This loop of Ubc9 is also involved in the recognition of the SUMO consensus motif (ΨKXE/D, where Ψ is a bulky hydrophobic residue and X is any residue) for the direct interaction with its substrates (Bernier-Villamor *et al*, 2002) (Supplementary Figure S5). The second part of Ubc9 that deviates from other known structures is a β-hairpin that protrudes from the Ubc9 core domain into the solvent (loop2). The conformation of this loop varies between all Ubc9 structures and so is likely to be intrinsically flexible (Figure 1B).

Extensive interactions mediate Ubc9 recognition by Imp13

Ubc9 fits into the N-terminal arch of Imp13 formed by HEATs 1–9 with direct interactions at two main areas of Imp13 inner surface (Figures 1B, 2A and B). Ubc9 contacts Imp13 mainly through interactions at loop1, loop5 and loop6 (Figure 2A and B and Supplementary Figure S2). A subset of these interacting residues is conserved (Supplementary Figure S2). The first patch of interactions is largely hydrophobic and is facilitated on Ubc9 by loop6 as well as the helix α3 itself, which packs against both helices of HEAT 1 and the B helix of HEAT 2 of Imp13. In particular, Ile125 of Ubc9 ($Ile125_{Ubc9}$) contacts the side chains of Tyr34 of Imp13 ($Tyr34_{Imp}$), $Glu73_{Imp}$ and $Tyr76_{Imp}$ while a second hydrophobic residue, $Tyr134_{Ubc9}$ points towards $Leu33_{Imp}$ and $Tyr34_{Imp}$ (Figure 2A).

The next set of interactions involves HEAT 6–9 of Imp13. Loop1 (the loop between helix α1 and the β-sheet) of Ubc9 packs tightly against HEAT 7, whereas HEAT 7, 8 and 9 of Imp13 are contacted via two positively charged amino acids from the first helix α1 of Ubc9. The interactions on this binding interface are largely polar and involve several positively charged residues contributed by Ubc9. $Arg17_{Ubc9}$ approaches the side chains of $Asp426_{Imp}$ (HEAT 9) and $Leu361_{Imp}$ (HEAT 8), while $Lys18_{Ubc9}$ points towards the residues $Val313_{Imp}$, $Glu317_{Imp}$ and $Asn318_{Imp}$ (HEAT 7). $Thr362_{Imp}$ on HEAT 8 forms polar contacts to both residues of Ubc9. Moreover, two salt bridges are formed between $Asp415_{Imp}$ of HEAT 9 and $Lys59_{Ubc9}$, and between $Glu261_{Imp}$ at HEAT 6 and $Lys110_{Ubc9}$ (Figure 2B).

A smaller set of interactions is formed by loop5 (the β-sheet to α2 loop) of Ubc9 and Imp13 HEAT 4 up to the inter-repeat loop between HEAT 4 and HEAT 5 (Supplementary Figure S2). A closer look reveals that $Asp102_{Ubc9}$ forms a polar interaction with $Thr179_{Imp}$ (at HEAT 4) (Figure 2A).

Thus, the N-terminal arch of Imp13 clamps Ubc9 with specific interactions (Supplementary Figure S2). The Imp13 grasps the Ubc9 as if between an opposing thumb (the N-terminal 2 HEAT repeats) and fingers (the B helices of HEAT repeats 6 to 9) (Figures 1A, B, 2A and B). Consistent with the structural analysis, mutations of both $Tyr34_{Imp}$ and $Tyr35_{Imp}$ to arginine (on the thumb) or of $Asp426_{Imp}$ to arginine (on the fingers) reduced or abolished the binding to Ubc9 in pull-down assays (Figure 2C, lanes 9 and 12 and Supplementary Figure S4C).

Imp13 uses different surfaces to bind Ubc9 and Mago-Y14

The binding mode of Ubc9 to Imp13 is different to that observed with Mago-Y14 and with other karyopherins. The N-terminus of Imp13 shares the highest degree of conservation with the other members of the karyopherin family as it is the binding site for their common regulator, RanGTP (Görlich *et al*, 1997). This is also the region wherein Ubc9 binds. In other importin structures solved to date, cargo molecules are usually found associated with the C-terminal arch of the importin (Cingolani *et al*, 1999; Lee *et al*, 2003, 2006; Cansizoglu *et al*, 2007; Imasaki *et al*, 2007; Wohlwend *et al*, 2007; Mitrousis *et al*, 2008; Bhardwaj and Cingolani, 2010). The only previously observed exception is a cargo of importin-β, the parathyroid hormone-related protein (PTHrP) that binds in an extended conformation at the N-terminal arch between HEAT 2 and 11 (Cingolani *et al*, 2002) (Supplementary Figure S4).

While Ubc9 interaction requires only the N-terminal half of Imp13 (Figures 3D and 4A), Mago-Y14 binding engages HEAT repeats from 5 to the very last helix of HEAT 20. Moreover,

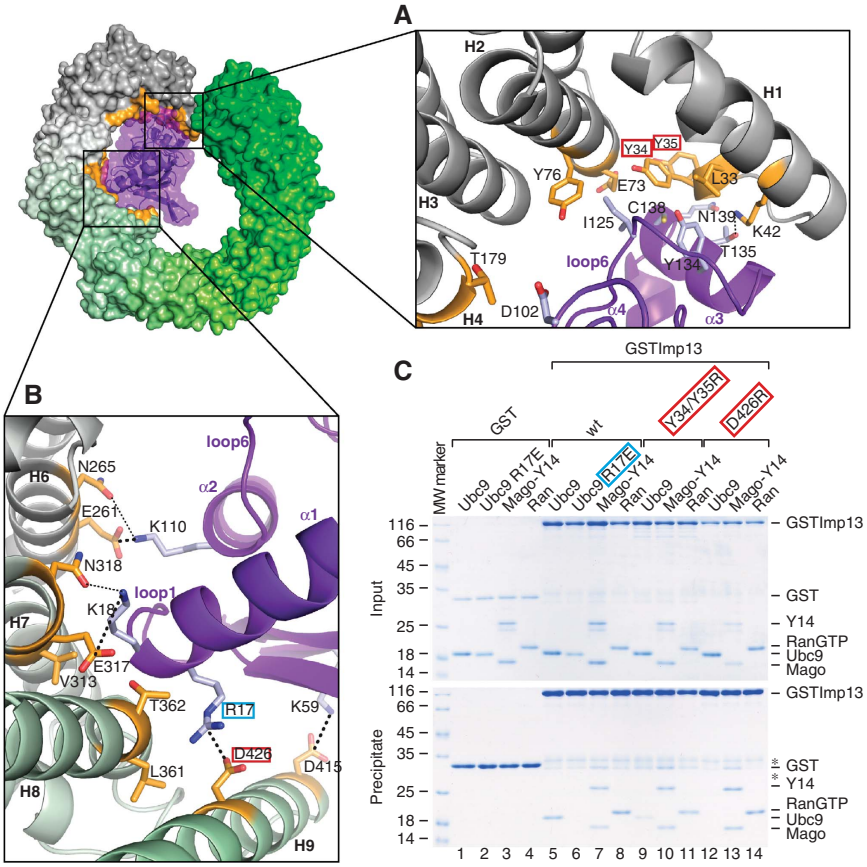

Figure 2 Details of the interactions between Imp13 and Ubc9. (**A**, **B**) show close up views of the interactions between Imp13 and Ubc9. In the upper left, the molecule is rendered as surface in a similar colour code and in a similar orientation as in Figure 1B. Interacting residues on Imp13 are in orange and interacting side-chains on Ubc9 are in pale blue for clarity. The views show the interaction between HEATs 1, 2 and 4 of Imp13 and the loop6 of Ubc9 (**A**), HEATs 7–9 of Imp13 and the loop1 of Ubc9, and between HEAT 6 and the helix α2 of Ubc9 (**B**). Residues of Imp13 and Ubc9 are labelled and HEAT repeats are in black (bold). Secondary structure elements of Ubc9 are labelled in purple. H bonds and charged interactions are shown as regular dotted lines and bold dotted lines, respectively. See also the corresponding electron density in Supplementary Figure S1. Residues mutated in 2C are highlighted with a red (Imp13) or blue (Ubc9) box. (**C**) Protein co-precipitations by GST pull-down assays. GST-tagged Imp13 wild type (wt) or mutant (labelled with a red box) was incubated with Ubc9 wt or mutant (blue box) in a buffer containing 50 mM NaCl. One-sixth of the sample was kept as input control (upper panel) and the rest was co-precipitated with glutathione sepharose beads (lower panel). Both input and pull-down samples were analyzed on Coomassie stained 15% SDS–PAGE. Lanes 1–4 show binding to GST as control. The far left lane was loaded with a molecular weight marker. The gels show some contamination between 35 and 25 KDa (marked with *), probably resulting from degradation of GSTImp13.

the two cargoes bind to the inner surface of Imp13 shifted towards opposite sides: Ubc9 is shifted towards the protruding N-terminal HEAT repeats and at the intra-repeat loops, whereas Mago-Y14 is enclosed by Imp13 on the side of the inter-repeat loops. The conformation of Imp13 in the two complexes is dramatically different (r.m.s.d. 8.4 Å over 792 Cα atoms). In complex with Mago-Y14, Imp13 has an open toroid conformation with the edges of HEAT 1 and HEAT 20 in close proximity (~22 Å distance) while in the complex with Ubc9, the edges of the superhelix are twisted and displaced ~43 Å apart (Figure 3A and C). Ubc9 and Mago-Y14 bind to non-overlapping sites at the inner surface of Imp13. HEAT 8 and HEAT 9 are contacted by both cargoes but at opposite ends of the B helices. While Ubc9 binds towards the tip of the helices of HEAT 4 and 6, Y14 binds adjacently at the following inter-repeat loops (Figure 3, Supplementary Figures S2 and S4). Consistent with these different binding modes, mutations of the human Imp13 corresponding to *Drosophila* mutations that were previously described to impair Mago-Y14 binding (Bono *et al*, 2010) do not affect Ubc9 binding to Imp13 (Figure 3D, lane 7 and Supplementary Figure S4). Moreover, a C-terminally truncated version of Imp13 (Imp13ΔC; HEATs 1–14, residues 1–672) retains its binding ability to Ubc9 and RanGTP (see below) but not to Mago-Y14. Indeed, more than half of Mago-Y14 interaction sites at the C-terminus of Imp13 are missing in the truncated mutant.

Both Ubc9 and Mago-Y14 are nuclear proteins at steady state (Seufert *et al*, 1995; Firestein and Feuerstein, 1998; Kataoka *et al*, 2000; Le Hir *et al*, 2001; Rodriguez *et al*, 2001). Ubc9 can sumoylate targets such as RanGAP in the cytoplasm (Matunis *et al*, 1996; Mahajan *et al*, 1997) and Mago-Y14 shuttles to the cytoplasm as part of the mRNP-associated EJC (Le Hir *et al*, 2001). Given that Ubc9 and Mago-Y14 are both specifically imported by Imp13 and that they sit at opposite sides of Imp13, we asked whether the two cargoes could bind concomitantly to be transported by Imp13 at the same time. A superposition of the two structures does not indicate any obvious steric clashes between the two import cargoes; however, the two structures could not be

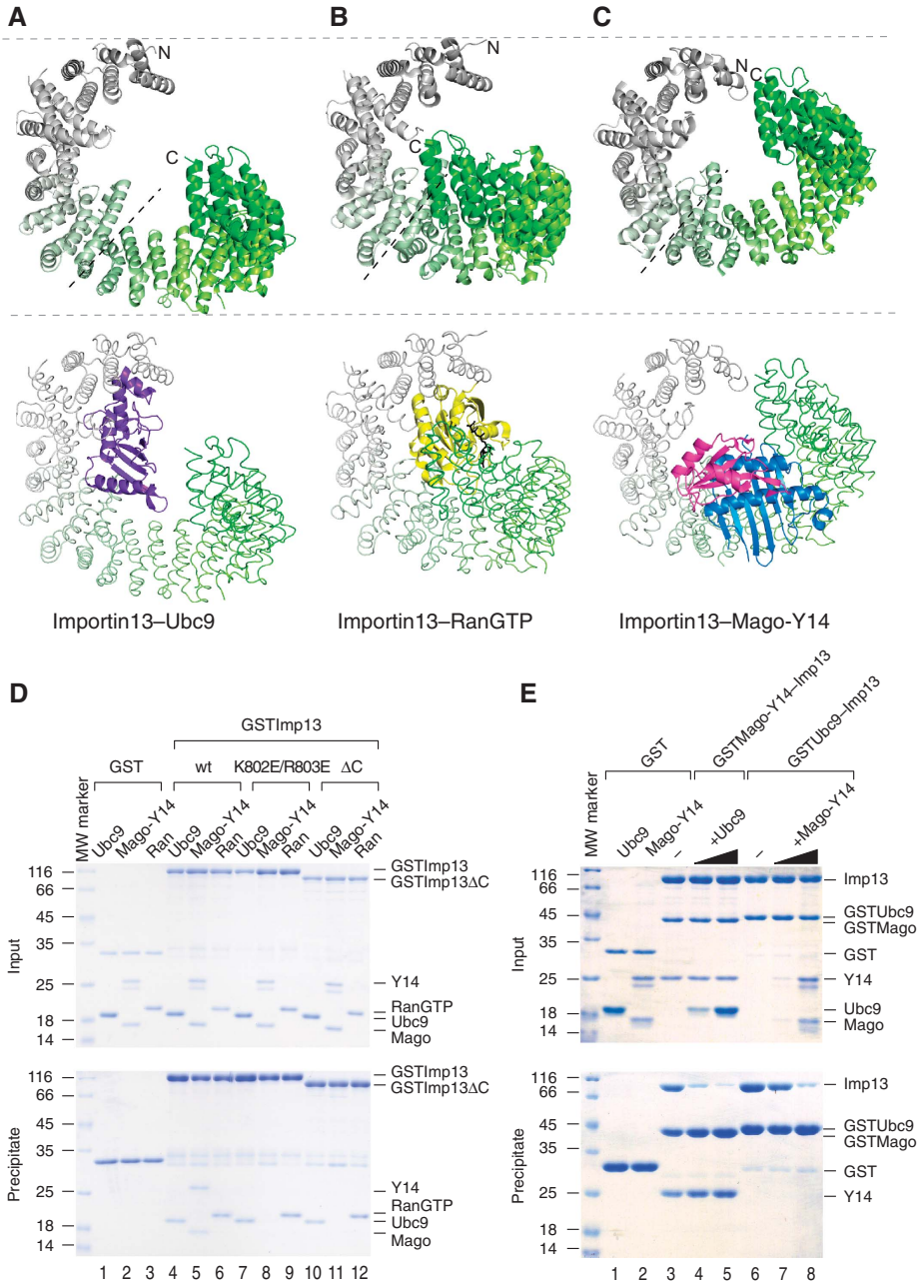

Figure 3 Conformational changes and binding mode of Imp13 in different complexes. (**A**–**C**) Conformational changes of Imp13 bound to (**A**) Ubc9, (**B**) RanGTP and (**C**) Mago-Y14. In the upper panel, the bound molecules are removed for clarity. Imp13 is represented as a cartoon with the same colour coding and view as in Figure 1A. The hinge point at HEAT 10 is represented as a dashed line in black. In the lower panel, Imp13 is represented as a ribbon trace while the bound molecules are shown as a cartoon. Ubc9 is in purple (**A**), Ran in yellow and GTP in black (**B**), Mago in blue, and Y14 in magenta (**C**). (**D**) Protein co-precipitation of GSTImp13 wt, of a GSTImp13 double mutant that was previously shown to impair the binding to Mago-Y14 (Bono *et al*, 2010) and of a GSTImp13 C-terminally truncated mutant (GSTImp13ΔC, H1–14). Both Imp13 K802E/R803E and GSTImp13ΔC mutants retain their ability to bind Ubc9 (lane 7, 10) and RanGTP (lane 9, 12). (**E**) On the left, competition assay of Ubc9 to Imp13–Mago-Y14 and on the right side of Mago-Y14 to Imp13–Ubc9. Both cargoes can displace each other and no concomitant binding is detected. In this competition experiment, 4 μg of GST, GST–Ubc9-Imp13 or GST–Mago-Y14-Imp13 were incubated on beads and competing amounts of Ubc9 (lanes 4 and 5) or of Mago-Y14 (lanes 7 and 8) were added (1 μg and 4 μg lanes 4, 7 and 5, 8, respectively).

optimally aligned because of the large conformational differences. Competition experiments show that increasing amounts of Ubc9 displace Imp13 bound to an immobilized GST fusion of Mago-Y14 (GST–Mago-Y14) and vice versa, clearly indicating that the binding of the two import cargoes is mutually exclusive (Figure 3E). This suggests that the different conformations of the two import complexes prevent mutual binding, allowing only one import cargo to bind at a time.

Mechanism of Ubc9 release from Imp13 by RanGTP

The Imp13–Ubc9 complex forms in the cytosol and translocates through the NPCs into the nucleus. There, on RanGTP binding to Imp13, Ubc9 is dissociated. RanGTP has three main attachment surfaces on Imp13. The first encompasses HEATs 1–4. The second interaction surface is centred at the protruding B helix of HEAT 9, which is in analogous position to the acidic loop at HEAT 8 in other importins. The last

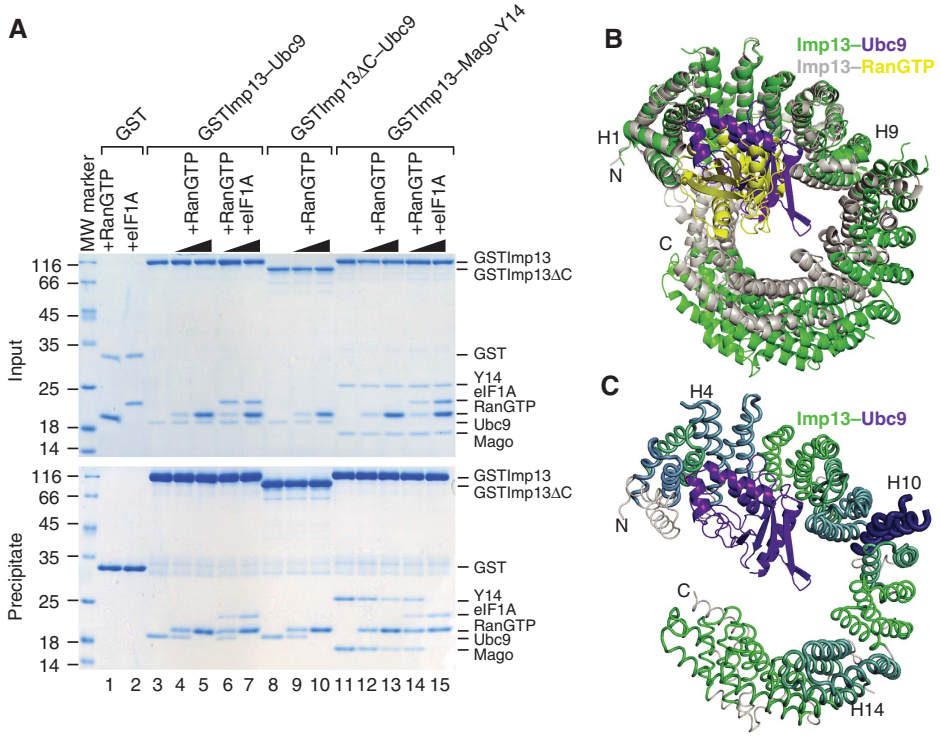

Figure 4 Cargo release by RanGTP. (**A**) Cargo release by increasing amounts of RanGTP (lanes 4, 5, 9, 10, 12, 13) and of RanGTP + eIF1A (lanes 6, 7, 14, 15) is shown in a competition assay on Imp13–Ubc9 (lanes 4–7), Imp13ΔC (HEATs 1–14)–Ubc9 (lanes 9, and 10) and Imp13–Mago-Y14 (lanes 12–15). RanGTP promotes the full dissociation of Ubc9 bound to Imp13ΔC (lane 10). Lanes 1 and 2 show binding of RanGTP and eIF1A to GST as control. (**B**) Superposition of Imp13–Ubc9 and Imp13–RanGTP (PDB ID 2X19). Imp13–Ubc9 is shown in green with a similar view as in Figure 1 after a 180° rotation around the *y* axis, after optimal superposition of the N-termini. Imp13 in complex with RanGTP is shown in grey, Ran is shown in yellow (Supplementary Figure S4C). (**C**) Sausage-like representation of the conformational differences between Imp13 in complex with Ubc9, and Imp13 in complex with RanGTP (calculated according to (Cook *et al*, 2009)). The wider the section of the ribbon and the darker the color, the more variability exists between the two structures. The complex is in the same orientation as in panel 4B. Hinge regions are labelled.

interaction surface involves HEAT 16–19 by which RanGTP bridges the gap between the N-and C-terminal edges of Imp13 (Bono *et al*, 2010). The comparison of the Imp13–Mago-Y14 structure and the Imp13–RanGTP structure shows that a dramatic conformational change takes place on Ran binding, whereupon the Imp13 assumes a more closed conformation. Mago-Y14 and Ran are bound on opposite sides of the molecule and the reverse-charge mutation of $Lys802_{Imp}$ and $Arg803_{Imp}$ to glutamate residues (corresponding to Lys814 and Lys815 in *Drosophila* Imp13) impairs Mago-Y14 binding but not RanGTP or Ubc9 binding (Figure 3D, lanes 7–9 and Supplementary Figure S4).

Surprisingly, Ubc9- and Ran-binding surfaces largely overlap at the N-terminal half of Imp13, with Ubc9 only lacking the C-terminal contact region (Figure 4B). On Imp13, Ubc9 and RanGTP bury a surface area of 1438.6 $Å^2$ and 1567.7 $Å^2$, respectively (as determined by the PISA server; (Krissinel and Henrick, 2007)). Ubc9 and RanGTP interact with Imp13 at several conserved positions on Imp13 but of all the conserved residues at the Ubc9 interface, only two are specific for this cargo (Supplementary Figure S2). Comparison of the Imp13 conformation in the Ubc9-bound complex and in the RanGTP-bound complex shows that the overall conformation of the N-terminal arch is quite similar (r.m.s.d. 1.4 Å over 320 atoms) in the two structures, whereas the C-terminal arch assumes a more open conformation in the Ubc9-bound form (Figure 3A and B). The hinge regions, where more significant movements occur on RanGTP binding, are located at HEAT 4, at HEAT 10 and around HEAT 14 (Figure 4C).

As the Ubc9-interacting surface overlaps with that of RanGTP, cargo release is initiated by direct competition rather than steric hindrance as shown for Mago-Y14 dissociation (Bono, 2010). In the Imp13–Ubc9 complex, the C-terminal binding site of RanGTP is exposed, suggesting that it could nucleate RanGTP association with Imp13. However, RanGTP is able to promote Ubc9 dissociation from Imp13ΔC (Figure 4A, lanes 9–10). Thus, the C-terminal interacting surface of Imp13 is not required as a docking point for Ran to start Ubc9 dissociation. The docking of RanGTP on Imp13–Ubc9, likely occurs at the first HEAT repeat and some flexibility to remove Ubc9 might be needed, possibly around HEAT 4, one of the hinge regions (Figure 4C). Interestingly, efficient Mago-Y14 dissociation *in vitro* requires not only RanGTP but also Imp13 export cargo, eIF1A, while eIF1A alone is not sufficient to promote cargo dissociation (Supplementary Figure S6). These results indicate that release from Imp13 might occur via different mechanisms for Ubc9 and Mago-Y14 or that Mago-Y14 binds with higher affinity to Imp13 than Ubc9, requiring the additive effect of eIF1A to be completely displaced (Figure 4A). This suggests that Mago-Y14 release and subsequent incorporation into the nascent mRNP might only occur efficiently when there is abundant eIF1A in the nucleus and, therefore, could point towards a regulatory role for Imp13 in delivering and releasing the cargoes in the appropriate cellular location.

Accessibility of Ubc9 active sites in the structure

The catalytic groove with the conserved Cys93 and the active site residues $Asn85_{Ubc9}$, $Tyr87_{Ubc9}$ is located between the fourth strand and the second α-helix (loop5) (Bernier-Villamor *et al*, 2002) (Figures 1A and 5A). $Cys93_{Ubc9}$ is the catalytic residue that forms a thioester bond with the C-terminal glycine of SUMO. In the Imp13–Ubc9 complex, loop5 is exposed to solvent and its conformation does not show major changes compared with other Ubc9 structures. As mentioned, loop6 of Ubc9 is involved in the recognition of the SUMO consensus motif present on many SUMO targets. In particular, the consensus motif is recognized by residues $Asp127_{Ubc9}$, $Pro128_{Ubc9}$, $Ala129_{Ubc9}$, $Gln130_{Ubc9}$ and $Ala131_{Ubc9}$ on loop6 (Bernier-Villamor *et al*, 2002), all of which are partially accessible in the complex with Imp13 (Supplementary Figure S5A). The main attachment site of SUMO in autosumoylated Ubc9 is the side chain of $Lys14_{Ubc9}$ in helix α1 (Hannich *et al*, 2005; Knipscheer *et al*, 2008; Makhnevych *et al*, 2009) (Figures 1A and 5A). This residue is disordered in the structure and is not involved in Imp13 recognition.

Functional implication for sumoylation in Ubc9 import

Many proteins are modified by SUMO following extra- and intracellular stimuli. In many instances, regulation of sumoylation can occur at the level of the target through post-translational modification (phosphorylation on proximal residues and/or competing modifications of the acceptor Lys) (reviewed in Geiss-Friedlander and Melchior, 2007). However, it can also be regulated via changes in the activity, abundance or localization of the enzymes involved in the SUMO pathway. As mentioned above, although Ubc9 is the only cellular E2 SUMO-conjugating enzyme, it can also be an acceptor protein for sumoylation. Mammalian Ubc9 sumoylation takes places at a non-canonical consensus site in the α1 helix and it modulates target selection (Figure 5A and B and Supplementary Figure S2). It has been shown that the modification efficiency by SUMO conjugated Ubc9 (Ubc9*SUMO) is reduced in the case of RanGAP and is enhanced in the case of Sp100 (Knipscheer *et al*, 2008). The crystal structure of Ubc9*SUMO confirmed SUMO attachment at $Lys14_{Ubc9}$ and revealed a newly created binding surface involving both Ubc9 and SUMO that provides a rationale for improved Sp100 binding.

Superposition of Ubc9 in complex with Imp13 with Ubc9*SUMO (PDB ID 2VRR, (Knipscheer *et al*, 2008) suggests that binding of the modified cargo to Imp13 could be possible (only minor side chain clashes at HEATs 8 and 10 are visible) (Figure 5A and B). The C-terminal arch of Imp13 is not involved in the binding to Ubc9 and as such, is potentially free to accommodate further molecules. To address this issue, we performed *in vitro* sumoylation reactions in presence of the E1 activating enzyme, the heterodimer Aos1–Uba2 (here Aos–Uba for simplicity), SUMO1 (here SUMO for simplicity) and Ubc9. In these reactions, Ubc9 has the double functionality of the E2 enzyme and the target. We then performed *in vitro* pull-down assays to assess the binding capability of Ubc9*SUMO to immobilized GSTImp13. Western blot analysis shows that Imp13 indeed binds to sumoylated Ubc9 showing that modified Ubc9 could also be an import substrate for Imp13 (Figure 5C).

It has been shown that mutations of $Arg17_{Ubc9}$ and $Lys18_{Ubc9}$ significantly reduce SUMO1 conjugation activity *in vitro* probably because of inefficient SUMO transfer to Ubc9 from the E1 activating enzyme (Tatham *et al*, 2003). The same patch of residues of Ubc9 is involved in the binding of SUMO1 in a non-covalent manner (Knipscheer *et al*, 2007; Capili and Lima, 2007a). Structural analysis of the Imp13–Ubc9 interaction surface shows that these two conserved residues are involved in the binding to Imp13 (Figure 2B and above). A reverse charge mutant at $Arg17Glu_{Ubc9}$ loses the ability to bind Imp13 in pull-down assays (Figure 2C, lane 6), indicating that this catalytically inactive version of Ubc9 cannot be imported into the nucleus by Imp13 and showing that this conserved surface on Ubc9 serves multiple roles (Figure 5D, lane 3).

When in complex with Imp13, Ubc9 is no longer able to catalyze autosumoylation reactions (Figure 5D, lane 4) and the addition of RanGTP partially restores the activity by releasing Ubc9 from Imp13. This implies that full activity of Ubc9 is most likely resumed in the nucleus only after dissociation from Imp13 by RanGTP.

Given that Ubc9 catalytic Cys93, site of thioester attachment, is exposed to solvent in our structure, we asked whether SUMO modified Ubc9 via thioester bond (Ubc9∼SUMO) could also associate with Imp13 and whether Ubc9 in complex with Imp13 could accept SUMO from the E1 (Aos–Uba). We observe formation of Ubc9∼SUMO when Ubc9 is bound to Imp13 (Figure 5E, lane 6) with a similar efficiency to Ubc9 apo (Figure 5E, lane 5). Sensitivity of Ubc9–SUMO to a reducing environment indicates that SUMO is indeed attached via a thioester bond. Precipitation of the same reaction on GST beads shows that Ubc9∼SUMO is stably bound to Imp13. However, we cannot exclude that Ubc9 could be in a dynamic equilibrium with Imp13 and could dissociate to accept the thioester from E1–SUMO to then re-associate to Imp13 after attachment.

As previously mentioned, the active-site residues of Ubc9, essential for E2 activity, are mostly exposed to solvent in the complex with Imp13, suggesting that sumoylation of some sets of targets could still occur. However, all other Ubc9 structures solved to date would sterically clash with Imp13, suggesting that no other Ubc9 complex could associate with Imp13 (Supplementary Figure S3). In particular, structural superposition of Ubc9 in complex with SUMO targets RanGAP and E2-25K with Ubc9 in complex with Imp13 show strong steric clashes at the N-terminal arch of Imp13 (Supplementary Figures S3D, E and S5A) that appear to hamper the docking of these substrates to the appropriate position for the reaction. To clarify this issue, we performed a SUMO conjugation reaction of both these targets with Ubc9 alone or in complex with Imp13 (Figure 5F), according to published protocols (Pichler *et al*, 2002; Knipscheer *et al*, 2009). In the conditions used, we observe the appearance of weak bands at the molecular weight predicted for the sumoylated forms of both targets (lane 3 and 6, E2-25K and RanGAP, respectively), as compared with the controls (lanes 2 and 5). This result could indicate that Ubc9 is partially functional in conjugation as most of its active site is exposed although the binding sites of the substrates on Ubc9 are occluded by Imp13 binding. However, we cannot rule out that undetectable amounts of Ubc9 could dissociate from Imp13 and catalyze the reaction, while most of Ubc9 in complex with Imp13 is not

functional. Indeed, from the structural superposition of Ubc9 in complex with Imp13 and in complex with RanGAP*SUMO, it appears that Imp13 could block interaction with the SUMO consensus motif of the target by partially occluding the recognition site for the hydrophobic residue that precedes the Lys (in this case, a Leu) (Supplementary Figure S5A). This

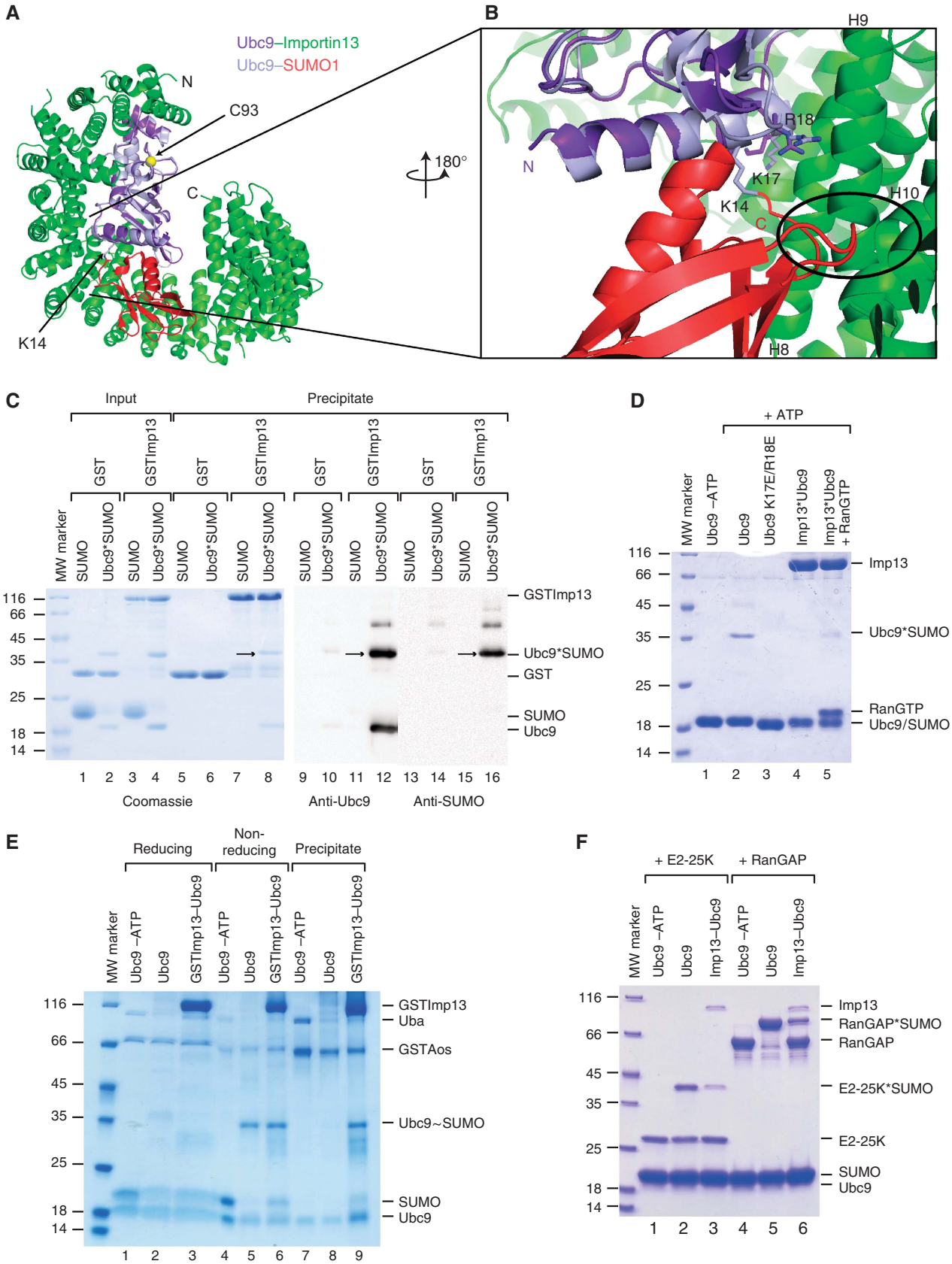

suggests that Imp13 binding could generally interfere with any SUMO consensus motif and supports the hypothesis that the residual activity that we observe in our assay is likely because of dissociation of the Imp13–Ubc9 complex.

Conclusions

We present the structure of Imp13 bound to the import cargo Ubc9. Imp13 has also recently been solved in complex with another import cargo, the Mago-Y14 heterodimer and in its RanGTP-bound nuclear state (Bono *et al*, 2010). Comparison of the three states of Imp13 shows that Imp13 can access a spectrum of conformations, from a tight ring-like structure to a wide, open superhelix.

Ubc9 recognition involves only the N-terminal half of Imp13 and overlaps with the RanGTP-binding surface, showing an unusual mode of binding for an import cargo. The internal surface of the C-terminal arch of Imp13 that provides an extensive cargo-binding surface for Mago-Y14, is not required for the interaction with Ubc9. Although the binding surfaces of the two Imp13 import cargoes mostly differ, concomitant binding is mutually exclusive. Both cargoes can displace each other from Imp13 to a similar extent, suggesting that the discrimination between Ubc9 versus Mago-Y14 in the cytosol perhaps depends on their spatio-temporal abundance and availability.

Binding of RanGTP to Imp13 is required to displace its import cargoes, but it seems that this is achieved through two very different mechanisms. Mago-Y14 is released by a steric hindrance mechanism by RanGTP whereas Ubc9 is released through direct competition for binding at the very N-terminus of Imp13. Interestingly, when Ubc9 dissociation is recapitulated *in vitro,* it works efficiently on RanGTP addition. Conversely, Mago-Y14 release by RanGTP is less efficient and requires the additional presence of Imp13 export cargo, eIF1A, suggesting that the two different modes of binding might also give rise to different requirements for dissociation in the nucleus.

Imp13 binds to two distinct regions on opposite sides of Ubc9, loop1 and 6, through a series of conserved contacts. The interacting surface centred around loop1 is multifunctional and Imp13 binding is not compatible with other known interactions such as non-covalent SUMO binding (Knipscheer *et al*, 2007; Capili and Lima, 2007a) and may also prevent E3 ligase binding (Supplementary Figure S3). Ubc9 is not able to autocatalyze SUMO conjugations when bound to Imp13. This suggests that during import and up to release in the nucleus, Ubc9 is held in a partially inactive state. Conversely, the catalytic cysteine of Ubc9, that mediates the SUMO thioester formation, is not involved in binding Imp13 and is exposed to solvent along with many of the active site residues. Interestingly, Ubc9∼SUMO is also able to associate to Imp13 and Ubc9 can also accept the thioester transfer when in the complex.

A limited number of enzymes function in the sumoylation pathway and target specificity is achieved at different levels in a way that is not fully understood. SUMO modification of the E2 enzyme, Ubc9, can alter substrate specificity (Knipscheer *et al*, 2008). Imp13 is able to associate with both non-modified and covalently modified Ubc9, although the functional significance of this finding is still unclear. Regulated nuclear import of Ubc9 could add yet another level of modulation to the system, tuning the availability of the E2 enzyme in the correct cellular compartment. Indeed it has been shown in mouse germ cells that Ubc9 nuclear localization is dependent on stage-specific Imp13 expression (Yamaguchi *et al*, 2006) and that Imp13 expression in rat and human systems is hormonally and developmentally regulated (Zhang *et al*, 2000). Imp13 might thus provide a molecular link between the cytoplasmic and nuclear function of Ubc9 with a possible regulatory role. Furthermore, the fact that the release of at least some cargoes requires the loading of another cargo points towards another regulatory role of Imp13. In this case, one could envision that efficient transport would occur with abundant cargoes but when some cargoes

Figure 5 Imp13 can bind Ubc9 in different sumoylation states. (**A**) Ubc9 structure superposition of Imp13–Ubc9 and Ubc9*SUMO (PDB ID 2VRR). The view is similar as in Figure 1A. The catalytic cysteine (C93, as a yellow sphere) and the main SUMO-modified lysine (K14) on Ubc9 are labelled. (**B**) Detailed view of the superposition rotated 180° along the *y* axis. Marked with a circle are a loop and the very C-terminal portion of SUMO that might sterically clash with HEAT 8 and 10 of Imp13. K17 and R18 are shown, as well as K14, wherein the C-terminus of SUMO is covalently linked. (**C**) Pull-down analysis of the binding of Ubc9*SUMO to Imp13 (Coomassie stained gel on the left side), revealed by western blot with an anti-Ubc9 (middle panel) and an anti-SUMO antibody (right panel). The arrow indicates the band corresponding to Ubc9*SUMO at the expected molecular weight (lane 8) and specifically detected both by anti-Ubc9 (lane12) and anti-SUMO antibodies (lane 16) (Supplementary Figure S5B). In this experiment, SUMO is His-tagged and, therefore, in the gel shows a molecular weight higher than Ubc9. (**D**) *In vitro* sumoylation reaction in the presence of the purified E1 enzyme, SUMO and Ubc9 (wt or mutated) apo or in complex with Imp13 with or without RanGTP, and ATP. On lane 4, Ubc9 is not modified by SUMO when in complex with Imp13 whereas Ubc9 apo (lane 2) functions as SUMO substrate as shown by the appearance of a band of ∼35 KDa corresponding to Ubc9*SUMO. A K17E/R18E Ubc9 double mutant is catalytically inactive in this condition (lane 3). The same mutant is unable to bind Imp13 (not shown and Figure 2C, lane 6). On lane 1 is the same reaction composition as in lane 2, without ATP as a negative control. (**E**) *In vitro* thioester formation reaction in the presence of the purified E1 enzyme (GSTAos–Uba), SUMO (HisSUMO in this reaction) and Ubc9 apo or in complex with Imp13 with or without ATP and in presence (reducing) or absence (non-reducing) of DTT. Ubc9 is modified by SUMO via formation of the thioester bond both in the apo form (lane 5) and when in complex with Imp13 (lane 6) as shown by the appearance of a band of ∼35 KDa corresponding to Ubc9∼SUMO. A similar reaction in reducing condition does not show the appearance of a band of the same molecular weight, confirming that the band in lanes 5 and 6 corresponds indeed to Ubc9∼SUMO. The three rightmost lanes of the gel correspond to a GST protein co-precipitation of the reactions performed in non-reducing conditions. On lane 9, it is clear that SUMO∼Ubc9 can bind to Imp13. GSTAos also precipitates on the beads but it is not bound to Ubc9 or SUMO∼Ubc9 as judged by the absence of the corresponding bands (lane 8). On lane 1 is the same reaction composition as in lane 2, without ATP and in reducing conditions, while on lanes 4 and 7 is the same reaction composition as in lane 5 and 8, without ATP and in non-reducing conditions as a negative controls. (**F**) SUMO conjugation of Ubc9 substrates E2-25K and RanGAP. The reaction was performed by incubating the purified E1 enzyme, SUMO (HisSUMO in this reaction) and Ubc9 apo or in complex with Imp13 in the presence either of E2-25K (lanes 1–3) or of RanGAP (lanes 4–6). Appearance of a weak band corresponding to SUMO conjugated E2-25K (∼45 KDa) in lane 3 and to RanGAP*SUMO in lane 6, indicates that in presence of Imp13 the reaction is less efficient. In the positive controls, stronger bands appear in presence of Ubc9 apo (lanes 2 and 5). Lanes 1 and 4 are loaded with the same reactions in the absence of ATP as negative controls. On the leftmost lane of all gels the molecular weight markers were loaded.

are depleted, a 'stalled' situation could occur. The absence of one cargo would then also block transport of other cargoes in the opposite direction.

The structure presented here demonstrates that the recognition and release of different cargo proteins by the same molecule can occur with very different mechanisms. Furthermore, we have shown that not only does Imp13 recognize different forms of Ubc9, it can also affect the activity of this cargo. Further structural investigations are needed to understand how Imp13 recognizes other import cargoes and how it promotes export.

Materials and methods

Protein expression and purification

Human Imp13 was expressed in *E. coli* and purified as previously described (Bono *et al*, 2010). Human Ubc9 was cloned in a pETMCN vector, derived from pET Novagen series (C Romier, IGBMC). The protein was expressed as an N-terminal hexahistidine fusion in the *E. coli* strain BL21 (DE3) Gold pLysS (Stratagene) in autoinducing medium (Studier, 2005) at 20°C overnight. Proteins were purified from cleared cell lysates by Ni^{2+}NTA affinity chromatography in buffer A (20 mM Tris (pH 7.5), 300 mM NaCl, 5 mM Imidazole and 1 mM β-mercaptoethanol) with a gradient of 5–250 mM imidazole, followed by proteolytic removal of the affinity tag with the TEV protease during dialysis into buffer B (20 mM Tris (pH 7.5), 100 mM NaCl and 1 mM dithiothreitol (DTT)). After a second pass over the Ni^{2+}NTA column, the collected flow through was further purified by cation-exchange chromatography in buffer B with a gradient of 0.1–1 M NaCl. The human Mago-Y14 full-length was prepared with a similar protocol as previously described, both as an His- or as a GST-tagged complex (Bono *et al*, 2006). Human SUMO1 was cloned in the same pETMCN vector as described for Ubc9. The expression of the protein was carried out in the *E. coli* strain BL21 (DE3) Gold for 3 h at 37°C by induction with 0.5 mM IPTG. The protein was purified by Ni^{2+}NTA affinity chromatography as described for Ubc9, with a further purification by size-exclusion chromatography. pGEX-2TK–Aos1 and pET28a–Uba2 were co-expressed in *E. coli* BL21 (DE3) Gold pLysS at 20°C overnight and purified by Ni^{2+} affinity chromatography as described for Ubc9. A second affinity step on glutathione sepharose beads (Macherey-Nagel) with buffer B was performed and the proteins were eluted with 20 mM reduced glutathione. The purification was completed by a size-exclusion chromatography. For complex formation, proteins were mixed in a 1:1.5 ratio (Imp13/Ubc9 or Imp13/Mago-Y14) in complex buffer (20 mM Tris (pH 7.5), 50 mM NaCl and 1 mM DTT) and incubated on ice for 1 h. The complex was subsequently purified by size-exclusion chromatography (Superdex200 10/300 GL column). Human E2-25K and RanGAP1 were expressed as GST fusion proteins in *E. coli* BL21 DE3 Gold in autoinducing medium at 20°C overnight. The proteins were affinity purified in batch on glutathione sepharose beads with buffer B. After proteolytic cleavage of the GST tag, they were further purified by anion-exchange chromatography followed size-exclusion chromatography as above.

Crystallization, data collection and structure determination

Initial crystals of Imp13–Ubc9 (14 mg/ml) were obtained at 18°C in 50 mM MES (pH 6) and 25% PEG 400 by vapour diffusion. Crystals were optimized by microseeding in 50 mM MES (pH 6.5), 20–25% PEG 300 and grew as needles to a size of $\sim 20 \times 20 \times 200$ μm. They diffracted to 2.8 Å resolution and contained one complex per asymmetric unit. They belong to space group $P2_12_12_1$ with cell dimensions $a = 69$ Å, $b = 127$ Å, $c = 184$ Å, $\alpha = \beta = \gamma = 90°$. Crystallographic data were measured at the PXII beamline at the Swiss Light Source. For data collection, crystals were stabilized in a solution consisting of the mother liquor supplemented with gradually increasing amount of glycerol up to 30% and flash cooled in liquid nitrogen. Data were processed and scaled using XDS (Kabsch, 1993). The structure was solved by MR using PHASER (McCoy *et al*, 2007). The search models included the Imp13 structure (PDB entry 2X19) and Ubc9 structure (PDB entry 1U9A). Owing to the large conformational change in Imp13–Ubc9 compared with the search model, the successful MR solution was only obtained when the Imp13 search model was separated into four fragments encompassing the HEAT repeats ranges H1–H5, H6–H9, H10–H13 and H16–H20 that behaved like rigid bodies. Refinement was carried out using iterative cycles of model building in COOT (Emsley and Cowtan, 2004) and O (Jones *et al*, 1990) and restrained refinement in CNS 1.2 (Brünger *et al*, 1998).

In vitro binding assays

GST-tagged recombinant Imp13, Ubc9 or Mago were mixed with purified binding partners (4 μg of each) in binding buffer (20 mM HEPES (pH 7.5), 50 mM NaCl, 1 mM DTT, 10% glycerol and 0.01% (v/v) Nonidet P40) in a final volume of 60 μl and incubated for 1 h at 4 °C. Attempts to measure the affinity of the interaction between Imp13 and Ubc9 either by surface plasmon resonance (SPR) or by isothermal titration calorimetry (ITC) failed, mainly because a significant percentage of Imp13 aggregates over time (as detected by static light scattering measurement) (data not shown). For the competition experiments, pre-formed complexes were purified by size-exclusion chromatography and 8 μg of complex was mixed with increasing amounts of the competitor proteins. Complexes were immobilized on 15 μl of glutathione agarose beads (Macherey-Nagel) and incubated for 1 h at 4°C. The resin was washed three times with 500 μl of binding buffer and eluted with 10 μl of SDS loading buffer, boiled and loaded on 15% SDS–PAGE with a protein molecular weight marker. Proteins were visualized by Coomassie staining.

In vitro sumoylation assays and western blot analysis

The Ubc9 *in vitro* modification assay was performed essentially as described by Knipscheer *et al*, 2008. For small-scale experiments, 38.5 μg Ubc9 or 270 μg of Imp13–Ubc9 ± 38 μg RanGTP, 1.6 μg Aos1–Uba2 and 7.6 μg SUMO1 (in this paper, SUMO for simplicity) were used in a final volume of 50 μl. The reaction was started by adding 5 mM ATP and incubated for 5 h at 37°C. Large-scale reactions were performed increasing the above components by ~570 folds in the same conditions, before purification. Ubc9*SUMO was purified on an anion-exchange column in buffer C (20 mM Tris (pH 7.5), 100 mM NaCl, 1 mM DTT and 0.1 mM AEBSF) and eluted with a salt gradient of 0.1–1M NaCl, followed by size-exclusion chromatography. After *in vitro* binding assays, the samples were separated by SDS–PAGE and transferred on a nitrocellulose membrane (Whatman). Immunoblotting was performed with mouse anti-SUMO (Zymed, 33–2400, dilution 1:3500) and goat anti-Ubc9 (Abcam, ab21193, dilution 1:3500). Western blots were developed using ECL Plus Western Blotting Detection System (GE Healthcare).

The thioester formation assay was done according to Pichler *et al*, 2002. In the reaction, 2 μg Aos1–Uba2, 1.2 μg SUMO and either 1.2 μg Ubc9 apo or 12 μg of pre-formed GSTImp13–Ubc9 complex and 5 mM ATP were incubated in a total volume of 60 μl for 3 h at 30°C. Of each reaction, 10 μl was treated with reducing buffer and 10 μl with non-reducing loading buffer. The *in vitro* binding assay was performed as described above in non-reducing condition. The remaining of the reaction was immobilized on 20 μl glutathione agarose beads (Macherey-Nagel) for 45 min at 4°C. *In vitro* sumoylation of E2-25K and RanGAP1 was performed as described by Knipscheer *et al*, 2009 in a total volume of 50 μl. The reactions were done with 2 μM Ubc9 or 2 μM pre-formed Imp13–Ubc9 complex respectively. To avoid unspecific binding, in case of RanGAP1, 2 μg BSA was added. The samples were loaded on a SDS–PAGE (Any kD Mini-PROTEAN TGX Precast Gel, BIORAD).

Accession numbers

The coordinates and structure factors have been deposited in the Macromolecular Structure Database of the European Bioinformatic Institute (EBI) with ID code 2xwu.

Supplementary data

Supplementary data are available at *The EMBO Journal* Online (http://www.embojournal.org).

Acknowledgements

We wish to thank Guido Sauer for mass spectrometry analysis and for the SUMO clone, Jerome Basquin, Karina Valer Saldana and Sabine Pleyer at the MPI-Martinsried crystallization facility and

Claire Basquin for biophysical measurements (MPI-Martinsried). We also thank Dirk Görlich (MPI, Goettingen) for the Human Ubc9 clone, Stefan Müller (MPI, Martinsried) for the E1 clones and the staff of the PX beamlines at the Swiss Light Source (Villigen, Switzerland) for assistance during data collection. We thank Oliver Weichenrieder for help with data collection and discussion. We thank Atlanta Cook, Gretel Buchwald, Elisa Izaurralde and Elena Conti for discussion and critical reading of the paper and Thomas Holder and Aleksandar Basara for help with some figures. This study was supported by the Max Planck Gesellshaft and by the DFG grant BO3588/1-1.

Conflict of interest

The authors declare that they have no conflict of interest.

References

Andrade MA, Petosa C, O'Donoghue SI, Müller CW, Bork P (2001) Comparison of ARM and HEAT protein repeats. *J Mol Biol* **309:** 1–18

Bernier-Villamor V, Sampson DA, Matunis MJ, Lima CD (2002) Structural basis for E2-mediated SUMO conjugation revealed by a complex between ubiquitin-conjugating enzyme Ubc9 and RanGAP1. *Cell* **108:** 345–356

Bhardwaj A, Cingolani G (2010) Conformational selection in the recognition of the snurportin importin beta binding domain by importin beta. *Biochemistry* **49:** 5042–5047

Bono F, Cook AG, Grunwald M, Ebert J, Conti E (2010) Nuclear import mechanism of the EJC component Mago-Y14 revealed by structural studies of Importin 13. *Mol Cell* **37:** 211–222

Bono F, Ebert J, Lorentzen E, Conti E (2006) The crystal structure of the exon junction complex reveals how it maintains a stable grip on mRNA. *Cell* **126:** 713–725

Brünger AT, Adams PD, Clore GM, DeLano WL, Gros P, Grosse-Kunstleve RW, Jiang JS, Kuszewski J, Nilges M, Pannu NS, Read RJ, Rice LM, Simonson T, Warren GL (1998) Crystallography & NMR system: a new software suite for macromolecular structure determination. *Acta Crystallogr D Biol Crystallogr* **54:** 905–921

Cansizoglu AE, Lee BJ, Zhang ZC, Fontoura BMA, Chook YM (2007) Structure-based design of a pathway-specific nuclear import inhibitor. *Nat Struct Mol Biol* **14:** 452–454

Capili AD, Lima CD (2007a) Structure and analysis of a complex between SUMO and Ubc9 illustrates features of a conserved E2-Ubl interaction. *J Mol Biol* **369:** 608–618

Capili AD, Lima CD (2007b) Taking it step by step: mechanistic insights from structural studies of ubiquitin/ubiquitin-like protein modification pathways. *Curr Opin Struct Biol* **17:** 726–735

Cingolani G, Bednenko J, Gillespie MT, Gerace L (2002) Molecular basis for the recognition of a nonclassical nuclear localization signal by importin beta. *Mol Cell* **10:** 1345–1353

Cingolani G, Petosa C, Weis K, Müller CW (1999) Structure of importin-beta bound to the IBB domain of importin-alpha. *Nature* **399:** 221–229

Cook A, Bono F, Jinek M, Conti E (2007) Structural biology of nucleocytoplasmic transport. *Annu Rev Biochem* **76:** 647–671

Cook AG, Conti E (2010) Nuclear export complexes in the frame. *Curr Opin Struct Biol* **20:** 247–252

Cook AG, Fukuhara N, Jinek M, Conti E (2009) Structures of the tRNA export factor in the nuclear and cytosolic states. *Nature* **461:** 60–65

Emsley P, Cowtan K (2004) Coot: model-building tools for molecular graphics. *Acta Crystallogr D Biol Crystallogr* **60:** 2126–2132

Firestein R, Feuerstein N (1998) Association of activating transcription factor 2 (ATF2) with the ubiquitin-conjugating enzyme hUBC9. Implication of the ubiquitin/proteasome pathway in regulation of ATF2 in T cells. *J Biol Chem* **273:** 5892–5902

Geiss-Friedlander R, Melchior F (2007) Concepts in sumoylation: a decade on. *Nat Rev Mol Cell Biol* **8:** 947

Giraud MF, Desterro JM, Naismith JH (1998) Structure of ubiquitin-conjugating enzyme 9 displays significant differences with other ubiquitin-conjugating enzymes which may reflect its specificity for sumo rather than ubiquitin. *Acta Crystallogr D Biol Crystallogr* **54:** 891–898

Görlich D, Dabrowski M, Bischoff FR, Kutay U, Bork P, Hartmann E, Prehn S, Izaurralde E (1997) A novel class of RanGTP binding proteins. *J Cell Biol* **138:** 65–80

Görlich D, Kutay U (1999) Transport between the cell nucleus and the cytoplasm. *Annu Rev Cell Dev Biol* **15:** 607–660

Hannich JT, Lewis A, Kroetz MB, Li S-J, Heide H, Emili A, Hochstrasser M (2005) Defining the SUMO-modified proteome by multiple approaches in Saccharomyces cerevisiae. *J Biol Chem* **280:** 4102–4110

Hayashi T, Seki M, Maeda D, Wang W, Kawabe Y-i, Seki T, Saitoh H, Fukagawa T, Yagi H, Enomoto T (2002) Ubc9 is essential for viability of higher eukaryotic cells. *Exp Cell Res* **280:** 212–221

Imasaki T, Shimizu T, Hashimoto H, Hidaka Y, Kose S, Imamoto N, Yamada M, Sato M (2007) Structural basis for substrate recognition and dissociation by human transportin 1. *Mol Cell* **28:** 57–67

Johnson ES (2004) Protein modification by SUMO. *Annu Rev Biochem* **73:** 355–382

Jones TA, Bergdoll M, Kjeldgaard M (eds) (1990) *O: A Macromolecular Modeling Environment*. Springer-Verlag Press, pp 189–195

Kabsch W (1993) Automatic processing of rotation diffraction data from crystals of initially unknown symmetry and cell constants. *J Appl Cryst* **26:** 795–800

Kahle J, Baake M, Doenecke D, Albig W (2005) Subunits of the heterotrimeric transcription factor NF-Y are imported into the nucleus by distinct pathways involving importin beta and importin 13. *Mol Cell Biol* **25:** 5339–5354

Kataoka N, Yong J, Kim VN, Velazquez F, Perkinson RA, Wang F, Dreyfuss G (2000) Pre-mRNA splicing imprints mRNA in the nucleus with a novel RNA-binding protein that persists in the cytoplasm. *Mol Cell* **6:** 673–682

Knipscheer P, Flotho A, Klug H, Olsen JV, van Dijk WJ, Fish A, Johnson ES, Mann M, Sixma TK, Pichler A (2008) Ubc9 sumoylation regulates SUMO target discrimination. *Mol Cell* **31:** 371–382

Knipscheer P, Klug H, Sixma TK, Pichler A (2009) Preparation of sumoylated substrates for biochemical analysis. *Methods Mol Biol* **497:** 201–210

Knipscheer P, van Dijk WJ, Olsen JV, Mann M, Sixma TK (2007) Noncovalent interaction between Ubc9 and SUMO promotes SUMO chain formation. *EMBO J* **26:** 2797–2807

Krissinel E, Henrick K (2007) Inference of macromolecular assemblies from crystalline state. *J Mol Biol* **372:** 774–797

Le Hir H, Gatfield D, Braun IC, Forler D, Izaurralde E (2001) The protein Mago provides a link between splicing and mRNA localization. *EMBO Rep* **2:** 1119–1124

Lee BJ, Cansizoglu AE, Süel KE, Louis TH, Zhang Z, Chook YM (2006) Rules for nuclear localization sequence recognition by karyopherin beta 2. *Cell* **126:** 543–558

Lee SJ, Sekimoto T, Yamashita E, Nagoshi E, Nakagawa A, Imamoto N, Yoshimura M, Sakai H, Chong KT, Tsukihara T, Yoneda Y (2003) The structure of importin-beta bound to SREBP-2: nuclear import of a transcription factor. *Science* **302:** 1571–1575

Mahajan R, Delphin C, Guan T, Gerace L, Melchior F (1997) A small ubiquitin-related polypeptide involved in targeting RanGAP1 to nuclear pore complex protein RanBP2. *Cell* **88:** 97–107

Makhnevych T, Sydorskyy Y, Xin X, Srikumar T, Vizeacoumar FJ, Jeram SM, Li Z, Bahr S, Andrews BJ, Boone C, Raught B (2009) Global map of SUMO function revealed by protein-protein interaction and genetic networks. *Mol Cell* **33:** 124–135

Matunis MJ, Coutavas E, Blobel G (1996) A novel ubiquitin-like modification modulates the partitioning of the Ran-GTPase-activating protein RanGAP1 between the cytosol and the nuclear pore complex. *J Cell Biol* **135:** 1457–1470

McCoy A, Grosse-Kunstleve R, Adams P, Winn M, Storoni L, Read R (2007) Phaser crystallographic software. *J appl crystallogr* **40:** 658–674

Melchior F (2000) SUMO—nonclassical ubiquitin. *Annu Rev Cell Dev Biol* **16:** 591–626

Mingot JM, Kostka S, Kraft R, Hartmann E, Görlich D (2001) Importin 13: a novel mediator of nuclear import and export. *EMBO J* **20:** 3685–3694

Mitrousis G, Olia AS, Walker-Kopp N, Cingolani G (2008) Molecular basis for the recognition of snurportin 1 by importin beta. *J Biol Chem* **283:** 7877–7884

Nacerddine K, Lehembre F, Bhaumik M, Artus J, Cohen-Tannoudji M, Babinet C, Pandolfi PP, Dejean A (2005) The SUMO pathway is essential for nuclear integrity and chromosome segregation in mice. *Dev Cell* **9:** 769–779

Pichler A, Gast A, Seeler JS, Dejean A, Melchior F (2002) The nucleoporin RanBP2 has SUMO1 E3 ligase activity. *Cell* **108:** 109–120

Reverter D, Lima CD (2005) Insights into E3 ligase activity revealed by a SUMO-RanGAP1-Ubc9-Nup358 complex. *Nature* **435:** 687–692

Rodriguez MS, Dargemont C, Hay RT (2001) SUMO-1 conjugation *in vivo* requires both a consensus modification motif and nuclear targeting. *J Biol Chem* **276:** 12654–12659

Sekiyama N, Arita K, Ikeda Y, Hashiguchi K, Ariyoshi M, Tochio H, Saitoh H, Shirakawa M (2010) Structural basis for regulation of poly-SUMO chain by a SUMO-like domain of Nip45. *Proteins* **78:** 1491–1502

Seufert W, Futcher B, Jentsch S (1995) Role of a ubiquitin-conjugating enzyme in degradation of S- and M-phase cyclins. *Nature* **373:** 78–81

Tang Z, Hecker CM, Scheschonka A, Betz H (2008) Protein interactions in the sumoylation cascade: lessons from X-ray structures. *FEBS J* **275:** 3003–3015

Tatham MH, Kim S, Yu B, Jaffray E, Song J, Zheng J, Rodriguez MS, Hay RT, Chen Y (2003) Role of an N-terminal site of Ubc9 in SUMO-1, -2, and -3 binding and conjugation. *Biochemistry* **42:** 9959–9969

Terry LJ, Shows EB, Wente SR (2007) Crossing the nuclear envelope: hierarchical regulation of nucleocytoplasmic transport. *Science* **318:** 1412–1416

Tong H, Hateboer G, Perrakis A, Bernards R, Sixma TK (1997) Crystal structure of murine/human Ubc9 provides insight into the variability of the ubiquitin-conjugating system. *J Biol Chem* **272:** 21381–21387

Walker P, Doenecke D, Kahle J (2009) Importin 13 mediates nuclear import of histone fold containing chrac heterodimers. *J Biol Chem* **284:** 11652–11662

Wang J, Hu W, Cai S, Lee B, Song J, Chen Y (2007) The intrinsic affinity between E2 and the Cys domain of E1 in ubiquitin-like modifications. *Mol Cell* **27:** 228–237

Wohlwend D, Strasser A, Dickmanns A, Ficner R (2007) Structural basis for RanGTP independent entry of spliceosomal U snRNPs into the nucleus. *J Mol Biol* **374:** 1129–1138

Yamaguchi YL, Tanaka SS, Yasuda K, Matsui Y, Tam PPL (2006) Stage-specific Importin13 activity influences meiosis of germ cells in the mouse. *Dev Biol* **297:** 350–360

Yoshida K, Blobel G (2001) The karyopherin Kap142p/Msn5p mediates nuclear import and nuclear export of different cargo proteins. *J Cell Biol* **152:** 729–740

Yunus AA, Lima CD (2006) Lysine activation and functional analysis of E2-mediated conjugation in the SUMO pathway. *Nat Struct Mol Biol* **13:** 491–499

Zhang C, Sweezey NB, Gagnon S, Muskat B, Koehler D, Post M, Kaplan F (2000) A novel karyopherin-beta homolog is developmentally and hormonally regulated in fetal lung. *Am J Respir Cell Mol Biol* **22:** 451–459

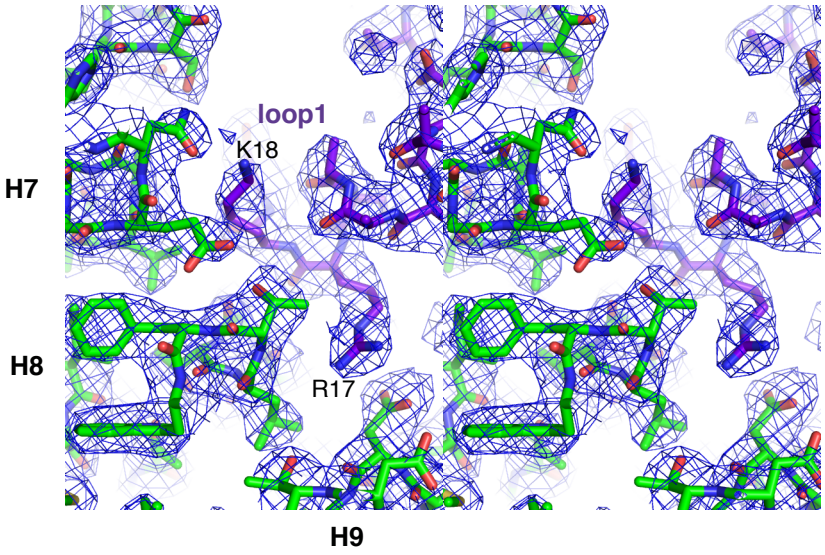

Figure S1. Electron density of a region of the interacting surface of Imp13 and Ubc9.
Stereo view of the electron density of the 2Fo-Fc map after refinement. The electron density is shown as a blue mesh contoured at 1σ. The final model is rendered as sticks representation, in green for Imp13 and in purpleblue for Ubc9. The zoom-in view shows the interaction between HEATs 7-8-9 of Imp13 with loop1 of Ubc9 in a similar view as in Fig. 2B. K18 and R17 of Ubc9 contact Imp13 at HEATs 7 and 8-9, respectively. Mutation of R17 to Glutamate impairs binding of Ubc9 to Imp13 (Fig. 2C).

Figure S2. Structure-based sequence alignment of Imp13 and Ubc9.
The alignment includes Imp13 and Ubc9 orthologues from *H. sapiens* (Hs), *D. melanogaster* (Dm) and *S. pombe* (Sp) and not shown, from *A. thaliana* and *C. elegans*. Highlighted in green and purple are conserved residues for Imp13 and Ubc9, respectively. The secondary structure elements of Hs Imp13 and Ubc9 are shown below the sequences as rectangles and arrows with the same color-code. The A and B helices of the 20 HEAT repeats are labeled. Above the sequences, colored circles highlight the residues involved in the interaction with Ubc9 (purple), and Imp13 (green) as identified using the AquaProt server (Reichmann et al., 2007). Interactions with Ran (yellow), Mago (blue),Y14 (magenta), SUMO (red) are labeled as circles. The red arrow marks SUMO1 covalent attachment site and the orange arrow, the catalytic Cysteine.

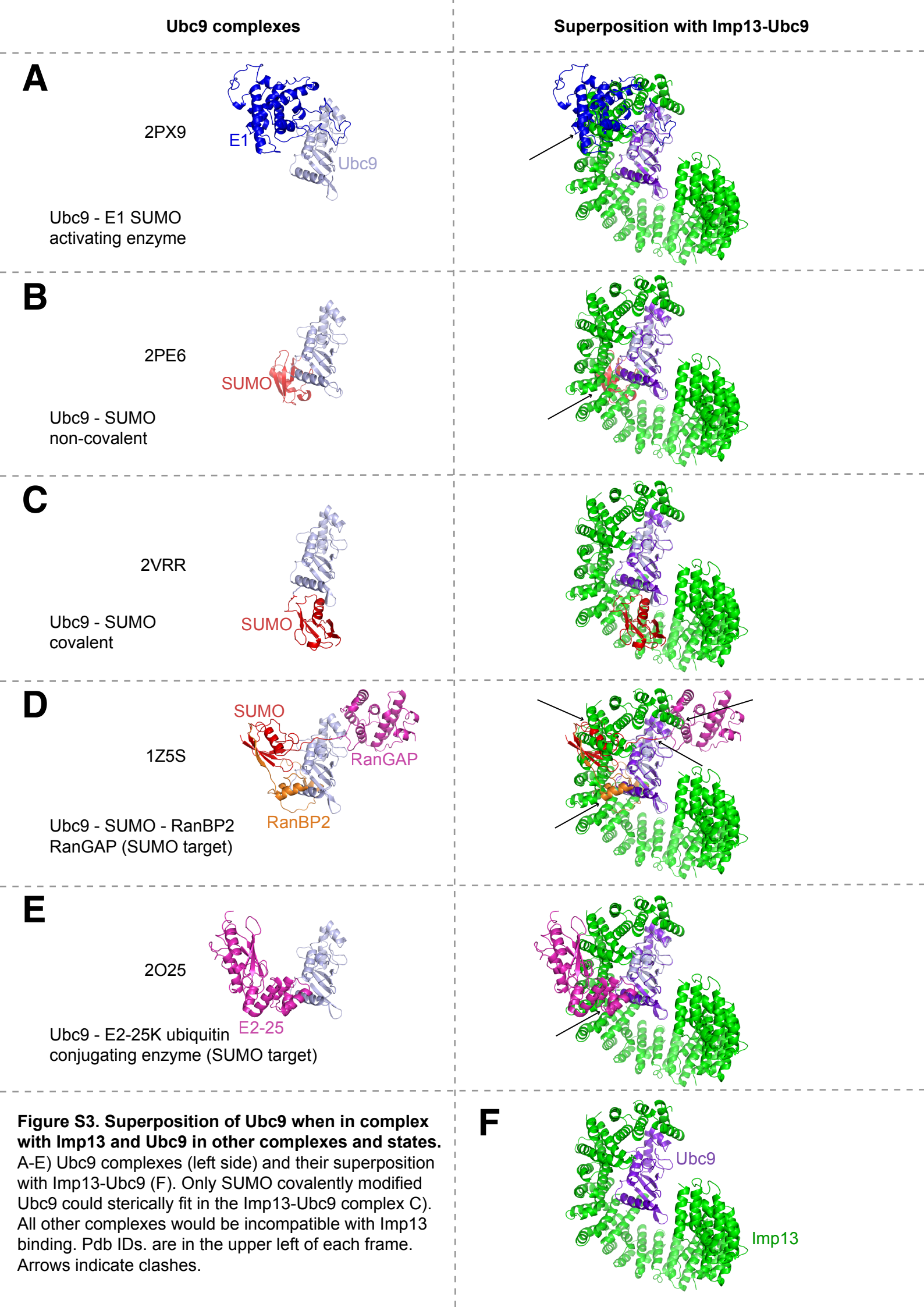

Figure S3. Superposition of Ubc9 when in complex with Imp13 and Ubc9 in other complexes and states. A-E) Ubc9 complexes (left side) and their superposition with Imp13-Ubc9 (F). Only SUMO covalently modified Ubc9 could sterically fit in the Imp13-Ubc9 complex C). All other complexes would be incompatible with Imp13 binding. Pdb IDs. are in the upper left of each frame. Arrows indicate clashes.

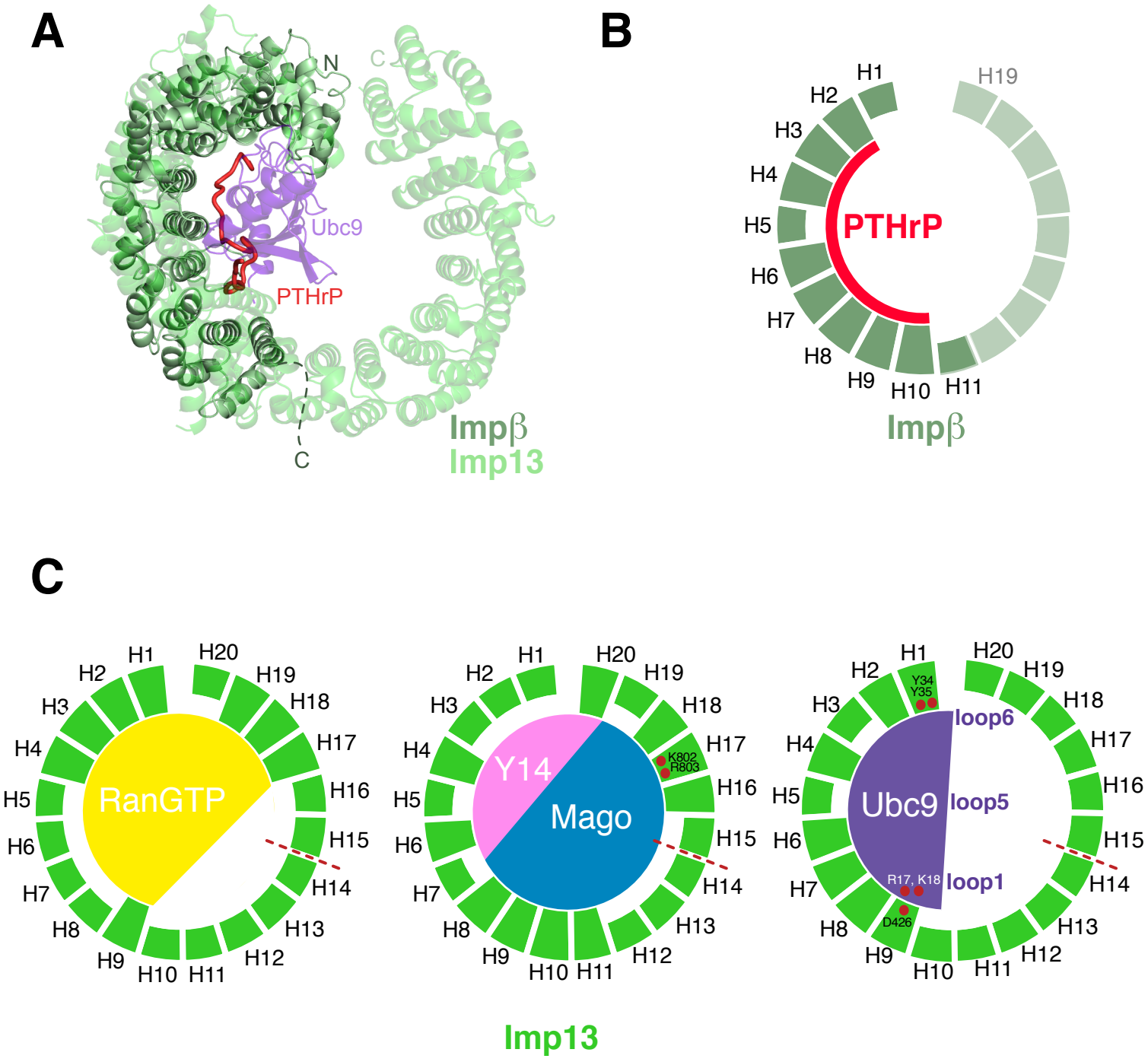

Figure S4. Comparison of Imp13-Ubc9 with Impβ-PTHrP peptide and schematics of Imp13 binding. A) N-terminal superposition of Imp13 and Impβ (HEAT 1-11) in complex with Ubc9 and with the PTHrP peptide (pdb id. 1M5N; Cingolani, 2002), respectively. The structures are viewed in a similar orientation as in Fig. 1B. Imp13 and Ubc9 are in the same color coding as before but with a transparent rendering for clarity; Impβ fragment is in smudge green and the PTHrP peptide in red. B) Scheme of the interaction between PTHrP and Impβ in the same view as in Fig. 1B. C) Schemes of the interaction of Imp13 with RanGTP (on the left side), with Mago-Y14 and with Ubc9 (on the right side). The proteins are represented with a similar color coding as in Fig. 3. HEAT repeats are labeled. Red dots represent residues mutated in this study and the dotted lines represent the C-terminus of Imp13ΔC mutant.

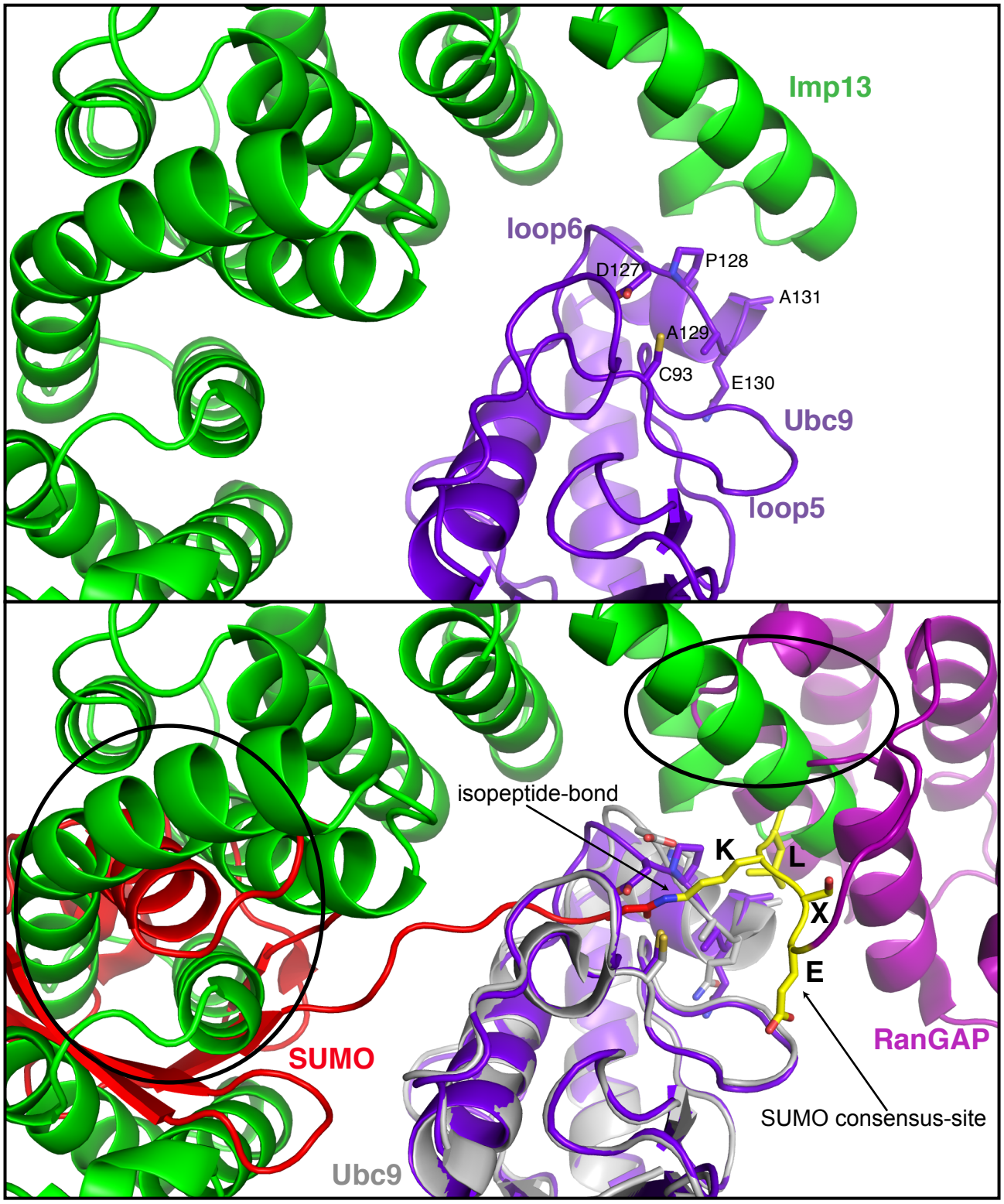

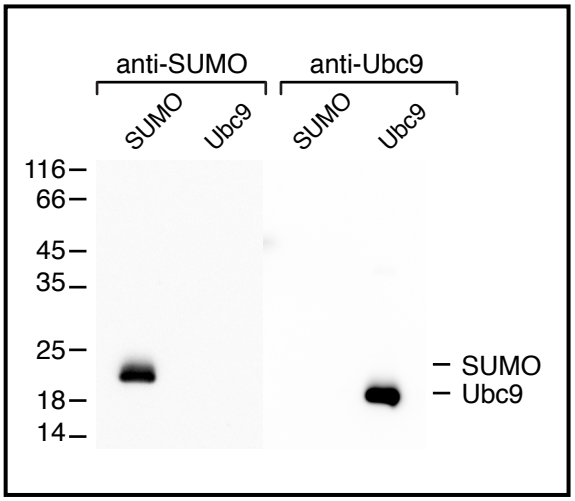

Figure S5. A) Steric incompatibility for the concomitant binding of RanGAP~SUMO-Ubc9 and Imp13.
On top, zoomed in view of the interaction between Imp13 and Ubc9 in a similar orientation as in Fig. 2A. Ubc9 active site residues are labeled. Lower panel, superposition of Ubc9 after SUMO conjugation to RanGAP (PDB ID 1Z5S; RanBP2 removed for clarity) and of Ubc9 in complex with Imp13. Steric clashes are marked with a circle. Important residues are labeled; the SUMO consensus-site residues are in yellow.
B) anti-SUMO and anti-Ubc9 do not cross-react.
On the left side, western blot with anti-SUMO antibody and on the right side with anti-Ubc9. As shown by an absence of staining of Ubc9 with anti-SUMO and by an absence of staining of SUMO (His-tagged) when the membrane is stained for anti-Ubc9, it is evident that there is no cross-reactivity of the two antibody in the conditions used.

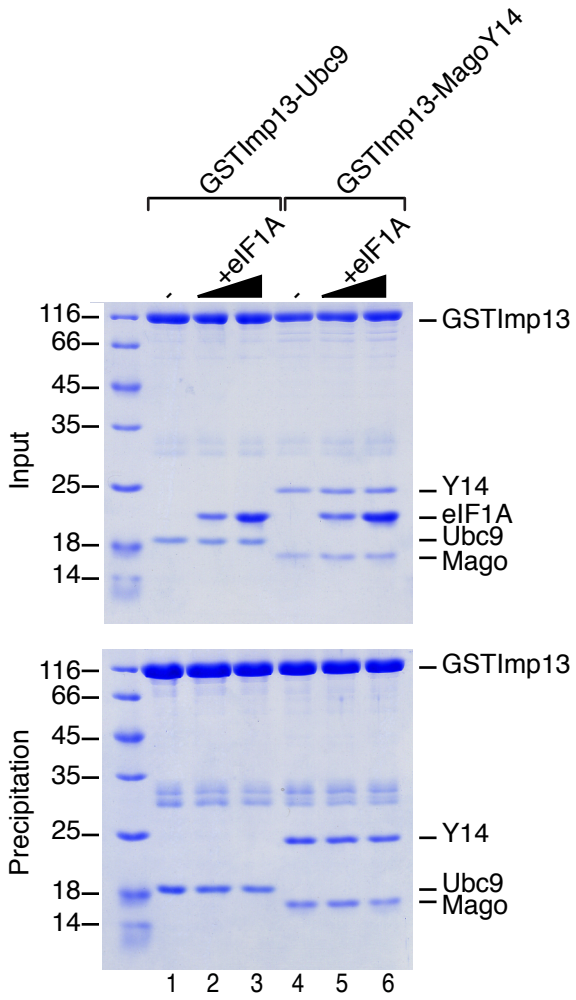

Figure S6. eIF1A does not displace Ubc9 and Mago-Y14 from Imp13 in competition assays. In this competition experiment, 8μg of GSTImp13-Ubc9 were incubated on beads and competing amounts of eIF1A were added (1μg in lanes 2 and 5; 4μg in lanes 3 and 6. No significant binding of eIF1A is detectable, suggesting that eIF1A can not promote the release of Ubc9 (lanes 2 and 3) and Mago-Y14 (lanes 5 and 6) in the absence of RanGTP.

5.3 Structural basis for the nuclear export activity of Importin13

This work has been originally published in following article:

Structural basis for the nuclear export activity of Importin13

Marlene Grünwald, Daniella Lazzaretti and Fulvia Bono
EMBO Journal, 2013, 23(6):899-913

The EMBO Journal (2013) 32, 899–913
www.embojournal.org

TRANSPARENT PROCESS

THE EMBO JOURNAL

Structural basis for the nuclear export activity of Importin13

Marlene Grünwald, Daniela Lazzaretti and Fulvia Bono*

Max Planck Institute for Developmental Biology, Tübingen, Germany

Importin13 (Imp13) is a bidirectional karyopherin that can mediate both import and export of cargoes. Imp13 recognizes several import cargoes, which include the exon junction complex components Mago-Y14 and the E2 SUMO-conjugating enzyme Ubc9, and one known export cargo, the translation initiation factor 1A (eIF1A). To understand how Imp13 can perform double duty, we determined the 3.6-Å crystal structure of Imp13 in complex with RanGTP and with eIF1A. eIF1A binds at the inner surface of the Imp13 C-terminal arch adjacent and concomitantly to RanGTP illustrating how eIF1A can be exported by Imp13. Moreover, the 3.0-Å structure of Imp13 in its unbound state reveals the existence of an open conformation in the cytoplasm that explains export cargo release and completes the export branch of the Imp13 pathway. Finally, we demonstrate that Imp13 is able to bind and export eIF1A *in vivo* and that its function is essential.

The EMBO Journal (2013) **32,** 899–913. doi:10.1038/emboj.2013.29; Published online 22 February 2013
Subject Categories: membranes & transport; structural biology
Keywords: eIF1A; export; Importin13; nucleo-cytoplasmic transport

Introduction

In eukaryotic cells, the nuclear envelope selectively separates the nucleus, where transcription and splicing occur, from the cytoplasm, where translation takes place. Proteins and RNAs can cross this barrier through the nuclear pore complexes (NPCs). Small molecules, up to ~20–40 kDa, can passively diffuse across the NPCs, while other molecules need to be actively transported (Görlich and Kutay, 1999; Mohr *et al*, 2009). Active nucleo-cytoplasmic transport is mainly mediated by a superfamily of proteins, known as karyopherins. Karyopherins can be divided into two groups based on their directionality: importins translocate cargoes from the cytoplasm to the nucleus, while exportins transport their cargoes from the nucleus into the cytoplasm. The directionality of both import and export is determined by the same driving force: a gradient of the small GTPase Ran. Importins bind their cargoes in the cytoplasm and release them upon binding to the GTP-bound form of Ran (RanGTP), which is confined to the nucleus. Conversely, exportins require RanGTP to stably bind their cargo in the nucleus; the dissociation of the export complex is then triggered in the cytoplasm by the hydrolysis of Ran-bound GTP to GDP (Görlich and Kutay, 1999; Cook *et al*, 2007). So far, only a few karyopherins including Importin13 (Imp13), Exportin4 and Msn5, have been characterized as bidirectional transport factors being able to both import and export cargoes from the nucleus (Mingot *et al*, 2001; Yoshida and Blobel, 2001; Gontan *et al*, 2009).

In *Drosophila* larvae, Imp13 affects neurotransmitter release at the neuromuscular junctions and homozygous *imp13* mutations are lethal (Giagtzoglou *et al*, 2009). In humans, Imp13 has been involved in the import of the core exon junction complex components Mago-Y14, the E2 SUMO-conjugating enzyme Ubc9 (Mingot *et al*, 2001), histone fold-containing and paired-type homeodomain transcription factors (Ploski *et al*, 2004; Kahle *et al*, 2005; Walker *et al*, 2009), the glucocorticoid receptor (Tao *et al*, 2006) and the actin-binding protein myopodin (Liang *et al*, 2008). The only export cargo of Imp13 known so far is the eukaryotic initiation factor 1A (eIF1A) (Mingot *et al*, 2001). However, the function and importance of this export pathway have not yet been addressed *in vivo*.

eIF1A is a protein conserved across eukaryotes with multiple functions in translation initiation (Jackson *et al*, 2010; Hinnebusch, 2011). Together with another translation initiation factor, eIF1, it directly associates to the small ribosomal subunit and is required for the assembly of the pre-initiation complex (Jackson *et al*, 2010; Aitken and Lorsch, 2012). The two initiation factors cooperate in promoting an 'open', scanning-competent conformation of the 40S subunit (Passmore *et al*, 2007). eIF1A consists of an oligonucleotide-binding (OB) β-barrel fold followed by an extended helix, and two unstructured tails at the N- and C-termini (Battiste *et al*, 2000). Due to its small size (17 kDa), eIF1A is thought to passively diffuse through the NPCs; its active export might therefore be required both to deplete eIF1A from the nucleus and to maintain sufficient cytoplasmic levels (Mingot *et al*, 2001). Despite the importance of eIF1A in translation, limited information is available on its localization.

Several structures of karyopherins have been determined to date, comprising two nuclear import factors (Importin β (Impβ) and Transportin (Tpn)) (Cingolani *et al*, 1999; Vetter *et al*, 1999a; Bayliss *et al*, 2000; Lee *et al*, 2003, 2005; Cansizoglu and Chook, 2007; Cansizoglu *et al*, 2007; Cook *et al*, 2007; Imasaki *et al*, 2007; Wohlwend *et al*, 2007; Mitrousis *et al*, 2008; Bhardwaj and Cingolani, 2010; Forwood *et al*, 2010; Xu *et al*, 2010; Zhang and Chook, 2012) and four nuclear export factors (Cse1, Crm1, Expo5 and Xpo-t) (Matsuura and Stewart, 2004; Cook *et al*, 2005, 2009; Monecke *et al*, 2009; Okada *et al*, 2009; Dong *et al*, 2009a, b; Güttler *et al*, 2010) but it is still unclear how a

*Corresponding author. Research Groups, Max Planck Institute for Developmental Biology, Spemannstrasse 35, Tübingen 72076, Germany. Tel.: +49 7071 6011367; Fax: +49 7071 6011308;
E-mail: fulvia.bono@tuebingen.mpg.de

Received: 7 November 2012; accepted: 28 January 2013; published online: 22 February 2013

transport factor, such as Imp13, can have a mixed transport competence. How RanGTP binding to bidirectional karyopherins can cause opposite effects, dissociation of the cargo to be imported and association of the cargo to be exported, is an open question in the nuclear transport field. Our previous work on the structures of the Imp13-RanGTP intermediate state and the Imp13-Mago-Y14 and Imp13-Ubc9 cargo complexes have provided key insights into import cargo recognition and dissociation by RanGTP (Bono *et al*, 2010; Grünwald and Bono, 2011). Well-characterized import factors such as Impβ and Tpn normally recognize only a small portion of their cargos as an import signal (Cingolani *et al*, 1999, 2002; Cansizoglu and Chook, 2007; Imasaki *et al*, 2007; Wohlwend *et al*, 2007; Mitrousis *et al*, 2008; Bhardwaj and Cingolani, 2010; Forwood *et al*, 2010; Xu *et al*, 2010; Zhang and Chook, 2012). Remarkably, Imp13 recognizes the folded domains of the import cargoes Ubc9 and Mago-Y14, predominantly via charged and polar residues distributed over the entire proteins. RanGTP binding to Imp13 is similar to RanGTP binding by Impβ and Tpn although Imp13 lacks the acidic loop that is found in the canonical import factors (Cook *et al*, 2007). Imp13 uses non-overlapping surfaces for the recognition of different import cargoes. As a consequence, the release mechanism of these cargoes is different: Mago-Y14 is released via a steric hindrance mechanism, while Ubc9 and RanGTP directly compete for the same binding surface on Imp13 (Bono *et al*, 2010; Grünwald and Bono, 2011).

Our structural and biochemical studies of Imp13 in its unbound state and the Imp13-RanGTP-eIF1A trimeric complex shed light on how bidirectional karyopherins can perform double duty and also be regulated in opposite ways by RanGTP. We further address the functional basis by which the nuclear transport factor Imp13 is able to recognize both import and export cargoes and deliver them in the appropriate cellular compartment and the *in vivo* relevance of Imp13 function.

Results and Discussion

Structure determination and quality

We determined the crystal structures of Imp13 in its nuclear export complex with RanGTP and eIF1A and also in the unbound form that corresponds to a cytosolic state. For the crystallization of the ternary export complex, human (Hs) Imp13, Ran and eIF1A were expressed separately in *E. coli*. While Imp13 was used as a full-length construct, the small GTPase Ran was truncated to contain the residues 1–180 and a Gln69Leu mutation to inhibit GTP hydrolysis, as previously described (Bischoff *et al*, 1994; Matsuura and Stewart, 2004; Lee *et al*, 2005; Cook *et al*, 2009; Monecke *et al*, 2009; Bono *et al*, 2010) (Figure 1A; Supplementary Figure 1A). Attempts to crystallize the trimeric complex in presence of full-length eIF1A were not successful probably due to the two large unstructured regions at the N- and C-termini (Battiste *et al*, 2000) (NTT and CTT, respectively). Therefore, a truncated version of eIF1A was used that includes the residues from 1 to 112 and lacks the CTT portion of the protein (eIF1AΔC; Figure 1A and Supplementary Figure 1A). The complex was reconstituted *in vitro* with an excess of RanGTP and eIF1A and purified to homogeneity by size exclusion chromatography (SEC). The export complex crystallized in a centred monoclinic space group (*C*2). Initial phases for the structure were obtained by molecular replacement (MR) with the Imp13-RanGTP structure as a search model (Bono *et al*, 2010; pdb id.: 2x19). Although density for eIF1A could be observed, a reliable MR solution could not be obtained when using available structures of eIF1A as search models (Battiste *et al*, 2000; pdb ids: 2oqk and 2dgy). We manually placed the crystal structure of eIF1A from *Cryptosporidium parvum* (pdb id.: 2oqk; 75% sequence identity over the region encompassed by our construct) into the electron density using an anomalous Fourier map of a seleno-methionine (SeMet) substituted eIF1A as a guide (Supplementary Figure 1A). This eIF1A was mutated to include a third methionine residue so that the structure could be positioned accurately by using three anomalous difference peaks (Supplementary Figures 1A and 2A). A view of the quality of the electron density of eIF1A is shown in Supplementary Figure 2B. Model building of the complex was also verified by single-wavelength anomalous diffraction (SAD) structure solution of a trimeric complex reconstituted with a SeMet substituted Imp13 (unpublished observation).

The asymmetric unit is composed of three distinct complexes. Complexes 1 and 2 present the ternary export complex and are very similar (r.m.s.d. of 0.634 Å over 868 Cα atoms). Complex 3 does not show density for eIF1A and superposes with an r.m.s.d. of 2.0 Å over 855 Cα atoms to complex 1. Complex 1 shows the best quality electron density and therefore, throughout the paper, we will refer to complex 1, unless explicitly stated. The model was refined to 3.6 Å resolution with an *R*free and *R*work of 29.9 and 26.8%, respectively, and good stereochemistry (Table I). Disordered regions are at the very N- and C-termini of Imp13 as well as a long inter-repeat loop at residues 655–672. The NTT of eIF1A is not observed (residues 1–27) together with several loop regions (residues 54–56; 97–100; 109–112) (Figure 1A and B). In complex 2, additional regions of the C-terminal arch of Imp13 and eIF1A are disordered.

The *Drosophila* (Dm) Imp13 apo form crystallized in space-group $P4_32_12$ and the crystals diffracted to 3.0 Å (Figure 1D). The structure was solved by MR using Dm Imp13 as a search model (Bono *et al*, 2010; pdb id.: 2x1g) fragmented into three portions. The refined model has an *R*free of 31% with good stereochemistry (Table I). For a sample of the electron density map, see Supplementary Figure 2C. In the unbound Imp13 structure, some N-terminal regions (residues 1–53; 78–117; 100–121), intermediate loops as well as the very C-terminus (residues 968–971) are not well defined and could not be modelled (Figures 1D and 6A).

Architecture of Imp13 in the export complex and in the unbound state

As previously shown, Imp13 folds into 20 consecutive HEAT repeats (Bono *et al*, 2010; Grünwald and Bono, 2011). HEAT repeats are motifs consisting of two helices (A and B) connected by a short loop (intra-repeat). Each HEAT repeat stacks against the following one, via an inter-repeat loop, to generate a superhelical arrangement (Cook *et al*, 2007). The A helices form the outer surface of the superhelix, while the B helices form the inner concave surface. The C-terminus of Imp13 is stabilized by a HEAT-like repeat motif composed of three helices (A–C). A hinge region around HEAT10 (H10) divides Imp13 into two arches, the N- and C-terminal arches.

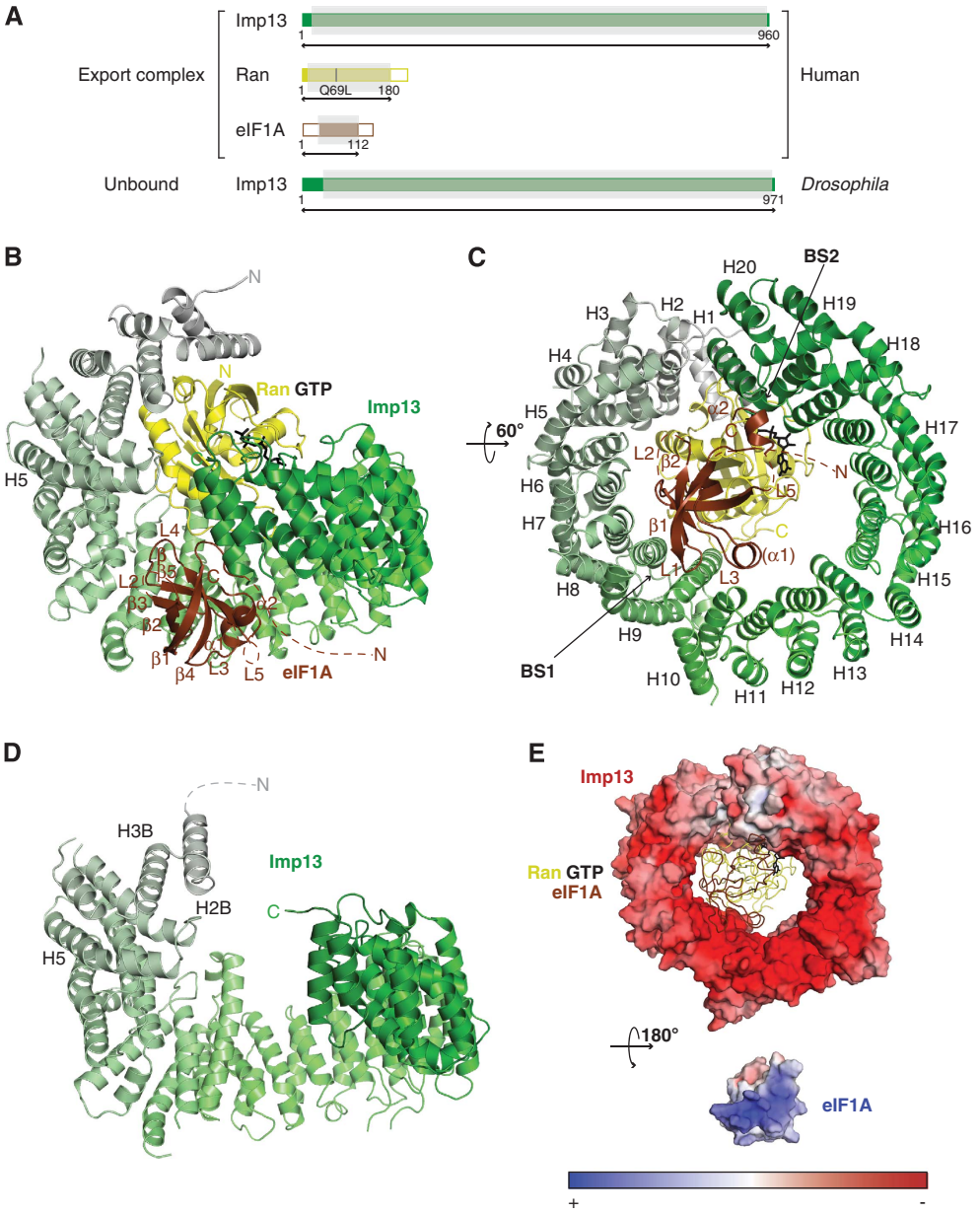

Figure 1 Structure of the ternary export complex Imp13-RanGTP-eIF1A and constructs used. (**A**) Schematic representation of the architecture of the proteins used in this study. Colour-filled areas in the scheme identify structural domains, which include the Ran core (in yellow) and the OB-fold of eIF1A (in brown). The residue numbers corresponding to the constructs used are indicated. The portions of the polypeptides ordered in the three-dimensional structure are shaded in grey. Cartoon view (**B**) and view rotated 60° along the x axis (**C**) of the export complex. Imp13 is shown in a colour gradient from grey (N-terminus) to green (C-terminus). Ran is in yellow with GTP as a stick model in black and eIF1A is coloured in brown. Secondary structure elements and HEAT repeats are labelled. (**D**) Imp13 apo structure in a similar colour code and view as in (**A**). (**E**) Surface rendering representation of Imp13 (top) and of eIF1A (bottom) in the export complex. The surface is coloured according to the electrostatic potential. Top, eIF1A and Ran, in the same colour code as above, are shown as loops with GTP as stick model in black. For the electrostatic potential calculation of eIF1A, the backbone was used as a template to include all the side chains with MODELLER (Sali and Blundell, 1993) (r.m.s.d. of 0.277 Å over 1121 atoms). These and all other protein structure figures were generated using PyMOL (http://www.pymol.org).

Two further hinge regions at H4 and H14 increase the protein's conformational flexibility (Bono *et al*, 2010; Grünwald and Bono, 2011).

In complex with RanGTP and eIF1A, Imp13 adopts a toroidal conformation with the N- and C-terminal edges offset by 8.2 Å and an inner diameter of ~58 Å (Figure 1B and C). The C helix of H20 approaches the N-terminal tip of H5 (Figures 1B and 6D). Both arches of Imp13 are engaged in complex formation. As in the Imp13-RanGTP structure, RanGTP binds to the inner concave surface of the N-terminal arch shifted towards the intra-repeat loops (Bono *et al*, 2010). However, when in complex with the export cargo, the toroidal conformation of Hs Imp13 is less compact than in the Imp13-RanGTP complex, with the C-terminal arch more open to accommodate eIF1A (Figure 1B). In the complex with Imp13 and eIF1A, the structure and conformation of Hs RanGTP is very similar to the structure of RanGTP in complex with RanBD1 (r.m.s.d. of 0.48 Å over 168 Cα atoms) and of

Table I Crystallographic statistics

Data collection			
Data set	Imp13-RanGTP-eIF1A	Imp13-RanGTP-eIF1A SAD	Imp13 unbound
Beamline	SLS PXII	SLS PXII	SLS PXII
Space group	*C*2	*C*2	$P4_32_12$
Unit cell (Å)	$a=186.5$, $b=100.4$, $c=274.7$, $\alpha=\gamma=90^\circ$, $\beta=90.9$	$a=185.7$, $b=100.9$, $c=273.3$, $\alpha=\gamma=90^\circ$, $\beta=90.5$	$a=b=167.7$, $c=95.6$, $\alpha=\beta=\gamma=90^\circ$
Wavelength (Å)	0.97919	0.97952	1.0409
Resolution range (Å)[a]	50–3.6 (3.7–3.6)	50–3.8 (3.9–3.8)	100–3.0 (3.1–3.0)
Total no. of observations	195 637	686 292	415 721
Unique reflections	57 267 (4046)	97 665 (7340)	27 903 (2557)
Redundancy	3.4 (3.2)	7.0 (7.3)	14.9 (12.5)
Completeness (%)[a]	96.6 (87.4)	99.9 (100.0)	99.9 (100.0)
$I/\sigma(I)$[a]	11.35 (2.08)	11.96 (2.37)	16.36 (2.28)
R_{sym}(%)[a]	8.2 (94.1)	10.7 (74.1)	10.7 (116.7)
Refinement			
Resolution range (Å)	50–3.6		50–3.0
No. of reflections	57266		27853
No. of reflections in test set	2843		1394
R_{free} (%)[a]	29.92		31.09
R_{work} (%)[a]	26.84		26.82
No. of atoms			
Protein	21782		6106
Ligand/ion	99		—
Water	—		—
B factors			
Protein	139.3		106.2
Ligand/ion	166.4		—
Water	—		—
R.m.s.d. bond (Å)	0.003		0.003
R.m.s.d. angle (deg)	0.775		0.737
Ramachandran values[b]			
Favoured (%)	98.2 (outliers 0.1)		97.2 (outliers 0.0)
Allowed (%)	99.9		100
Molprobity score (with H)	1.83		2.18

Data collection and refinement statistics of the crystal structure of Imp13-RanGTP-eIF1A complex and of Imp13 apo.
[a]Values in parentheses correspond to the highest resolution shell.
[b]Molprobity (Chen *et al*, 2010).

RanGTP in the binary complex with Imp13 (r.m.s.d. of 0.34 Å over 147 Cα atoms) and has been extensively described elsewhere (Vetter *et al*, 1999b; Bono *et al*, 2010).

In the structure of Dm Imp13 in the unbound state, the karyopherin toroidal structure is in an open conformation (Figure 1D). H1 and the external helices of H2 and 3 are disordered in the structure, suggesting flexibility at the very N-terminus of the protein. Flexibility in this region might be required for the docking of RanGTP in the nucleus to displace the import cargoes (Grünwald and Bono, 2011) (Figures 1D, 6A and B) and to recognize cargoes that bind at the N-terminal arch of Imp13, such as Ubc9.

Export cargo recognition by Imp13 and RanGTP

The OB-fold of eIF1A is composed of five β strands (β1–β5 strands of eIF1A: $\beta1_E$–$\beta5_E$) forming an elliptic cavity interrupted by a loop between $\beta3_E$ and $\beta4_E$ ($L3_E$) that folds into a small helix ($\alpha1_E$). C-terminal to the β-barrel eIF1A features an additional helix ($\alpha2_E$). Although the NTT of eIF1A was present in the construct that was crystallized, no density for this part of the structure was observed in the trimeric export complex, likely due to conformational flexibility in this region (Battiste *et al*, 2000). When the full-length solution structure is superposed on the export complex, the NTT points into solvent (Supplementary Figure 6B). To rule out the possibility that the NTT is required for binding and the possibility that the NTT was not observed due to the relatively low resolution map, we performed SEC with truncated versions of eIF1A. These experiments show that the folded part of eIF1A (residues 26–115; ΔNΔC) is sufficient for binding to Imp13 (Figure 2D and E).

eIF1A can be approximated to a triangle that is recognized at its vertices on three main interaction surfaces, two on Imp13 and one on RanGTP. The two corners at the base of the triangle $\beta2_E$ and $L3_E$, and $\alpha2_E$ interact at two opposite surface areas (BS1 and BS2, respectively) that bridge the inner central part of Imp13 and its very C-terminus (Figures 1B, C, 2A, B and 3A). The interaction surface of eIF1A to Imp13 contains several conserved, positively charged residues, which complement the negatively charged inner binding surface of Imp13 (Figure 1E).

The larger area of interactions (BS1) is centred around H9 of Imp13 and stretches across the hinge between the N- and C-terminal arches involving H7-11 on the side of the inter-repeat loops. On eIF1A the loop $L1_E$ points to the groove between H8 and 9 (Figure 2A); $\beta3_E$ and the N-terminal stretch of $L3_E$ contact H8 and H10-11, respectively, while the N-terminal part of $\beta5_E$ and $L4_E$ interacts with H7-8. A series of salt bridges are likely to stabilize this interface: Asp369 on H8 of Imp13 ($Asp369_I$) points to Lys88 of eIF1A ($Lys88_E$) on

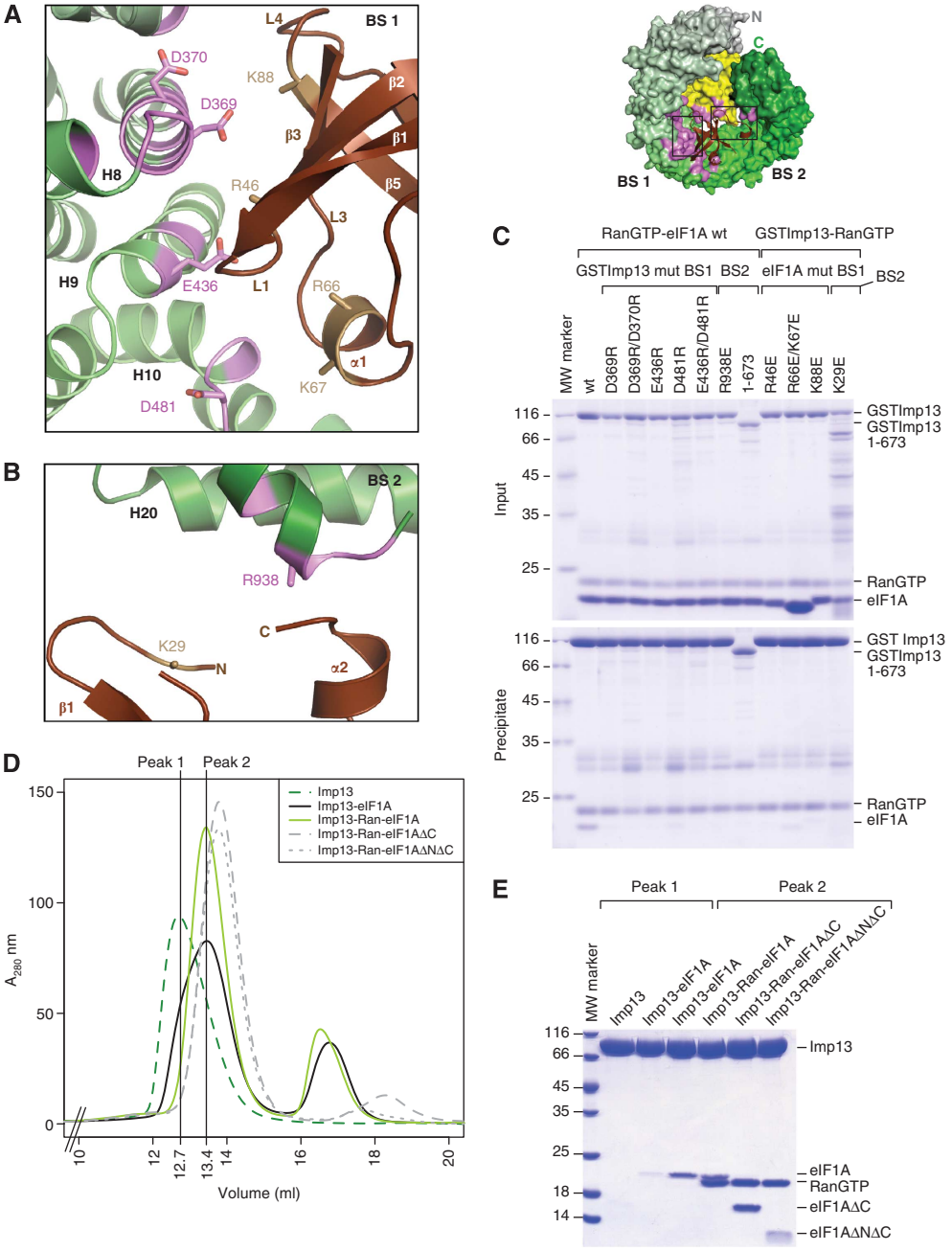

Figure 2 Detailed view of the interaction between Imp13 and eIF1A. Top right, the export complex is rendered with Imp13 and RanGTP as surface and eIF1A as cartoon in the same colour coding as in Figure 1B. The interaction surface of eIF1A on Imp13-RanGTP is in pink. (**A**) Close-up view of the eIF1A interaction with Imp13 at BS 1 in a similar view as in Figure 1B. Residues involved in the interaction on eIF1A and Imp13 are shown as sand and pink sticks, respectively. HEAT repeats are labelled in black and secondary structure elements of eIF1A are marked in brown or white. (**B**) Zoomed in view of the BS 2 interaction site. (**C**) Protein co-precipitation by GST-tagged Imp13 incubated with RanGTP and eIF1A with either wt or mutant proteins. In this experiment, Ran was His tagged for better separation from eIF1A on gel. For the input control, 1/6 of the samples were kept (upper panel) and the rest was co-precipitated with glutathione sepharose beads (lower panel) and analysed on Coomassie-stained 15% SDS–PAGE. The far left lane was loaded with a molecular weight marker. Some contaminations likely from degradation of GSTImp13 are visible between 25 and 35 kDa. GST controls for this experiment are in Supplementary Figure 6A. (**D**) Overlay of SEC plots of Imp13 alone or together with different eIF1A constructs with or without RanGTP. (**E**) Samples of the peaks fractions were analysed on Coomassie-stained SDS–PAGE (Any kD, BIORAD). The far left lane was loaded with a molecular weight marker.

$\beta5_E$; on H9, $Glu436_I$ approaches $Arg46_E$ on $L1_E$; $Asp481_I$ at the inter-repeat loop between H10-11 is in proximity to $Arg66_E$ and $Lys67_E$ on $L3_E$.

At the smaller interaction surface, helix $\alpha2_E$ packs end-on to the C-terminal helix of Imp13. At this site, $Arg938_I$ approaches helix $\alpha2_E$ as well as the N-terminal stretch of eIF1A (Figure 2B; Supplementary Figure 1). Consistent with the structural analysis, reverse charge mutations of $Asp369_I$, $Asp370_I$, $Glu436_I$ and $Asp481_I$ to arginine in BS1 or of $Arg938_I$ to glutamate in BS2 resulted in reduction or loss of binding to eIF1A in pull-down assays (Figure 2C; Supplementary Figure 1). Although structurally less well defined (many side chains of eIF1A do not have visible electron density), the contribution of positively charged residues of eIF1A

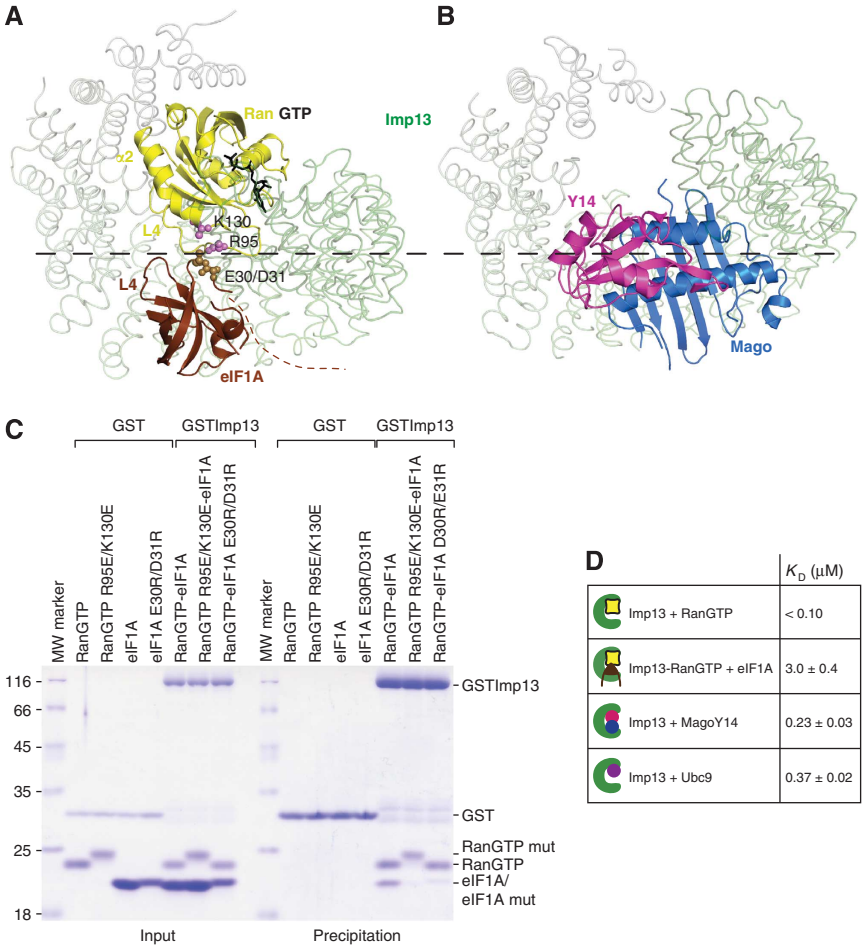

Figure 3 Structural basis of Imp13 bidirectionality and K_D affinities in the Imp13 cycle. (**A**) RanGTP and eIF1A concomitant interaction in the ternary export complex. Interacting residues on Ran and eIF1A are rendered as spheres in pink and sand, respectively. (**B**) Imp13-Mago-Y14 structure oriented as in Figure 3A (pdb ids.: 2x1g). Imp13 is represented as loop trace. A dashed line in black marks the boundary between compatible and hindered binding. (**C**) Protein co-precipitations by GST-tagged Imp13 incubated together with His-RanGTP and eIF1A with either wt or mutant proteins performed as in the previous figure. (**D**) Table representing K_D values determined by DSF from at least three independent experiments.

to Imp13 binding could also be confirmed using reverse charge mutations. Residues $Lys29_E$, $Arg46_E$, $Arg66/Lys67_E$ and $Lys88_E$ are conserved (Supplementary Figure 1A) and mutations to negatively charged residues impeded binding to Imp13, as confirmed by pull-down assays (Figure 2C; Supplementary Figure 6A).

Similarly to the import cargoes Ubc9 and Mago-Y14, eIF1A is primarily recognized by Imp13 as a folded domain. This indicates that both import and export signals recognized by Imp13 are complex ones, therefore different from the linear and semi-linear canonical NLSs and NESs recognized by Impβ, Tpn and Crm1 (Xu *et al*, 2010; Zhang and Chook, 2012). The structural and mutational analyses show that Imp13 recognizes its cargoes by a combination of shape and charge together with specific contacts at conserved positions on eIF1A.

Imp13 uses shape complementarity of cargoes to perform bidirectional transport

In the export complex, the β-barrel and the very tip of helix $\alpha2_E$ of eIF1A bind adjacent to RanGTP at the inner surface of Imp13. The structure strongly suggests that eIF1A is in direct contact with RanGTP in the complex with Imp13. L4 of Ran ($L4_R$, between $\beta5_R$-6_R) is adjacent to $L4_E$ and to the N-terminus of eIF1A (Figure 3A). Here, $Glu30_E$ and $Asp31_E$ point towards the $L4_R$ and towards $Lys130$ of Ran ($Lys130_R$) while $L4_E$ approaches $Arg95_R$ at helix $\alpha2_R$ (Figure 3A; Supplementary Figure 1A). Consistently, mutants of $Glu30_E$ and $Asp31_E$ to arginine and of $Arg95_R$ and $Lys130_R$ to glutamate impair binding of Imp13-RanGTP to eIF1A (Figure 3C).

To further understand Imp13 bidirectionality, we compared the mode of binding of Imp13 in the export complex with the structure of Imp13 bound to the import cargo Mago-Y14 (Bono *et al*, 2010). As we have previously shown, when the latter structures are superposed, RanGTP and Mago-Y14 assume an adjacent but overlapping position that precludes concomitant binding of Mago-Y14 with RanGTP due to steric hindrance (Bono *et al*, 2010). In the complex of Imp13 with RanGTP and eIF1A, the export cargo is much smaller than Mago-Y14 so that it fits neatly into the hole created by the C-terminal arch. In this case there is not a clash with RanGTP, instead the complementary charge interactions with RanGTP stabilize the binding and increase the binding affinity (Figure 3D). Consistently, SEC experiments of Imp13-eIF1A complexes show only a partial binding of eIF1A in the

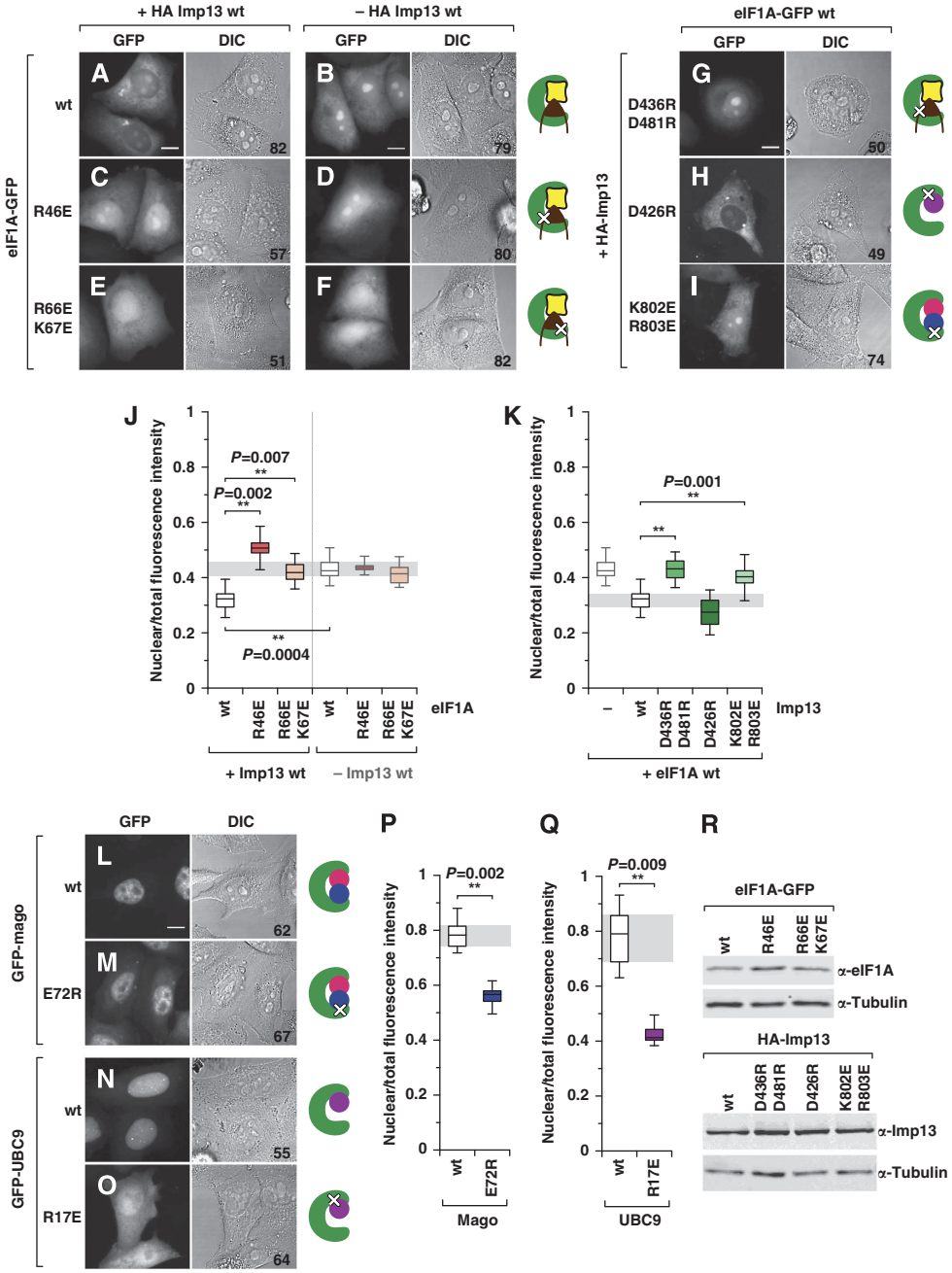

Figure 4 Imp13 binds and exports eIF1A *in vivo*. (**A**–**F**) Fluorescence microscopy images and the corresponding differential interference contrast (DIC) images of living HeLa cells expressing GFP-tagged eIF1A (eIF1A-GFP) wt or mutants. Localization of wt or mutant eIF1A-GFP in the presence (**A**, **C**, **E**) or absence (**B**, **D**, **F**) of HA-Imp13. (**G**–**I**) Localization of wt eIF1A-GFP in the presence of the indicated HA-Imp13 mutants. (**J**, **K**) Relative quantification of the fluorescence intensity in the nuclear compartment for each construct, in the absence (−) or presence (+) of Imp13 wt or of the indicated Imp13 constructs. (**L**–**O**) Fluorescence microscopy images and the corresponding DIC images of living HeLa cells expressing GFP-tagged Mago or Ubc9 wt or mutants. (**P**, **Q**) Relative quantification of the fluorescence intensity in the nuclear compartment for each construct. Box plots: the bottom and top of the box depict the first (qu1) and the third (qu3) quartiles, respectively, with the central line indicating the median (qu2); the upper and lower whiskers represent the maximum and minimum values, respectively. At least three independent experiments were performed; the number of analysed cells is indicated for each condition at the bottom right of the corresponding DIC image. Statistical significance was calculated by comparing the means of each experimental replicate with the means of the appropriate control conditions, with one-tail *t*-tests (α 0.05). Scale bar: 10 μm. (**R**) Western blot showing the expression levels of HA-Imp13 wt and mutants, or eIF1A-GFP wt and mutants; note that all mutants are expressed at levels similar to the corresponding wt. α-Tubulin served as a loading control.

absence of RanGTP (Figure 2D and E). Imp13 is therefore able to discriminate between cargoes based on their structural features and can therefore promote either cooperative binding (for export) or antagonistic binding (for import).

Comparison of the Imp13-RanGTP-eIF1A complex with the Imp13-Mago-Y14 structure also shows that the binding of Mago-Y14 and eIF1A is mutually exclusive. The release of Mago-Y14 by RanGTP is less efficient *in vitro* as compared to

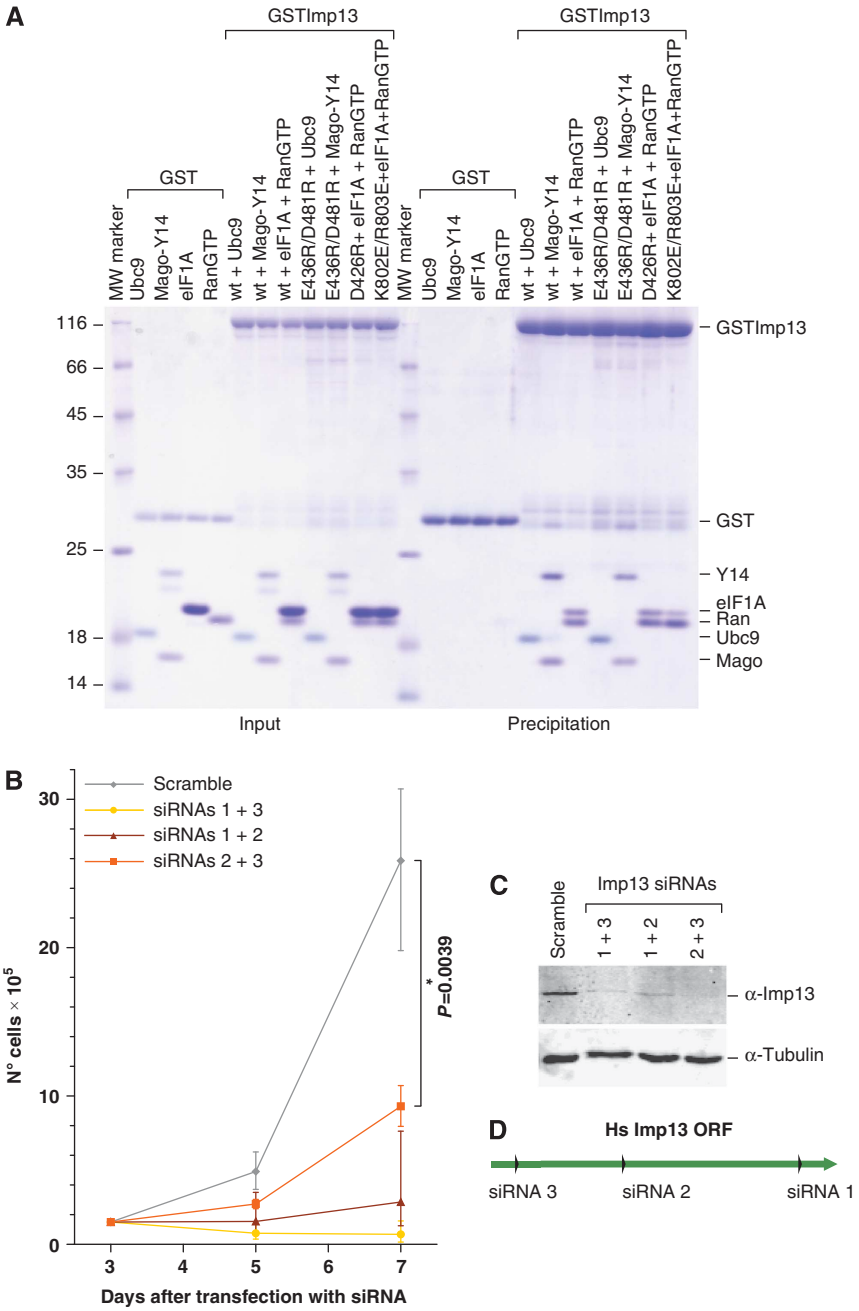

Figure 5 Imp13 function is essential *in vivo*. (**A**) Coomassie gel of co-precipitations to demonstrate that the Imp13 mutants impaired in the binding of one of the cargoes analysed are still able to associate to the other two cargoes. (**B**) HeLa cells were transfected with different siRNA combinations and counted at the indicated time points. Six independent experiments were performed. Statistical significance of the cell counts between knockdown and control condition was assessed with Wilcoxon–Mann–Whitney test (α 0.05). (**C**) Western blot showing the levels of endogenous Imp13 in the control and the Imp13 knockdown condition; α-tubulin served as a loading control. (**D**) Schematic representation of Imp13 open reading frame (ORF) showing the target sites of the siRNAs used.

that of another import cargo, Ubc9, which shows a different mode of binding. We have previously shown that addition of eIF1A together with RanGTP enhances the release of Mago-Y14 from Imp13 (Grünwald and Bono, 2011; Figure 3A and B). In contrast, a comparison of the Imp13 export complex with Imp13-Ubc9 import complex shows no major clashes between the cargoes (Figure 6D and E). However, a simultaneous binding of eIF1A and Ubc9 to Imp13 *in vitro* is not possible (Grünwald and Bono, 2011). The structural and biochemical data suggest that the shape complementarity of eIF1A and its overlap with the Mago-Y14 binding site is critical for achieving the directionality of Mago-Y14 import. RanGTP likely destabilizes Mago-Y14 binding by preventing optimal association with Imp13. Further association of eIF1A with Imp13 would lock the importin in an export conformation, preventing re-association of Mago-Y14 and imparting directionality to this nuclear import step.

To better understand the mechanism of the Imp13 import/export cycle, we measured the K_D values by

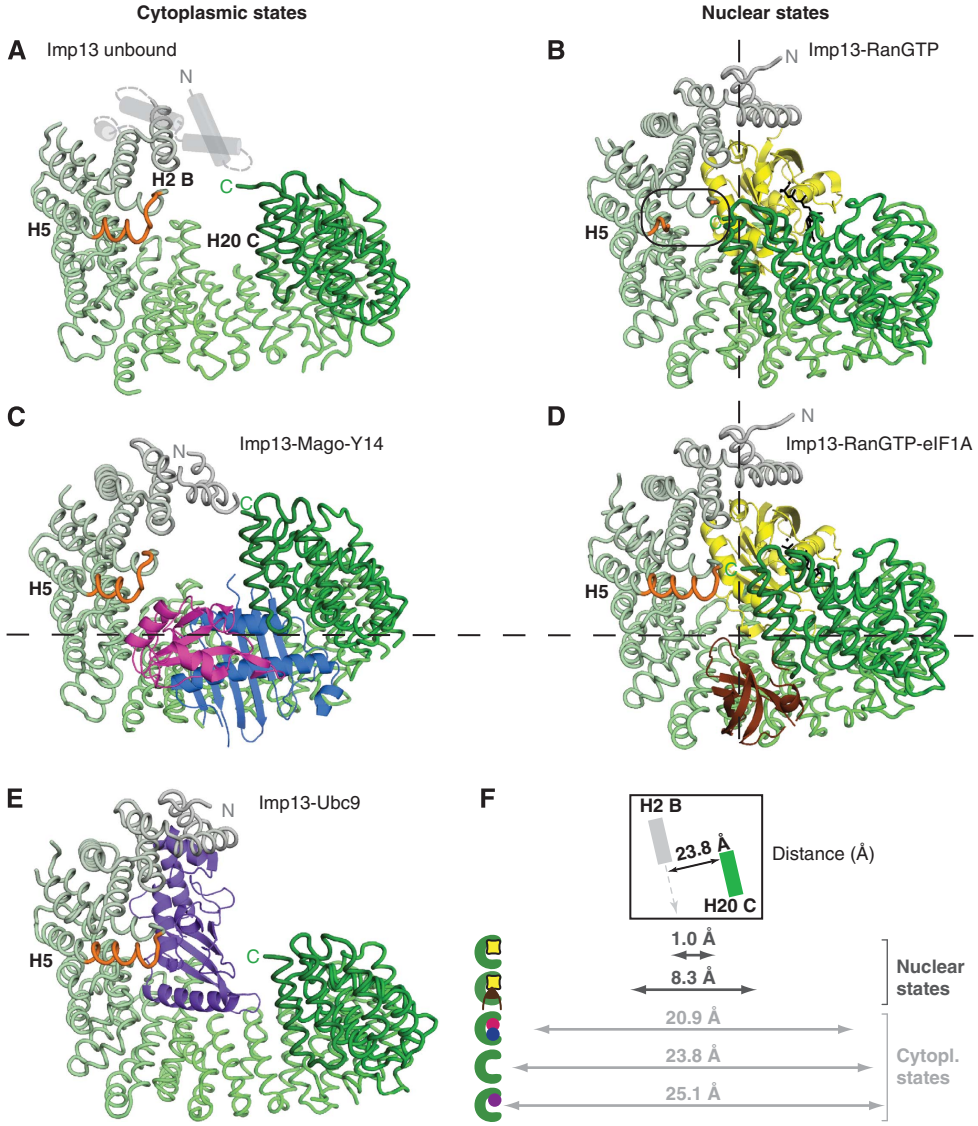

Figure 6 Imp13 samples an ample spectrum of conformations. Cytoplasmic (**A**, **C**, **E**) and nuclear (**B**, **D**) states of Imp13 in the same view as in Figure 1B. Imp13 is represented as a tube trace in a colour gradient from grey to green. All cargoes are shown as cartoons with Ubc9 in purple-blue, Mago in blue, Y14 in magenta, Ran in yellow with GTP in black and eIF1A in brown. (**F**) Graphical representation of the distance from N-terminus to C-terminus measured from the line connecting H2B and H20C as shown in the box (top).

differential scanning fluorimetry (DSF) (Niesen *et al*, 2007) (Figure 3D; Supplementary Figure 3). The estimated K_D for the two import cargoes Mago-Y14 and Ubc9 is in a similar range with a value of 235 ± 30 nM and 370 ± 20 nM, respectively. The K_D value for RanGTP binding to Imp13, although not accurately calculated due to the upper detection limit of the method, falls in the low nanomolar or picomolar range (< 100 nM) and is consistent with values measured for other karyopherins (Bischoff and Görlich, 1997; Deane *et al*, 1997; Görlich *et al*, 1997; Lipowsky *et al*, 2000). The dissociation constant of the export cargo eIF1A to a preformed Imp13-RanGTP complex is 3 ± 0.38 μM, 10-fold higher than the K_D values of the import cargoes (Figure 3D). The rather weak affinity of Imp13-RanGTP for its export cargo eIF1A is comparable to that displayed by Crm1 for most NES, such as HIV Rev (K_D of about 0.5 μM) (Askjaer *et al*, 1999; Paraskeva *et al*, 1999). One exception is Snurportin that binds to CRM1 with much higher affinity because it is recognized through additional interactions (K_D ~ 10 nM) (Paraskeva *et al*, 1999). Xpot also binds tRNAs with high affinity (K_D ~ 3 nM) (Kutay *et al*, 1998; Lipowsky *et al*, 1999). The binding of CAS/Cse1 to Impα and RanGTP is highly cooperative and cargo binding cannot be disjointed from RanGTP binding (Kutay *et al*, 1997).

Imp13 exports eIF1A in vivo and its function is required for cell viability

eIF1A is able to passively diffuse through the NPCs and thus reach the nuclear compartment and it has previously been proposed that active export is necessary to deplete eIF1A from the nucleus and contribute in preventing nuclear translation (Mingot *et al*, 2001). Surprisingly, we observed that endogenous eIF1A is enriched in nucleoli in HeLa cell lines (Supplementary Figure 4A and D). An overexpressed, GFP-tagged version of the protein shows a similar localization in fixed cells (Supplementary Figure 4C); however, the same construct displays a significantly higher cytoplasmic

fraction in living cells (Figure 4B), suggesting that fixation affects eIF1A localization to some extent. All together, our results indicate that endogenous eIF1A is localized to both nucleoli and cytoplasm.

Overexpression of Imp13 causes an accumulation of wild-type (wt) eIF1A in the cytoplasm (Figure 4A), indicating that Imp13 can bind and export eIF1A *in vivo*. This redistribution of eIF1A in the cell depends on its ability to bind to Imp13, since Arg46Glu$_E$ and Arg66Glu/Lys67Glu$_E$ mutants, which are impaired in their interaction with Imp13 (Figure 2C), do not change their nucleo-cytoplasmic distribution upon Imp13 overexpression (Figure 4C, E and J) despite being expressed at similar levels (Figure 4R). Conversely, only wt Imp13, but not Asp436Arg/Asp481Arg$_I$ mutant, which is unable to bind to eIF1A (Figure 2C) but still associates with Mago-Y14 and Ubc9 (Figure 5A), triggers eIF1A depletion from the nucleus (Figure 4G and K). This effect is not due to a lower expression level of the mutants compared to wt Imp13 (Figure 4R). In the absence of Imp13 overexpression, however, eIF1A wt, Arg46Glu$_E$ and Arg66Glu/Lys67Glu$_E$ reverse-charge mutants show a similar nucleo-cytoplasmic distribution (Figure 4B, D and F), as shown in the quantification (Figure 4J). These results indicate that other pathways are probably involved in eIF1A localization *in vivo*.

Since eIF1A is present in the nucleolus, the site of ribosome assembly, we hypothesized that it might be exported together with other complexes. A possible association could be with the small ribosomal subunit, which is exported via a Crm1-dependent export pathway (Thomas and Kutay, 2003) and, at least in yeast, by a recently identified Mex67/Mtr2-dependent pathway (Faza *et al*, 2012). It has previously been shown that eIF1A cannot directly bind Crm1 (Mingot *et al*, 2001). We therefore analysed the localization of eIF1A wt and mutants in the presence of leptomycin B (LMB), a specific inhibitor of Crm1 (Wolff *et al*, 1997). LMB treatment causes a small but consistent and significant nuclear retention of eIF1A, regardless its capacity to bind to Imp13 (Supplementary Figure 5), suggesting that at least a fraction of eIF1A might be exported via a Crm1-dependent pathway reflecting an as yet unidentified association of eIF1A with other nuclear complexes.

We also examined the *in vivo* localization of two previously characterized Imp13 import cargoes, Mago-Y14 and Ubc9 (Bono *et al*, 2010; Grünwald and Bono, 2011). As expected, both cargoes are predominantly nuclear in HeLa cells (Kataoka *et al*, 2000, 2001; Rodriguez *et al*, 2001; Saitoh *et al*, 2002) (Figure 4L and N). Mutations previously shown to disrupt their interaction with Imp13 have also a strong impact on the localization of these cargoes (Bono *et al*, 2010; Grünwald and Bono, 2011) (Figure 4M and O–Q), suggesting that Imp13 is probably the main factor involved in Mago-Y14 and UBC9 import *in vivo*. Notably, an Imp13 mutant unable to bind to Mago-Y14 (Lys803Glu/Arg803Glu$_I$) is also less efficient in exporting eIF1A *in vivo* (Figure 4I and K), reflecting a reduction in binding to eIF1A *in vitro* (Figure 5A). Conversely, the Asp426Arg$_I$ Imp13 mutant, impaired in Ubc9 binding (Figure 5A), is as efficient as Imp13 wt in exporting eIF1A (Figure 4H and K).

To gain further insights into the role of Imp13-mediated transport *in vivo*, we depleted endogenous Imp13 in HeLa cells using three different siRNAs targeted to the Imp13 open reading frame (ORF) (Figure 5C and D). With every siRNA and combination of siRNAs, we observed a significant decrease in cell viability (Figure 5B), suggesting that Imp13 might be an essential protein.

Conformational changes of Imp13 in the cytoplasmic and nuclear states

Imp13 shows a marked conformational change when the cytoplasmic and nuclear states are compared (Figure 6). Dm Imp13 in the unbound state adopts an open conformation measuring about 24 Å between H2 and 20 (Figure 6A and F). In the cytoplasmic states of Imp13 bound to Mago-Y14 and Ubc9, the karyopherin also has a more extended conformation (Figure 6C, E and F). In the nucleus where it is associated with RanGTP, Imp13 is more compact with the C-terminal arch approaching the N-terminus (Figure 6B, D and F). Here, maximal compactness is observed in the binary complex with RanGTP (1 Å between H2 and H20). In complex 3, Imp13 shows a conformation similar to the one observed when in complex to RanGTP (Bono *et al*, 2010) (r.m.s.d. of 0.548 Å over 903 Cα) (Supplementary Figure 7C and D), suggesting that eIF1A is indeed missing in this complex. In the ternary complex with RanGTP and eIF1A, the C-terminus of Imp13 moves slightly away from the N-terminus to fit the export cargo within the C-terminal arch.

Remarkably, helix A of H5 undergoes partial melting and appears to work as a spacer to sense the RanGTP-bound state. In the RanGTP-bound state, helix H5B contacts the last helix H20C and therefore closes Imp13 into a ring (Figure 6B). In contrast, upon eIF1A binding, the H5A helix of Imp13 folds into a longer helix, breaking the H5B contact and establishing a new contact between the newly formed H5A helix and H20C helix (Figure 6D). Thereby, the toroidal ring of Imp13 opens up slightly at the hinge region at H14 to accommodate eIF1A, which concomitantly contacts the beginning of the H20C helix replacing the H5 interaction. In all Imp13 open conformation states, the import complexes as well as the unbound Imp13, the helix at H5 is also structured.

The spectrum of conformations sampled by Imp13 reflects the cumulative effect of changes distributed over the entire molecule with more prominent changes at the three hinge regions (Grünwald and Bono, 2011).

The structures of several exportins in complex with an export cargo have been solved. A comparison between the different export complexes of Cse1, Crm1, Xpo5 and Xpot with Imp13-RanGTP-eIF1A shows similar topology of Imp13 and Crm1 in the export cargo bound state (Matsuura and Stewart, 2004; Cook *et al*, 2009; Monecke *et al*, 2009; Okada *et al*, 2009; Dong *et al*, 2009b) (Supplementary Figure 7A and B). Although both karyopherins have a closed ring-like conformation, Imp13 binds the export cargo mainly with the inner concave surface, whereas Crm1 binds its cargoes on its outer surface (Monecke *et al*, 2009; Dong *et al*, 2009b). As in most exportins with the exception of Crm1, the positively charged interface of RanGTP directly contacts the cargo. In the apo form, Xpot and Imp13 demonstrate an overall open conformation that closes up upon RanGTP binding (Cook *et al*, 2009).

Export cargo dissociation and directionality of Imp13 transport

In the nucleus, RanGTP is very abundant and its binding to karyopherins is very tight, thus eIF1A will likely encounter

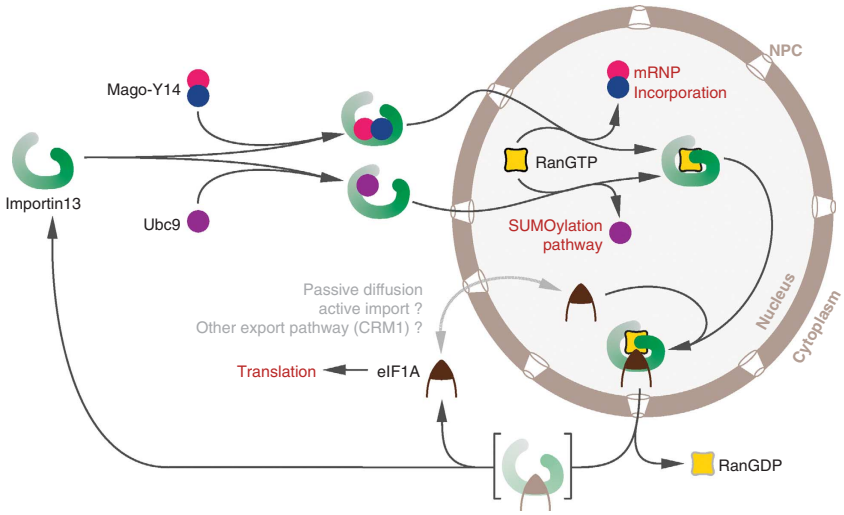

Figure 7 The Imp13 pathway. Schematic display of the dynamic interactions that take place between Imp13 and its protein partners in the cell. In the cytoplasm, Imp13 in the unbound state adopts an open conformation that probably facilitates association of the cargoes to be imported. In the binary import complexes with Mago-Y14 or Ubc9, Imp13 maintains a rather open conformation and translocates through the NPCs into the nucleus. Here, high concentration and the high affinity binding of RanGTP to Imp13 promotes release of the import cargoes. Mago-Y14 is then free to be re-incorporated into an EJC on a newly transcribed and processed mRNP, while Ubc9 promotes SUMOylation of a large number of nuclear targets. In the binary complex with RanGTP, Imp13 adopts a compact conformation that favours the docking of eIF1A. A slight opening of Imp13 conformation at the C-terminal arch accommodates eIF1A side-by-side with RanGTP. The trimeric export complex crosses the NPCs to deliver the export cargo in the cytoplasm upon RanGTP extraction and hydrolysis. Some residual- or re-binding of eIF1A to Imp13 in the absence of RanGTP might occur in the cytoplasm. In this case, import cargo association to Imp13 will competitively displace eIF1A. Due to its small size that allows its diffusion through the NPCs (or possibly via a yet unknown active import mechanism) eIF1A is found in the nucleus at steady state. eIF1A export from the nucleus is not unique to Imp13 and might involve other export factors, such as Crm1, and might occur in complex with other proteins.

Imp13-RanGTP complex in the closed conformation that will then open at the C-terminal arch to accommodate the cargo. In the cytoplasm, the disassembly of the export cargo-receptor complex is coupled to the activation of the GTPase activity of Ran by RanGAP, a cytoplasmic enhancer of RanGTPase activity (Bischoff *et al*, 1994). Prior to GTP hydrolysis, RanGTP is likely to be extracted from the complex by the concomitant recognition of the C-terminal region of RanGTP and the Ran binding domain of RanBP1. Similarly to what has been observed with other RanGTP-karyopherin complexes (Hellmuth *et al*, 1998; Kutay *et al*, 1998; Vetter *et al*, 1999b; Koyama and Matsuura, 2010), when the RanGTP-RanBP1 complex is superposed on the export complex, RanBP1 would clash with H14-15 of Imp13 whereas the extended acidic tail at the C-terminus of Ran would clash with H13 (Supplementary Figure 6C). This indicates that the mechanism for removing RanGTP and ending the export cycle is likely similar in Imp13 as in other karyopherins.

Comparison of Imp13 export complex and Imp13 apo structures gives insights into the directionality of the transport. In the apo form, the contact of eIF1A with RanGTP is missing. Moreover, if we optimally superpose the eIF1A binding site at H8-9 of Imp13 in the export complex and in the apo structure (residues 357–438 of Hs Imp13 in complex with RanGTP and eIF1A and 370–452 of Dm Imp13 unbound), the contact at the C-terminus of Imp13 is lost, together with the contact at the inter-loop between H10-11 (Supplementary Figure 6D). The latter includes $Asp481_I$, which is involved in binding to eIF1A (Figure 2A and C) and is displaced in the apo structure. Therefore, in the Imp13 apo form, the complementarity for eIF1A is partially lost, with only the interaction surface at H7-10 being in place. The remaining contacts that compose the intact binding surface in the trimeric complex (at H6 and 11) are also displaced due to a divergence of the N- and C-termini of Imp13 that pushes them away from the eIF1A binding site (Supplementary Figure 6D). Therefore, apo Imp13 has a shape that is incompatible with eIF1A binding. This open form could provide expanded flexibility to allow Imp13 to associate with a variety of different import cargoes that it can recognize in the cytoplasm. It is likely that the tighter binding import cargoes will displace any residual association between eIF1A and Imp13 in the cytoplasm.

Whether the cytoplasmic import cargo-bound form of Imp13, after RanGTP hydrolysis and export cargo release, occurs through an unbound or eIF1A-bound intermediate is unclear. Our binding studies show that eIF1A binds poorly to Imp13 in the absence of RanGTP (Figure 2D and E). In addition, an Imp13 mutant with a C-terminal deletion (residues 1–673) is impaired in the binding to eIF1A indicating that the C-terminal contact of Imp13 to eIF1A is important for the binding (Figure 2C). However, our SEC data indicate that eIF1A remains partially associated with Imp13 in the absence of RanGTP, and so association with import cargoes might be necessary to clear residual eIF1A from Imp13 in the cytoplasm. This would imply that Imp13 could take two pathways after entry to the cytoplasm, one where binding of an import cargo is directly coupled to eIF1A ejection and one where Imp13 is released in an apo state before binding to other cargoes (Figure 7).

Conclusions

Imp13 is an essential import factor that also has a critical role as an export factor. The structure of the export complex of Imp13 with RanGTP and eIF1A shows how Imp13 can

perform this dual duty. Imp13 in this complex adopts a compact conformation where eIF1A recognizes the inner surface of the C-terminal arch of Imp13 and is engaged in a stabilizing contact with RanGTP. eIF1A association with Imp13 is compatible with the presence of RanGTP, since the export cargo overall shape/structure does not clash with Ran and the binding sites do not overlap. Contacts on Imp13 and on RanGTP stabilize cargo binding for export. The binding mode of eIF1A to Imp13 is similar and spatially overlapping to the binding mode of Mago-Y14 to Imp13. In the latter case, however, the association with RanGTP is mutually exclusive. Due to the higher affinity of binding to Imp13 and high nuclear concentration of the small GTPase, the import cargo is released in the nucleus. At each stage of the import/export cycle Imp13 adopts a shape that allows complementary cargoes to compete for binding in the same compartment. The combination of shape, charge and size of the bound cargo will drive the concomitant or exclusive interactions with RanGTP and ultimately determine the directionality of the transport and the delivery of the cargoes in the appropriate compartment. The mechanism by which Imp13 can act as a bidirectional transport factor could be exploited by more karyopherins, suggesting that the range of bifunctional receptors might be larger than believed so far.

The apo structure explains the directionality of eIF1A export. In this state of Imp13, the binding site for eIF1A is partially distorted and the shape complementarity for eIF1A is lost. These data suggest two pathways for importin association in the cytoplasm: either Imp13 is released as a free apo molecule after RanGTP has been extracted, or import cargoes directly displace the export cargo concomitantly with RanGTP release (Figure 7).

We demonstrate that eIF1A is exported by Imp13 *in vivo*. However, the intracellular localization of eIF1A mutants designed based on the structure show that Imp13 export is functionally redundant and that a Crm1-dependent pathway might be important for eIF1A localization. We also show that Imp13 function is required for viability in human cells, though this may relate to its role in other transport pathways. Further investigations will clarify eIF1A function in the nucleus and eIF1A alternative export pathways.

Materials and methods

DNA constructs

For mammalian expression, Hs Imp13, Mago, Y14 and Ubc9 were cloned in a pEGFP-C1 vector (Clontech); to obtain HA-tagged fusion proteins, the EGFP sequence was deleted and substituted with one encoding for the HA epitope (YPYDVPDYA). Hs eIF1A was cloned in a pEGFP-N3 vector (Clontech). Hs fibrillarin (FBL) was amplified from HeLa cDNA and cloned into a modified pEGFP-C1 vector, in which the sequence encoding EGFP was replaced by the ORF of mCherry (pmCherry-C1). GFP-NES was obtained by inserting an oligonucleotide encoding for the nuclear export signal (NES) of the protein kinase A inhibitor (PKI) (Güttler *et al*, 2010) into the *Xho*I/*Hin*dIII sites of the pEGFP-C1 vector.

Protein expression and purification

Recombinant Hs and Dm Imp13 were expressed as described before (Grünwald and Bono, 2011). Hs Ran Q69L (1–180) and Hs eIF1A full-length and truncated constructs were cloned in a pETMCN vector (Diebold *et al*, 2011) with an N-terminal hexahistidin tag. The recombinant Hs Ran was prepared similarly to the yeast orthologue (Bono *et al*, 2010). The eIF1A constructs were expressed in the *E. coli* strain BL21 (DE3) Gold in autoinducing medium (Studier, 2005) at 20°C overnight. The cleared cell lysates were affinity purified by Ni^{2+} NTA in buffer A (20 mM Tris pH 7.5, 300 mM NaCl, 5 mM imidazole and 1 mM β-mercaptoethanol) with a gradient of 5–250 mM imidazole, followed by dialysis in the presence of TEV protease in buffer B (20 mM Tris pH 7.5, 300 mM NaCl, 1 mM DTT). The protein was further purified by a second step of Ni^{2+} NTA chromatography and the collected flow-through applied to a cation-exchange column in buffer B with a gradient of 300–1000 mM NaCl.

Site-directed mutagenesis was used to introduce a third methionine at residue 65 in pETMCN His eIF1A (1–112). To produce eIF1A Leu65Met 1–112 SeMet-labelled protein, the construct was expressed in the *E. coli* strain DL41 auxotroph for methionine in M9 medium and starved before addition of SeMet. The protein was purified as described above for the unmodified protein.

For complex formation, proteins were mixed in a 1:1.5:2 ratio of Imp13-RanGTP-eIF1A in complex buffer A (20 mM Tris pH 7.5, 50 mM NaCl, 4 mM $MgCl_2$ and 1 mM DTT) and incubated for 1 h at 4°C. The complexes were further purified by SEC and concentrated to 15 mg/ml prior to setting up crystallization trials.

Analytical SEC

For analytical SEC, 1 mg of Imp13 was injected directly or after incubation for 1 h at 4°C with 1.5 × excess of RanGTP and/or 2 × excess of different eIF1A constructs. The runs were carried out with a Superdex 200 10/300GL gel filtration column (GE Healthcare) using the UV absorbance at 280 nm. A sample of each peak fraction was analysed by 15% SDS–PAGE. Proteins were visualized by Coomassie staining.

Crystallization, data collection and analysis

Optimized crystals of the ternary export complex were obtained in 6% PEG 8000, 0.1 M Na-citrate, pH 5.8 grown at 18°C by vapour diffusion. For data collection, crystals were cryo-protected with mother liquor supplemented with 30% glycerol and flash frozen in liquid nitrogen. The crystals diffracted to 3.6 Å resolution and belong to the spacegroup *C*2 with cell dimensions of $a = 186.50$ Å, $b = 100.4$ Å, $c = 274.72$ Å, $\alpha = \gamma = 90°$ $\beta = 90.909°$. The asymmetric unit contains three independent complexes. Data were processed and scaled using XDS (Kabsch, 1993). The structure was solved by MR using PHASER (McCoy *et al*, 2007) and the Imp13-RanGTP structure (pdb id.: 2x19) as a search model. For placing eIF1A into the electron density, SAD data of the SeMet substituted eIF1A Leu65Met in complex with Imp13 and RanGTP were collected and an anomalous Fourier map was calculated. Refinement was carried out using iterative cycles of model building in COOT (Emsley and Cowtan, 2004) and restrained refinement including NCS in BUSTER (Smart *et al*, 2012) and B-group refinement in PHENIX (Adams *et al*, 2010).

Crystals of unbound Dm Imp13 grew in 0.1 M NaoAc, pH 4.9 with addition of 0.8 M ammonium tartrate at 18°C by vapour diffusion method (8 mg/ml). The crystals diffracted to 3 Å and belonged to spacegroup $P4_32_12$ with cell dimensions of $a = b = 167.72$, $c = 95.630$ and $\alpha = \beta = \gamma = 90°$. The structure was solved by MR using PHASER and Dm Imp13 as a search model (pdb id.: 2x1g) fragmented into three regions encompassing H2-8, H9-12; H15-20. Iterative cycles of model building and restrained refinement were carried out in COOT and PHENIX (Emsley and Cowtan, 2004; Adams *et al*, 2010).

All diffraction data were collected at the PXII beamline of the Swiss Light Source (Villigen, Switzerland).

In vitro binding assays

For binding assays, GST-tagged Imp13 was incubated with purified binding partners (7 μg of eIF1A or 4 μg of each of the other proteins) in binding buffer (20 mM HEPES pH 7.5, 50 mM NaCl, 4 mM $MgCl_2$, 10% glycerol, 0.01% (v/v) Nonidet P40 and 1 mM DTT) in a final volume of 60 μl for 1 h at 4°C. The GST-tagged protein was immobilized on 15 μl of glutathione agarose beads (Macherey-Nagel) and incubated for 1 h at 4°C. The beads were washed three times with 500 μl of binding buffer and eluted with 8 μl of SDS loading buffer. The eluted proteins were analysed by 15% SDS–PAGE and visualized by Coomassie staining.

Cell culture and transfection

HeLa cells were maintained in Dulbecco's Modified Eagle's medium (DMEM) supplemented with fetal bovine serum (10%), L-glutamine (2 mM), penicillin (100 units/ml) and streptomycin (100 μg/ml; all from Invitrogen). Cells were grown in a humidified incubator with 5% CO_2 at 37°C. Transfections were performed using Lipofectamine 2000 (Invitrogen), following manufacturer's recommendations.

Knockdown efficiency was assessed by western blot using anti-Imp13 antibody (produced in-house) and anti-tubulin as a loading control (1:10 000; Sigma).

For immunofluorescence, the cells were grown directly on glass coverslips, in 24-well plates. The transfection mixtures contained 600 ng of one or more plasmids encoding GFP-, mCherry- or HA-protein fusions. The cells were fixed 48 h after transfection.

For live-cell imaging, the cells were grown in 24-well plates. The transfection mixtures contained 600 ng of one or more plasmids encoding GFP-, mCherry- or HA-protein fusions. The day after transfection, the cells were transferred in 35 mm glass-bottom dishes (Greiner Bio-One). The cells were imaged 48 h after transfection. Where indicated, the cells were treated with 20 ng/ml Leptomycin B (LMB; Sigma-Aldrich) for 5 h before imaging.

Fluorescence microscopy, image processing and data analysis

For immunofluorescence, HeLa cells were fixed with 4% paraformaldehyde in PBS for 10 min, and permeabilized for 10 min with PBS containing 0.5% Triton X-100. Anti-eIF1AY (1:50, #Y055246, abm) and anti-Imp13 were used for detection. Incubation with the primary antibodies was performed in 0.1 M Tris–HCl pH 8 with 5% donkey serum, for 60 min at room temperature. Cells were then washed 2 × in 0.1 M Tris–HCl pH 8 and 3 × in 0.1 M Tris–HCl pH 8 with 1 M NaCl. Appropriate Alexa Fluor 488- or Alexa Fluor 555-coupled secondary antibodies (Molecular Probes) were diluted 1:1.000 in 0.1 M Tris–HCl pH 8 with 1 M NaCl and incubated 45 min at room temperature; where stated, Alexa 633-phalloidin (Molecular Probes) was also included. DNA was stained with Hoechst 33342 (Molecular Probes). Samples were mounted using Fluoromount-G (Southern Biotechnology Associates, Inc.). For live imaging, HeLa cells grown in 35 mm glass-bottom dishes were maintained in CO_2-independent medium (Gibco) supplemented with fetal bovine serum (1%).

Images were acquired on an Olympus FluoView FV1000 confocal microscope, equipped with a UPLSAPO 60X NA:1.20 water objective. Z-stacks were taken to scan the cell volume, with slices every 0.49 μm. Where indicated, DIC images were also acquired to define the boundaries of cytoplasm and nucleus. Image processing and quantification was performed with ImageJ. Briefly, all the slices of a Z-stack were summed and, after background subtraction, total fluorescence intensity was measured for each cellular compartment. The values obtained for the nuclear compartment were then expressed as a fraction of the corresponding total fluorescence. Statistical representation and analysis were performed with gnumeric (http://projects.gnome.org/gnumeric/).

Differential scanning fluorimetry

Previous attempts at measuring binding affinities with ITC and Biacore proved unsuccessful due to aggregation and precipitation of Imp13. For this reason, we used DSF to determine the dissociation constants of Imp13 with various cargoes (Niesen *et al*, 2007). The cargo was titrated in 18–20 steps to a fixed concentration of Imp13 in buffer containing 20 mM HEPES pH 7.5, 100 mM NaCl, 4 mM $MgCl_2$ and 15% glycerol in a 96-well plate (BIOZYME). For Mago-Y14 and RanGTP Q69L (residues 1–180), a fixed concentration of 0.5 μM Imp13 was used, while Ubc9 was titrated to 1 μM Imp13. eIF1A was titrated to 1 μM of preformed and purified Imp13-RanGTP complex. To each titration step, 5 × SYPRO Orange (SIGMA) was added, the wells were sealed with Flat Caps Strips (BIOZYME) and incubated for 30 min at RT. Melting curves were measured with BIO-RAD DNA Engine Chromo4 with a temperature gradient from 25 to 85 °C with an increment of 1°C/s and an adjustment time of 5 s. Two channels, SYBR and CY3, were used for excitation and absorption. The melting temperature (*T*m) was calculated with the program GraphPad PRISM5 by fitting the Boltzman equation to the measured melting curves. For the calculation of the K_D, the *T*m was plotted against the concentration of the cargo and fitted with an exponential equation.

Accession numbers

The coordinates and structure factors have been deposited in the Macromolecular Structure Database of European Bioinformatic Institute (EBI) with ID code 3zjy and 3zkv for Imp13 ternary export complex and unbound form, respectively.

Supplementary data

Supplementary data are available at *The EMBO Journal* Online (http://www.embojournal.org).

Acknowledgements

We wish to thank J Basquin, K Valer-Saldana and S Pleyer at the MPI-Martinsried crystallization facility and C Basquin and Y Grömping for advice on biophysical measurements. We also thank E Izaurralde (MPI-Tübingen) for plasmids, W Antonin (MPI-Tübingen) and F Baumann (Hertie Institut, Tuebingen) for cell lines, R Neher for advice on statistical analysis and the staff at the Swiss Light Source synchrotron for assistance during data collection. We are grateful to C Liebig and G Jékely for help in fluorescence microscopy data acquisition and analysis and to S Wachter for help with protein purification. We thank A Cook and E Conti for discussion and critical reading of the manuscript. This study was supported by the Max Planck Gesellshaft and by the DFG grant BO3588/1-1.

Author contributions: Biochemical, biophysical and structural work was done by MG; cell-based assays by DL; FB supervised the project. All authors wrote the paper.

Conflict of interest

The authors declare that they have no conflict of interest.

References

Adams PD, Afonine PV, Bunkóczi G, Chen VB, Davis IW, Echols N, Headd JJ, Hung L-W, Kapral GJ, Grosse-Kunstleve RW, McCoy AJ, Moriarty NW, Oeffner R, Read RJ, Richardson DC, Richardson JS, Terwilliger TC, Zwart PH (2010) PHENIX: a comprehensive Python-based system for macromolecular structure solution. *Acta Crystallogr D Biol Crystallogr* **66:** 213–221

Aitken CE, Lorsch JR (2012) A mechanistic overview of translation initiation in eukaryotes. *Nat Struct Mol Biol* **19:** 568–576

Askjaer P, Bachi A, Wilm M, Bischoff FR, Weeks DL, Ogniewski V, Ohno M, Niehrs C, Kjems J, Mattaj IW, Fornerod M (1999) RanGTP-regulated interactions of CRM1 with nucleoporins and a shuttling DEAD-box helicase. *Mol Cell Biol* **19:** 6276–6285

Battiste JL, Pestova TV, Hellen CU, Wagner G (2000) The eIF1A solution structure reveals a large RNA-binding surface important for scanning function. *Mol Cell* **5:** 109–119

Bayliss R, Littlewood T, Stewart M (2000) Structural basis for the interaction between FxFG nucleoporin repeats and importin-beta in nuclear trafficking. *Cell* **102:** 99–108

Bhardwaj A, Cingolani G (2010) Conformational selection in the recognition of the snurportin importin beta binding domain by importin beta. *Biochemistry* **49:** 5042–5047

Bischoff FR, Görlich D (1997) RanBP1 is crucial for the release of RanGTP from importin beta-related nuclear transport factors. *FEBS Lett* **419:** 249–254

Bischoff FR, Klebe C, Kretschmer J, Wittinghofer A, Ponstingl H (1994) RanGAP1 induces GTPase activity of nuclear Ras-related Ran. *Proc Natl Acad Sci USA* **91:** 2587–2591

Bono F, Cook AG, Grünwald M, Ebert J, Conti E (2010) Nuclear import mechanism of the EJC component Mago-Y14 revealed by structural studies of importin 13. *Mol Cell* **37:** 211–222

Cansizoglu AE, Chook YM (2007) Conformational heterogeneity of karyopherin beta2 is segmental. *Structure (London, England: 1993)* **15:** 1431–1441

Cansizoglu AE, Lee BJ, Zhang ZC, Fontoura BMA, Chook YM (2007) Structure-based design of a pathway-specific nuclear import inhibitor. *Nat Struct Mol Biol* **14:** 452–454

Chen VB, Arendall WB, Headd JJ, Keedy DA, Immormino RM, Kapral GJ, Murray LW, Richardson JS, Richardson DC (2010) MolProbity: all-atom structure validation for macromolecular crystallography. *Acta Crystallogr D Biol Crystallogr* **66:** 12–21

Cingolani G, Bednenko J, Gillespie MT, Gerace L (2002) Molecular basis for the recognition of a nonclassical nuclear localization signal by importin beta. *Mol Cell* **10:** 1345–1353

Cingolani G, Petosa C, Weis K, Müller CW (1999) Structure of importin-beta bound to the IBB domain of importin-alpha. *Nature* **399:** 221–229

Cook A, Bono F, Jinek M, Conti E (2007) Structural biology of nucleocytoplasmic transport. *Annu Rev Biochem* **76:** 647–671

Cook A, Fernandez E, Lindner D, Ebert J, Schlenstedt G, Conti E (2005) The structure of the nuclear export receptor Cse1 in its cytosolic state reveals a closed conformation incompatible with cargo binding. *Mol Cell* **18:** 355–367

Cook AG, Fukuhara N, Jinek M, Conti E (2009) Structures of the tRNA export factor in the nuclear and cytosolic states. *Nature* **461:** 60–65

Deane R, Schäfer W, Zimmermann HP, Mueller L, Görlich D, Prehn S, Ponstingl H, Bischoff FR (1997) Ran-binding protein 5 (RanBP5) is related to the nuclear transport factor importin-beta but interacts differently with RanBP1. *Mol Cellular Biol* **17:** 5087–5096

Diebold M-L, Fribourg S, Koch M, Metzger T, Romier C (2011) Deciphering correct strategies for multiprotein complex assembly by co-expression: application to complexes as large as the histone octamer. *J Struct Biol* **175:** 178–188

Dong X, Biswas A, Chook YM (2009a) Structural basis for assembly and disassembly of the CRM1 nuclear export complex. *Nat Struct Mol Biol* **16:** 558–560

Dong X, Biswas A, Süel KE, Jackson LK, Martinez R, Gu H, Chook YM (2009b) Structural basis for leucine-rich nuclear export signal recognition by CRM1. *Nature* **458:** 1136–1141

Emsley P, Cowtan K (2004) Coot: model-building tools for molecular graphics. *Acta Crystallogr D Biol Crystallogr* **60:** 2126–2132

Faza MB, Chang Y, Occhipinti L, Kemmler S, Panse VG (2012) Role of Mex67-Mtr2 in the Nuclear Export of 40S Pre-Ribosomes. *PLoS Genet* **8:** e1002915

Forwood JK, Lange A, Zachariae U, Marfori M, Preast C, Grubmüller H, Stewart M, Corbett AH, Kobe B (2010) Quantitative structural analysis of importin-β flexibility: paradigm for solenoid protein structures. *Structure (London, England: 1993)* **18:** 1171–1183

Giagtzoglou N, Lin YQ, Haueter C, Bellen HJ (2009) Importin 13 regulates neurotransmitter release at the Drosophila neuromuscular junction. *J Neurosci* **29:** 5628–5639

Gontan C, Guttler T, Engelen E, Demmers J, Fornerod M, Grosveld FG, Tibboel D, Gorlich D, Poot RA, Rottier RJ (2009) Exportin 4 mediates a novel nuclear import pathway for Sox family transcription factors. *J Cell Biol* **185:** 27–34

Grünwald M, Bono F (2011) Structure of Importin13-Ubc9 complex: nuclear import and release of a key regulator of sumoylation. *EMBO J* **30:** 427–438

Görlich D, Dabrowski M, Bischoff FR, Kutay U, Bork P, Hartmann E, Prehn S, Izaurralde E (1997) A novel class of RanGTP binding proteins. *J Cell Biol* **138:** 65–80

Görlich D, Kutay U (1999) Transport between the cell nucleus and the cytoplasm. *Annu Rev Cell Dev Biol* **15:** 607–660

Güttler T, Madl T, Neumann P, Deichsel D, Corsini L, Monecke T, Ficner R, Sattler M, Görlich D (2010) NES consensus redefined by structures of PKI-type and Rev-type nuclear export signals bound to CRM1. *Nat Struct Mol Biol* **17:** 1367–1376

Hellmuth K, Lau DM, Bischoff FR, Künzler M, Hurt E, Simos G (1998) Yeast Los1p has properties of an exportin-like nucleocytoplasmic transport factor for tRNA. *Mol Cell Biol* **18:** 6374–6386

Hinnebusch AG (2011) Molecular mechanism of scanning and start codon selection in eukaryotes. *Microbiol Mol Biol Rev* **75:** 434–467 first page of table of contents

Imasaki T, Shimizu T, Hashimoto H, Hidaka Y, Kose S, Imamoto N, Yamada M, Sato M (2007) Structural basis for substrate recognition and dissociation by human transportin 1. *Mol Cell* **28:** 57–67

Jackson RJ, Hellen CUT, Pestova TV (2010) The mechanism of eukaryotic translation initiation and principles of its regulation. *Nat Rev Mol Cell Biol* **11:** 113–127

Kabsch W (1993) Automatic processing of rotation diffraction data from crystals of initially unknown symmetry and cell constants. *J Appl Cryst* **26:** 795–800

Kahle J, Baake M, Doenecke D, Albig W (2005) Subunits of the heterotrimeric transcription factor NF-Y are imported into the nucleus by distinct pathways involving importin beta and importin 13. *Mol Cell Biol* **25:** 5339–5354

Kataoka N, Diem MD, Kim VN, Yong J, Dreyfuss G (2001) Magoh, a human homolog of Drosophila mago nashi protein, is a component of the splicing-dependent exon-exon junction complex. *EMBO J* **20:** 6424–6433

Kataoka N, Yong J, Kim VN, Velazquez F, Perkinson RA, Wang F, Dreyfuss G (2000) Pre-mRNA splicing imprints mRNA in the nucleus with a novel RNA-binding protein that persists in the cytoplasm. *Mol Cell* **6:** 673–682

Koyama M, Matsuura Y (2010) An allosteric mechanism to displace nuclear export cargo from CRM1 and RanGTP by RanBP1. *EMBO J* **29:** 2002–2013

Kutay U, Bischoff FR, Kostka S, Kraft R, Görlich D (1997) Export of importin alpha from the nucleus is mediated by a specific nuclear transport factor. *Cell* **90:** 1061–1071

Kutay U, Lipowsky G, Izaurralde E, Bischoff FR, Schwarzmaier P, Hartmann E, Görlich D (1998) Identification of a tRNA-specific nuclear export receptor. *Mol Cell* **1:** 359–369

Lee SJ, Matsuura Y, Liu SM, Stewart M (2005) Structural basis for nuclear import complex dissociation by RanGTP. *Nature* **435:** 693–696

Lee SJ, Sekimoto T, Yamashita E, Nagoshi E, Nakagawa A, Imamoto N, Yoshimura M, Sakai H, Chong KT, Tsukihara T, Yoneda Y (2003) The structure of importin-beta bound to SREBP-2: nuclear import of a transcription factor. *Science (New York, NY)* **302:** 1571–1575

Liang J, Ke G, You W, Peng Z, Lan J, Kalesse M, Tartakoff AM, Kaplan F, Tao T (2008) Interaction between importin 13 and myopodin suggests a nuclear import pathway for myopodin. *Mol Cell Biochem* **307:** 93–100

Lipowsky G, Bischoff FR, Izaurralde E, Kutay U, Schäfer S, Gross HJ, Beier H, Görlich D (1999) Coordination of tRNA nuclear export with processing of tRNA. *RNA (New York, NY)* **5:** 539–549

Lipowsky G, Bischoff FR, Schwarzmaier P, Kraft R, Kostka S, Hartmann E, Kutay U, Görlich D (2000) Exportin 4: a mediator of a novel nuclear export pathway in higher eukaryotes. *EMBO J* **19:** 4362–4371

Matsuura Y, Stewart M (2004) Structural basis for the assembly of a nuclear export complex. *Nature* **432:** 872–877

McCoy A, Grosse-Kunstleve R, Adams P, Winn M, Storoni L, Read R (2007) Phaser crystallographic software. *J Appl Crystallogr* **40:** 658–674

Mingot JM, Kostka S, Kraft R, Hartmann E, Görlich D (2001) Importin 13: a novel mediator of nuclear import and export. *EMBO J* **20:** 3685–3694

Mitrousis G, Olia AS, Walker-Kopp N, Cingolani G (2008) Molecular basis for the recognition of snurportin 1 by importin beta. *J Biol Chem* **283:** 7877–7884

Mohr D, Frey S, Fischer T, Güttler T, Görlich D (2009) Characterisation of the passive permeability barrier of nuclear pore complexes. *EMBO J* **28:** 2541–2553

Monecke T, Güttler T, Neumann P, Dickmanns A, Görlich D, Ficner R (2009) Crystal structure of the nuclear export receptor CRM1 in complex with Snurportin1 and RanGTP. *Science (New York, NY)* **324:** 1087–1091

Niesen FH, Berglund H, Vedadi M (2007) The use of differential scanning fluorimetry to detect ligand interactions that promote protein stability. *Nat Protoc* **2:** 2212–2221

Okada C, Yamashita E, Lee SJ, Shibata S, Katahira J, Nakagawa A, Yoneda Y, Tsukihara T (2009) A High-Resolution Structure of the Pre-microRNA Nuclear Export Machinery. *Science (New York, NY)* **326:** 1275–1279

Paraskeva E, Izaurralde E, Bischoff FR, Huber J, Kutay U, Hartmann E, Lührmann R, Görlich D (1999) CRM1-mediated recycling of snurportin 1 to the cytoplasm. *J Cell Biol* **145:** 255–264

Passmore LA, Schmeing TM, Maag D, Applefield DJ, Acker MG, Algire MA, Lorsch JR, Ramakrishnan V (2007) The eukaryotic

translation initiation factors eIF1 and eIF1A induce an open conformation of the 40S ribosome. *Mol Cell* **26:** 41–50

Ploski JE, Shamsher MK, Radu A (2004) Paired-type homeodomain transcription factors are imported into the nucleus by karyopherin 13. *Mol Cell Biol* **24:** 4824–4834

Rodriguez MS, Dargemont C, Hay RT (2001) SUMO-1 conjugation *in vivo* requires both a consensus modification motif and nuclear targeting. *J Biol Chem* **276:** 12654–12659

Saitoh H, Pizzi MD, Wang J (2002) Perturbation of SUMOlation enzyme Ubc9 by distinct domain within nucleoporin RanBP2/Nup358. *J Biol Chem* **277:** 4755–4763

Sali A, Blundell TL (1993) Comparative protein modelling by satisfaction of spatial restraints. *J Mol Biol* **234:** 779–815

Smart OS, Womack TO, Flensburg C, Keller P, Paciorek W, Sharff A, Vonrhein C, Bricogne G (2012) Exploiting structure similarity in refinement: automated NCS and target-structure restraints in BUSTER. *Acta Crystallogr D Biol Crystallogr* **68:** 368–380

Studier FW (2005) Protein production by auto-induction in high density shaking cultures. *Protein Expr Purif* **41:** 207–234

Tao T, Lan J, Lukacs GL, Haché RJG, Kaplan F (2006) Importin 13 regulates nuclear import of the glucocorticoid receptor in airway epithelial cells. *Am J Respir Cell Mol Biol* **35:** 668–680

Thomas F, Kutay U (2003) Biogenesis and nuclear export of ribosomal subunits in higher eukaryotes depend on the CRM1 export pathway. *J Cell Sci* **116:** 2409–2419

Vetter IR, Arndt A, Kutay U, Görlich D, Wittinghofer A (1999a) Structural view of the Ran-Importin beta interaction at 2.3 A resolution. *Cell* **97:** 635–646

Vetter IR, Nowak C, Nishimoto T, Kuhlmann J, Wittinghofer A (1999b) Structure of a Ran-binding domain complexed with Ran bound to a GTP analogue: implications for nuclear transport. *Nature* **398:** 39–46

Walker P, Doenecke D, Kahle J (2009) Importin 13 mediates nuclear import of histone fold containing chrac heterodimers. *J Biol Chem* **284:** 11652–11662

Wohlwend D, Strasser A, Dickmanns A, Ficner R (2007) Structural basis for RanGTP independent entry of spliceosomal U snRNPs into the nucleus. *J Mol Biol* **374:** 1129–1138

Wolff B, Sanglier JJ, Wang Y (1997) Leptomycin B is an inhibitor of nuclear export: inhibition of nucleo-cytoplasmic translocation of the human immunodeficiency virus type 1 (HIV-1) Rev protein and Rev-dependent mRNA. *Chem Biol* **4:** 139–147

Xu D, Farmer A, Chook YM (2010) Recognition of nuclear targeting signals by Karyopherin-β proteins. *Curr Opin Struct Biol* **20:** 782–790

Yoshida K, Blobel G (2001) The karyopherin Kap142p/Msn5p mediates nuclear import and nuclear export of different cargo proteins. *J Cell Biol* **152:** 729–740

Zhang ZC, Chook YM (2012) Structural and energetic basis of ALS-causing mutations in the atypical proline-tyrosine nuclear localization signal of the Fused in Sarcoma protein (FUS). *Proc Natl Acad Sci USA* **109:** 12017–12021

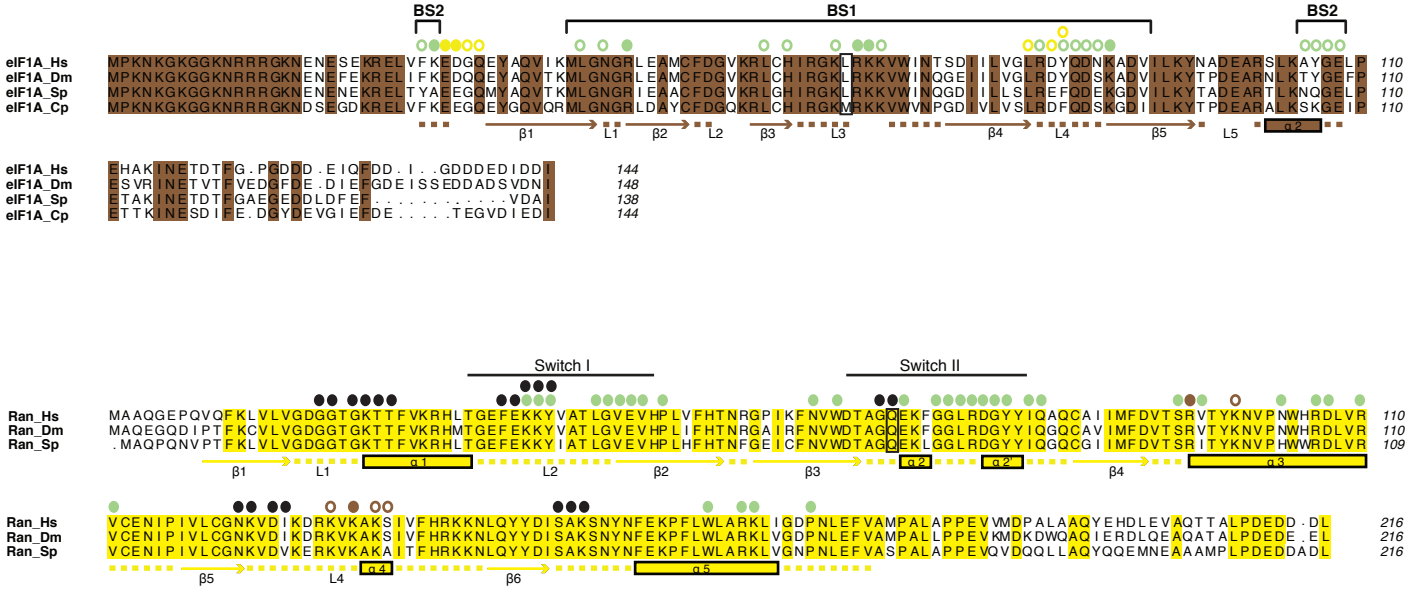

Supplementary Figure 1A. Structure-based sequence aligment of eIF1A and RanGTP.
The alignment shows eIF1A and RanGTP orthologues from *H. sapiens* (Hs), *D. melanogaster* (Dm) and *S. pombe* (Sp). The eIF1A alignment is complemented with the orthologue from *C. parvum* (Cp), which was used as a structural model in MODELLER. The conserved residues are highlighted in brown and yellow, respectively. The secondary structure elements are indicated as rectangles for α-helices and arrows for β-strands in the same color code. Dotted lines indicated loop regions. The eIF1A L65M mutation, used for the SAD data set, and the catalytic mutation of Ran Q69L are marked with a black rectangle. Interacting residues for Imp13 (green), Ran (yellow) and GTP (black), which were identified by the AquaProt server (Reichmann et al., 2007), are marked with colored circles above the sequence. For identifications of potential interacting residues of eIF1A with Imp13 and Ran, a MODELLER based model including all sidechains was analyzed with PISA (Krissinel and Henrick, 2007) and marked in the same color code with empty circles. Residues that were shown in co-precipitations to participate in the interaction, are marked with color-filled circles.

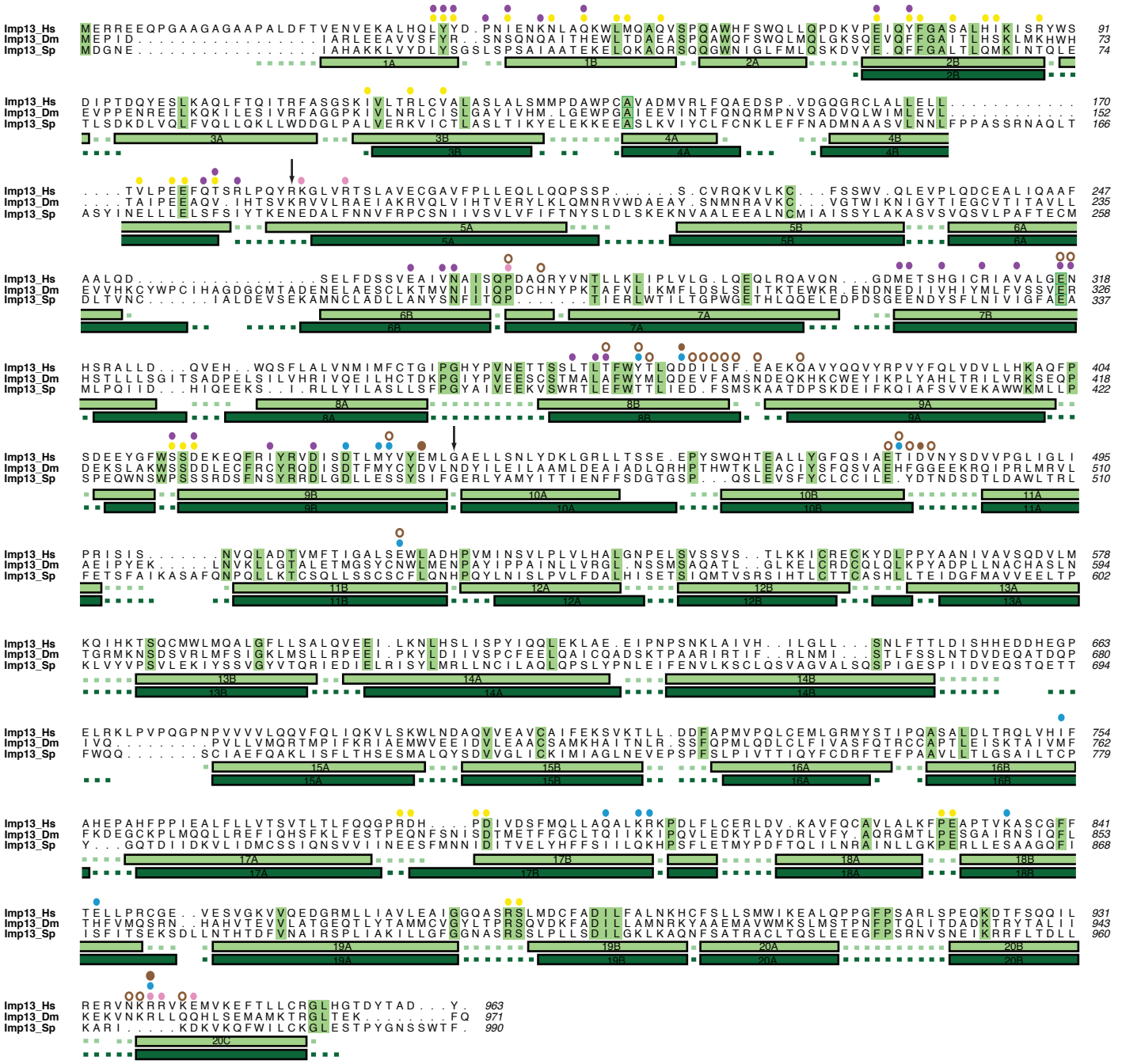

Supplementary Figure 1B. Structure-based sequence aligment of Imp13.
The alignment shows Imp13 orthologues from *H. sapiens* (Hs), *D. melanogaster* (Dm) and *S. pombe* (Sp). The conserved residues are highlighted in green. The HEAT-repeats of Hs and Dm Imp13 are shown below the sequence as light and dark green rectangles, respectively. Dotted lines represent loop regions. The two hinge regions of Imp13 are marked with a black arrow. Interacting residues for Ran (yellow), Ubc9 (purple), Mago (blue) and Y14 (magenta), which were identified by the AquaProt server (Reichmann et al., 2007), are marked with colored circles above the sequence. For identifications of potential interacting residues of eIF1A with Imp13, a MODELLER based model including all sidechains was analyzed with PISA (Krissinel and Henrick, 2007) and marked with empty brown circles. Residues, which were shown in co-precipitation to participate in the interaction, are marked with color-filled brown circles.

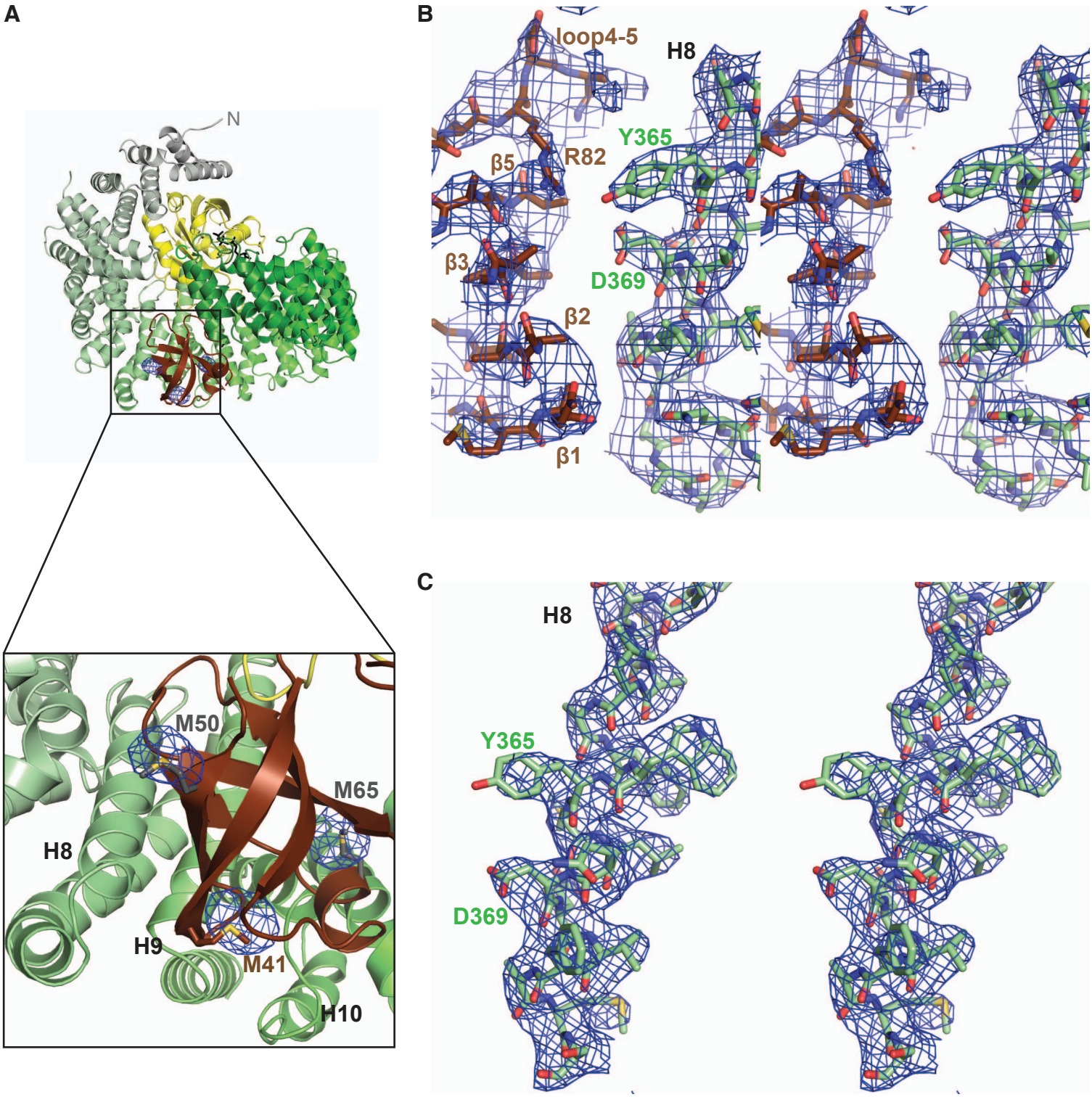

Supplementary Figure 2. Quality of the electrondensity. (**A**) Cartoon view and zoom-in (tilted) of the Imp13-RanGTP-eIF1A complex in the same color code and view as in Fig. 1A with an overlay of the anomalous Fourier map of the SeMet substitued eIF1A L65M SAD data set contoured at 4σ. The three methionine peaks of eIF1A L65M are shown as a blue mesh. The two methionine sidechains shown in coal were modeled in Coot (Emsley and Cowtan, 2004). (**B**) Stereo view of the eletron density of the 2Fo-Fc maps of the Imp13-RanGTP-eIF1A complex and of the Imp13 apo structure (**C**) after refinement and in a similar view. The interaction between Imp13 (green) and eIF1A (brown) is shown in a similar view as in Fig. 2A after a 180 rotation around the y-axis. The electron density is visualized as a blue mesh contoured at 1σ.

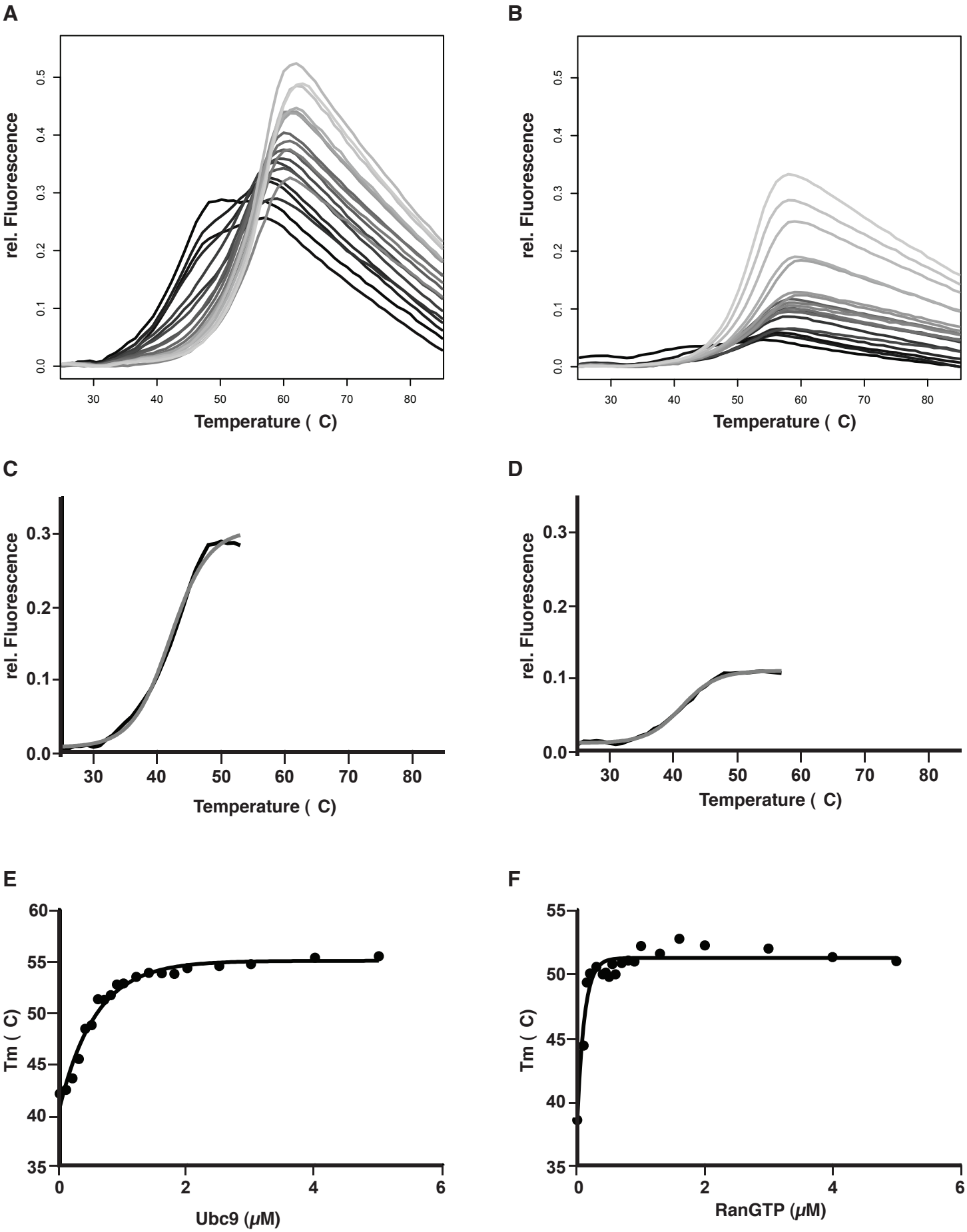

Supplementary Figure 3. Representative DSF curves. (**A**) and (**B**) show melting curves of Imp13 in dependence of increasing concentration of either Ubc9 (**A**) or RanGTP (**B**). The melting curves are plotted from black to gray according to increasing concentration of the ligand. (**C**) and (**D**) represent the melting curve of the first step of Ubc9 or RanGTP titration, respectively. The curves were fitted with the Boltzmann equation for the calculation of the Tm. (**E**) and (**F**) represent a plot of Tm against the concentration of Ubc9 (**E**) and RanGTP (**F**) with an exponential equation fitted. For the calculation of the K_D values, at least three independend measurement were carried out. Note that the RanGTP curve is too steep for a precise calculation of the K_D.

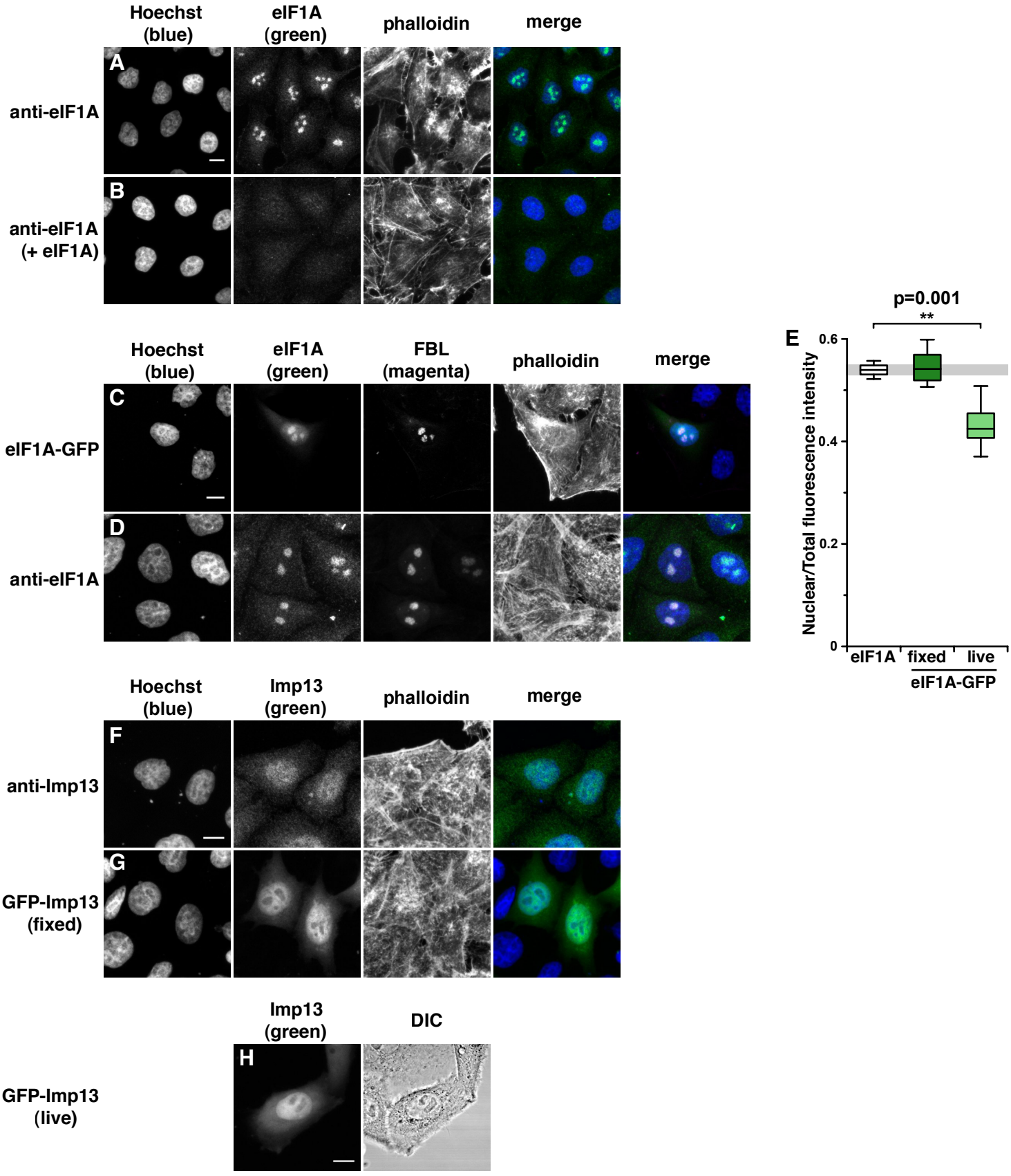

Supplementary figure 4. Localization of eIF1A and Imp13.
(**A-F**) Fluorescence microscopy images of fixed HeLa cells; the merged images show the nuclei (blue), the depicted endogenous or overexpressed protein (green) and, where indicated, the nucleolar protein FBL fused to mCherry (magenta). (**A, D**) Localization of endogenous eIF1A; in **B** the anti-eIF1A antibody was incubated with recombinant eIF1A prior to immunostaining. (**C**) Localization of GFP-tagged eIF1A (eIF1A-GFP). (**E**) Relative quantification of the fluorescence intensity in the nuclear compartment for endogenous eIF1A and eIF1A-GFP, both in fixed samples and live imaging (see also Fig. 5). (**F**) Localization of endogenous Imp13. (**G-H**) Localization of GFP-tagged Imp13 (GFP-Imp13) in fixed (**G**) and in live cells (**H**); DIC: differential interference contrast. At least three independent experiments were performed. Statistical significance was assessed with one tailed t-tests on the means of each experimental replicate, between the indicated conditions; the exact probabilities for alpha=0.05 are shown. (**) $p<0.01$, (*) $p<0.05$.Scale bar: 10µm.

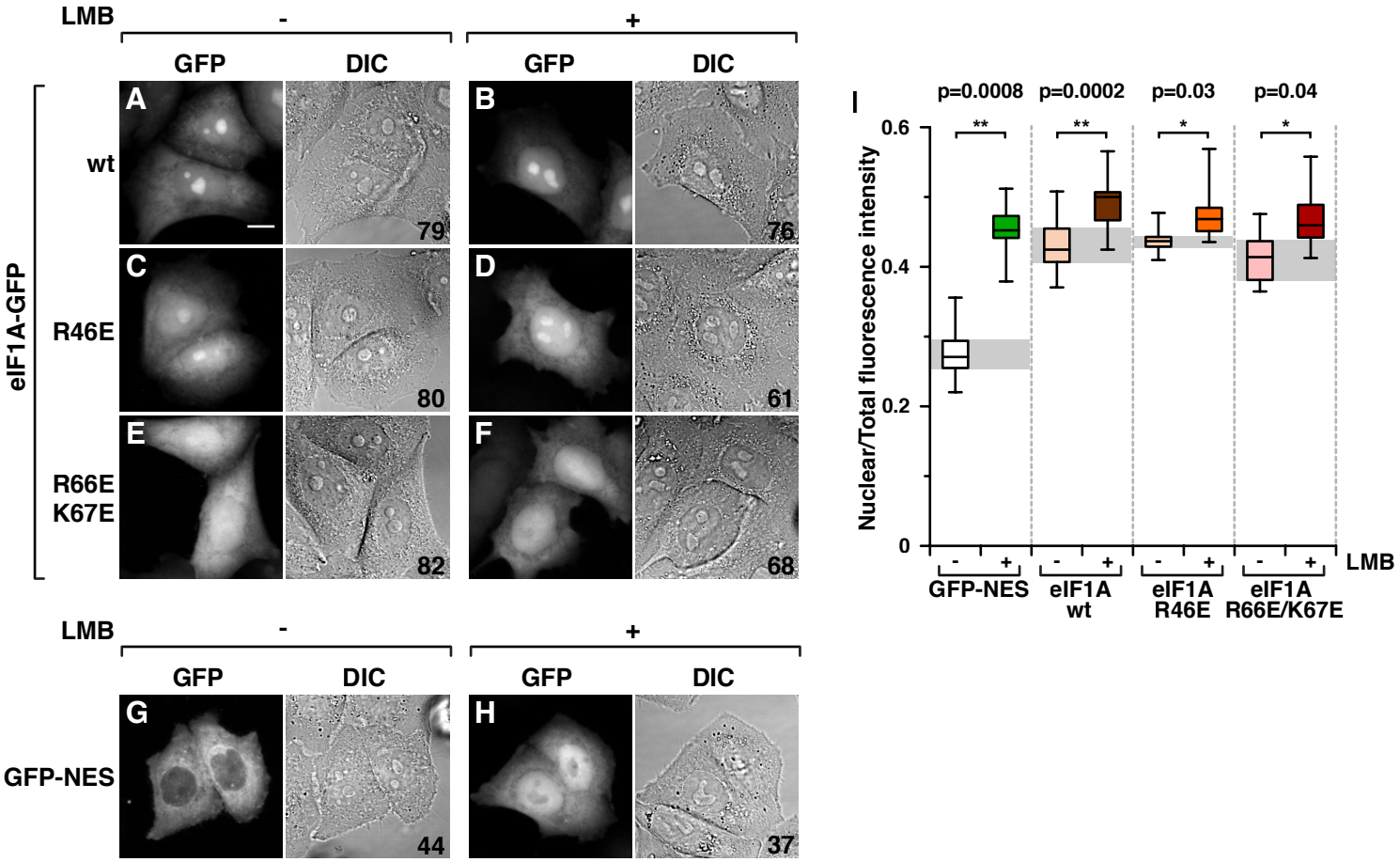

Supplementary Figure 5. CRM1 contributes to eIF1A localization.
(**A-H**) Fluorescence microscopy images and the corresponding DIC images of living HeLa cells expressing GFP-tagged eIF1A (eIF1A-GFP) wild type (wt, **A-B**) or mutants (**C-F**), or GFP fused to the nuclear export signal (GFP-NES) of the protein kinase A inhibitor (**G-H**). Localization of each construct in the absence (**A, C, E, G**) or presence (**B, D, F, H**) of Leptomycin B (LMB) is shown. (**I**) Relative quantification of the fluorescence intensity in the nuclear compartment for each construct, in the absence (-) or presence (+) of LMB. At least three independent experiments were performed; the number of analysed cells is indicated for each condition. Statistical significance was assessed with one tailed t-tests between the indicated conditions; the exact probabilities are shown. (**) $p<0.01$, (*) $p<0.05$. Scale bar: 10 µm.

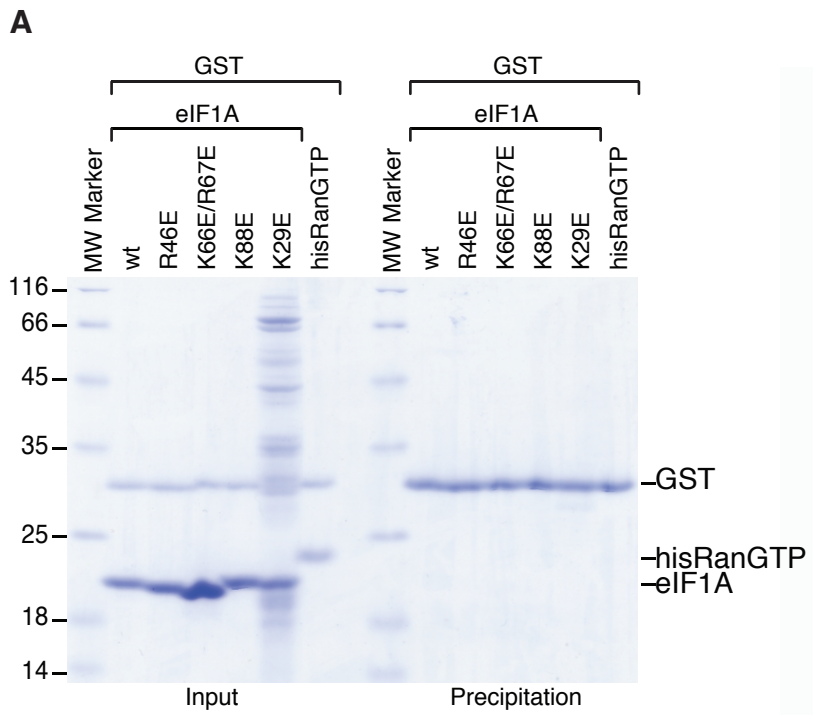

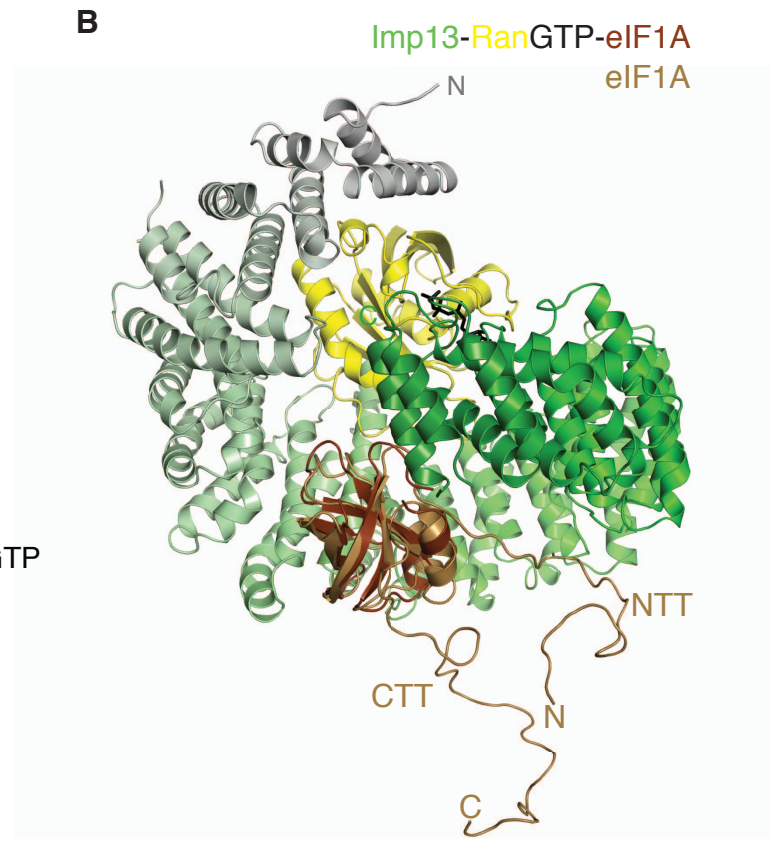

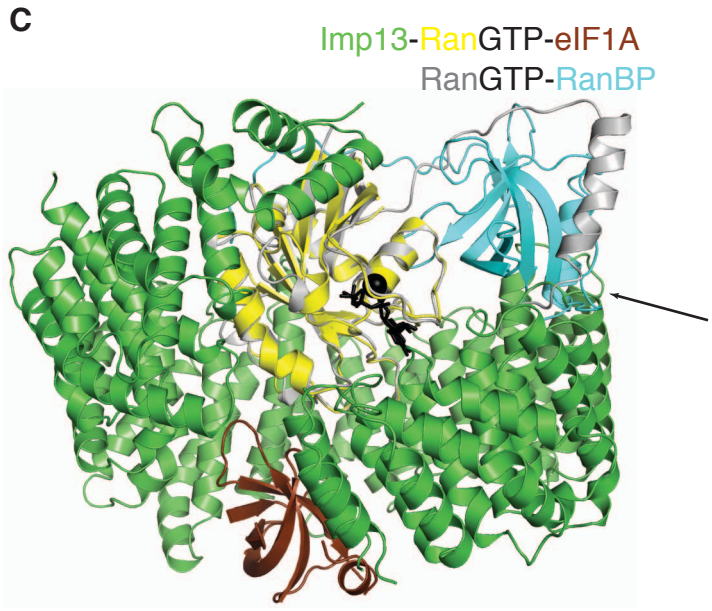

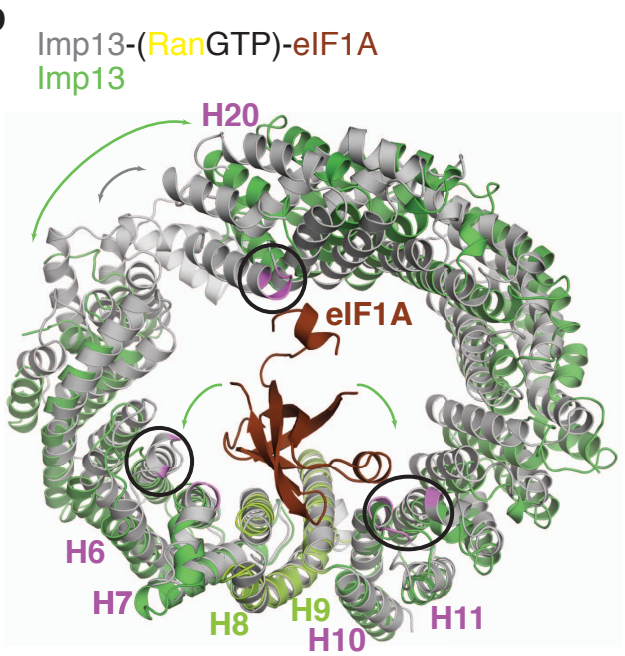

Supplementary Figure 6. (**A**) Protein co-precipitation by GST incubated together with RanGTP and eIF1A either with wild type (wt) or mutant. For the input control 1/6 of the samples were kept (upper panel) and the rest was co-precipitated with glutathione sepharose beads and analyzed on Coomassie stained 15 % SDS-PAGE. The far left lane was loaded with a molecular weight marker. Refers to Figure 2c (**B**) Cartoon view of a superposition of the NMR solution structure of human eIF1A (sand) (pdb id.: 1d7q) (Battiste et al., 2000) to eIF1A in the trimeric export complex Imp13-RanGTP-eIF1A. The Imp13-RanGTP-eIF1A structure is shown in the same color code and view as Figure 1b. (**C**) Superposition of Imp13-RanGTP-eIF1A with RanGTP-RanBP structure (pdb id: 1rrp)(Vetter et al., 1999), in grey and in cyan, respectively (**D**) eIF1A binding site on Imp13 apo and on Imp13 in the trimeric complex. Imp13 unbound is in green and in the export complex in grey, eIF1A is in brown and RanGTP is not shown for clarity. In pale green, the portion of eIF1A binding-site optimally superposed. Other interaction sites between Imp13 and eIF1A in the export complex are labeled in pink. Circled in red eIF1A interactions lost in the Imp13 apo conformation. Arrows highlight the compacting movement between the two Imp13 states.

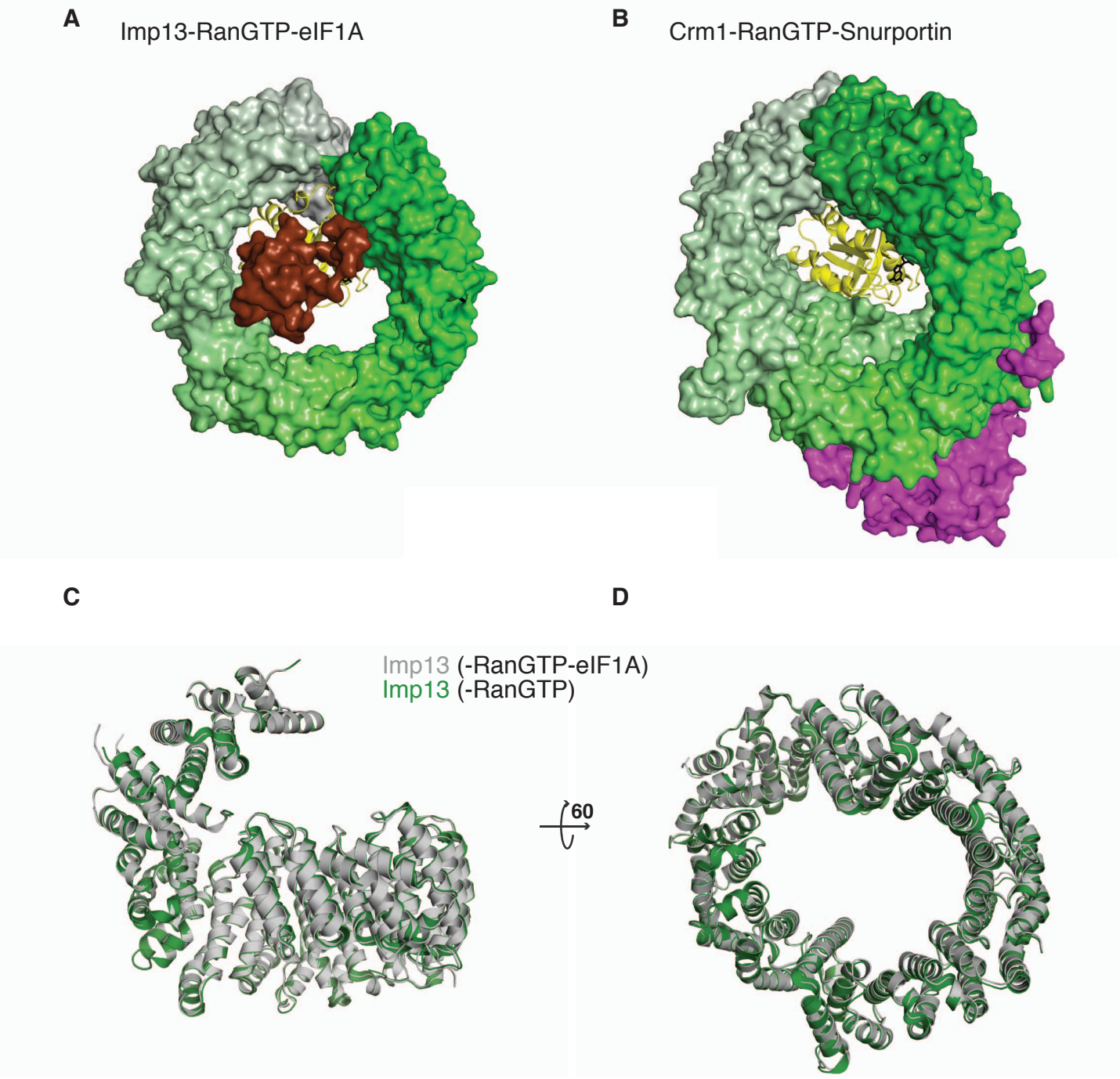

Supplementary Figure 7. Comparison of different karyopherin complexes.
A) and **B**) Surface view of different export-complexes in a similar view as in Fig1B turned 180 around the z axis. The exportins are shown in a gray to green color gradient. Ran is visible as yellow cartoon with the bound GTP in black. The export cargo eIF1A (**A**) is rendered as a surface in brown, while Snurportin bound to Crm1 (**B**) (Monecke et al, 2009; pdb id.: 3gjx) is in magenta. **C**) and **D**) Cartoon representation of Imp13 in complex 3 superposed to Imp13 in the previously described binary complex (Bono et al., 2010; pdb id.: 2x19) in a similar view as in Fig. 1B, C. Other components of the complexes are removed for clarity.